

**MEETING OFF-GRID TRANSPORTATION ENERGY NEEDS: A
RESOURCE EVALUATION MODEL FOR A SOLAR VORTEX POWER
GENERATION SYSTEM**

A Dissertation
Presented to
The Academic Faculty

By

Amy Marie Moore

In Partial Fulfillment
of the Requirements for the Degree
Doctor of Philosophy in Civil Engineering in the
School of Civil and Environmental Engineering

Georgia Institute of Technology
December 2016

Copyright © 2016 Amy Marie Moore

**MEETING OFF-GRID TRANSPORTATION ENERGY NEEDS: A
RESOURCE EVALUATION MODEL FOR A SOLAR VORTEX POWER
GENERATION SYSTEM**

Approved by:

Dr. Michael O. Rodgers, Advisor
School of Civil and Environmental
Engineering
Georgia Institute of Technology

Dr. Randall Guensler, Committee Member
School of Civil and Environmental
Engineering
Georgia Institute of Technology

Dr. Susan Burns, Committee Member
School of Civil and Environmental
Engineering
Georgia Institute of Technology

Dr. Ari Glezer, Committee
Member
Woodruff School of Mechanical
Engineering
Georgia Institute of Technology

Dr. William Drummond,
Committee Member
School of City and Regional
Planning
Georgia Institute of Technology

Date Approved: November 9, 2016

TABLE OF CONTENTS

LIST OF TABLES	vii
LIST OF FIGURES	viii
CHAPTER 1: INTRODUCTION	1
1.1 Global Climate Change	1
1.2 Transportation Sector's Impact on Global Climate Change	2
1.2.1 Reducing the Transportation Sector's Impact	4
1.2.2 The Need for Off-Grid Energy Production	5
1.2.3 The National Parks: Reducing the Transportation Sector's Impact at the Micro-Level	5
CHAPTER 2: TRANSPORTATION IN THE NATIONAL PARKS	7
2.1 Overview of Transportation Energy Needs at the National Parks	7
2.2 Ongoing Efforts at the National Parks	9
2.2.1 Green Parks Plan	9
2.2.2 Clean Cities Program	9
2.3 Renewable Energy Usage at National Parks	10
2.3.1 Small Scale	10
2.3.2 Utility Scale	11
2.4 Electric Vehicle Charging Stations at National Parks	12
2.5 Electric Buses	15
2.6 Transit in National Parks	16
2.6.1 Features of Park Transit	18
2.6.1.1 Transit Funding	18
2.6.1.2 Parking Problems on Park Property	19
2.6.1.3 Park Visitors' Perception of Park Transit	19
2.6.1.4 Park Transit's Influence on Park Visitation	22
2.6.1.5 Park Transit's Influence on Surrounding Communities	22
CHAPTER 3: SHORT-TERM SOLUTIONS AT THE NATIONAL PARKS AND OTHER OFF-GRID LOCATIONS: LOWER IMPACT FUELS	24
3.1 Green Bus Fleets	24

3.2 Propane	25
3.3 Compressed Natural Gas.....	26
3.4 Liquefied Natural Gas.....	27
3.5 Biofuels	28
3.5.1 Ethanol	28
3.5.2 Biodiesel	29
3.6 Long-Term Solutions for the National Parks and Other Off-Grid Locations: Power from Renewable Sources	30
3.6.1 Cogeneration	31
3.6.2 Bio-waste	32
3.7 Wind and Solar Technologies	32
3.7.1 Wind Technologies	33
3.7.2 Solar Technologies.....	34
3.7.2.1 Solar PV arrays	34
3.7.2.2 Concentrated Solar Power.....	36
CHAPTER 4: WIND AND SOLAR RESOURCE MODELS	39
4.1 Solar Resource Model.....	39
4.2 Wind Resource Model	41
4.3 Concentrated Wind Resource Model	44
CHAPTER 5: EMERGING TECHNOLOGY	45
5.1 The Solar Vortex (SoV)	45
5.1.1 Design Concept.....	46
5.1.2 Initial SoV Prototype	50
5.1.3 Renewable Power from SoVs	53
5.1.4 Comparison of SoV with Wind and Solar	54
5.1.5 Renewable Power from SoVs at National Parks.....	55
5.1.6 SoV Resource Model	56
CHAPTER 6: CONCENTRATED WIND RESOURCE MODEL	58
6.1 The GIS Model	59
6.2 MODIS.....	60
6.2.1 MODIS Data	64

6.3 Weather Station Variables	84
6.3.1 Obtaining Data from NOAA's NCDC Weather Stations	84
6.4.2 Weather Station Variable Data in ArcGIS	86
6.4 Calculation of Sensible and Latent Heat Flux	93
6.4.1 Gamma Calculation	95
6.4.2 Delta Calculation	96
6.4.3 $psat^*$ and VPD Calculation	96
6.4.4 pv Calculation.....	97
6.4.5 pd Calculation	97
6.4.6 ρ Calculation.....	97
6.4.7 Sensible Heat Calculation	98
6.4.8 Latent Heat Calculation	115
6.4.9 Saturation Vapor Pressure.....	115
6.4.10 Actual Vapor Pressure	115
6.4.11 Saturation and Actual Vapor Pressure Deficit	116
6.5 Raster Calculator.....	116
6.6 Contour Elevation Files	117
6.6.1 Creation of Digital Elevation Model.....	118
6.7 Creation of the Slope Model.....	123
6.7.1 ArcPy Scripts Involved in the Creation of the Slope Model	123
6.8 Threshold Model.....	129
6.8.1 Representative Distributions	129
6.8.2 Analysis of In-Situ Data.....	132
6.8.3 Threshold Model Steps	135
6.9 Linear Model.....	141
6.9.1 Final Model Assumptions	141
6.9.1.1. Vortex Power Assumption.....	141
6.9.1.2 Daytime Electrical Power Produced by SoV	142
6.9.1.3 Average Daytime Electrical Power Produced by SoV	142
6.9.1.4 Average Monthly Daytime Electrical Power Produced by SoV.....	143
6.9.1.5 Average Daytime Electrical Power Produced by SoV for All Locations	143

6.9.1.6 Relationship between Sensible and Latent Heat and Slope	143
6.9.1.7 Potential Withdrawal of Power	144
6.9.1.8 Mesa, Arizona Calculation Methods.....	144
CHAPTER 7: THE NATIONAL PARKS	148
7.1 Locating National Parks Using NREL’s Wind and Solar Models.....	148
7.1.1 Parks Suitable for Wind Facilities	148
7.1.2 Parks Suitable for Solar PV Facilities.....	153
CHAPTER 8: ANALYSIS, RESULTS, AND DISCUSSION OF CASE STUDY IN ZION NATIONAL PARK	158
8.1 Overview of Zion National Park.....	159
8.2 Calculation of Vortex Energy Potential Using Models	161
8.3 Results from the Linear Model	163
8.4 Results from the Threshold Model	169
8.5 Discussion	175
CHAPTER 9: CONTRIBUTIONS, LIMITATIONS, AND FUTURE WORK.....	176
9.1 Contributions.....	176
9.2 Limitations	176
9.3 Future Work	177
APPENDIX A.....	178
APPENDIX B	187
APPENDIX C	204
APPENDIX D.....	209
REFERENCES	213

LIST OF TABLES

Table 1: Proposed EV Station Sites at National Parks (American Progress, 2015)	15
Table 2: Emissions for Different Bus Types (results from GREET software) (CCW, 2015)	25
Table 3: NREL Wind Resource Model Wind Classes (NREL, 2014).....	42
Table 4: MODIS Spectral Bands 1-19 (NASA, 2015)	63
Table 5: Variables Needed for Sensible and Latent Heat Calculation.....	95
Table 6: Suitable National Parks for Wind Facilities	150
Table 7: Suitable National Parks for Solar PV Facilities.....	155
Table 8: Additional SoV Site Selection Criteria.....	158

LIST OF FIGURES

Figure 1: U.S. Greenhouse Gas Emissions 2013 (EPA, 2015)	1
Figure 2: Sources of Greenhouse Gas Emissions (EPA, 2015)	2
Figure 3: 2014 Estimated Energy Use (DOE, 2015)	3
Figure 4: Greenhouse Gas Emissions from Transportation (EPA, 2015)	4
Figure 5: National Parks (NPS, 2011)	8
Figure 6: National Parks with EVs and EV Stations (American Progress, 2015)	14
Figure 7: 2014: U.S. Energy Consumption by Source (EIA, 2015)	31
Figure 8: Wind Turbine Diagram (Clean Technica, 2014)	33
Figure 9: Solar PV Diagram (GreenSunRising, 2015)	35
Figure 10: Diagram of Concentrated Solar Configurations (Solar Tower UK, 2016)	37
Figure 11: Concentrated Solar Configurations (Solar Tower UK, 2016)	38
Figure 12: NREL's Solar Resource Model in ArcGIS (NREL, 2015)	40
Figure 13: NREL's Wind Resource Model in ArcGIS (NREL, 2015)	43
Figure 14: Dust Devil and Initial SoV Prototype (Georgia Tech, 2012)	46
Figure 15: Dust Devil and Initial SoV Prototype (Georgia Tech, 2012)	48
Figure 16: Diagram of SOV Vanes (Georgia Tech, 2012)	49
Figure 17: Diagram of SOV (Georgia Tech, 2012)	49
Figure 18: SoV Prototype (Georgia Tech, 2016)	51
Figure 19: Diagram of SoV Prototype (Georgia Tech, 2016)	52
Figure 20: Diagram of SoV Prototype (Georgia Tech, 2016)	53
Figure 21: Levelized Cost of Energy (Georgia Tech, 2012)	55
Figure 22: Model Development Flow Chart	58

Figure 23: EOS System (NASA, 2015)	61
Figure 24: MODIS Location on Terra Satellite (NASA, 2015).....	62
Figure 25: MODIS (NASA, 2015)	62
Figure 26: Sensible Heat Flux of Tibetan Plateau (Ma et al, 2010)	64
Figure 27: MODIS Reprojection Tool (USGS, 2011)	65
Figure 28: Raster Calculator with MODIS Null Cell Exclusion Formula.....	67
Figure 29: MODIS Land Surface Temperature (LST) and Emissivity, January, 2011 (10:30 am)	68
Figure 30: MODIS Land Surface Temperature (LST) and Emissivity, January, 2011 (10:30 pm)	69
Figure 31: MODIS Land Surface Temperature (LST) and Emissivity, January, 2013 (10:30 am)	70
Figure 32: MODIS Land Surface Temperature (LST) and Emissivity, January, 2013 (10:30 pm)	71
Figure 33: MODIS Land Surface Temperature (LST) and Emissivity, April, 2011 (10:30 am) .	72
Figure 34: MODIS Land Surface Temperature (LST) and Emissivity, April, 2011 (10:30 pm) .	73
Figure 35: MODIS Land Surface Temperature (LST) and Emissivity, April, 2013 (10:30 am) .	74
Figure 36: MODIS Land Surface Temperature (LST) and Emissivity, April, 2013 (10:30 pm) .	75
Figure 37: MODIS Land Surface Temperature (LST) and Emissivity, July, 2011 (10:30 am) ...	76
Figure 38: MODIS Land Surface Temperature (LST) and Emissivity, July, 2011 (10:30 pm) ...	77
Figure 39: MODIS Land Surface Temperature (LST) and Emissivity, July, 2013 (10:30 am) ...	78
Figure 40: MODIS Land Surface Temperature (LST) and Emissivity, July, 2013 (10:30 pm) ...	79

Figure 41: MODIS Land Surface Temperature (LST) and Emissivity, October, 2011 (10:30 am)	80
Figure 42: MODIS Land Surface Temperature (LST) and Emissivity, October, 2011 (10:30 pm)	81
Figure 43: MODIS Land Surface Temperature (LST) and Emissivity, October, 2013 (10:30 am)	82
Figure 44: MODIS Land Surface Temperature (LST) and Emissivity, October, 2013 (10:30 pm)	83
Figure 45: Locations of 216 NCDC Weather Stations	86
Figure 46: Air Temperature Interpolation	88
Figure 47: Dewpoint Temperature Interpolation	89
Figure 48: Wetbulb Temperature Interpolation	90
Figure 49: Weather Station Pressure Interpolation	91
Figure 50: Relative Humidity Interpolation	92
Figure 51: Sensible Heat Flux, January, 2011 (10:30 am)	99
Figure 52: Sensible Heat Flux, January, 2011 (10:30 pm)	100
Figure 53: Sensible Heat Flux, January, 2013 (10:30 am)	101
Figure 54: Sensible Heat Flux, January, 2013 (10:30 pm)	102
Figure 55: Sensible Heat Flux, April, 2011 (10:30 am)	103
Figure 56: Sensible Heat Flux, April, 2011 (10:30 pm)	104
Figure 57: Sensible Heat Flux, April, 2013 (10:30 am)	105
Figure 58: Sensible Heat Flux, April, 2013 (10:30 pm)	106
Figure 59: Sensible Heat Flux, July, 2011 (10:30 am)	107

Figure 60: Sensible Heat Flux, July, 2011 (10:30 pm)	108
Figure 61: Sensible Heat Flux, July, 2013 (10:30 am)	109
Figure 62: Sensible Heat Flux, July, 2013 (10:30 pm)	110
Figure 63: Sensible Heat Flux, October, 2011 (10:30 am)	111
Figure 64: Sensible Heat Flux, October, 2011 (10:30 pm)	112
Figure 65: Sensible Heat Flux, October, 2013 (10:30 am)	113
Figure 66: Sensible Heat Flux, October, 2013 (10:30 pm)	114
Figure 67: Raster Calculator Tool in ArcGIS	117
Figure 68: ArcPy Window in ArcGIS with DEM Script	120
Figure 69: ArcPy Window in ArcGIS with Symbology Script	121
Figure 70: Completed Digital Elevation Model in ArcGIS	122
Figure 71: ArcPy Window in ArcGIS with Feature to Raster Conversion Script	124
Figure 72: ArcPy Window in ArcGIS with Raster Reprojection Script	125
Figure 73: ArcPy Window in ArcGIS with Script that Applies the Slope Function	126
Figure 74: ArcPy Window in ArcGIS with Script that Applies a Unified Symbology	127
Figure 75: Completed Slope Model in ArcGIS	128
Figure 76: Physiographic Region Types Across U.S. with Ameriflux Sites	131
Figure 77: Representative Distributions from Ameriflux Sites	132
Figure 78: Bimodal Distribution of Heat Flux at Santa Rita Creosote Site	134
Figure 79: Measured vs. Predicted (Santa Rita Creosote site)	134
Figure 80: R Code Used in Estimation of Power Output	135
Figure 81: Threshold Model Assumptions	137
Figure 82: Power Output Estimation for California and Baja California	138

Figure 83: 2011 Annual Power Output (from Threshold Model).....	139
<i>Figure 84: 2013 Annual Power Output (from Threshold Model).....</i>	<i>140</i>
Figure 85: Mesa, Arizona Summer 2013 Vortex Energy (Low Estimate)	145
Figure 86: Mesa, Arizona Summer 2013 Vortex Energy (Medium Estimate)	146
Figure 87: Mesa, Arizona Summer 2013 Vortex Energy (High Estimate).....	147
Figure 88: ArcPy Script for Selecting Areas with Assigned Wind Classes Greater than, or Equal to Three	149
Figure 89: ArcPy Script for Selecting National Parks within Areas with Wind Classes Greater than, or Equal to Three.....	150
Figure 90: National Parks in Areas with Assigned Wind Class of 3 to 7 (NREL, 2015).....	152
Figure 91: ArcPy Script for Selecting Areas with Kilowatts per Square Meter per Day (kw/m2d) Greater than, or Equal to Five	153
Figure 92: ArcPy Script for Selecting National Parks within Areas with Kilowatts per Square Meter per Day (kw/m2d) Greater than, or Equal to Five.....	154
Figure 93: National Parks in Areas with kw/m2d ≥ 5	157
Figure 94: Zion National Park Boundary (Google Earth)	159
Figure 95: Zion Shuttle Parking and Garage (Google Earth)	160
Figure 96: Area North of Shuttle Parking Considered for SoV Installation.....	161
Figure 97: Zion National Park Slope Model.....	162
Figure 98: Zion Monthly Average Daytime Vortex Energy (Low Estimate – Linear Model)...	163
Figure 99: Zion Monthly Average Daytime Vortex Energy (Medium Estimate– Linear Model)	164
Figure 100: Zion Monthly Average Daytime Vortex Energy (High Estimate– Linear Model) .	165

Figure 101: Zion Shuttle Parking, Visitor Center, and Potential SoV Facility Locaiton (Low Estimate – Linear Model)	166
Figure 102: Zion Shuttle Parking, Visitor Center, and Potential SoV Facility Locaiton (Medium Estimate – Linear Model)	167
Figure 103: Zion Shuttle Parking, Visitor Center, and Potential SoV Facility Locaiton (High Estimate – Linear Model)	168
Figure 104: Zion Monthly Average Daytime Vortex Energy (Low Estimate – Threshold Model)	169
Figure 105: Zion Monthly Average Daytime Vortex Energy (Medium Estimate – Threshold Model).....	170
Figure 106: Zion Monthly Average Daytime Vortex Energy (High Estimate – Threshold Model)	171
Figure 107: Zion Shuttle Parking, Visitor Center, and Potential SoV Facility Locaiton (Low Estimate – Threshold Model).....	172
Figure 108: Zion Shuttle Parking, Visitor Center, and Potential SoV Facility Locaiton (Medium Estimate – Threshold Model).....	173
Figure 109: Zion Shuttle Parking, Visitor Center, and Potential SoV Facility Locaiton (High Estimate – Threshold Model).....	174
Figure 110: January 2011: Average Monthly Daytime Power Output (using Threshold Model)	179
Figure 111: January 2013: Average Monthly Daytime Power Output (using Threshold Model)	180
Figure 112: April 2011: Average Monthly Daytime Power Output (using Threshold Model) ..	181

Figure 113: April 2013: Average Monthly Daytime Power Output (using Threshold Model) ..	182
Figure 114: July 2011: Average Monthly Daytime Power Output (using Threshold Model)....	183
Figure 115: July 2013: Average Monthly Daytime Power Output (using Threshold Model)....	184
Figure 116: October 2011: Average Monthly Daytime Power Output (using Threshold Model)	
.....	185
Figure 117: October 2013: Average Monthly Daytime Power Output (using Threshold Model)	
.....	186
Figure 118: January 2011 Latent Heat (10:30 AM).....	188
Figure 119: January 2011 Latent Heat (10:30 PM)	189
Figure 120: January 2013 Latent Heat (10:30 AM).....	190
Figure 121: January 2013 Latent Heat (10:30 PM)	191
Figure 122: April 2011 Latent Heat (10:30 AM).....	192
Figure 123: April 2011 Latent Heat (10:30 PM)	193
Figure 124: April 2013 Latent Heat (10:30 AM).....	194
Figure 125: April 2013 Latent Heat (10:30 PM)	195
Figure 126: July 2011 Latent Heat (10:30 AM)	196
Figure 127: July 2011 Latent Heat (10:30 PM)	197
Figure 128: July 2013 Latent Heat (10:30 AM)	198
Figure 129: July 2013 Latent Heat (10:30 PM)	199
Figure 130: October 2011 Latent Heat (10:30 AM)	200
Figure 131: October 2011 Latent Heat (10:30 PM).....	201
Figure 132: October 2013 Latent Heat (10:30 AM)	202
Figure 133: October 2013 Latent Heat (10:30 PM).....	203

Figure 134: January 2013 Power Output (10:30 AM - Using Linear Model)	205
Figure 135: April 2013 Power Output (10:30 AM - Using Linear Model)	206
Figure 136: July 2013 Power Output (10:30 AM - Using Linear Model)	207
Figure 137: October 2013 Power Output (10:30 AM - Using Linear Model).....	208
Figure 138: January 2013: City of Atlanta 10:30 AM Power Production (Full Linear Model) .	209
Figure 139: April 2013: City of Atlanta 10:30 AM Power Production (Full Linear Model)	210
Figure 140: July 2013: City of Atlanta 10:30 AM Power Production (Full Linear Model)	211
Figure 141: October 2013: City of Atlanta 10:30 AM Power Production (Full Linear Model).	212

ACRONYMS AND SYMBOLS

α	Alpha: 50 w/m ² Threshold
ANOVA	Analysis of Variance
APS	American Physical Society
ARPA-E	Advanced Research Projects Agency – Energy
ASCE	American Society of Civil Engineers
ATS	Alternative Transportation System
β	Beta: 24.73 w/m ²
BLM	Bureau of Land Management
BTU	British Thermal Unit
BYD	Build Your Dreams
B100	Neat Biodiesel
C_a	Collection Area
C_E	Conversion Efficiency Factor
CHP	Combined Heat and Power
CMAQ	Congestion Mitigation and Air Quality Improvement
CNG	Compressed Natural Gas
CO ₂	Carbon Dioxide
c_p	Air Specific Heat at Constant Pressure
C2ES	Center for Climate and Energy Solutions
DEM	Digital Elevation Model
Δ	Delta: Slope of the Saturation Vapor Pressure Deficit at Air Temperature

DNI	Direct Normal Irradiance
DOE	Department of Energy
EPA	Environmental Protection Agency
e_a	Actual Vapor Pressure
e_s	Saturation Vapor Pressure
ESRI	Environmental Systems Research Institute
E10	Ethanol 10
FFV	Flexible Fuel Vehicles
FTA	Federal Transit Administration
γ	Gamma: Psychrometric Constant
G_E	Generation Efficiency Factor
GHG	greenhouse gas emissions
GIS	Geographic Information System
H	Sensible Heat
HDF	Hierarchical Data Format
IDLE	Integrated Development Environment
KM	Kilometer
KML	Keyhole Markup Language
KWE	Kilowatt Electric
KWH	Kilowatt-Hour
KW/M2D	Kilowatt per Meter Square per Day
λE	Latent Heat
LNG	Liquefied Natural Gas

LONO	Low or No Emission Vehicle Deployment Program
LST	Land Surface Temperature and Emissivity
MAP-21	Moving Ahead for Progress in the 21 st Century
M_d	Molar Mass of Dry Air
M_v	Molar Mass of Vapor
MODIS	Moderate Resolution Imaging Spectroradiometer
MWE	Megawatt Electric
NASA	National Aeronautics and Space Administration
NCDC	National Climatic Data Center
NED	National Elevation Dataset
NEDIS	National Environment Satellite Data and Information Service
NOAA	National Oceanographic and Atmospheric Administration
NPS	National Parks Service
NREL	National Renewable Energy Lab
p	Pressure Recorded at Measuring Station
p_d	Partial Pressure of Dry Air
PD	Saturation and Actual Vapor Pressure Deficit
φ	Phi: Relative Humidity
PNNL	Pacific Northwest National Laboratory
p_{sat}^*	Saturation Pressure of Water Vapor at Wetbulb Temperature
PV	Photovoltaic
p_v	Partial Pressure of Water Vapor
ρ	Air Density

R	Universal Gas Constant
r_{ah}	Aerodynamic Resistance for Heat Transfer Between Land and Surface
R_F	Regional Factor
SAFETEA-LU	Safe, Accountable, Flexible, Efficient Transportation Equity Act A Legacy for Users
SEIA	Solar Energy Industries' Association
δ	Slope
SoV	Solar Vortex
T_a	Air Temperature (Celsius)
T_d	Dewpoint Temperature (Celsius)
T_0	Surface Temperature
TIFF	Tag Image File Format
T^*	Wetbulb Temperature (Celsius)
UK	United Kingdom
US	United States
USGS	United States Geological Survey
UTRC	University Transportation Research Center
VE	Vortex Energy
VE_{AD}	Average Daytime Electrical Power Produced
VE_{AM}	Average Monthly Daytime Electrical Power
VE_D	Daytime Electrical Power
VPD	Vapor Pressure Deficit
W/M2	Watts per Meter Square

SUMMARY

The transportation sector is responsible for 27 percent of overall greenhouse gas emissions (GHG), and this is due to a heavy reliance on petroleum-based fuels. Therefore, electrification of transportation is desired to reduce this reliance. Alternative energy sources, mainly solar and horizontal wind, are currently the focus for meeting transportation energy needs. Emerging technologies are being developed, which are suitable for off-grid locations, making them appropriate for meeting transportation energy needs at remote locations, such as many of the National Parks. One such technology, the Solar Vortex (SoV), which was developed at Georgia Tech, relies on concentrated wind to generate power.

The National Renewable Energy Lab (NREL) currently has GIS resource models representing solar and horizontal wind resources across the 48 conterminous United States. However, a concentrated wind GIS resource model does not exist. A primary objective of this research was to develop a concentrated wind resource model that is comparable in resolution to NREL's existing solar and horizontal wind resource models. This was performed using ArcGIS to calculate sensible and latent heat for the 48 conterminous United States, using MODIS surface heat flux data, and methods used by Ma et al (2010 and 2013) and Bonan (2002).

A digital elevation model (DEM) was developed using contour line data from the 1/3 arc-second National Elevation Dataset (NED) from USGS. The DEM was then used to create a slope model for the 48 conterminous United States, which was created in ArcGIS using ArcPy programming language. A power output estimation model was then developed using R software, which used the calculated sensible heat values to estimate average, monthly power output potential based on actual sensible heat data obtained from Ameriflux. The results from the

model were then used in-conjunction with the slope model, and calculated diurnal sensible and latent heat values to develop a final model for estimating power output for the SoV.

Using NREL's solar and horizontal wind resource models, suitable locations of parks within the National Parks Service for solar and/or horizontal wind power generation were obtained. Upon completion of the final model, a case study was performed using Zion National Park. Zion was chosen for the case study based on its applicability for using the SoV due to its concentrated wind resource availability, and due to its remote location. The case study provides suggestions for the park based on its potential to use SoV units to power electric park vehicles.

CHAPTER 1: INTRODUCTION

1.1 Global Climate Change

There is substantial evidence that the Earth's climate is changing, and the changes that have taken place, even in recent decades, are striking: rising surface air temperatures and subsurface ocean temperatures; rising sea levels; and massive arctic glaciers that are decreasing in size (NASA, 2016). Noticeable changes have taken place since 1950, and these changes have been attributed to anthropogenic forces: a massive increase in greenhouse gas emissions, as shown in *Figure 1: U.S. Greenhouse Gas Emissions 2013* (EPA, 2015), namely: carbon dioxide, chlorofluorocarbons, methane, and nitrous oxide. It is believed that if society continues to function in the same manner, with few changes being made to reduce greenhouse gas (GHG) emissions, there will be severe repercussions. "If no mitigating actions are taken, significant disruptions in the Earth's physical and ecological systems, social systems, security and human health are likely to occur. We must reduce emissions of greenhouse gases beginning now" (APS, 2007).

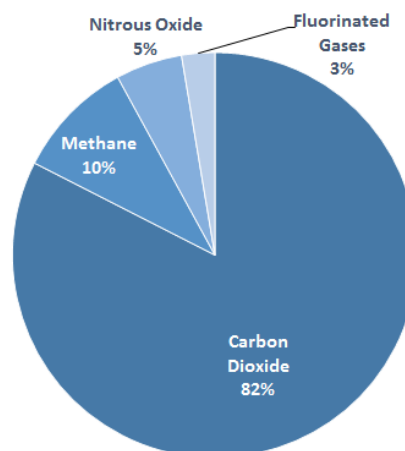


Figure 1: U.S. Greenhouse Gas Emissions 2013 (EPA, 2015)

1.2 Transportation Sector's Impact on Global Climate Change

Currently, the transportation sector alone accounts for 27 percent of overall GHG emissions, which is a 16 percent increase since 1990, as shown in *Figure 2: Sources of Greenhouse Gas Emissions (EPA, 2015)* and *Figure 3: 2014 Estimated Energy Use (DOE, 2015)*. These emissions consist mainly of carbon dioxide (CO₂), resulting from combustion of gasoline, diesel, and other petroleum-based fuels, with most of the emissions being contributed to heavy usage of passenger vehicles and light-duty trucks (EPA, 2015) as shown in *Figure 4: Greenhouse Gas Emissions from Transportation (EPA, 2015)*.

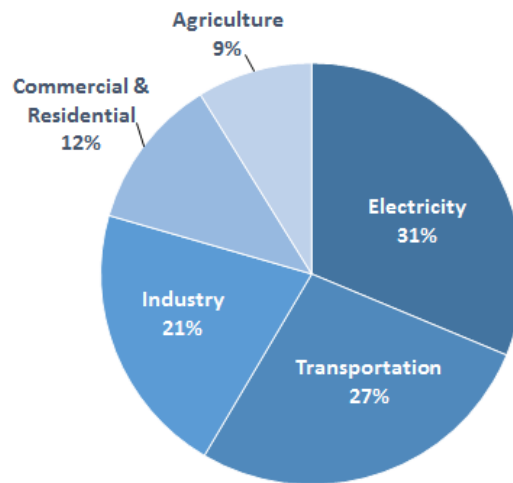
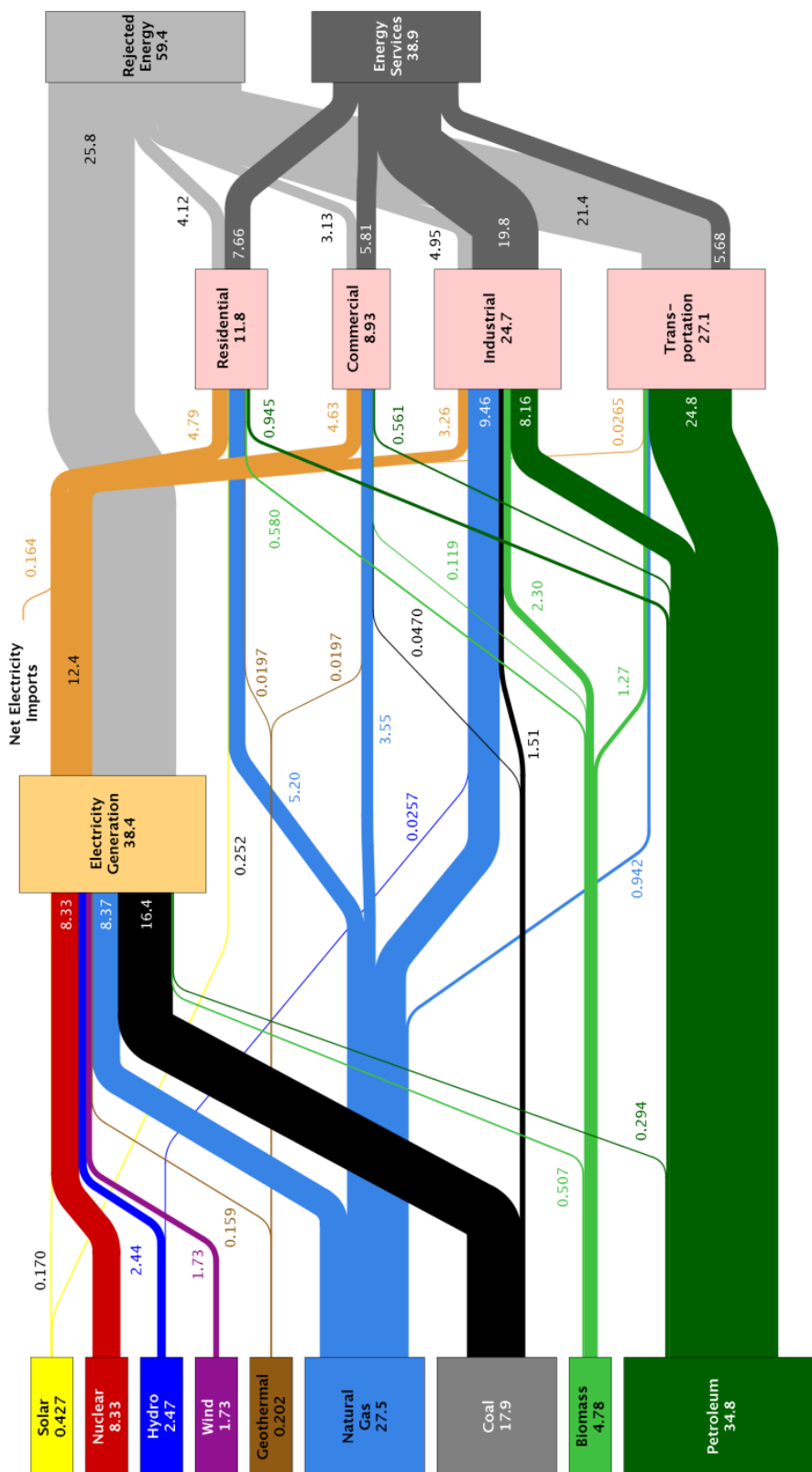


Figure 2: Sources of Greenhouse Gas Emissions (EPA, 2015)

Estimated U.S. Energy Use in 2014: ~98.3 Quads



Source: LLNL 2015. Data is based on DOE/EIA-0035(2015-03), March, 2014. If this information or a reproduction of it is used, credit must be given to the Lawrence Livermore National Laboratory and the Department of Energy, under whose auspices the work was performed. Distributed electricity represents only retail electricity sales and does not include self-generation. EIA reports consumption of renewable resources (i.e., hydro, wind, geothermal and solar) for electricity in BTU-equivalent values by assuming a typical fossil fuel plant "heat rate." The efficiency of electricity production is calculated as the total retail electricity delivered divided by the primary energy input into electricity generation. End use efficiency is estimated as 65% for the residential and commercial sectors and 80% for the industrial sector, and 21% for the transportation sector. Totals may not equal sum of components due to independent rounding. LLNL-MI-410527

Figure 3: 2014 Estimated Energy Use (DOE, 2015)

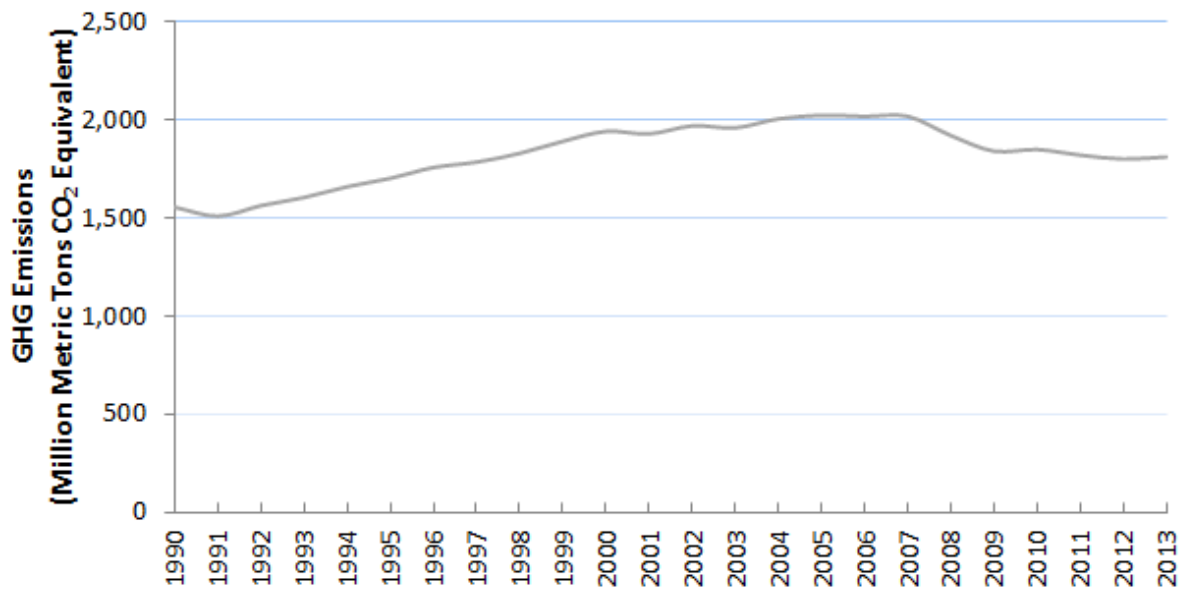


Figure 4: Greenhouse Gas Emissions from Transportation (EPA, 2015)

1.2.1 Reducing the Transportation Sector's Impact

Changes need to be made to reduce the transportation sector's impact on overall GHG emissions, both on a macro and micro-scale. The EPA recommends changes that need to be made to reduce the impact that the transportation sector has on overall GHG emissions, including: reducing the number of passenger vehicle trips, by increasing the availability of transit; making improvements to the structure of the built environment so that more places are conducive to transit and alternative forms of transportation; using lower impact fuels, both for passenger vehicles and transit vehicles; increasing the usage of electric vehicles, and, relevant to this study, using electricity from renewable sources to provide power to these electric vehicles (EPA, 2015).

1.2.2 The Need for Off-Grid Energy Production

There is a global interest in off-grid energy production. In many remote locations, power is needed, and in most cases, generators are used. However, in an effort to become less oil-dependent, renewable sources of energy production are becoming more common, even in remote locations. Solar photovoltaic (PV) arrays, small-scale wind turbines, and even microhydro-electric systems are sustainable sources of energy production that can be found in remote locations. The National Parks Service (NPS) is an example of an organization needing more sustainable off-grid energy production, due to the fact that many of the Nation's parks are located in remote locations.

1.2.3 The National Parks: Reducing the Transportation Sector's Impact at the Micro-Level

A prime example for understanding broader issues of global climate change, and actions that can be taken to reduce emissions, especially with regards to transportation, is the National Parks Service. The National Parks Service (NPS) consists of hundreds of parks, all with varying energy needs. Because the National parks have millions of visitors each year, they are major consumers of electricity, with Yellowstone National Park being the largest consumer (NPS, 2016). The NPS also has varying transportation needs that must be considered and met in a sustainable way, and because many of the National parks are in rural and secluded locations, grid-independence is crucial in helping the parks become self-sustaining, while reducing financial and environmental costs associated with the transportation of fuels, and reliance on electricity produced from the burning of fossil fuels.

Examining the transportation energy needs of the NPS, which includes large geographical areas, and has similar transportation needs of other large organizations, can help in better

understanding how to meet overall transportation energy needs in more sustainable ways. One goal of this research is to examine the transportation energy needs of the NPS and consider current changes that have been made to reduce emissions at the National parks, namely increasing park transit and encouraging electric vehicle usage. Major considerations will be given to increasing the usage of renewable sources of energy at many of the National parks, and methods will be provided regarding locating suitable locations for renewable energy production facilities to further promote sustainability.

CHAPTER 2: TRANSPORTATION IN THE NATIONAL PARKS

2.1 Overview of Transportation Energy Needs at the National Parks

The National Parks Service (NPS), like many other large organizations, is making efforts to reduce overall carbon emissions and incorporate sustainable practices into maintenance and daily functions on park property. The NPS consists of 409 parks across the Country, as shown in *Figure 5: National Parks (NPS, 2011)*, which includes State and National parks, National forests, and National historic sites, and receives approximately 292,000,000 visitors annually (NPS, 2015). There are 48 National parks within the lower 48 states, and all of these parks have a variety of energy needs, especially transportation energy needs, that require more sustainable practices to accommodate the influx of visitors to park property. The NPS, as an organization whose goal has always been to preserve and protect the Country's natural landscape, acknowledges the importance of incorporating sustainable practices in order to maintain park property and improve park visitors' experiences, all while reducing their impact on the natural environment and on overall GHG emissions.

As the number of visitors to the National parks increases, and as the need for reducing GHG emissions and reducing reliance on petroleum becomes more imminent, accommodations will need to be made to ensure that the National parks continue to provide services to visitors in a sustainable manner that is characteristic of the goals of the NPS. A goal of this research is to assess the varying transportation energy needs of the NPS, including consideration of vehicle types for park transit and park maintenance, as well as accommodating increasing electric vehicle usage by park visitors. This research will examine these various types of transportation needed at the parks, and look at current measures that are being taken to meet these growing needs, while reducing emissions and reducing reliance on petroleum.

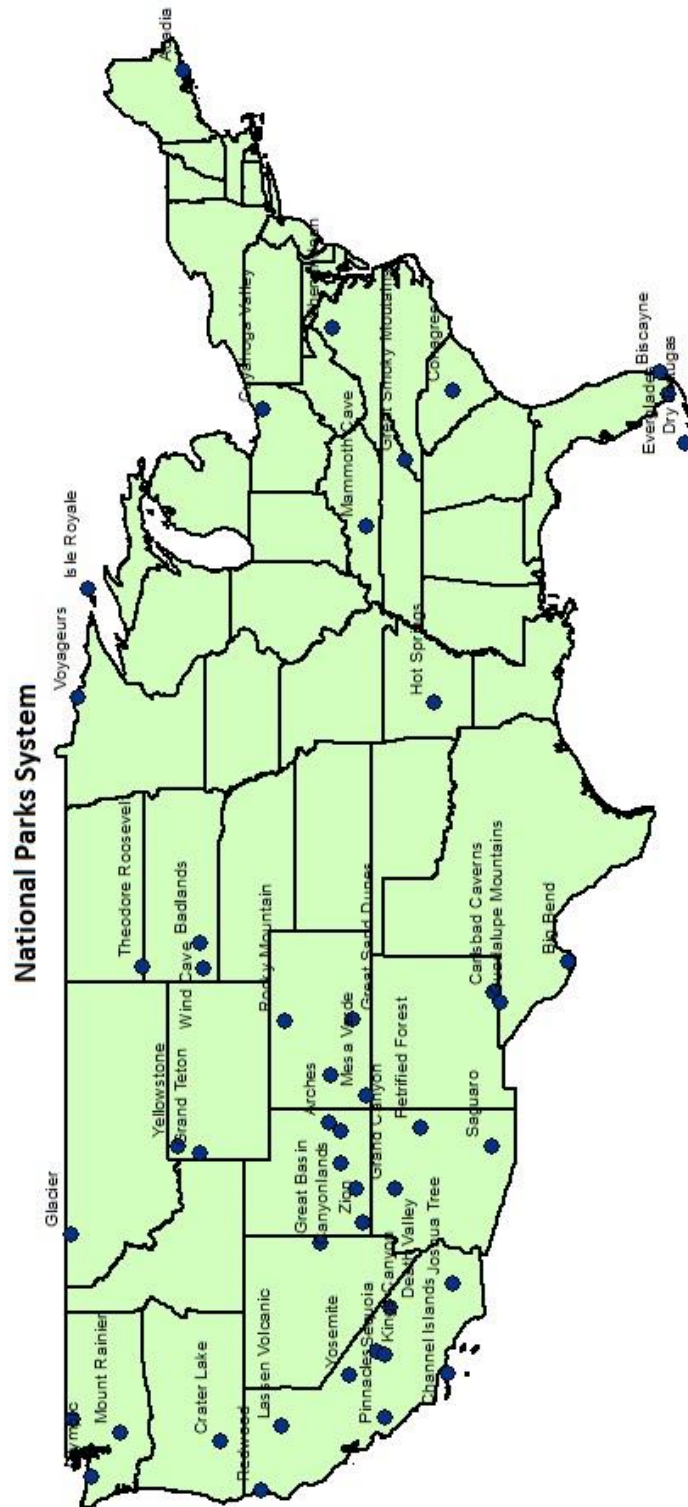


Figure 5: National Parks (NPS, 2011)

2.2 Ongoing Efforts at the National Parks

2.2.1 Green Parks Plan

The National Parks Service (NPS) has designed a strategic plan in order to carry out its commitment to protecting and preserving valuable lands and promoting sustainable practices. The goals of this plan include: meeting objectives to reduce the amount of water used at national parks; improving park recycling programs; decreasing energy usage at parks; installing renewable energy production facilities on park property; and incorporating the use of energy efficient and environmentally sound transportation (NPS, 2012). Ultimately, the NPS aims at reducing GHG emissions on park property, and this goal can be achieved by adhering to the aforementioned objectives outlined in the Green Parks Plan, with sustainable park transportation being a major component.

2.2.2 Clean Cities Program

Clean Cities, which is a public-private partnership, funded by the Department of Energy, has regional coalitions that support programs to reduce reliance on petroleum for transportation needs. According to the DOE: “Clean Cities advances the Nation's economic, environmental, and energy security by supporting local actions to reduce petroleum consumption in transportation. A national network of nearly 100 Clean Cities coalitions brings together stakeholders in the public and private sectors to deploy alternative and renewable fuels, idle-reduction measures, fuel economy improvements, and emerging transportation technologies” (DOE, 2015).

Through combined efforts with Clean Cities and the National Parks Service, transportation projects involving 29 National parks have been initiated. Mammoth Cave National Park in Kentucky received funding through Clean Cities and Green Parks to purchase propane

buses and biodiesel and ethanol fueled maintenance vehicles (Business Fleet, 2014).

Yellowstone and Grand Teton National Parks have also received grants through Clean Cities to install electric vehicle charging stations and purchase electric park maintenance and park security vehicles, as well as a hybrid electric transit bus (YTCleanCities, 2014).

Projects funded through Clean Cities aim to educate park visitors about the ways in which petroleum usage can be reduced, and help in supporting major changes in transportation at the National parks, such as installing electric vehicle charging stations for park staff and visitors, and conversion of park vehicle fleets, both for park transit and maintenance, to run on renewable energy sources. Through efforts made by NREL, the DOE, and Clean Cities, education and training is provided to NPS employees through the Green Rides Toolkit program, which is used to inform employees on ways to educate park visitors on sustainability practices. “These outreach materials help parks educate employees, partners, neighboring communities, and visitors about reducing vehicle emissions and cutting petroleum usage. The Green Rides Toolkit supports the Green Rides Objective under the Green Parks Plan, which defines a collective vision and long-term strategic plan for sustainable management of NPS operations” (DOE, 2015).

2.3 Renewable Energy Usage at National Parks

2.3.1 Small Scale

Many of the National parks currently have small-scale renewable energy production facilities on-site to provide power to visitor centers, ranger stations, and other buildings on park property. Many of these parks have installed solar photovoltaic facilities in-conjunction with battery pack power stations to store the energy generated by the solar PV arrays. A prime

example of this is Yellowstone National Park, which has incorporated the use of used Toyota battery packs from vehicles to store excess power generated by their solar facilities (Toyota, 2015).

2.3.2 Utility Scale

Due to the Southwest's climate, it is a prime location for proposed utility-scale renewable energy facilities, including solar, both solar photovoltaic and concentrated solar, and wind facilities (National Parks Conservation Association, 2012). Yosemite National Park, for example, currently has the largest, grid-connected solar facilities in the National Parks Service (National Parks Service, 2011). Sites for proposed utility-scale facilities are also in Arizona, Nevada, New Mexico, and other parts of California, in locations adjacent to National parks and National monuments. Although environmental impact analyses have been performed, there is still concern regarding the impact that the facilities will have on the adjacent park lands. "Despite the environmental reviews required for proposed projects, poorly sited projects have been approved that will harm natural and cultural resources shared between BLM [Bureau of Land Management] lands and desert National parks" (National Parks Conservation Association, 2012). Although the overall benefit of solar facilities is thought to outweigh any negative impacts on the physical environment at these sites, there is still concern for vulnerable species and habitats on the proposed sites and the adjacent park lands. "The resulting habitat fragmentation and destruction, impaired visual resources, and lost wildlife connectivity will affect not only BLM lands but adjacent national park lands as well. In short, while there are great benefits to harnessing sunlight for electricity generation, these benefits come at a significant cost to desert resources" (National Parks Conservation Association, 2012).

2.4 Electric Vehicle Charging Stations at National Parks

As a goal of both the Green Parks Plan and the Clean Cities Program, many of the National parks have installed electric vehicle charging stations on park property, while other parks within the NPS are planning on installing charging stations in the near future. Installation of these charging stations in parks allows for the conversion of current park vehicle fleets to fleets of electric vehicles to be used for park management and park transit. Installation of charging stations also encourages people who own electric vehicles to visit parks within the National Parks Service, while reducing emissions during long-distance trips to parks that are located in more secluded areas.

Currently, a major concern regarding electric vehicle use is the lack of charging stations in most public areas. An electric vehicle owner may chose not to take a long-distance trip to a National park if they are unsure about the location or availability of charging stations at, or near, their destination. By installing charging stations at National parks across the Country, more people may be able to enjoy the park and park facilities without worrying about the availability of electric vehicle charging stations nearby. Park visitors can charge their vehicle while taking hikes and other daytime activities. In parks that contain lodging, park visitors can simply charge their vehicle at night, which Zion National Park recommends (Zion National Park, 2016).

Currently, 21 of the National parks have electric park vehicles in-use, either for park transit or park maintenance, with charging stations located on park property. Several of these parks also have electric vehicle charging stations available for park visitors. 21 additional parks within the National Park Service are also being considered for installation of electric vehicle charging stations on park property (American Progress, 2015) as shown in *Figure 6: National Parks with EVs and EV Stations (American Progress, 2015)* and *Table 1: Proposed EV Station*

Sites at National Parks (American Progress, 2015). According to the Department of Energy (2015), the National parks of: Acadia, Catoclin, Glacier, Grand Canyon, Great Smoky Mountains, Petroglyph, Rocky Mountain, Shenandoah, Sleeping Bear Dunes, Yellowstone, and Zion have converted some of their fleets of park shuttles or maintenance vehicles to hybrid or all-electric vehicles (DOE, 2015), and Gateway National Recreation Area, Cumberland Islands National Seashore, and Lyndon B. Johnson National Historic Park currently have electric trams or buses in-use (NPS, 2003). All of these parks, excluding Great Smoky Mountains and Zion National Park, rely solely on electricity sourced from the grid to provide power to their electric vehicle charging stations for both park vehicles and visitors' personal vehicles. However, Great Smoky Mountains and Zion National Park have recently installed solar PV arrays located on park property to provide power to their electric vehicle charging stations, furthering their efforts to reduce overall emissions (Auto Evolution, 2015).



Figure 6: National Parks with EVs and EV Stations (American Progress, 2015)

Table 1: Proposed EV Station Sites at National Parks (American Progress, 2015)

	Proposed Sites for Electric Vehicle Charging Stations
1	Arches National Park
2	Bryce Canyon National Park
3	Blue Ridge Parkway
4	Cape Cod National Seashore
5	Cape Hatteras National Seashore
6	Chesapeake and Ohio Canal National Historical Park
7	Cuyahoga Valley National Park
8	Everglades National Park
9	Gateway National Recreation Area
10	Georgia Washington Memorial Parkway
11	Glacier National Park
12	Grand Canyon National Park
13	Gulf Islands National Seashore
14	Hawaii Volcanoes National Park
15	Hot Springs National Park
16	Lake Mead National Recreation Area
17	Mount Rushmore National Memorial
18	Natchez Trace Parkway
19	Olympic National Park
20	Redwood National Park
21	Yosemite National Park

2.5 Electric Buses

Many of the National parks have hybrid electric or fully electric park transit shuttles or buses, or electric park maintenance or security vehicles. According to the literature, this is a growing trend in the NPS, and will likely continue to grow, as fully electric vehicles are a means by which the National parks' goal of reducing emissions on park property can be met. Although electric park shuttles and buses and other park vehicles are becoming more commonplace within the National parks, the capital costs for purchasing large, fully electric buses, and installing the necessary charging facilities on-site, currently prevents the National parks from being able to convert all of their existing fleets. However, thanks to programs like Clean Cities, electric

vehicles have been purchased for many of the National parks (Navigant, 2014). Many other public entities including several cities, including Seneca, South Carolina, and Chattanooga, Tennessee, and even the Kings Canyon Unified School District in California's San Joaquin Valley, have also converted their bus fleets to all electric, while many other cities and municipal transportation agencies have converted some of their fleets to all electric and hybrid.

Companies such as BYD, Proterra, and Trans Tech design and build fully electric buses, with BYD recently aiming at being the manufacturer for the NPS (Navigant, 2014). Fully electric buses made by these manufacturers boast zero emissions, approximately 21 miles per gallon equivalent, at approximately \$0.20 per mile, (using approximately 1.92 kilowatt hours per mile), compared with traditional diesel powered buses with approximately 3.86 miles per gallon at \$0.84 per mile (BYD, 2015 and Proterra, 2015). Proterra also claims that electric buses save the owner \$700,000 in operations and maintenance costs (based on the expected 12-year life of most buses), compared to operation and maintenance costs for typical diesel buses (MacKechie, 2015). Fully-electric bus manufacturers such as BYD, Proterra, and Trans Tech also offer models with regenerative braking systems, which return power back to the battery during braking, allowing the bus to travel farther distances without stopping to be charged.

2.6 Transit in National Parks

Although the National parks were originally designed to accommodate personal vehicles, now that the National parks attract millions of visitors each year, parks are experiencing many negative effects due to the increase in vehicular traffic on park property. Many parks experience congestion along park roads, which can negatively impact visitors' experiences, and more importantly, the emissions from visitors' personal vehicles are detrimental to the air quality in and around the parks.

It is necessary for the National parks to provide transit systems in order to reduce the negative effects brought about by the increase in personal vehicle ridership on park property. “ATS [Alternative Transportation Systems] can reduce the potential environmental and experiential impacts of conventional automobile-based transportation in parks and related areas” (Anderson et al, 2015, p. 127). “[A] reduction in vehicle noise and air pollutants [through the use of transit] improves the quality of visitor experience. Most transit system goals aim at reducing traffic and parking congestion, improving safety for visitors, and mitigating environmental impacts of increasing visitation (Dunning, 2005, pp. 131-132). In a recent study conducted by Manning et al (2013), it was found that the use of the shuttle bus system at Acadia National Park and Zion National Park helped in significantly reducing emissions and noise pollution (Manning et al, 2013).

In the many National parks that offer transit services to park visitors, these services are often available free of charge, and provide park visitors with a more relaxing and enjoyable, park experience. Park transit systems provide safe and reliable transportation for park visitors in a manner that is better for the environment in several ways: park transit reduces the amount of vehicle emissions inside the park by reducing the number of vehicles on the road; it protects wildlife and natural habitats by preventing park visitors from parking alongside park roads when parking space is limited; it reduces noise and congestion, and aims at providing park visitors with an overall better park experience by reducing stress, and in some situations, even enhancing park visitors’ experiences by providing additional information through guided tours and informative sessions while using transit.

Many of the Nation’s parks that currently have a transit system rely on the use of buses or shuttles, and most of these are powered by fuels other than traditional diesel in an effort to be

more environmentally-conscious. Many of the National park transit systems use propane-powered buses (NPS, 2014). Although propane is a cleaner-burning fuel alternative to traditional diesel, fully-electric buses and shuttles are a better option for reducing emissions on park property.

2.6.1 Features of Park Transit

2.6.1.1 Transit Funding

For the past several years, funding for transit projects at National parks could be obtained through the Congestion Mitigation and Air Quality Improvement (CMAQ) program, as authorized by MAP-21 (Moving Ahead for Progress in the 21st Century) (Volpe National Transportation Systems Center, 2014). Prior to CMAQ, the Paul S. Sarbanes Transit in Parks program, which was authorized under SAFETEA-LU (Safe, Accountable, Flexible, Efficient Transportation Equity Act: A Legacy for Users), “was established to address the challenge of increasing vehicle congestion in and around our National parks and other federal lands. To address these concerns, this program provides funding for alternative transportation systems, such as shuttle buses, rail connections and even bicycle trails. The program seeks to conserve natural, historical, and cultural resources; reduce congestion and pollution; improve visitor mobility and accessibility; enhance visitor experience; and ensure access to all, including persons with disabilities” (USDOT, 2014). The Paul S. Sarbanes Transit in Parks program provided funding from 2006 until it was repealed by Congress under MAP-21 in 2013.

CMAQ provides funding for up to 80 percent of project costs, with the need for partner funding sources to cover the remaining costs (Volpe National Transportation Systems Center, 2014). Acadia National Park in Maine, and Rocky Mountain National Park in Colorado, both received CMAQ funding through their MPOs (Metropolitan Planning Organizations) or State

DOTs to improve existing park transit and transportation services in order to mitigate congestion and improve air quality at these parks and in the surrounding areas. According to Volpe National Transportation Systems Center (2014), there are many other parks within NPS, both with and without existing park transit services, that are eligible to obtain CMAQ funding “based on population and pollution levels in ozone (O₃), particulate matter (PM₁₀ and PM_{2.5}), and carbon monoxide (CO) nonattainment or maintenance areas designated by the EPA” (Volpe National Transportation Systems Center, 2014).

2.6.1.2 Parking Problems on Park Property

Parking is limited on park property, which poses a problem for visitors, and may prevent parks from increasing park visitation in certain locations where parking is limited. More importantly, visitors attempting to park in undesignated areas on park property can also endanger park staff, other visitors, and park wildlife and habitats. “Lack of parking often results in visitors parking along the road or in grassy areas, creating a safety concern for park officials and damage to potentially sensitive habitats” (Sims et al, 2005, p. 26). Providing park transit that allows visitors to park outside of park property and ride a bus or shuttle in and out of a park can help to remedy this problem.

2.6.1.3 Park Visitors’ Perception of Park Transit

It is important that National parks provide transit that visitors will want to use, thus, park visitors’ perception of the transit services provided at National parks has been explored in many studies. Researchers have surveyed visitors of National parks in an effort to gauge visitors’ reactions to different park transit options and features regarding the transit, such as: type of transit vehicle; scheduling frequency and routing; whether visitors perceived the park transit to benefit the park overall; and whether or not the park transit was perceived to improve visitors’

experience at the park. In one particular study, visitors were surveyed at Acadia National Park where it was determined that vehicle crowding, scenery, travel freedom, and travel convenience were the most significant factors to influence visitors' experiences (Hallo and Manning, 2001). The results from this study were not atypical. In survey research conducted on visitors' perceptions of park transit at Yosemite National Park and Rocky Mountain National Park, ease of use of the transit system, reduction in stress regarding finding parking and navigating park roads, lack of perceived congestion and crowding, and the perception that visitors maintain freedom to explore park property were all salient factors influencing park transit ridership (Taff et al, 2013, p. 45). In research conducted on different demographic groups of visitors to Rocky Mountain National Park, it was found that younger groups (age 40 and younger) were more likely to use park transit in areas of the park where congestion is common (Pettebone et al, 2011). Similar research was also conducted at Virginia's Colonial National Historical Park, where it was found that the factors influencing park shuttle ridership included: whether or not a fee was charged for driving a personal vehicle on park property; whether or not there was a park shuttle fare; the amount of time spent in and out of the vehicle; the shuttle headway; and whether or not live interpretation was provided on the shuttle (Shiftan et al, 3006, p. 58). The information obtained from this study, and others like it, can be beneficial in transit planning at all of the National parks because it provides insight into factors that may influence transit ridership.

Most of the National parks that provide transit do not make park transit mandatory for all visitors. In parks that have mandatory park transit ridership during the peak season, such as Zion National Park in Utah, survey research has been conducted to determine whether visitors perceived the mandatory park transit to improve their overall experience at the park or whether they felt that making park transit ridership mandatory hindered their ability to explore the park

and prevented them from having a more enjoyable time during their visit. According to the results from survey: “the shuttle will be perceived as successful and a preferred alternative by visitors so long as wait times are minimal (no greater than 15 min) and the main attractions in the canyon remain accessible from shuttle stops, enhancing visitor freedom” (Mace et al, 2013, p. 1282).

Survey research conducted on the Full Circle Trolley, which is a fully electric shuttle that provides a transit loop around the town of Woodstock, Vermont surrounding the Marsh-Billings-Rockefeller National Park found that there are several factors that have been found to influence transit ridership. “Alternative transportation systems (ATS) should have frequent scheduling (or headways), should include stops at destinations important to riders, should relieve traveler stress (e.g., reduce concern over lack of parking), should educate riders on the environmental benefits of ATS, and should include a strong element of rider orientation, education, and interpretation about the park and surrounding area” (Anderson et al, 2015, p. 127).

By encouraging transit ridership at the National parks, it is also hoped that if visitors perceive park transit to be positive, they may also be inclined to think more positively about other forms of transit in other locations besides the National parks. “ATS can reduce many of the environmental impacts of private automobiles while maintaining and even enhancing the quality of the visitor experience. And many visitors will take these positive experiences with more sustainable transportation back home with them, more prepared to support sustainability in all forms, and this will be good for National parks and the greater world” (Manning et al, 2014, p. 13).

2.6.1.4 Park Transit's Influence on Park Visitation

Studies have been conducted to determine the effects of transit services at National parks on levels of park visitation. Park rules regarding park transit vary by park, and therefore affect visitor ridership. “Factors such as perception of transit service quality, perception of private vehicle congestion, and private vehicle restrictions will affect trip-making for both visitors and local residents” (Dunning, p. 131, 2005). It has been noted that transit ridership at several National parks has increased in recent years, and has been observed to be a result of park visitors and residents of the nearby area’s familiarity with the transit services at parks. “Increasing ridership on these systems suggests that communities and visitors must grow accustomed over a few years to the systems before transit activity becomes a regular part of local transportation. Continuing efforts to improve and disseminate information about the systems should also affect patronage” (Dunning, p. 132, 2005).

2.6.1.5 Park Transit's Influence on Surrounding Communities

In some areas surrounding National parks, nearby residents will rely on park transit for daily commutes and leisurely trips. Although many of these residents may be seasonal employees of the park, residents who reside year-round in communities adjacent to park properties may also rely on park transit. “Although the shuttles were intended for tourists, local residents use the buses for all types of trips, including commute trips. This travel behavior should be encouraged because it helps reach identified goals of transit: it reduces traffic congestion and its associated safety hazards, frees parking spaces that would otherwise remain full all day, and reduces noise pollution and local emissions that are harmful to air quality” (Dunning, p. 133, 2005). However, in some locations, such as with Marsh-Billings-Rockefeller National Park in Woodstock, Vermont, survey research suggests that there needs to be more of a focus on

improving park transit in terms of scheduling and routing of park transit to accommodate residents living near National parks, including seniors and residents with disabilities. “For residents, it was noted that the trolley could also serve as a fun outing; however, the trolley’s route (limited to within town) and schedule (operating within working hours) were identified as limitations for residents’ transportation needs” (Anderson et al, 2015, p. 119).

Transit services inside National parks encourages visitors to remain in the park for the day, rather than making trips in and out of the park using personal vehicles, which reduces emissions and congestion in and around parks. However, because this prevents visitors from making trips in and out of the park during a visit, this can reduce the number of trips made by visitors to businesses outside of the parks. Studies have found that there are possible negative effects on the local economies of gateway communities: communities outside of National parks that rely on park visitors as their source of income. “Local businesses have observed that people riding transit prefer to spend the whole day in the park, rather than exiting at lunchtime and reentering” (Dunning, p. 131, 2005). However, ATS can help to promote tourism in surrounding communities around National parks through scheduling and routing decisions that incorporate local businesses into routes and stops. “Many communities near parks benefit from the jobs and economic opportunities generated by park tourism. By taking visitors to local restaurants, hotels, campgrounds, and shops, ATS can promote tourism. ATS can also generate jobs as staff is hired to operate and maintain new systems” (NPS, 2003).

CHAPTER 3: SHORT-TERM SOLUTIONS AT THE NATIONAL PARKS AND OTHER OFF-GRID LOCATIONS: LOWER IMPACT FUELS

As is evident in the literature, park transit services can help the National parks reach their goal of reducing emissions on park property, simply due to the fact that it reduces the number of personal vehicles in-use on park property. However, incorporating the use of buses and shuttles fueled by traditional fuels, such as diesel, is not the best solution. The National parks recognizes this, as is evident in the use of electric buses, shuttles, and maintenance vehicles at many of the parks, and many of the vehicles that are not fully-electric are fueled by lower impact fuels, mainly propane or compressed natural gas (NPS, 2015). Although these are short-term solutions, using lower impact, renewable sources to provide power to park vehicles is a better option than petroleum based fuels, as shown in *Table 2: Emissions for Different Bus Types (results from GREET software) (CCW, 2015)*.

3.1 Green Bus Fleets

The NPS, along with several cities, counties, and school districts across the Country with existing bus fleets have converted their fleets to accommodate the usage of lower impact fuels, or have invested in new technology. Whereas most bus fleets are powered by diesel, many fleets now consist of buses powered by propane, liquefied natural gas (LNG), compressed natural gas (CNG), biodiesel, hydrogen, and fully-electric and hybrid vehicles. These entities that have chosen to make these changes to their bus fleets have done so in efforts to reduce emissions, improve the air quality on buses, and cut down on operations and maintenance costs, especially in school districts (USA Today, 2013). While most buses are powered by diesel fuel; biodiesel, compressed natural gas, and propane are becoming popular alternatives to diesel (USA Today, 2013). School districts and other public and private entities have been able to make these

changes to their existing fleets through federal funding and grants, such as the LoNo (low or no emission vehicle deployment) program (FTA, 2014). Other programs such as the Alternative Fuels Excise Tax Credit provided alternative fuel users with tax credits, such as providing propane users with a \$0.50 per gallon tax credit (DOE, 2014).

Table 2: Emissions for Different Bus Types (results from GREET software) (CCW, 2015)

Bus Type	On road petroleum use (in bbl.)	GHG emission (Short ton)
Diesel	380	209
Diesel Hybrid	300	165
CNG	0	198
Electric	0	157
Electric with Renewable energy	0	5

3.2 Propane

Propane motor fuel, which consists of liquefied petroleum gas, is a cleaner-burning fuel alternative to diesel and gasoline because it has a lower carbon content. Liquefied petroleum gas (LPG), occurs during the processing of natural gas. Overall, it has a relatively lower impact on the environment and a reduction in vehicle emissions compared with traditional fuels such as diesel or gasoline. However, it still produces particulate matter, sulfur dioxide, nitrogen oxide, nitrous oxide, carbon monoxide, and methane.

Most of the propane consumed in the U.S. is produced locally and distributed using pipeline infrastructure. Although propane costs less per gallon compared with diesel or gasoline, an added cost can be in transporting it to areas that are not near infrastructure, although private

infrastructure can be established (DOE, 2015). Mammoth Cave National Park in Kentucky, for example, has an on-site propane fueling station on park property (Business Fleet, 2014).

Propane buses are the most widely-used type of lower impact fueled vehicles within the NPS, and this is mainly due to the fact that capital costs are lower versus other vehicle options (Navigant, 2014). Propane-powered buses are suitable for shorter routes, which makes them appropriate for park transit. Propane-powered buses typically get 10 percent fewer miles per gallon than traditional diesel-powered buses because of propane's lower BTU rating, and they cost about \$3,000-4,000 more than traditional diesel buses (USA Today, 2013). However, the cost per gallon of propane is significantly less than the cost per gallon of diesel, and propane has a higher octane rating than gasoline. Propane also has the potential to extend the life of the engine. "Propane's high octane combined with its low-carbon and low oil-contamination characteristics have resulted in improved engine life compared to conventional gasoline engines. Because the fuel's mixture of propane and air is completely gaseous, cold start problems associated with liquid fuel can be reduced" (DOE, 2015). Overall, there is a substantial savings in the amount of emissions and in operations and maintenance costs for propane-powered buses versus diesel-powered buses (USA Today, 2013). "Burning propane reduces greenhouse gas emissions by 22 percent compared to gasoline-powered buses or 6 percent compared to diesel" (New York Times, 2015).

3.3 Compressed Natural Gas

Compressed natural gas (CNG) is natural gas that is kept under pressure, usually around 3,100 pounds per square inch (psi) for vehicle fuel usage (California.gov, 2015). CNG dissipates quickly and is flammable when it mixes with air, but only when the mixture contains 5-15 percent natural gas (California.gov, 2015). Currently, around 99 percent of natural gas consumed

in the United States is sourced domestically. CNG is a cleaner-burning fuel alternative to gasoline and diesel, with an 80 percent reduction in vehicle emissions compared to traditional gasoline (California.gov, 2015). CNG costs about 15-40 cents less per gallon than gasoline, and like propane, CNG has a higher octane rating, leading to better engine performance. However, vehicles that run on CNG typically cost about \$3,500 more than gasoline-powered vehicles due to the higher cost of CNG fuel cylinders (All About CNG Vehicles, 2016). In the 1990s, many parks and historic sites within the NPS in and around the Washington, D.C. area began using CNG refuse haulers (NREL, 1998). Also, since 1998, Grand Canyon National Park has been using six CNG maintenance vehicles and 29 CNG shuttles (NPS, 2010). The CNG shuttles were purchased to replace the diesel and liquefied natural gas (LNG) shuttles that had previously been used at the park (NPS, 2008).

3.4 Liquefied Natural Gas

Liquefied natural gas (LNG) is produced through liquefaction by cooling natural gas to minus 259 degrees Fahrenheit, which cools the natural gas, consisting mainly of methane, to below its boiling point (California.gov, 2015). Like CNG, LNG is only flammable when mixed with air and when this mixture contains 5-15 percent LNG, and it is only explosive in enclosed spaces containing this mixture (California.gov, 2015). When used as a vehicle fuel, it is relatively less expensive and cleaner-burning than diesel, and it has a higher storage density than CNG (California.gov, 2015). Most of the world's LNG sources are in the countries of: Algeria, Australia, Brunei, Indonesia, Libya, Malaysia, Nigeria, Oman, Qatar, and Trinidad and Tobago (California Energy Commission, 2015). LNG is transported to the United States by large ships that can maintain the required low handling temperature of LNG. Currently, LNG terminals in the U.S. are located in Georgia, Louisiana, Maryland, Massachusetts, Mississippi, Texas, and

Puerto Rico. However, the NPS has opposed the installation of an LNG terminal and pipeline extension from Warrenton, Oregon due to concerns regarding damage to natural habitats in the surrounding area (Oregonian, 2012).

Although LNG is a lower impact fuel, LNG vehicles are not currently in-use at any of the National Parks. Grand Canyon National Park used LNG shuttle buses for years to transport visitors along the south rim of the Canyon, but these shuttles, along with diesel shuttles, were recently phased out and replaced with CNG shuttles (NPS, 2008). LNG has a short shelf life, requires extreme conditions to keep cool, and in the case of the location of many of the National parks, requires long distance trips to reach its destination where it will be used. It is also more suitable for long-haul vehicles, and vehicles that require constant fueling (Westport, 2013). Therefore, LNG typically isn't a good choice for transit shuttles and buses at the National parks.

3.5 Biofuels

3.5.1 Ethanol

Ethanol is ethyl alcohol, and is produced mainly by the fermentation and distillation of corn, sugar cane, and feedstock. Brazil is the largest producer of ethanol, which is produced using sugar cane, but the Midwestern states of Iowa, Illinois, Minnesota, and Nebraska are the largest producers of ethanol for the U.S. due to the large production of corn in these states. The costs of ethanol production are higher than production of petroleum fuels, but the government has tried to offset the costs of production of ethanol to increase competition with production of petroleum fuels (California.gov, 2015).

Ethanol is combined with gasoline to produce Ethanol 85 vehicle fuel, which is a mixture consisting of 85 percent ethanol and 15 percent gasoline, and can be used in vehicles that are

designed to run on higher concentrations of ethanol, which are called flexible fuel vehicles (FFVs). Ethanol 85 has a lower energy content than traditional gasoline, but it has a higher octane rating, resulting in improved engine performance (California.gov, 2015). Most vehicles can use fuel that is a mixture containing 10 percent or less ethanol with gasoline, which results in slightly lower vehicle emissions compared with gasoline only. The reduction in emissions is considered to be significant in vehicles that can use fuel like Ethanol 85, with higher concentrations of ethanol, because of the net reduction in carbon emissions, which considers the occurrence of an offset of emissions due to the production of crops (DOE, 2015).

Since the late 1990s, Yellowstone National Park has used E10 fuel to power its snowmobiles on park property (NPS, 2003). Mammoth Cave National Park also has E10 maintenance vehicles in-use (Business Fleet, 2014). Using FFVs or vehicles that are fueled by E10 and other mixtures of gasoline and ethanol are better choices for the National parks than traditional diesel fueled vehicles.

3.5.2 Biodiesel

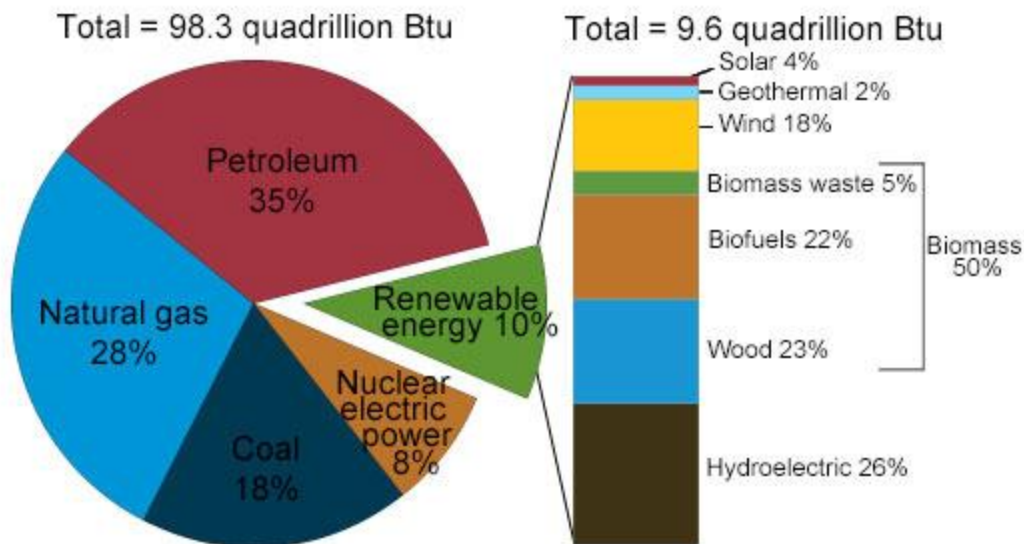
Biodiesel is produced using soybeans, vegetables, animal fats, and used restaurant grease, and it is biodegradable and is a cleaner-burning fuel than traditional petroleum fuels. Biodiesel can be used in most diesel engines, but is not recommended to be used in vehicles running in colder climates, which many of the National parks are located in, because it can crystallize, leading to engine failure (DOE, 2015). B100, also called neat biodiesel, is pure biodiesel, but biodiesel can also be mixed with petroleum diesel in different concentrations to create different fuels, such as B20, B2, and B5, which are commonly used, and are more suitable to be used in colder climates where biodiesel with higher concentrations is not recommended. The use of

biodiesel in diesel engines also results in significantly lower emissions, and the resulting emissions are 45-90 percent lower in toxins compared to traditional diesel. Biodiesel vehicles, including some watercraft, are currently being used at Channel Islands National Park and Yosemite National Park (California.gov, 2015).

3.6 Long-Term Solutions for the National Parks and Other Off-Grid Locations: Power from Renewable Sources

Due to the fact that fully-electric vehicles produce the least amount of emissions compared with traditional fuels and lower impact fuels, the National parks can benefit the most from, and be able to reach their goal of lowering overall emissions on park property, by incorporating electric park vehicles and installing electric vehicle charging stations on park property. Most of the National parks that currently have electric park vehicles and electric vehicle charging stations located on park property obtain power from the grid (excluding Zion and Smoky Mountains National Parks which have solar PV arrays located on park property). Many parks are located in remote areas, where there are additional costs associated with power provisions and transport of fuels. Also, the majority of power produced in the U.S. is produced from nonrenewable sources, as shown in *Figure 7: 2014: U.S. Energy Consumption by Source (EIA, 2015)*, which is thought to ultimately negate efforts at reducing emissions. Therefore, in order for the National parks to meet their goal of reducing overall emissions (not only on park property), they need long-term energy solutions; therefore, renewable energy sources should be considered.

U.S. energy consumption by energy source, 2014



Note: Sum of components may not equal 100% as a result of independent rounding.

Source: U.S. Energy Information Administration, *Monthly Energy Review*, Table 1.3 and 10.1 (March 2015), preliminary data



Figure 7: 2014: U.S. Energy Consumption by Source (EIA, 2015)

3.6.1 Cogeneration

Cogeneration, or combined heat and power (CHP), is the generation of electricity by the burning of different types of biogas or natural gas fuel, and the usage of the waste heat from the electricity generation to provide heat for hot water, or cold water for cooling purposes.

Cogeneration facilities are typically useful in areas that require constant power or consistent access to hot or cold water, such as hospitals, data centers, industrial facilities, and large residential facilities. Cogeneration facilities can produce electricity and hot water efficiently and cost-effectively, but capital costs for the facilities and operation and maintenance costs are extremely high (around \$45 million for construction costs only) (C2ES, 2014). Therefore, cogeneration facilities on park property would not be feasible for several reasons: the amount of

available land to build the facilities on park property will be limited; the capital costs of building the facilities is likely to be too high; and there isn't a need to provide constant heat or cooling to a large number of buildings on most park properties.

3.6.2 Bio-waste

Bio-waste is a product of farming, animal husbandry, and paper and wood products' processing and manufacturing. Bio-waste can take the form of tree limbs, crops, animal waste, paper and pulp, and grass, among other things. Bio-waste can be harvested and then used in special combustion furnaces containing generators to produce energy. Using bio-waste on-site to produce energy results in lower emissions, and the product of the burning process results in ash that can then be used as fertilizer (Natures Furnace, 2014). Energy production facilities using bio-waste are suitable for farms and large scale agriculture because capital costs are relatively low, and the bio-waste is on-site, does not require transportation from off-site locations, and is typically in constant supply. Therefore, such facilities would likely not be a viable option for many park locations because space for the facilities may not be available, and a sufficient supply of bio-waste would not be generated on-site and would need to be transported to the location, thus increasing costs.

3.7 Wind and Solar Technologies

For the purposes of this study, solar and wind technologies will be considered appropriate for providing power to meet the long-term, transportation energy needs of off-grid locations, mainly the National parks. Wind and solar technologies are typically more practical sources of energy production.

3.7.1 Wind Technologies

Wind power is the generation of electricity through the use of wind turbines. Wind turbines turn due to naturally-occurring moving air. There are two types of wind turbines: vertical axis turbines, and horizontal axis turbines; the second type being the most common. Wind moves the blades of a turbine, which is connected to a shaft that is connected to a generator, which produces electricity. Small scale wind turbines can be found in rural locations and can be used to provide power to homes and agricultural equipment, while large, utility-scale wind turbines (wind farms) can be found in many different locations and provide power to many homes and businesses, as shown in *Figure 8: Wind Turbine Diagram (Clean Technica, 2014)*.

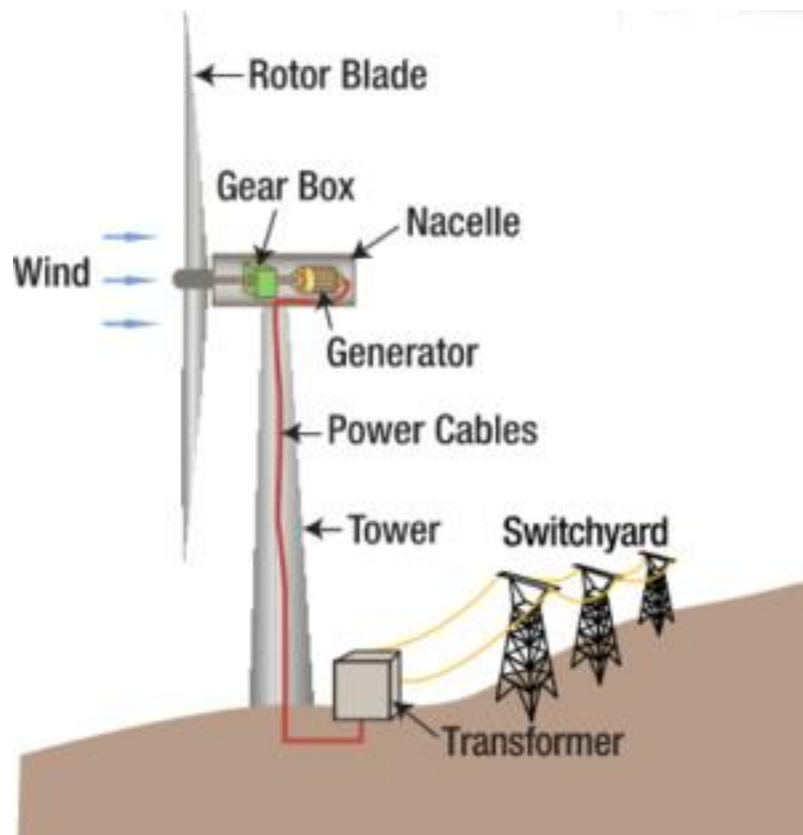


Figure 8: Wind Turbine Diagram (Clean Technica, 2014)

Although wind power is a renewable and a “free” source of energy, the capital costs and operation and maintenance costs of wind energy production facilities are high. Wind turbines are also very large and require large areas of land dedicated to them. Typical wind turbines have a blade span of 116 feet and a unit height of 328 feet (National Wind Watch, 2014). Even small scale wind turbines are expensive, and they typically only produce 100-300 kwh of energy per month (CleanTechnica, 2014), which would not be enough to provide power to fleets of electric vehicles on National park property. There are environmental concerns regarding the impact of wind farms on habitats, and the impact on bird and bat populations. Also, there are concerns regarding the aesthetics of wind farms and the impact of noise pollution (BLM, 2014). Currently, Channel Islands National Park in California has three wind turbines on Navy-owned San Clemente Island. These turbines were installed by the Department of Defense, DOE, and EPA, and have been in operation since 1998 (DOE, 2015).

3.7.2 Solar Technologies

3.7.2.1 Solar PV arrays

Solar photovoltaic (PV) devices generate energy through the use of semiconductors contained in panels, as shown in *Figure 9: Solar PV Diagram (GreenSunRising, 2015)*. Solar energy frees electrons within the material in the panels, and these electrons travel through a circuit: powering devices (vehicles, calculators, road signs, appliances in homes, etc.) or sending power to the grid. The most common type of solar PV uses crystalline silicon solar cells. This type of solar PV is very efficient and reliable, installation costs are low, they are capable of lasting a very long time (sometimes decades), and they can withstand extreme heat. Another type of solar PV uses thin film solar cells, which are less efficient, but are also less expensive to

manufacture (Dirjish, 2012). Currently, the Great Smoky Mountains National Park in Tennessee and North Carolina has both fleets of electric vehicles and electric vehicle charging stations available to visitors, and it relies on solar PV to provide power to its charging stations (National Parks Service, 2015). Yosemite, Canyonlands, Death Valley, and Zion National Parks also have solar PV facilities on park property.

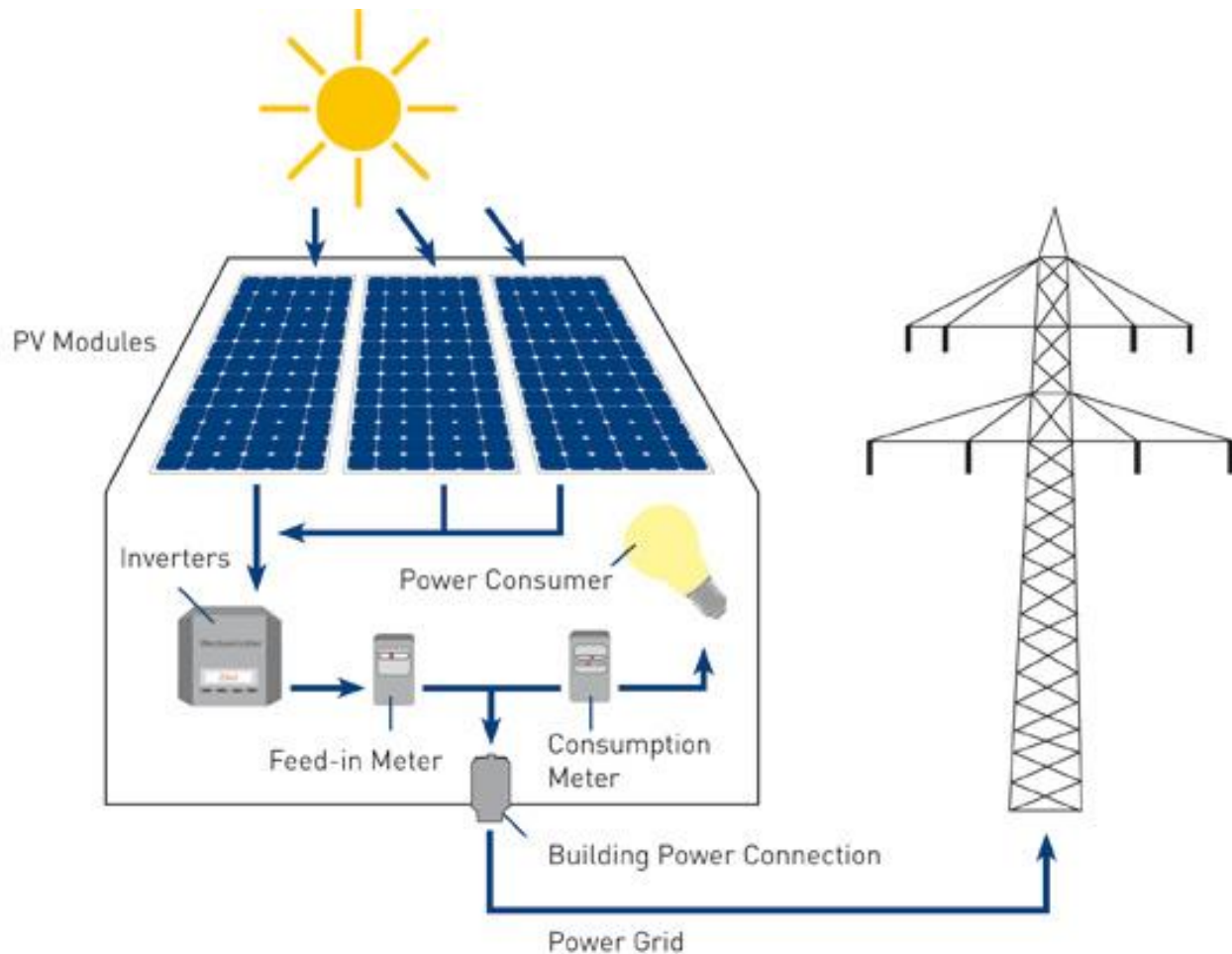


Figure 9: Solar PV Diagram (GreenSunRising, 2015)

3.7.2.2 Concentrated Solar Power

There are several types and configurations of concentrated solar power, as shown in *Figure 10: Diagram of Concentrated Solar Configurations (Solar Tower UK, 2016)* and *Figure 11: Concentrated Solar Configurations (Solar Tower UK, 2016)*. All of the configurations contain series of mirrors arranged in such a way that the sunlight that is reflected off of them is concentrated, and this concentrated energy is collected and used to heat water to create steam to generate energy by moving a turbine. One type is a parabolic trough, where curved mirrors are arranged, and focus the sun's rays onto a receiver, which contains oil that is heated to 750 degrees Fahrenheit, that is used to heat water to create steam. Another type is a compact linear Fresnel reflector, which contains rows of mirrors that reflect sunlight to receivers, which contain tubes of water, which boil and create steam. A third type is a power tower, which is similar to a parabolic trough in that the mirrors reflect sunlight to a receiver which contains oil that is heated to 1,000 degrees Fahrenheit. The difference between a power tower and a parabolic trough is in the mirror configuration: a power tower contains rows of mirrors which are programmed to track the sun. Lastly, the fourth type is a dish engine, which consists of large dishes of parabolic mirrors that concentrate sunlight on a receiver at the center of the dish. This receiver contains hydrogen, which is heated to 1,200 degrees Fahrenheit, and this heated hydrogen powers an engine (SEIA, 2015).

Concentrated solar power plants are very expensive to build (approximately \$600 million in capital costs, depending on the type). Concentrated solar power plants currently exist in California, Arizona, Nevada, and Colorado. These areas have high direct normal solar radiation, which is required for concentrated solar power plants to function, and these areas also have access to water resources, which is needed for steam production. Besides access to naturally-

occurring resources, these locations also have access to high voltage transmissions lines that is adjacent to large parcels of land suitable for accommodating rows of mirrors (SEIA, 2015).

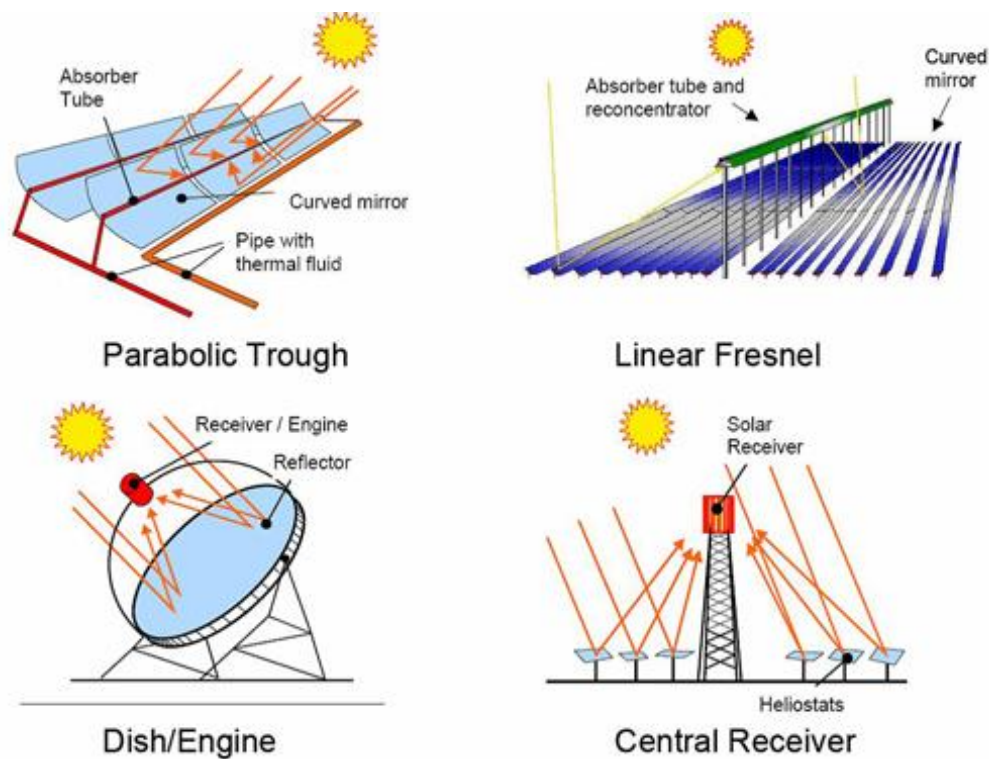


Figure 10: Diagram of Concentrated Solar Configurations (Solar Tower UK, 2016)

parabolic trough (PSA)



solar tower (SNL)



linear Fresnel (SPG/MAN)



parabolic dish (SBP)

Figure 11: Concentrated Solar Configurations (Solar Tower UK, 2016)

CHAPTER 4: WIND AND SOLAR RESOURCE MODELS

4.1 Solar Resource Model

The National Renewable Energy Laboratory (NREL) has a U.S. solar resource model, representing data obtained from SUNY Albany's solar radiation model. The data displayed in the resource model was collected from 1985 to 2009, depending on type, and contains average annual and monthly averages, measured in kilowatts per square meter, for the conterminous U.S. The resolution, depending on type, varies from approximately 10 to 40 square kilometers. Direct normal irradiance, global horizontal irradiance, and photovoltaic measurement types are provided (NREL, 2015).

For the purposes of this research, direct normal irradiance (in kilowatts per square meter) data were obtained for 2009. The data is in raster format, and was loaded into ArcGIS software, as shown in *Figure 12: NREL's Solar Resource Model in ArcGIS (NREL, 2015)*. The resolution for this dataset is in 10 square kilometers. A Bird Clear Sky model was used to calculate the clear sky Direct Normal Irradiance (DNI). The sources for the data used in the model include: radiance satellite imagery, snow coverage data, monthly average water vapor data, trace gases and aerosols data, and, where necessary, ground truth data. Due to variations in terrain and the existence of microclimates, the results of the model are accurate up to 15 percent of the measured values for each grid cell (NREL, 2012).

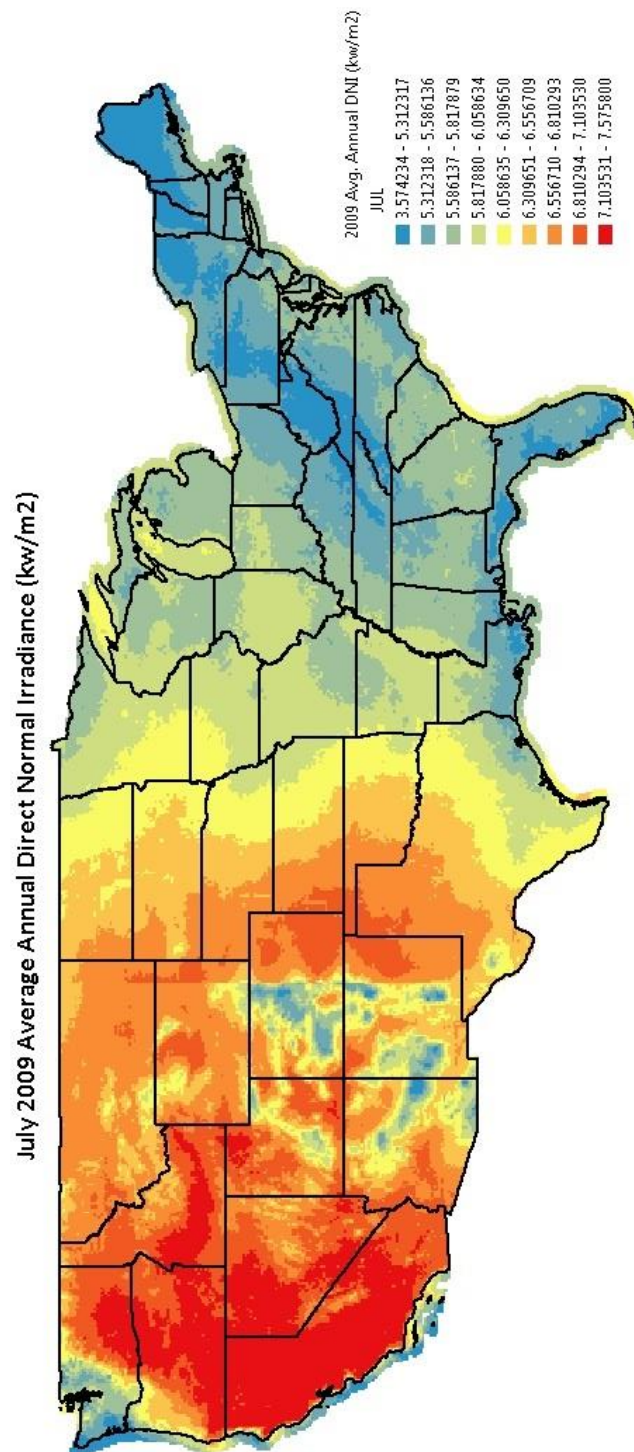


Figure 12: NREL's Solar Resource Model in ArcGIS (NREL, 2015)

4.2 Wind Resource Model

NREL's wind resource model displays estimated wind class values, as shown in *Table 3: NREL Wind Resource Model Wind Classes (NREL, 2014)*, for the conterminous U.S. using data obtained from the Pacific Northwest National Laboratory's (PNNL) wind resource model, developed in October 1986. The data used in the model is at a resolution of 200 meters to one kilometer, with state-level measured data (excluding Alabama, Florida, Louisiana, and Mississippi) at 50-meter height hubs, and national-level data measured at 25-kilometer height hubs. The data were used in-conjunction with a model produced by a consulting firm, AWS TruePower, along with the DOE, to enhance the model and estimate wind class values for areas that were excluded in PNNL's model (NREL, 2015).

The data accessed from the PPNL model excluded areas with low surface roughness, such as flat areas with low-lying vegetation, and it excluded areas with slopes greater than 20 percent. In areas with higher surface roughness, such as areas with forests and a thick vegetation canopy, the model assumes higher than actual wind potential. The model developed by AWS TruePower, and the DOE, estimates wind class values based on varying surface roughness and slopes. In areas with adequate data, surface wind, coastal marine, and upper-air data measurements were obtained. In areas where the data were unavailable, wind speeds were estimated based on topographic features, amount of vegetation affected by wind, and in coastal regions, the existence of sand dunes and other wind-influenced features.

Wind class values one to seven were assigned, based on measured or estimated wind speed or wind speed potential, and these values were dependent upon the amount of data available in the model, topography, and wind variability (NREL, 2015). Areas with an assigned

wind class of three to seven are considered suitable for large scale wind facilities, while areas with an assigned wind class of two are considered appropriate for small-scale and rural facilities. Areas with an assigned wind class of one are considered unsuitable for wind facilities (NREL, 2015).

For the purpose of this research, national-level data from August 2015 was obtained. The dataset created in-conjunction with AWS TruePower and the DOE was chosen because it did not contain any exceptions based on various topographic attributes. Because the data is at the national-level, it is measured at a height of 25 kilometers, and the resolution is at one square kilometer. ArcGIS software was also used to access the data, as shown in *Figure 13: NREL's Wind Resource Model in ArcGIS (NREL, 2015)*.

Table 1-1. Classes of wind power density at 10 m and 50 m(a)

Wind Power Class	10 m (33 ft)		50 m (164 ft)	
	Wind Power Density (W/m ²)	Speed (b) m/s (mph)	Wind Power Density (W/m ²)	Speed (b) m/s (mph)
1	0	0	0	
2	100	4.4 (9.8)	200	5.6 (12.5)
3	150	5.1 (11.5)	300	6.4 (14.3)
4	200	5.6 (12.5)	400	7.0 (15.7)
5	250	6.0 (13.4)	500	7.5 (16.8)
6	300	6.4 (14.3)	600	8.0 (17.9)
7	400	7.0 (15.7)	800	8.8 (19.7)
	1000	9.4 (21.1)	2000	11.9 (26.6)

a. Vertical extrapolation of wind speed based on the 1/7 power law.

b. Mean wind speed is based on Rayleigh speed distribution of equivalent mean wind power density. Wind speed is for standard sea-level conditions. To maintain the same power density, speed increases 3%/1000 m (5%/5000 ft) elevation.

*NOTE: Each wind power class should span two power densities. For example, Wind Power Class = 3 represents the Wind Power Density range between 150 W/m² and 200 W/m². The offset cells in the first column attempt to illustrate this concept.

Table 3: NREL Wind Resource Model Wind Classes (NREL, 2014)

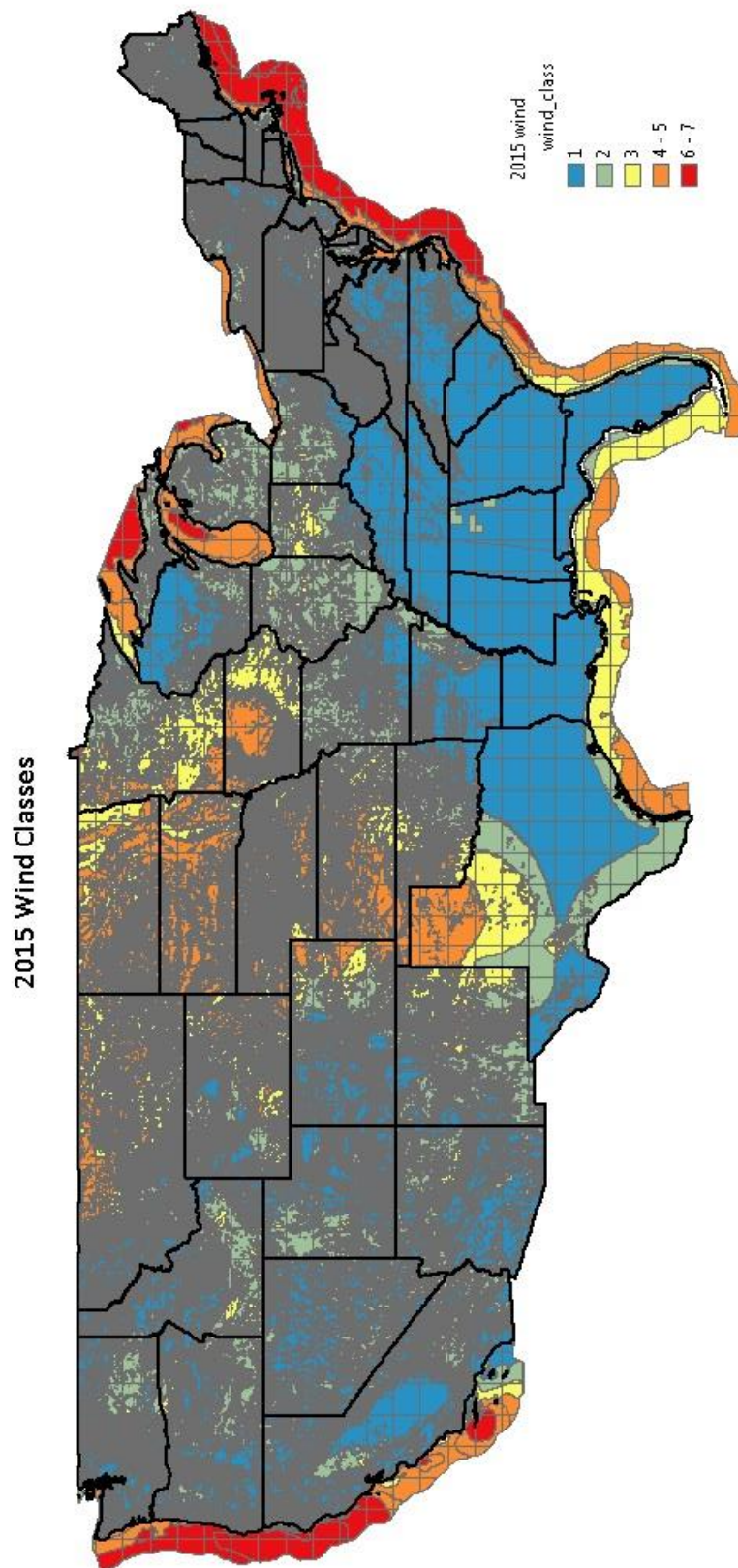


Figure 13: NREL's Wind Resource Model in ArcGIS (NREL, 2015)

4.3 Concentrated Wind Resource Model

The current wind and solar resource models are sufficient for determining feasible locations for concentrated and distributed solar, and for utility-scale, horizontal wind turbines. However, there is currently no resource model for concentrated wind. A concentrated wind resource model is necessary for locating areas of the Country that have convective potential, rather than advective potential, which is suitable for functional utility-scale wind turbines. Because convection is a small-scale resource, it is necessary that a concentrated wind resource model have a large resolution; one which is comparable to NREL's existing wind resource model (approximately one kilometer). Thus, an objective of this study is to create a resource model for a concentrated wind system. Such a resource model could be used to determine suitable locations for emerging technologies in concentrated wind.

CHAPTER 5: EMERGING TECHNOLOGY

5.1 The Solar Vortex (SoV)

Due to increasing concerns regarding the amount of GHG emitted into the atmosphere on a daily basis from the burning of fossil fuels, the need to find viable sources of alternative energy is becoming more pressing. Although improvements to renewable energy sources, including wind and solar photovoltaic technologies, have increased their prevalence, these technologies are still facing pressure, as the number of facilities in-use, the amount of power produced, and the efficiency and cost comparison with fossil fuels is such that only 14 percent of U.S. energy generation is produced by renewable sources (U.S. Energy Information Agency, 2014). This staggering figure is attributed to many issues faced by renewable energy technology, especially concerns with operation and maintenance costs. This desire to increase the percentage of overall power generation by renewable sources has prompted the development of new technologies, some of which are based on current technologies, and some are completely innovative.

The Solar Vortex (SoV) is an innovative means of energy production developed by a team of researchers, whose goal was to develop an entirely new source of harnessing alternative energy, based on simple principles of atmospheric physics, and to take advantage of naturally occurring physical conditions. The basic design concept behind the development of the Solar Vortex (SoV) is an anchored unit consisting of angled vanes that channel warm rising air from the ground's surface, where it meets slightly cooler air directly above it, causing a funnel to form inside the unit due to the existence of convection: the natural phenomenon where warm air tends to rise, while cooler air, which is denser, tends to sink. The funnel is then maintained inside the unit, as shown in *Figure 14: Dust Devil and Initial SoV Prototype (Georgia Tech, 2012)*, and after gaining momentum, has the potential to move a turbine inside the unit, which generates

energy. This basic design harnesses the potential to create and sustain movement of a vortex due to the existence of a temperature differential between the ground air and the air directly above it. This occurrence is similar to vortices found in nature, such as dust devils, which are commonly found in the Midwest and the Southwest United States.

The SoV is a new technology that the NPS, and other remote locations, can consider to generate on-site electricity to provide power to electric vehicles. The SoV units are small in comparison to wind turbines and other solar technologies. The expected capital costs, and operation and maintenance costs are also lower than wind and other solar technologies.

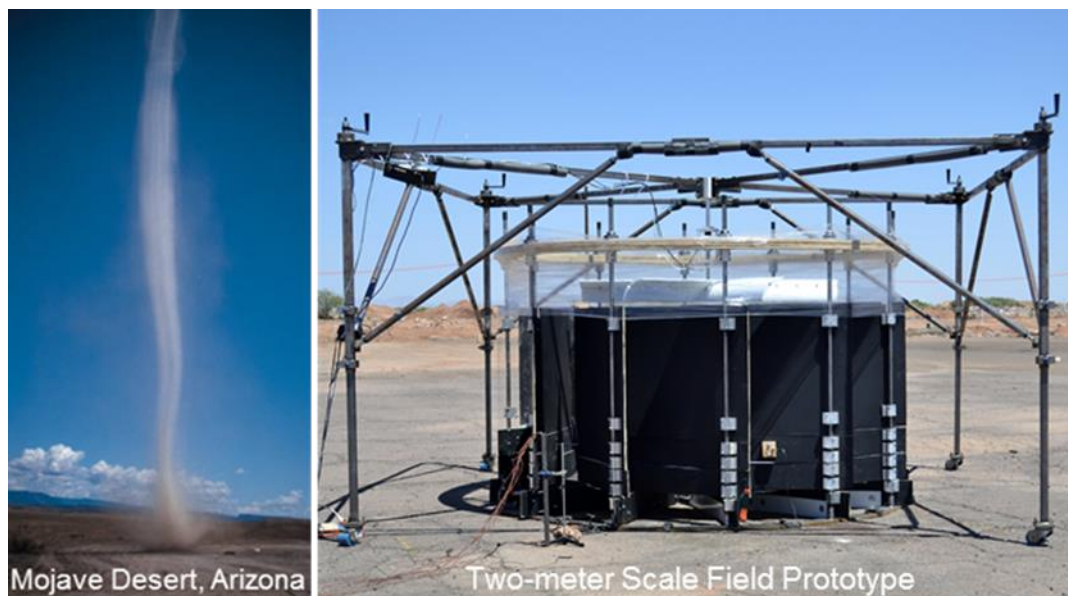


Figure 14: Dust Devil and Initial SoV Prototype (Georgia Tech, 2012)

5.1.1 Design Concept

The SoV design was based on the occurrence of naturally-occurring vortices that are found in nature: hurricanes (large scale); tornadoes (meso-scale), and dust devils (micro-scale),

These vortices form by the rising, warmer air next to the surface, which is heated by the sun, and the sinking, slightly cooler air located directly above this warm layer of sun-heated air. The funnels are an example of concentrated wind energy. Although these types of vortices, especially hurricanes and tornados, draw in energy from a large area, the energy is concentrated at the eye of the storm, as shown in *Figure 15: Dust Devil and Initial SoV Prototype (Georgia Tech, 2012)*. Thus, even a small dust devil, which has a diameter of approximately one meter, has the potential to draw energy from an area the size of a football field.

Based on the concept of vortex formation, the SoV design was based on the theory that a sustained vortex funnel could then be used to move a turbine in order to generate power. However, naturally-occurring dust devils typically cannot withstand a cross breeze and therefore, are incapable of being sustained for long periods of time. Therefore, a crucial part of the SoV design needed to be in sustainment of the vortex by anchoring the unit to the ground. “Unlike naturally occurring dust devil vortices that are free to wander laterally, and are hence susceptible to cross wind, each anchored columnar vortex is rendered stationary by an azimuthal array of tangential flow vanes” (Simpson et al, 2013).

The original concept for the SoV was designed by Dr. Ari Glezer, a mechanical engineering professor at the Georgia Institute of Technology. Dr. Glezer, along with a team of researchers from other universities and research institutions, collaborated to design, construct, and run the prototype and determine if the SoV is a viable means of alternative energy production, whether the unit would be marketable, and where units could theoretically be used to generate power. Currently, the study to determine if the SoV is a viable means of alternative energy production is in its early stages and it is being funded by the Advanced Research Projects Agency-Energy (ARPA-E).

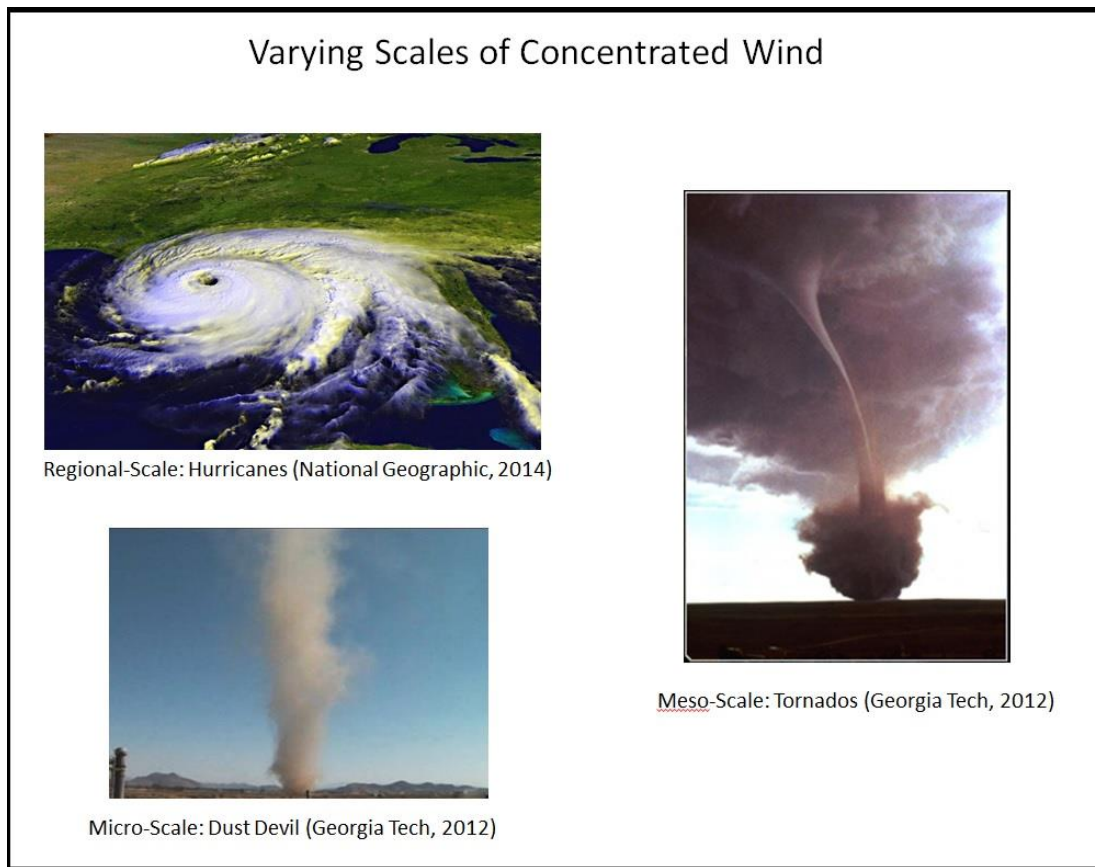


Figure 15: Dust Devil and Initial SoV Prototype (Georgia Tech, 2012)

As with other types of technology that harness alternative energy sources, the SoV was to be designed as a source of alternative energy production that can be constructed to take advantage of existing conditions, both naturally-occurring and man-made. A major consideration in the initial concept design was the existence of an abundance of solar heat that can be harnessed across the Earth's landscape. One-third of the Earth's land mass is desert, which allows for the capturing of solar heat, (on average 200 watts per square meter in a 24-hour period) that can then be used as a source of clean energy (Simpson et al, 2013). "Clean, renewable, electric power can be generated in hot climate or humid environments through exploitation of the thermal instability of the ground-heated air by deliberately triggering,

anchoring, and sustaining arrays of stationary solar-driven vortices, each of which is coupled to a vertical-axis turbine. This power generation approach is simple, scalable, and low-cost” (Simpson et al, 2013). These existing conditions were the basis for the concept of the SoV.

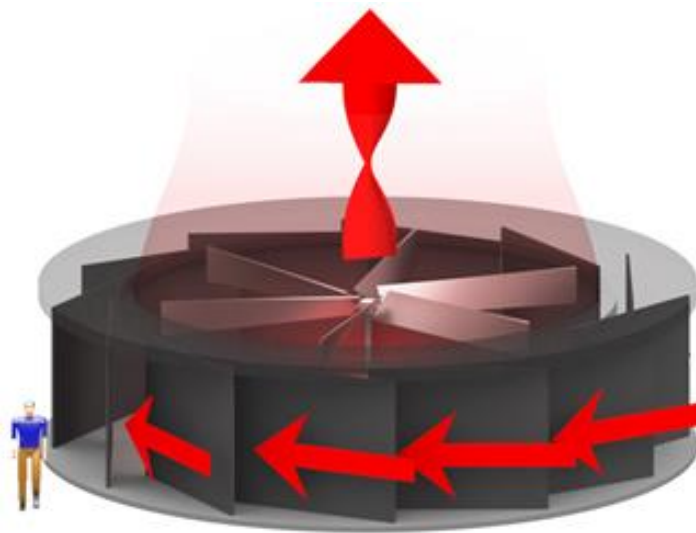


Figure 16: Diagram of SOV Vanes (Georgia Tech, 2012)

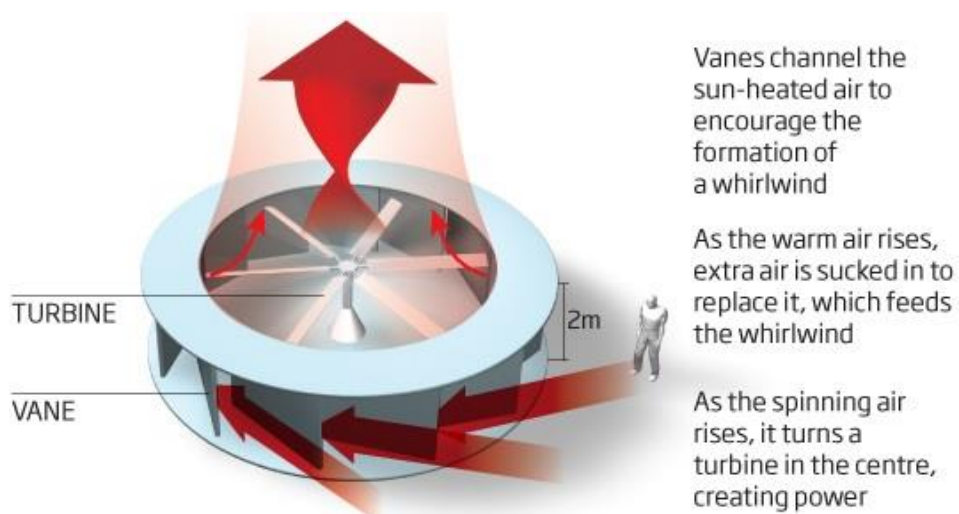


Figure 17: Diagram of SOV (Georgia Tech, 2012)

5.1.2 Initial SoV Prototype

An initial SoV prototype with a diameter of two meters was constructed in an area outside of Mesa, Arizona, which was the former General Motors proving grounds, and tested in July 2014 to determine if the unit could produce and sustain a vortex. A second prototype consisting of a unit six meters in diameter was also constructed in the same location in Mesa, Arizona in August 2015. Both units were stand-alone and did not contain a turbine. After initial testing of the prototypes, it was found that the units were able to successfully form and maintain a funnel inside the unit.

Testing of the initial prototype was crucial in determining the viability of the unit. Initial testing of the prototype provided information on the average time in which the unit shut down due to a lack of temperature differential after, but not immediately following, sundown. Testing provided information regarding the appropriate structure and angle of the vanes with which warm air was channeled into the unit in order to sustain formation and maintenance of the funnel inside the unit, as shown in *Figure 16: Diagram of SOV Vanes (Georgia Tech, 2012)*, *Figure 17: Diagram of SOV (Georgia Tech, 2012)*, *Figure 19: Diagram of SoV Prototype (Georgia Tech, 2016)* and *Figure 20: Diagram of SoV Prototype (Georgia Tech, 2016)*. Lastly, testing also provided information regarding the factors that may inhibit the sustainment of the vortex inside the unit, such as cross breezes, which were remedied by construction of a shroud over the unit, as shown in *Figure 18: SoV Prototype (Georgia Tech, 2016)*.



Figure 18: SoV Prototype (Georgia Tech, 2016)

A third prototype was tested July 2016. This unit was slightly larger than the previous prototypes, and contained a turbine. The prototype initially contained a total of eight, flat blades. Unfortunately, it was found that the turbine would not move. The research team decided that the number of blades needed to be reduced to half, and that the remaining blades needed to be angled. The turbine was also moved from the top of the structure to the bottom. After moving the turbine, it was found that very little airflow was able to enter the structure, and power could not be generated by the turbine.

During testing, frequent periods of rain delayed startup of the structure. Due to the prototype being located in the desert, the rain caused the sandy ground to become soaked, which required several dry days in order for the ground to dry sufficiently and the structure to function

properly. Unfortunately, while the research team was away from the testing site, a severe storm occurred in Mesa and destroyed a large portion of the structure. Thus, final testing and power generation results were never obtained. Further simulations are necessary to obtain power generation potential.

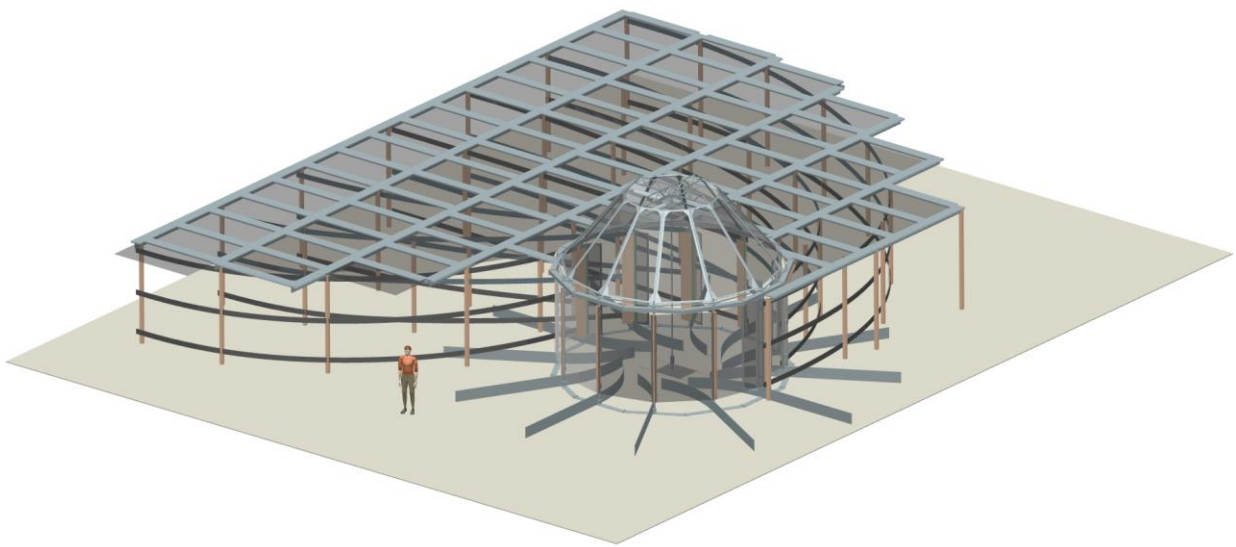


Figure 19: Diagram of SoV Prototype (Georgia Tech, 2016)

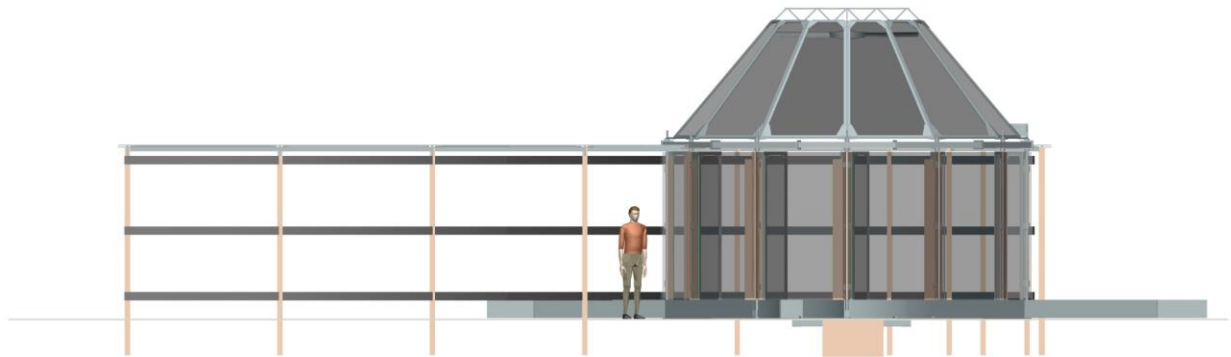


Figure 20: Diagram of SoV Prototype (Georgia Tech, 2016)

5.1.3 Renewable Power from SoVs

The SoV is an example of a source of concentrated wind energy production that the NPS, and other remote locations looking for off-grid sources of energy production can use for numerous reasons. Operation and maintenance costs are relatively low compared with horizontal wind and concentrated and distributed solar technologies (Simpson et al, 2013). The amount of energy theoretically produced by a unit is comparable to wind and solar PV, in terms of energy production. Unlike with horizontal wind and solar PV, which require particular environmental characteristics present at the location, SoV units can be constructed in a variety of locations, depending on the existence of a temperature differential; possibly making SoV units a suitable choice in areas that cannot support horizontal wind and distributed or concentrated solar facilities. Also, the fact that the units are smaller in size compared to the size of wind facilities, and the footprint of solar PV arrays, is such that they can be located close to buildings and in parking lots, possibly making them more suitable for providing power in locations where space is limited.

5.1.4 Comparison of SoV with Wind and Solar

Another important consideration given during the design phase of the SoV was in ensuring that the SoV would be comparable to other alternative sources of energy production, mainly horizontal wind and distributed and concentrated solar technologies. According to Simpson et al, (2013) with regards to an array of approximately 320 SoV units on a square kilometer: “such an array of vortices has an estimated output of 16 Mwe/km², comparing favorably to conventional wind turbines (3-6 Mwe/km²) and solar photovoltaic/concentrated solar power (15-25 Mwe/km²)” (Simpson et al, 2013).

Not only are SoV units comparable to horizontal wind and distributed and concentrated solar systems in terms of power output potential, but they are estimated to be less expensive to operative and maintain for a number of reasons, as shown in *Figure 21: Levelized Cost of Energy (Georgia Tech, 2012)*. When comparing SoV units to horizontal wind facilities, Simpson et al (2013) found that: “Because the vortex harvests energy from the thin thermal layer nearest to the ground, the vertical-axis turbines are relatively close to the ground level, reducing operational and maintenance costs. [Also,] in addition to the collection of the available gravitational potential energy in the solar-heated ground air layer, the azimuthal flow vanes can entrain considerable kinetic energy from ambient horizontal wind, independent of wind direction, thereby increasing the electric power generated” (Simpson et al, 2013). When comparing SoV units to solar facilities: “the system requires no electromechanical control system to track the sun, rendering the system mechanically simpler and reducing initial capital and maintenance costs. The vortex and turbine collect energy at a central location from a wide, unimproved area, so that the surface need not be tiled with expensive elements, again reducing the overall cost of the system. [Lastly,] the thermal ground storage capability renders the electric power produced

by buoyancy-induced vortices much less susceptible to cloud passage, and gives it much better diurnal predictable, [in that] the energy output of the vortex does not vanish immediately after sunset, and will, under some conditions, continue well into the evening” (Simpson et al, 2013). Finally, according to Simpson et al (2013): SoV units compare favorably in terms of costs of energy production, such that a 10-meter diameter unit, producing 50 Kwe, would cost \$0.066/kwh, compared with solar PV (\$0.18/kwh), and a horizontal wind turbine (\$0.084/kwh) (Simpson et al, 2013).

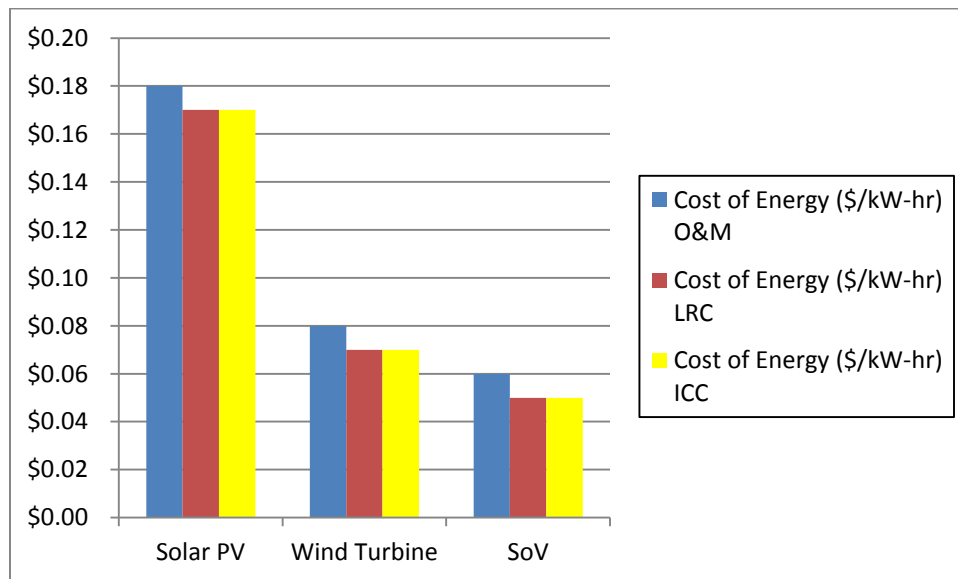


Figure 21: Levelized Cost of Energy (Georgia Tech, 2012)

5.1.5 Renewable Power from SoVs at National Parks

National parks can benefit from off-grid power generation systems, like the SoV, in many ways. One such way is in the SoV providing power to park lodges, office buildings, ranger stations, and other buildings located on the park property. If a park is located in an area that is suitable for SoV installation, the units can be installed on, or near, the park property and provide

power to park buildings. Due to the SoV being smaller in size compared with large-scale horizontal wind and solar facilities, the units can be installed in parking lots, or other locations on the property, without the concern of losing valuable space. Depending on the location, units can also theoretically be installed on rooftops of buildings to take advantage of heat radiating from buildings in colder climates.

Using renewable energy to charge electric vehicles, especially energy harnessed at the source, rather than accessed from the power grid, is an extremely sustainable practice for business or personal use, especially at National parks. If a park is in a location where SoV units can feasibly be installed, the units can provide power to electric vehicle charging stations on the park property, which can power electric park maintenance and service vehicles, park visitors' personal electric vehicles, which may prove to be an incentive for some electric vehicle owners to visit parks, and, most importantly for the focus of this study, provide renewable energy to charge electric park transit buses and shuttles.

5.1.6 SoV Resource Model

The SoV relies on the existence of a difference in temperature between the layer of warm air directly above the ground surface and the cooler air above the warmer layer. This temperature differential theoretically exists in nature in varying locations. Theoretically, it can also occur in locations where the temperature differential is not naturally-occurring, such as in man-made environments where there is a heat source located in a cooler environment. The SoV units rely on this temperature differential in order to create and sustain vortex formation within the unit. Therefore, it is necessary to locate areas where units could feasibly be constructed, such as in locations that are conducive to naturally-occurring convection. Currently, because the SoV is in

its early stages of research and development, a concentrated wind resource model is not available, and therefore, must be developed.

CHAPTER 6: CONCENTRATED WIND RESOURCE MODEL

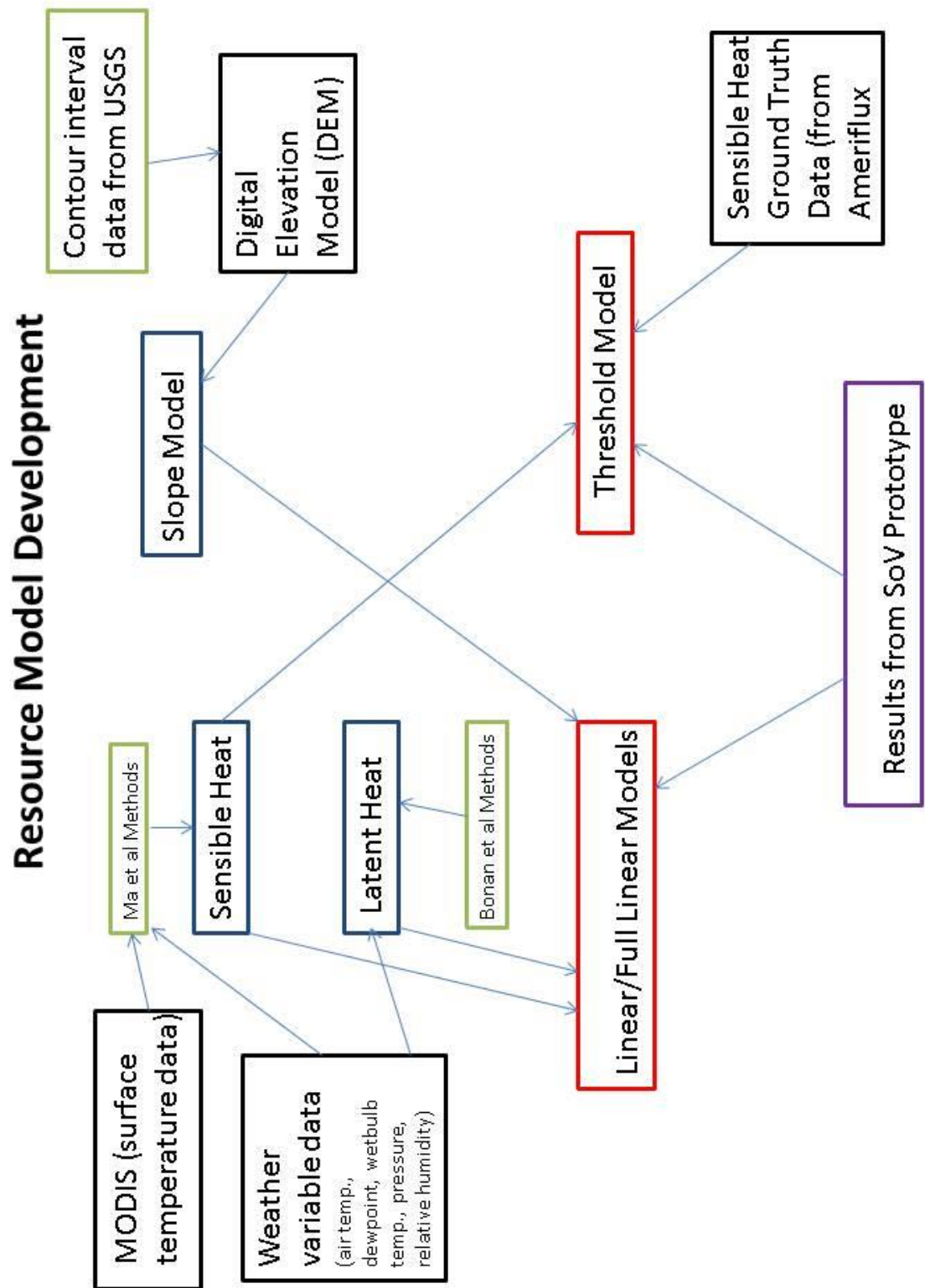


Figure 22: Model Development Flow Chart

6.1 The GIS Model

The GIS resource model developed for this study was crucial in locating potential areas where concentrated wind energy production systems, such as the SoV, could potentially be installed based on existing natural resources. This GIS resource model was an important component for determining the viability of the SoV in varying locations based on potential power output. More importantly, it was necessary for resource evaluation to determine appropriate locations that may be suitable for future installation of concentrated wind energy production systems based on naturally-occurring environmental attributes. The SoV relies on buoyancy. Many factors affect the SoV including: the density of air (based on the moisture content), ambient temperature, sensible heat flux at the surface, latent heat (also related to moisture content), and physical attributes (albedo and slope). The GIS resource model was used to calculate and pinpoint locations that contain the aforementioned resources necessary for potential funnel formation and sustainment within SoV units due to convection. By developing a GIS resource model that determines resource availability with regards to temperature and heat exchange for the entire United States, National park locations can potentially be considered for off-grid application of concentrated wind energy production facilities, like the SoV.

The GIS resource model in this study was created to: estimate heat flux values at one kilometer resolution, which is comparable to NREL's current horizontal wind resource model; estimate temporal distributions of heat flux, based on the methods used by Ma et al (2010); estimate theoretical daily, monthly, and annual average power output in watts per meter square and kilowatt-hours; develop a slope model of the entire U.S.; and refine the power output estimates based on the slope map. To achieve these tasks, the GIS resource model developed for

this study calculated sensible and latent heat for the 48 conterminous United States. The power output estimate models were developed based on the distribution of varying sensible and latent heat fluxes found at different geographical locations at different times, both morning and night, and at different times of year. Refer to *Figure 22: Model Development Flow Chart* for steps involved in development of the resource model.

Determination of power output estimates is crucial in locating areas where the power output potential is such that a concentrated wind energy production system, like the SoV, could be constructed and run successfully. The slope model was created to be used after obtaining the results from the power output estimates to determine geographical areas where systems could potentially be installed. The slope map is necessary in finding potential areas where the ground surface is level, with a very low gradient, or areas with low slope surrounded by adjacent areas with a higher slope to encourage upward or downward moving air to flow into a unit, influencing start-up time.

6.2 MODIS

The methods used by Ma et al (2010) were used in creating the GIS resource model, mainly the methods used to calculate sensible heat, as shown in *Figure 26: Sensible Heat Flux of Tibetan Plateau (Ma et al, 2010)*. Ma et al (2010) calculated sensible for the Tibetan Plateau using MODIS (Moderate Resolution Imaging Spectroradiometer) land surface temperature (LST) and emissivity satellite imagery data. MODIS, which is aboard the Terra satellite, as shown in *Figure 23: EOS System (NASA, 2015)*, *Figure 24: MODIS Location on Terra Satellite (NASA, 2015)*, and *Figure 25: MODIS (NASA, 2015)*, which is part of the EOS (Earth Observing Satellites) system, views the entire earth in approximately two days. MODIS obtains data with 36 spectral bands. However, for the purposes of this study, only bands 31 and 32 are needed

because those contain the surface and cloud coverage data and surface temperature data, as shown in *Table 4: MODIS Spectral Bands 1-19 (NASA, 2015)*.

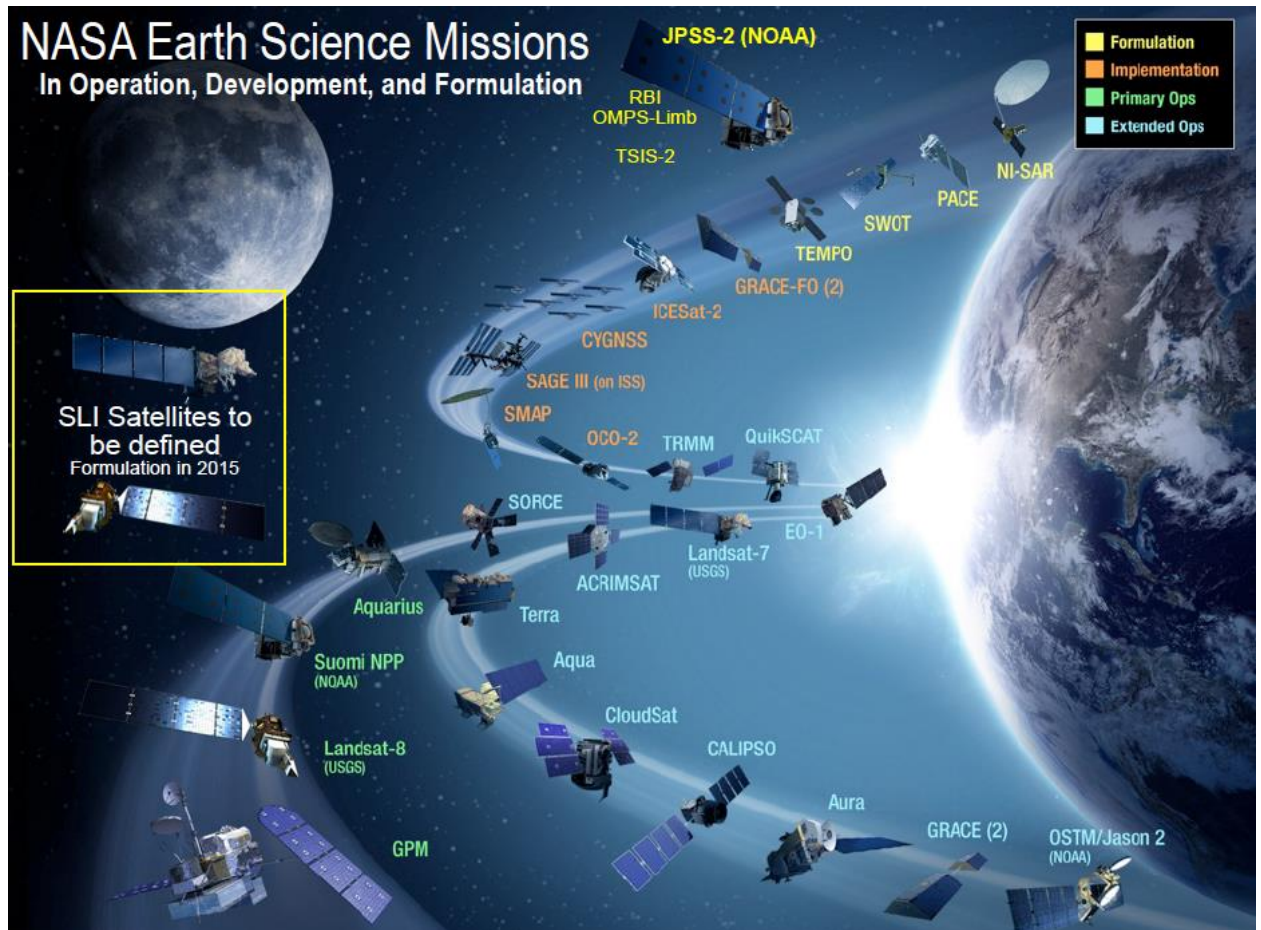


Figure 23: EOS System (NASA, 2015)

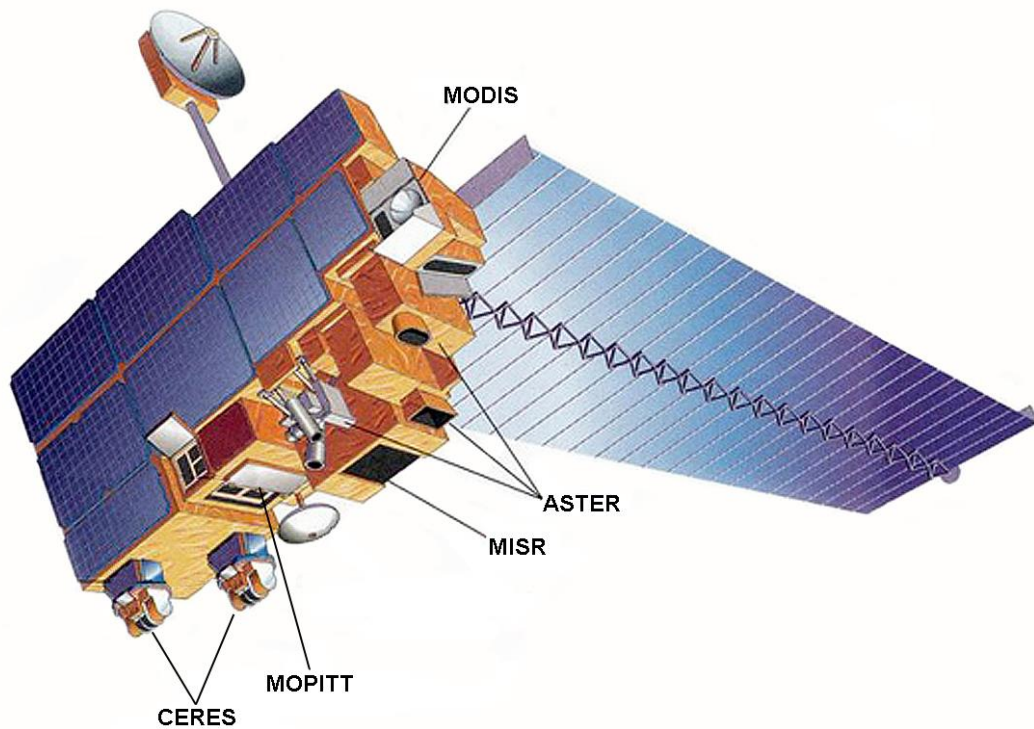


Figure 24: MODIS Location on Terra Satellite (NASA, 2015)

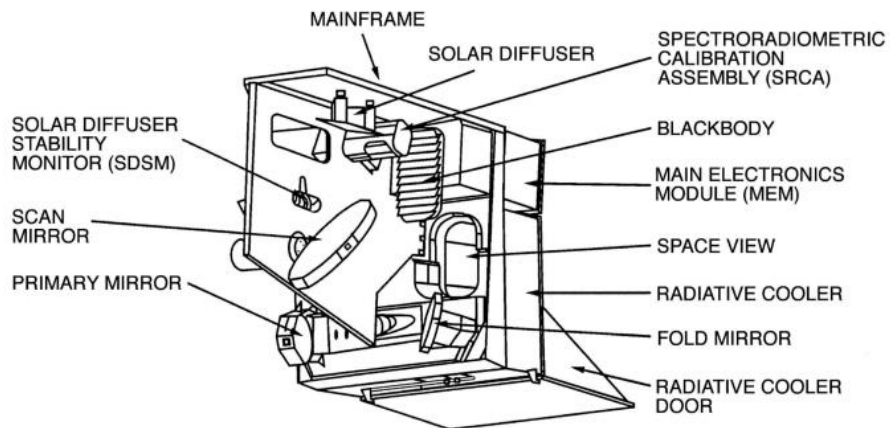


Figure 25: MODIS (NASA, 2015)

Primary Use	Band	Bandwidth	Spectral Radiance	Required NE[Δ]T(K) (Noise-Equivalent Temperature Difference)
Surface/Cloud Temperature	20	3.660 - 3.840	0.45(300K)	0.05
	21	3.929 - 3.989	2.38(335K)	2
	22	3.929 - 3.989	0.67(300K)	0.07
Atmospheric Temperature	23	4.020 - 4.080	0.79(300K)	0.07
	24	4.433 - 4.498	0.17(250K)	0.25
	25	4.482 - 4.549	0.59(275K)	0.25
Cirrus Clouds Water Vapor	26	1.360 - 1.390	6 150(SNR)	
	27	6.535 - 6.895	1.16(240K)	0.25
	28	7.175 - 7.475	2.18(250K)	0.25
Cloud Properties	29	8.400 - 8.700	9.58(300K)	0.05
Ozone	30	9.580 - 9.880	3.69(250K)	0.25
Surface/Cloud Temperature	31	10.780 - 11.280	9.55(300K)	0.05
	32	11.770 - 12.270	8.94(300K)	0.05
	33	13.185 - 13.485	4.52(260K)	0.25
Altitude	34	13.485 - 13.785	3.76(250K)	0.25
	35	13.785 - 14.085	3.11(240K)	0.25
	36	14.085 - 14.385	2.08(220K)	0.35

Primary Use	Band	Bandwidth	Spectral Radiance	Required SNR (Signal-to-Noise Ratio)
Land/Cloud/Aerosols	1	620 - 670	21.8	128
Boundaries	2	841 - 876	24.7	201
Land/Cloud/Aerosols	3	459 - 479	35.3	243
Properties	4	545 - 565	29	228
	5	1230 - 1250	5.4	74
	6	1628 - 1652	7.3	275
Ocean Color/	7	2105 - 2155	1	110
	8	405 - 420	44.9	880
	9	438 - 448	41.9	838
Biogeochemistry	10	483 - 493	32.1	802
	11	526 - 536	27.9	754
	12	546 - 556	21	750
	13	662 - 672	9.5	910
	14	673 - 683	8.7	1087
	15	743 - 753	10.2	586
	16	862 - 877	6.2	516
Atmospheric	17	890 - 920	10	167
Water Vapor	18	931 - 941	3.6	57
	19	915 - 965	15	250

Table 4: MODIS Spectral Bands 1-19 (NASA, 2015)

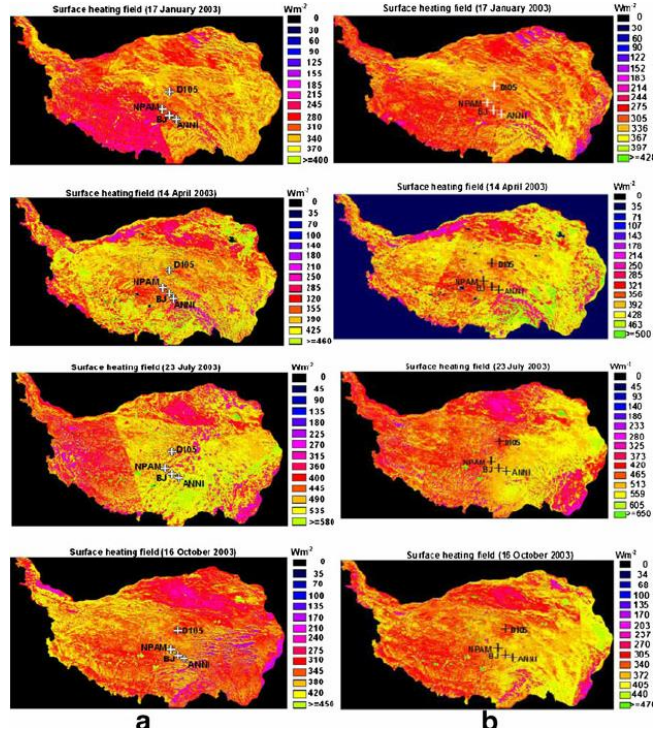


Figure 26: Sensible Heat Flux of Tibetan Plateau (Ma et al, 2010)

6.2.1 MODIS Data

The MODIS data were obtained from the MOLT database from USGS. The files were downloaded manually, although a Python script could have been written to automate the process. The files, which were an average temperature (in degrees Kelvin) of the first eight days of each month, were corrected for cloud coverage, and in raster format at one kilometer resolution, were downloaded directly from the database in hierarchical data format (HDF). The MODIS Reprojection Tool 4.1 (2011) was downloaded from USGS's Land Processes Distributed Active Archive Center Website, and each HDF file was loaded into the software and converted to a geotiff format file, as shown in *Figure 27: MODIS Reprojection Tool (USGS, 2011)*. There was a total of 13 MODIS raster files, covering the entire U.S., for four months (January, April, July, and October) for 2011 and 2013, at approximately 10:30 am and 10:30 pm (104 files total). The

MODIS data were obtained using the version MOD11A2 due to this version having the least amount of missing data compared with previous versions: MOD11A1.004 and MOD11A1.005.

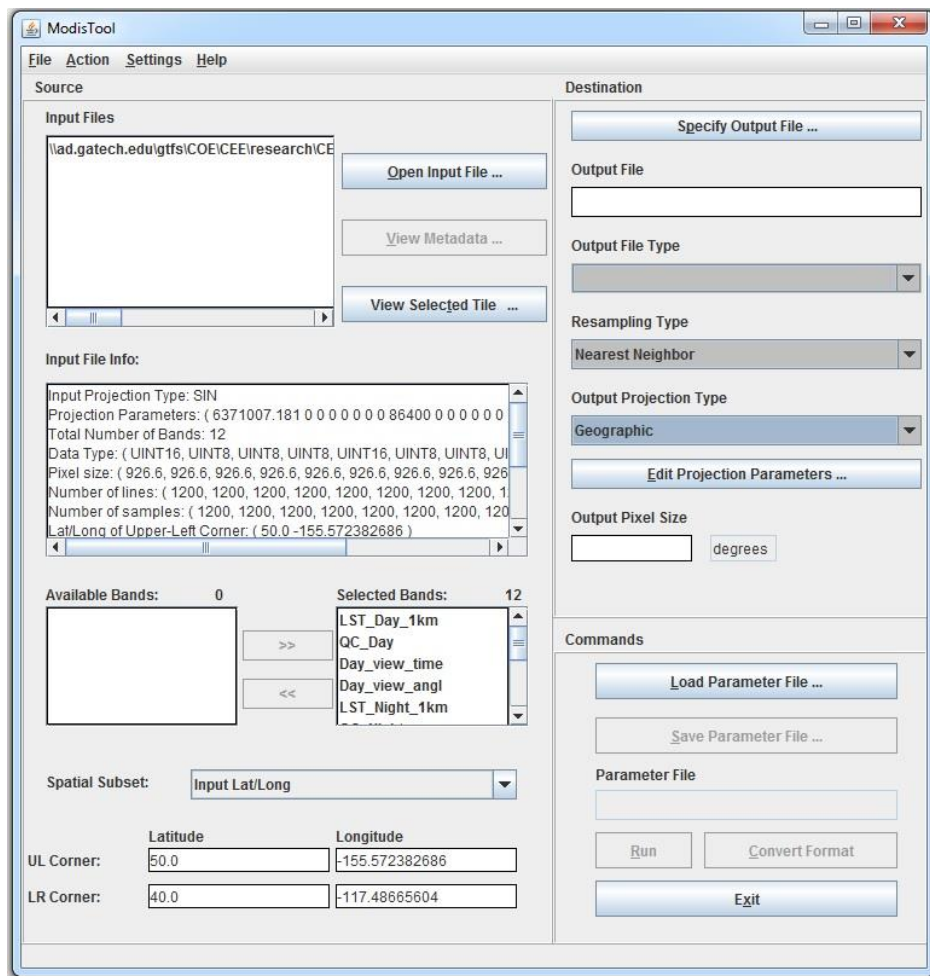


Figure 27: MODIS Reprojection Tool (USGS, 2011)

After the files were converted from hdf to geotiff format using the MODIS Reprojection Tool, the raster files were then loaded into ArcGIS, using the Sinusoidal projection. Because the files were in geotiff form, they loaded easily into ArcGIS as raster layers. However, although version MOD11A2 data were used, there were still large areas where there were missing raster cell values (the surface temperature for those cells was zero in the attribute table). This posed a

problem during calculations. To remedy this problem, a simple code was written in Python in the Raster Calculator tool in ArcGIS, as shown in *Figure 28: Raster Calculator with MODIS Null Cell Exclusion Formula*. This code, when run in Raster Calculator on all 104 raster layers, created new raster layers where the empty cells were excluded. The layers were then added to the Table of Contents in ArcGIS, and would then be used during sensible and latent heat calculations. The processed and reprojected MODIS images can be found in: *Figure 29: MODIS Land Surface Temperature (LST) and Emissivity, January, 2011 (10:30 am)* through *Figure 44: MODIS Land Surface Temperature (LST) and Emissivity, October, 2013 (10:30 pm)*.

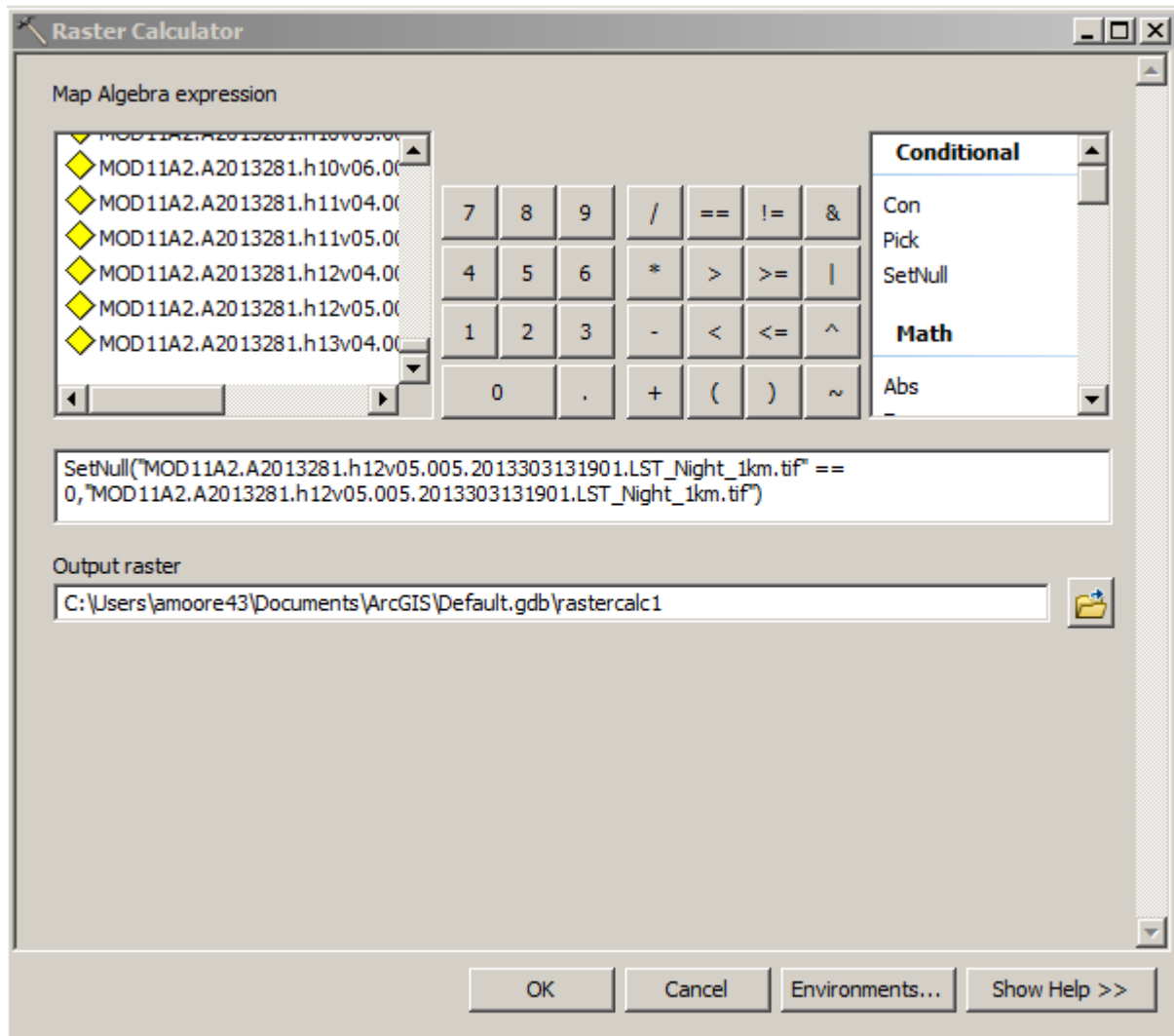


Figure 28: Raster Calculator with MODIS Null Cell Exclusion Formula

January 2011 10:30 am

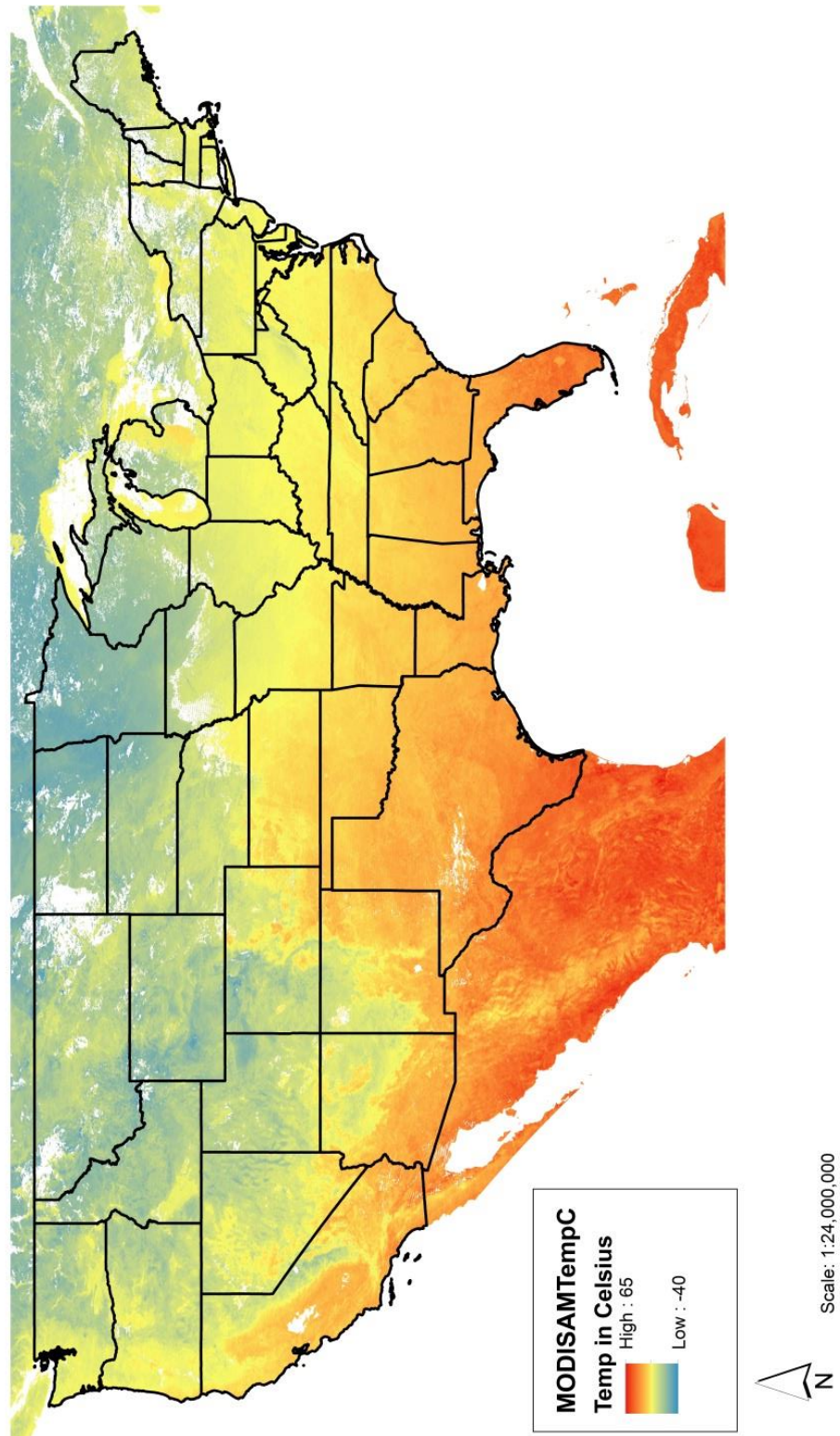


Figure 29: MODIS Land Surface Temperature (LST) and Emissivity, January, 2011 (10:30 am)

January 2011 10:30 pm

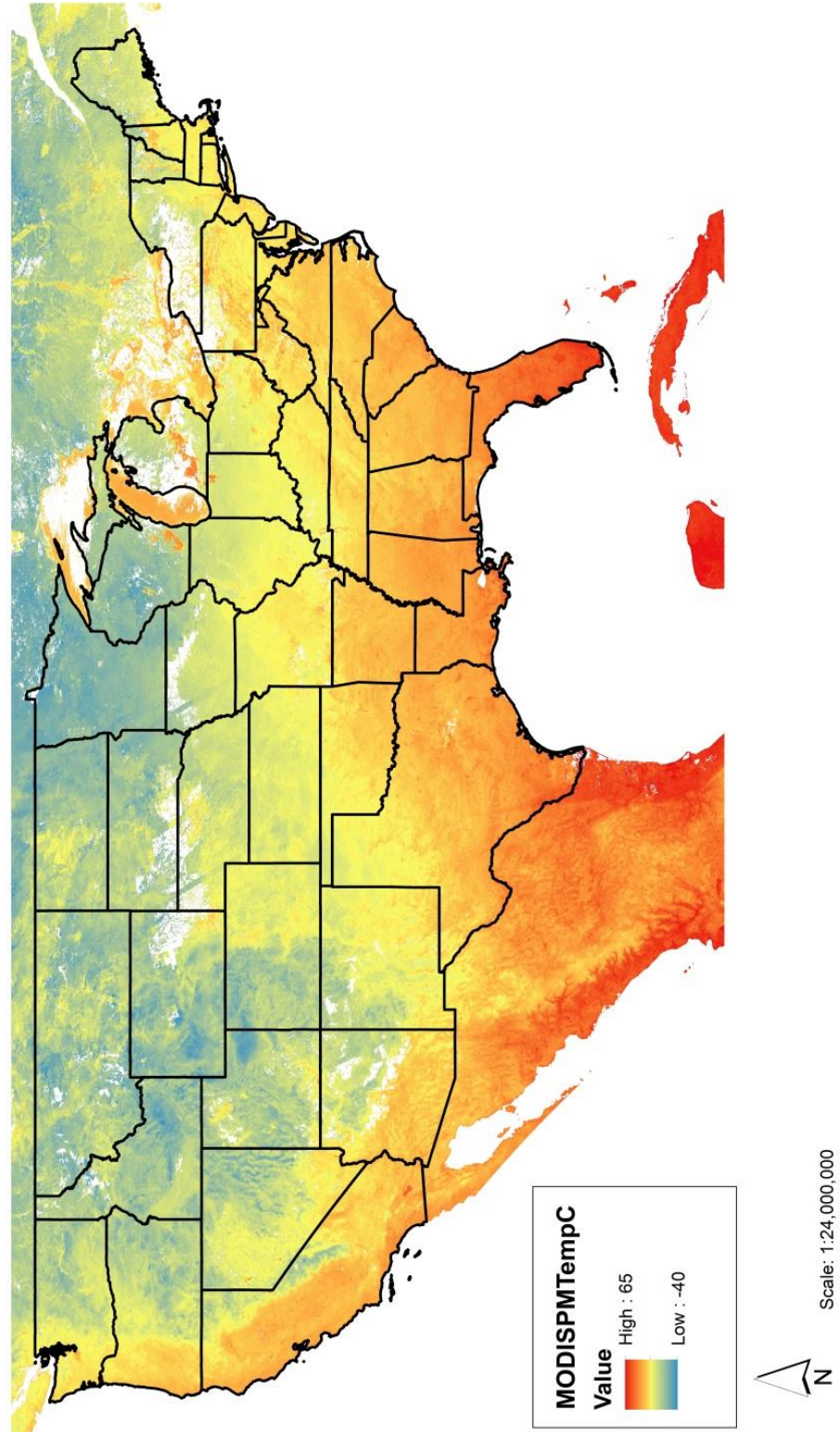


Figure 30: MODIS Land Surface Temperature (LST) and Emissivity, January, 2011 (10:30 pm)

January 2013 10:30 am

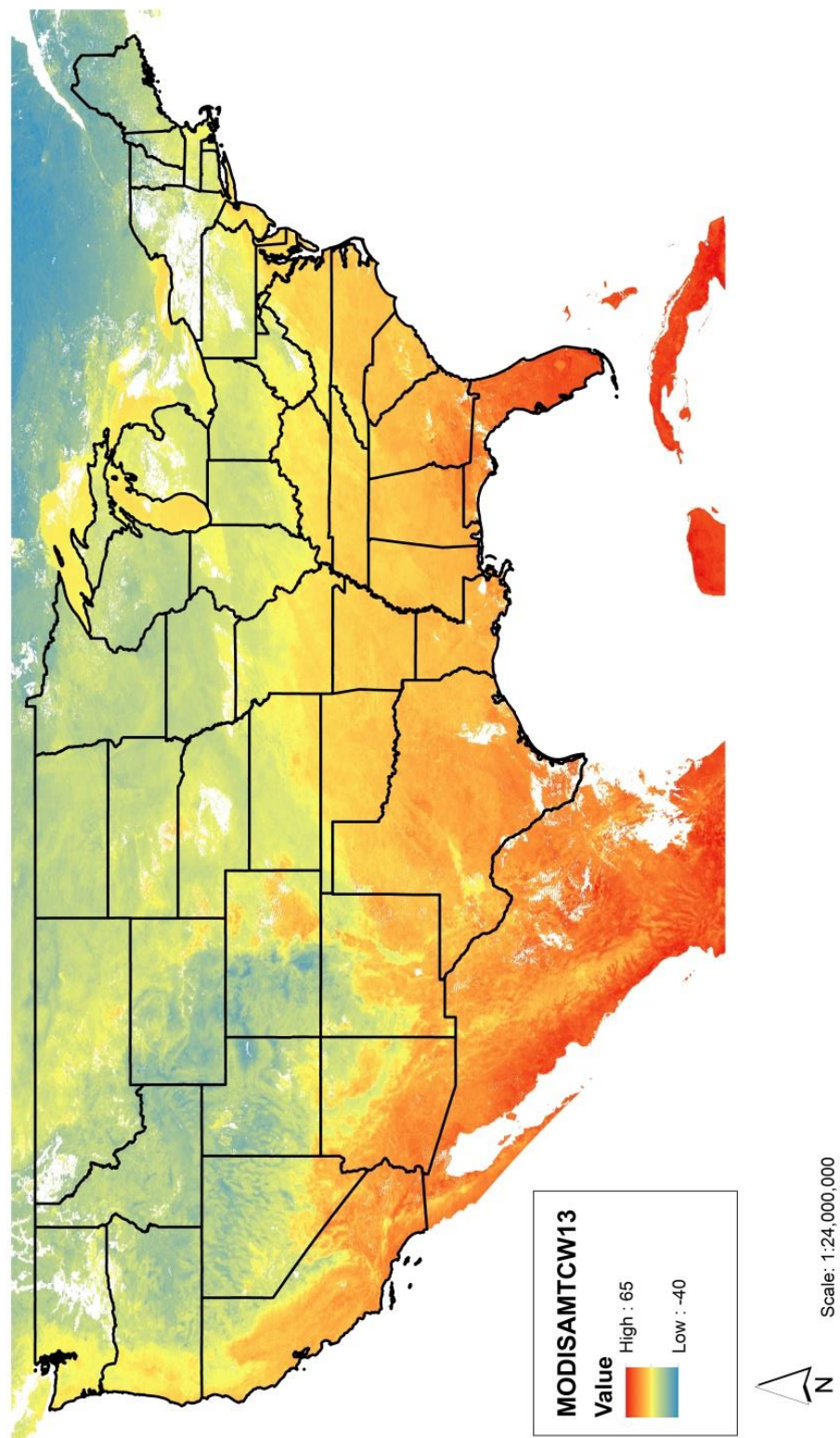


Figure 31: MODIS Land Surface Temperature (LST) and Emissivity, January, 2013 (10:30 am)

January 2013 10:30 pm

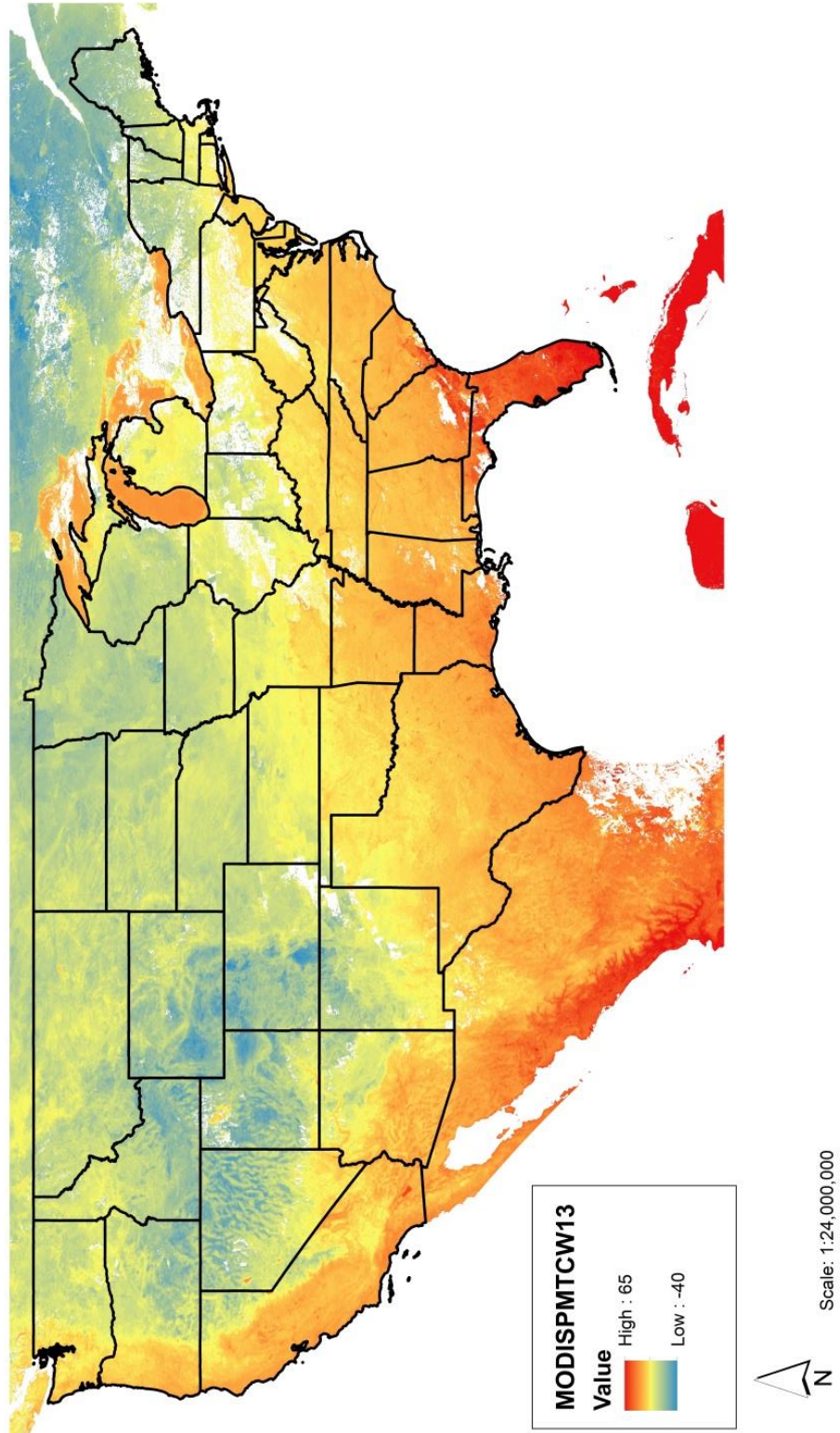


Figure 32: MODIS Land Surface Temperature (LST) and Emissivity, January, 2013 (10:30 pm)

April 2011 10:30 am

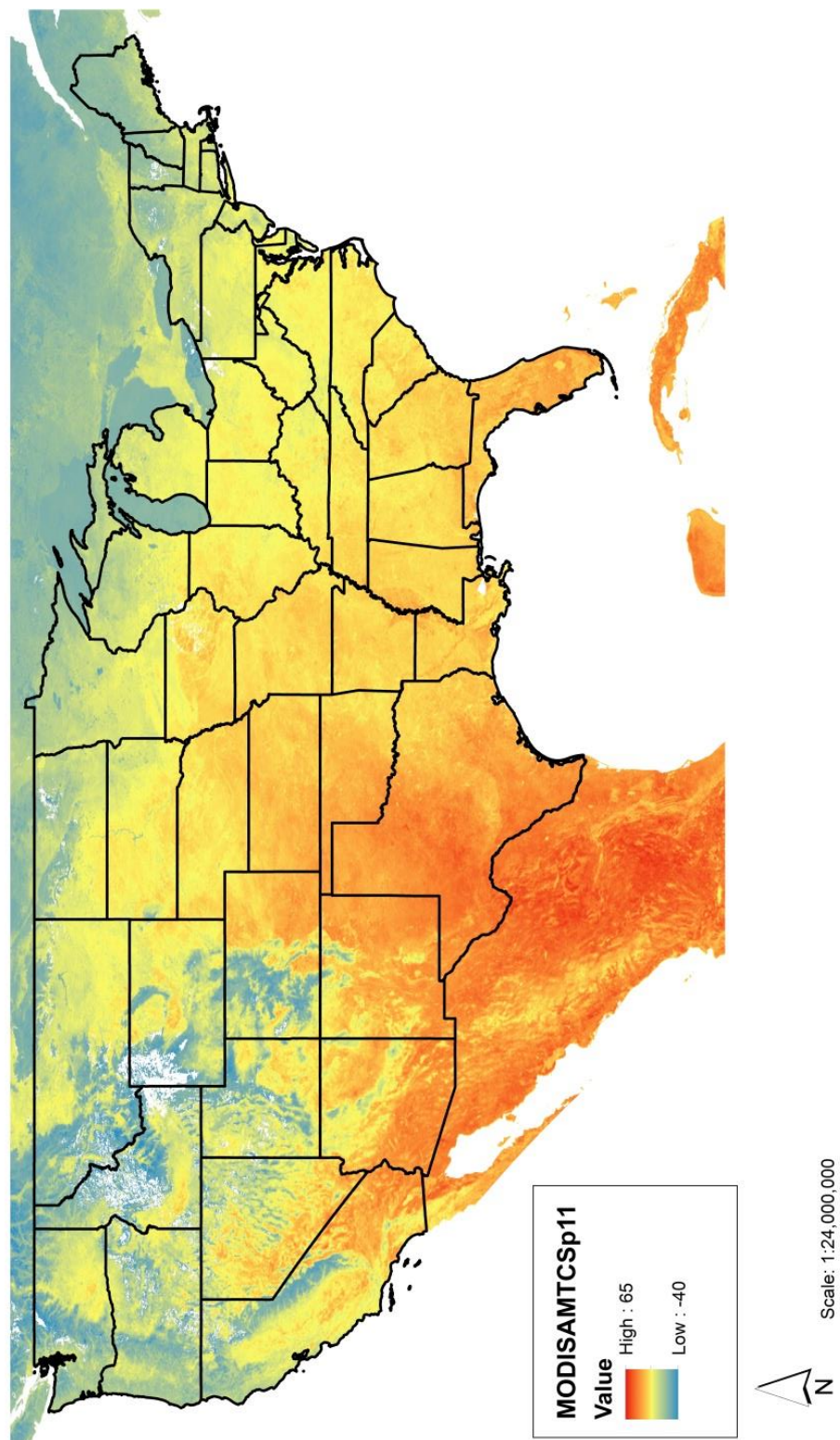


Figure 33: MODIS Land Surface Temperature (LST) and Emissivity, April, 2011 (10:30 am)

April 2011 10:30 pm

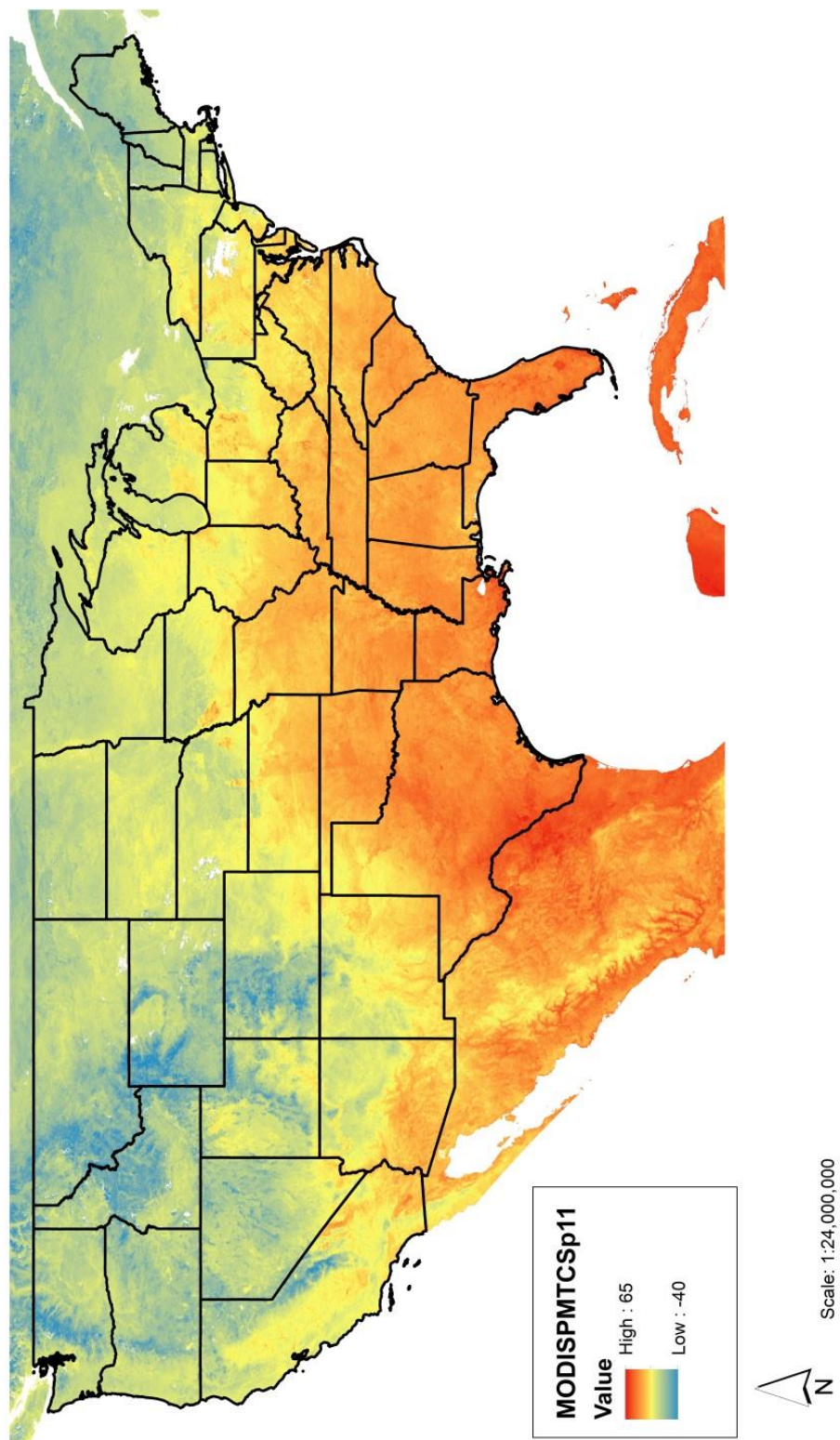


Figure 34: MODIS Land Surface Temperature (LST) and Emissivity, April, 2011 (10:30 pm)

April 2013 10:30 am

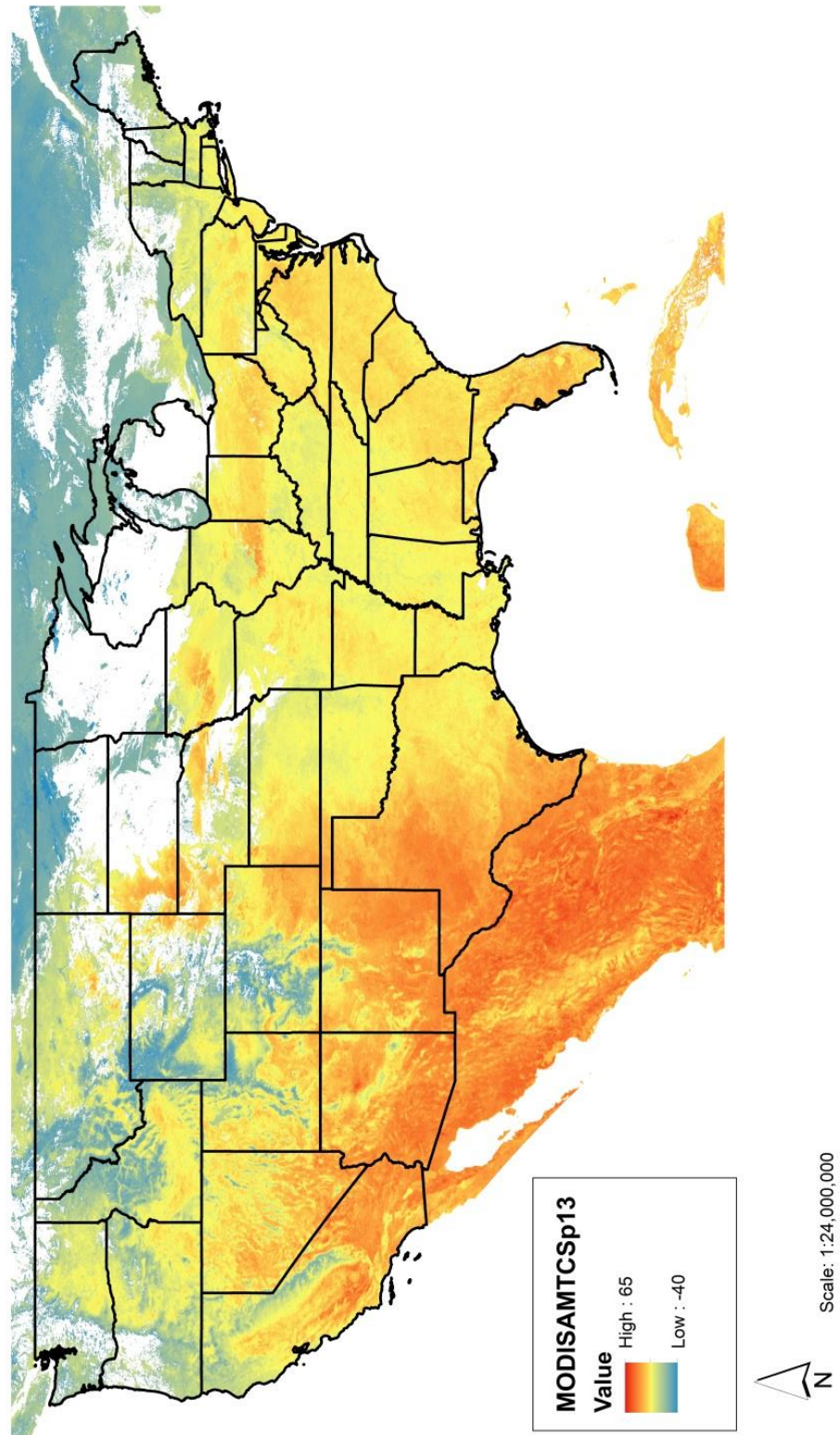


Figure 35: MODIS Land Surface Temperature (LST) and Emissivity, April, 2013 (10:30 am)

April 2013 10:30 pm

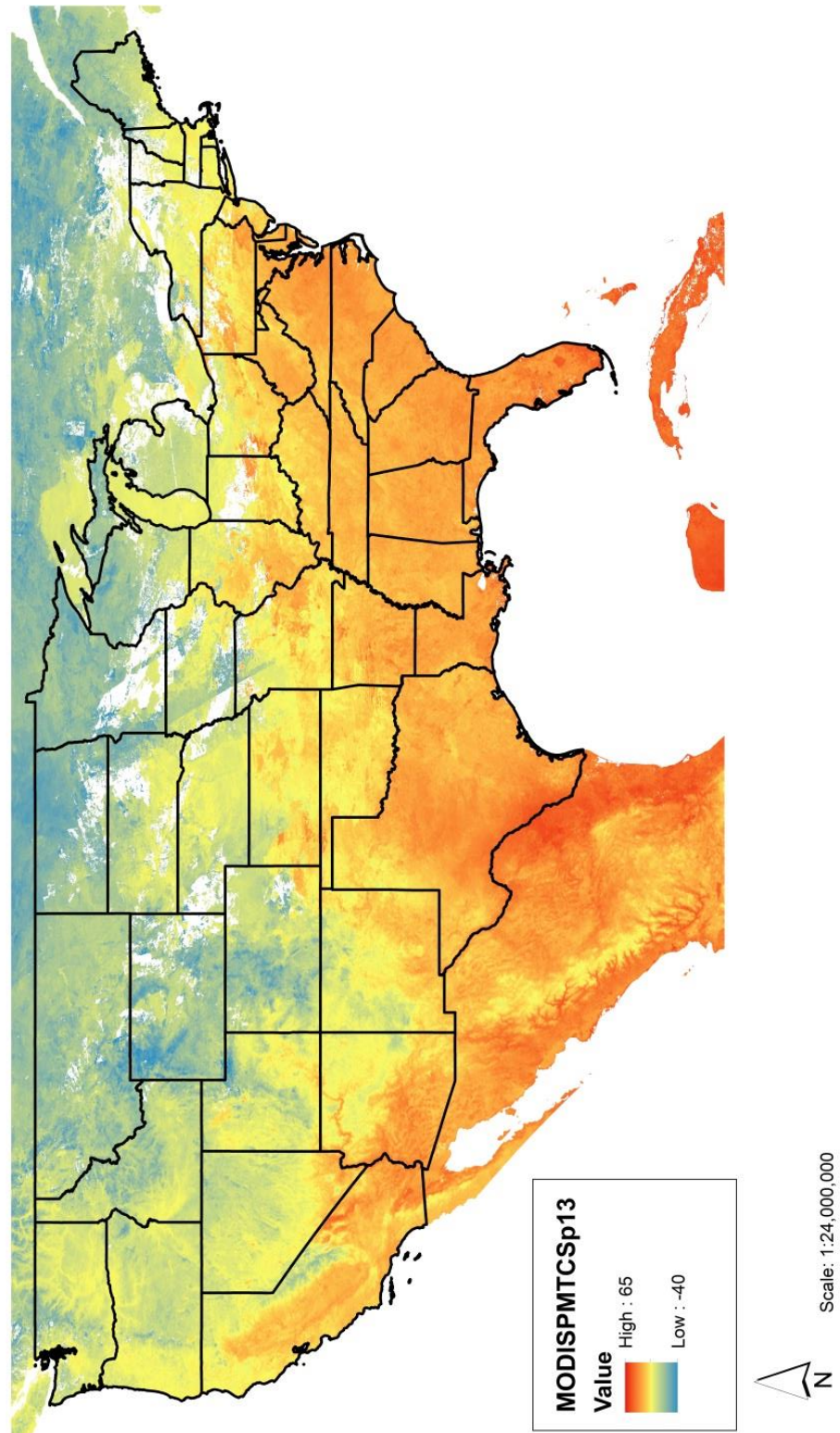


Figure 36: MODIS Land Surface Temperature (LST) and Emissivity, April, 2013 (10:30 pm)

July 2011 10:30 am

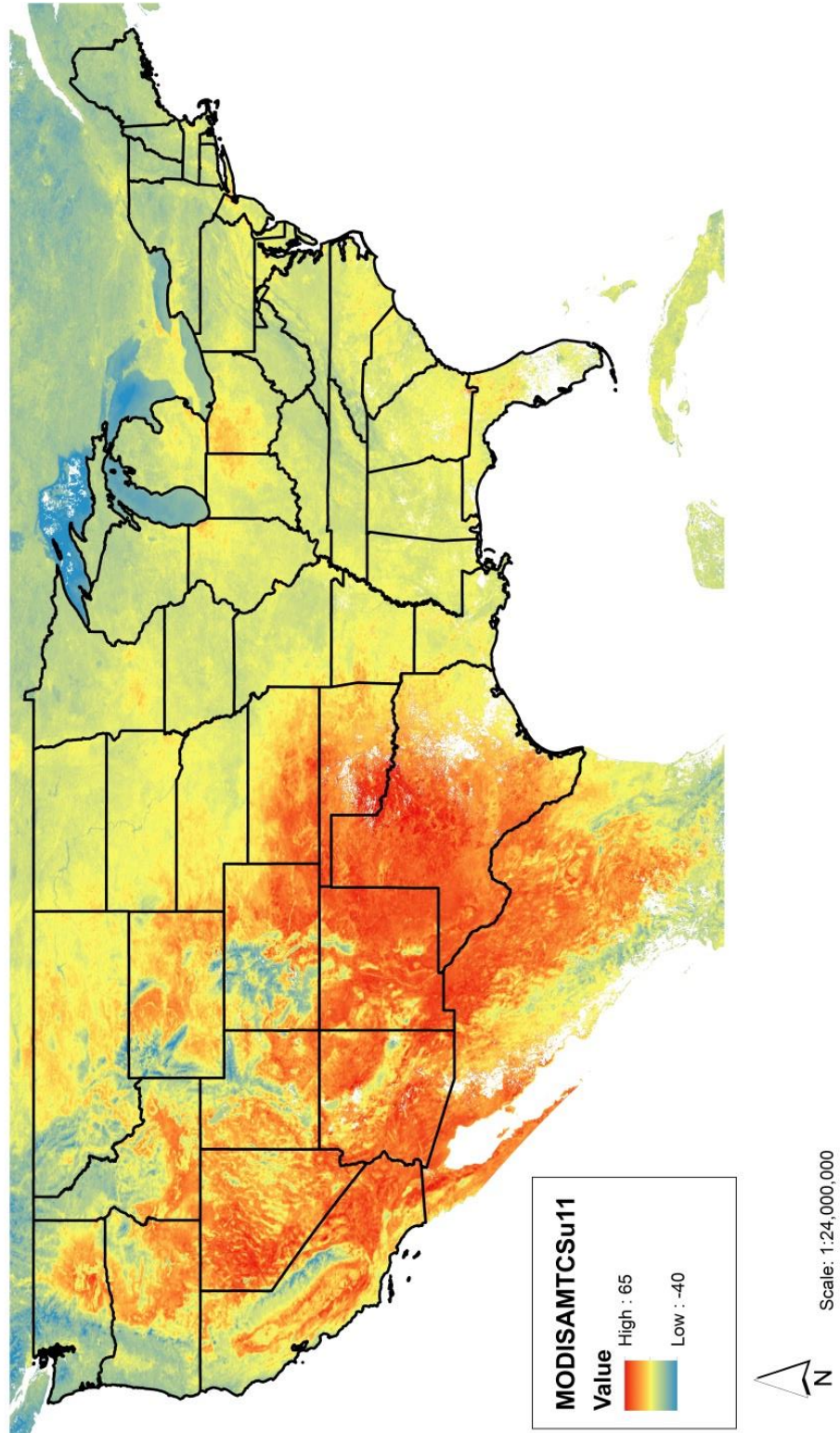


Figure 37: MODIS Land Surface Temperature (LST) and Emissivity, July, 2011 (10:30 am)

July 2011 10:30 pm

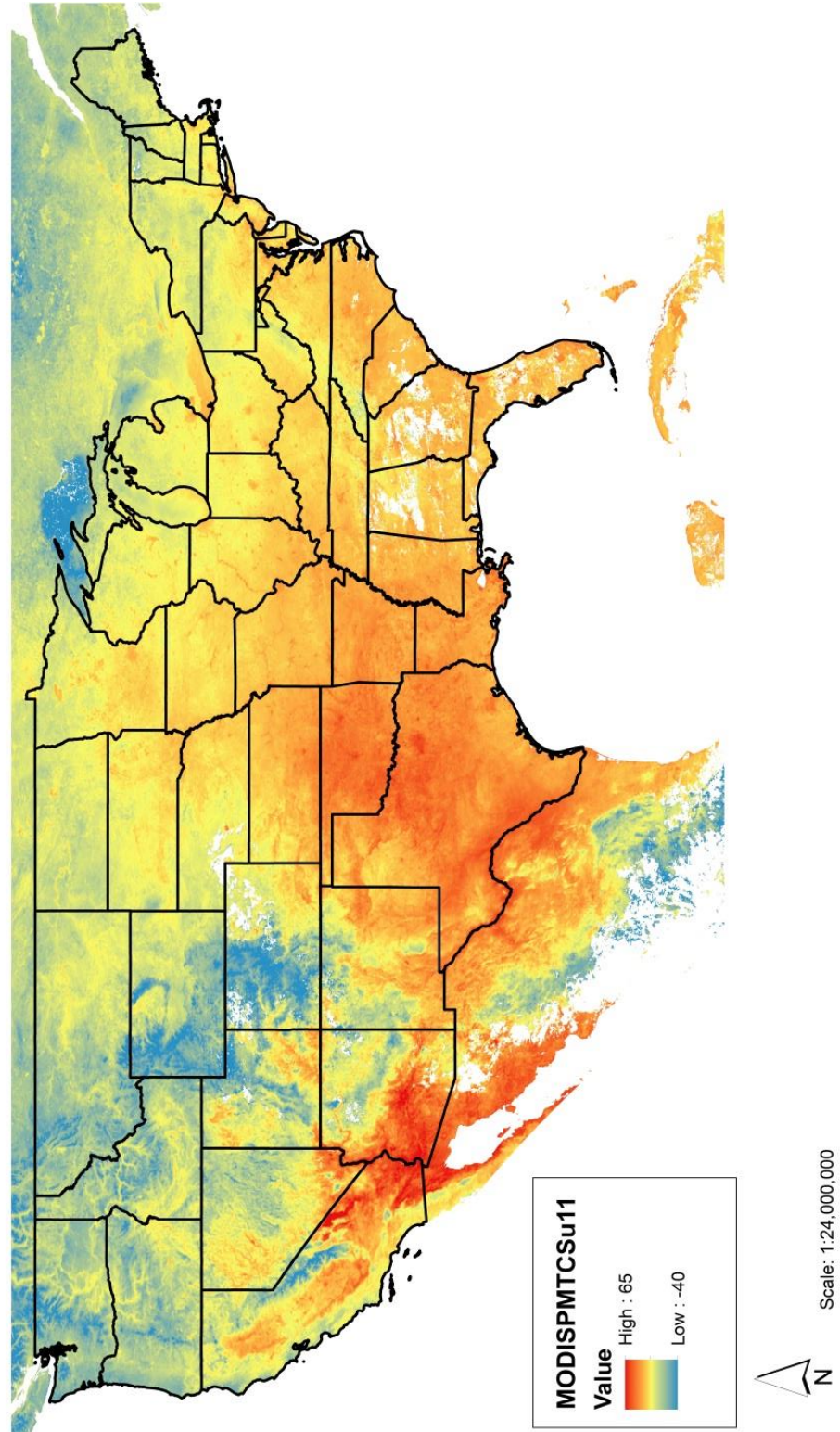


Figure 38: MODIS Land Surface Temperature (LST) and Emissivity, July, 2011 (10:30 pm)

July 2013 10:30 am

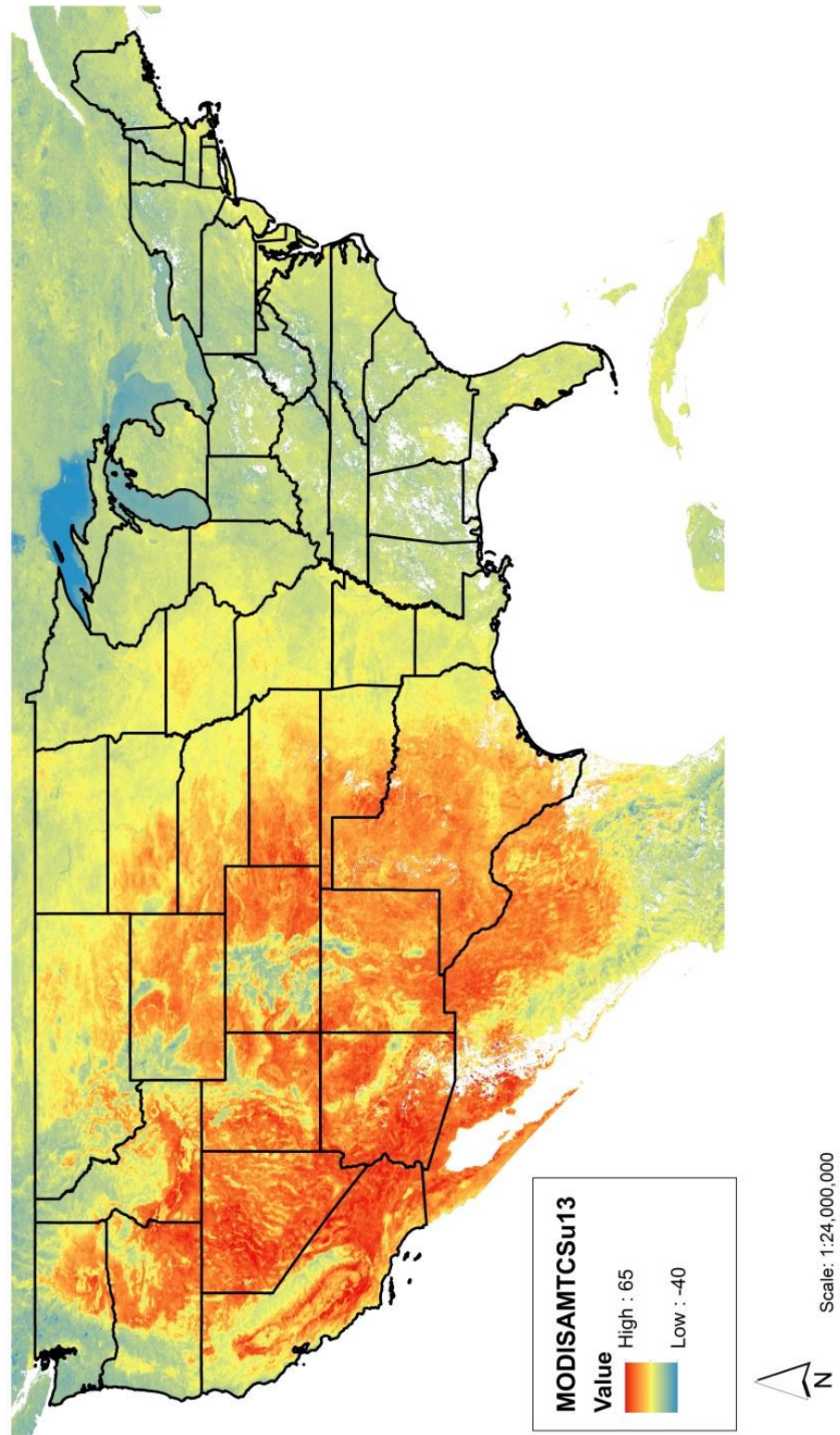


Figure 39: MODIS Land Surface Temperature (LST) and Emissivity, July, 2013 (10:30 am)

July 2013 10:30 pm

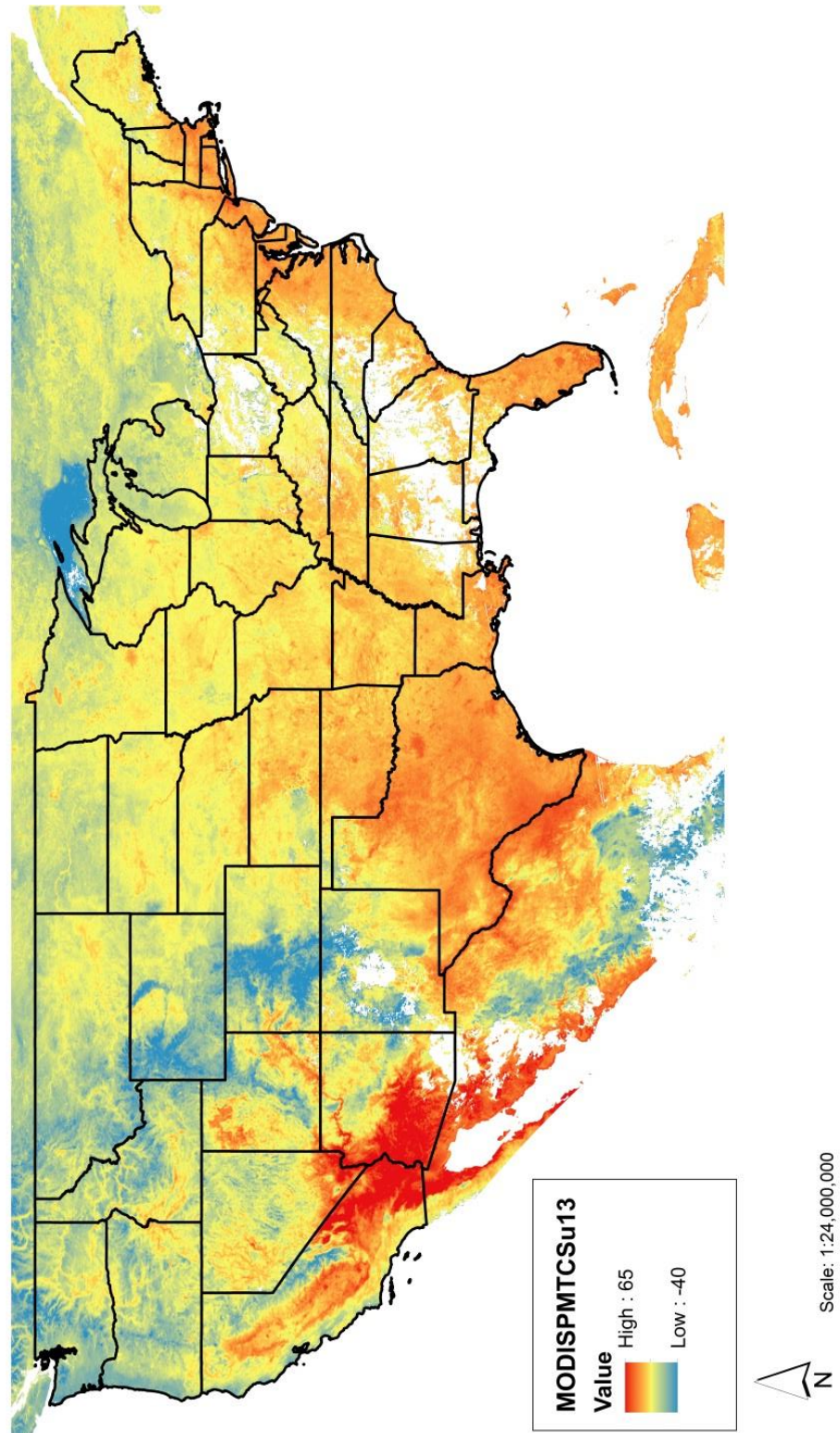


Figure 40: MODIS Land Surface Temperature (LST) and Emissivity, July, 2013 (10:30 pm)

October 2011 10:30 am

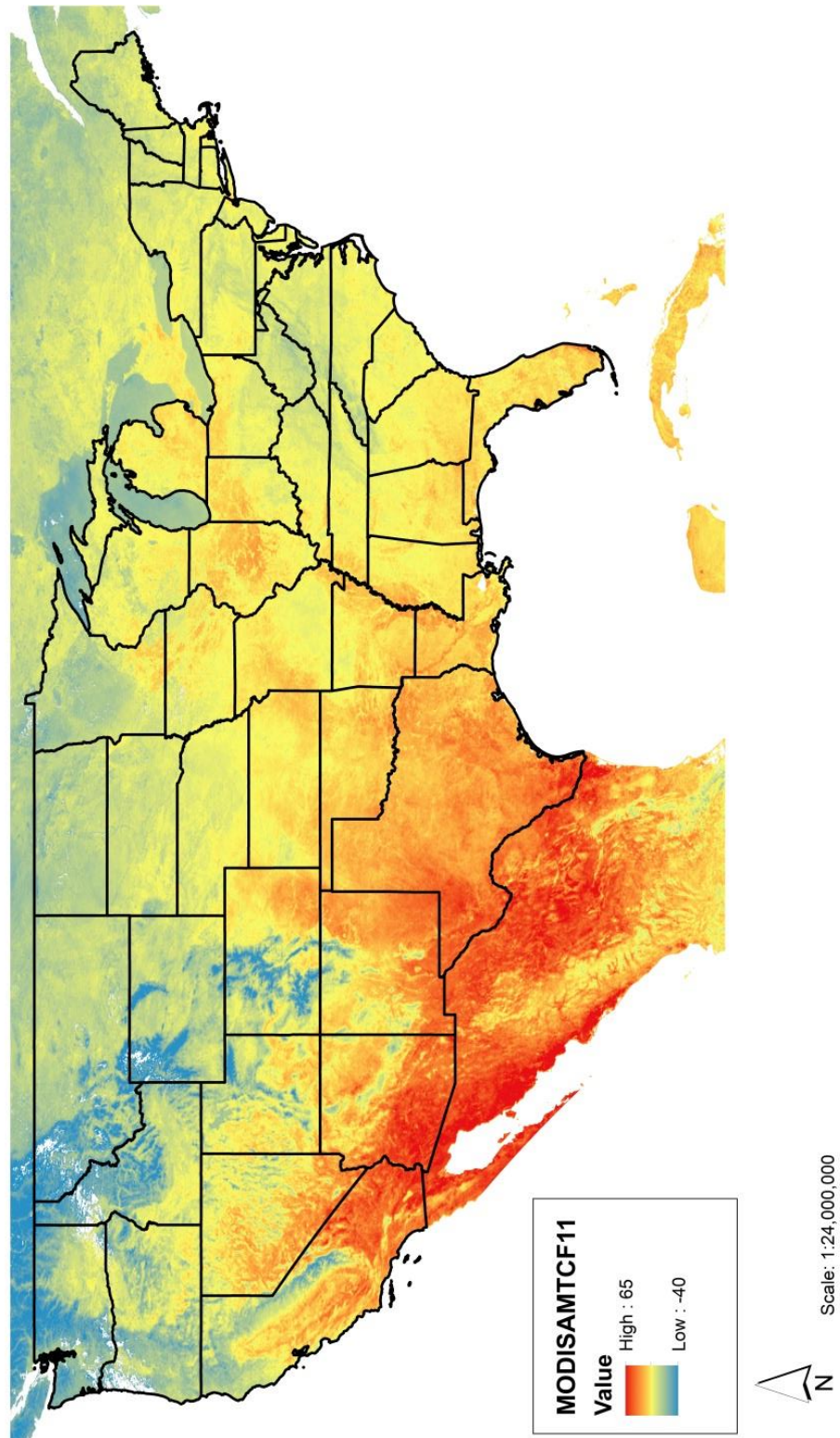


Figure 41: MODIS Land Surface Temperature (LST) and Emissivity, October, 2011 (10:30 am)

October 2011 10:30 pm

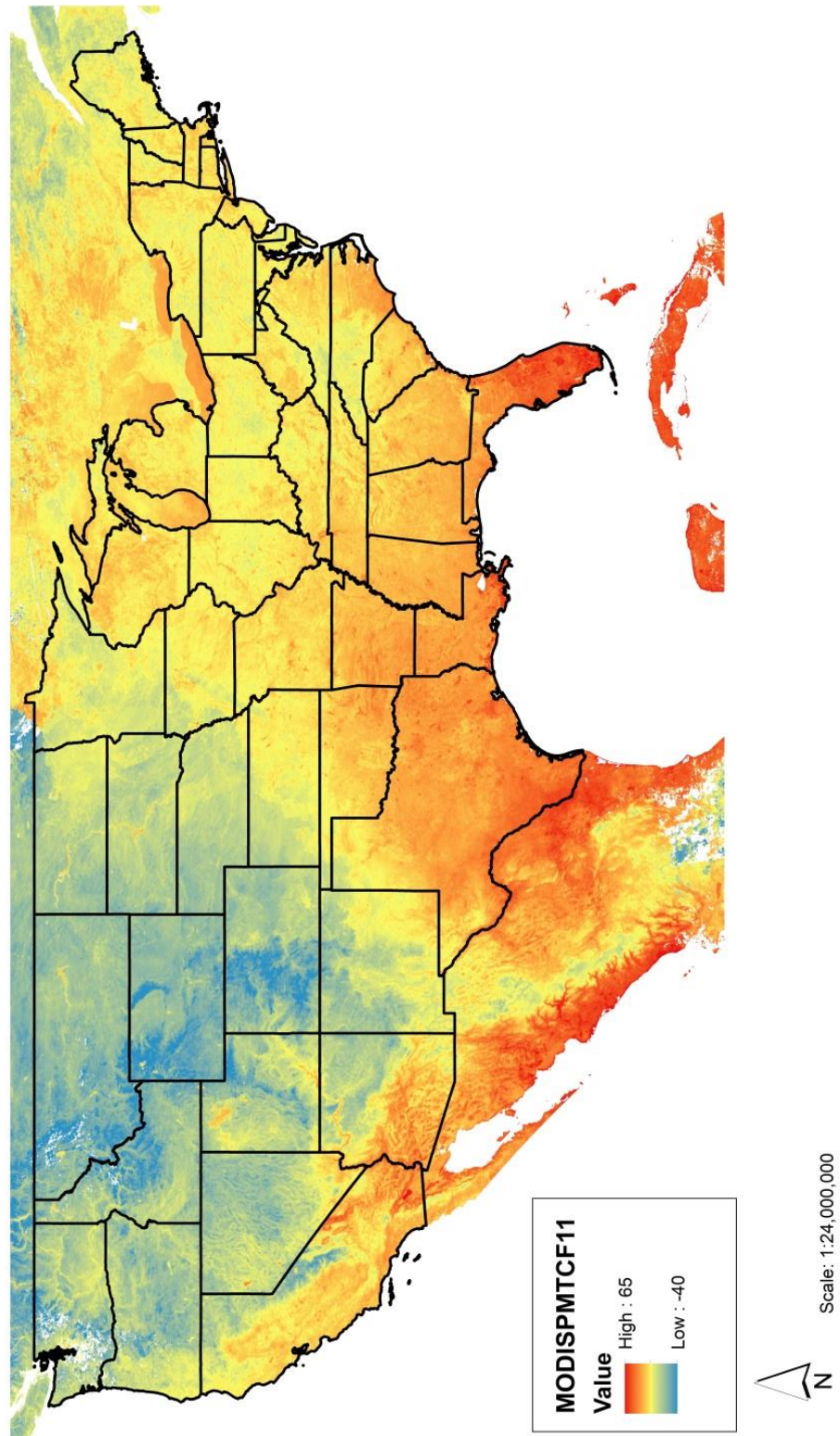


Figure 42: MODIS Land Surface Temperature (LST) and Emissivity, October, 2011 (10:30 pm)

October 2013 10:30 am

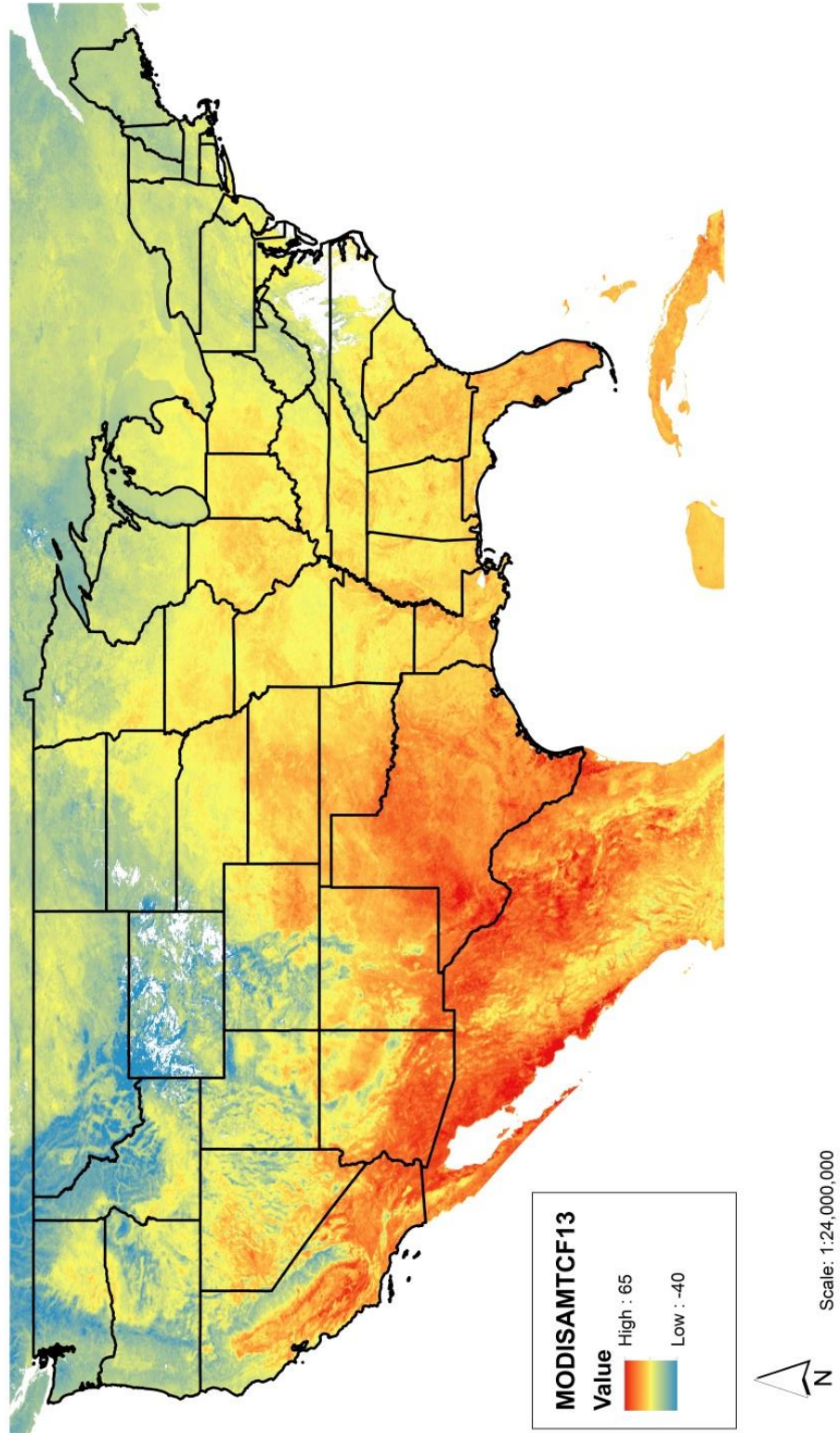


Figure 43: MODIS Land Surface Temperature (LST) and Emissivity, October, 2013 (10:30 am)

October 2013 10:30 pm

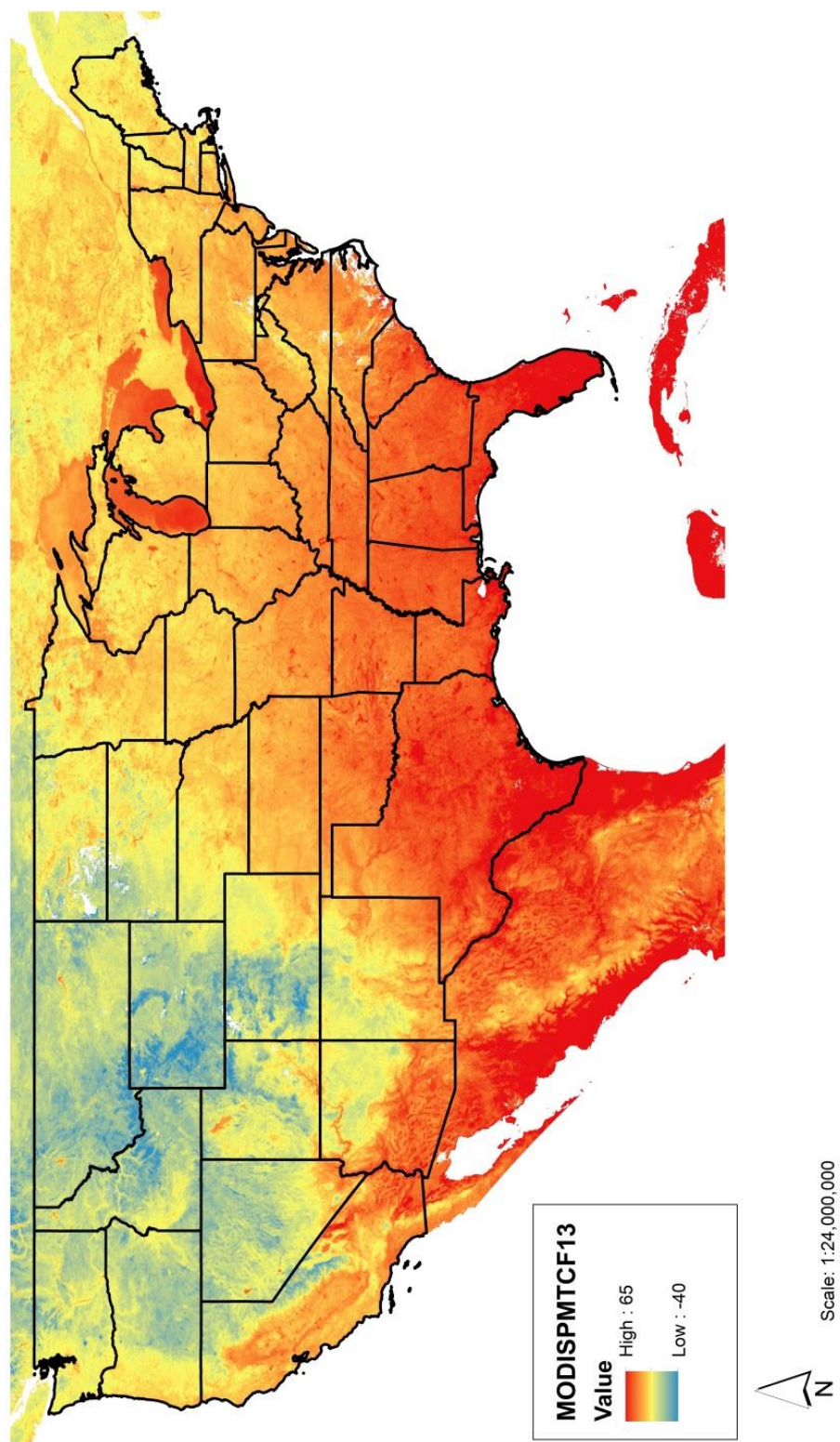


Figure 44: MODIS Land Surface Temperature (LST) and Emissivity, October, 2013 (10:30 pm)

6.3 Weather Station Variables

6.3.1 Obtaining Data from NOAA's NCDC Weather Stations

In order to calculate sensible heat for the conterminous U.S. using the methods outlined in Ma et al (2010), several weather variables were needed: air temperature (drybulb), wetbulb temperature, dewpoint temperature (all in degrees Celsius), relative humidity, and air pressure. Initially, using the state of Arizona as a trial area, weather data were obtained from Weather Underground (Wunderground.com, 2014) for the first days of the month for January, April, July, and October, of 2011 and 2013, and the data were then applied to physiographic areas, obtained from Ameriflux (2002), and loaded into ArcGIS. However, this created unrealistic cut-offs along the physiographic regions' boundary lines. It was then decided that data needed to be obtained from NOAA's National Climate Data Center's weather stations, and these data would be used to estimate the aforementioned weather variables for the conterminous U.S.

NOAA's National Environmental Satellite, Data, and Information Service (NESDIS), as part of NCDC, manages current and historical weather data for the entire U.S. that can easily be downloaded from the Website. For the purpose of this study, published climatological data were accessed for each state. Using the Website, each state was selected from a dropdown menu, for each state there were, on average, 12 different station locations to choose from in the dropdown menu. After choosing a station location, the appropriate month and year were then selected (January, April, July, and October, for 2011 and 2013). However, many stations did not have data for the years 2011 and 2013, so on average, each state only had about four station locations that had the necessary data. After selecting a station location with data for 2011 and 2013 from the dropdown menu, a link was provided which contained a tabular file to be downloaded.

After manually downloading all of the files for all 216 weather stations that had weather data for 2011 and 2013, the necessary weather variable data needed to be obtained. The files contained the necessary weather variable data at different times throughout the day for each day in the month. For the purpose of this study, only weather variable data at approximately 10:30 am and 10:30 pm were obtained (this varied depending on data availability). For each month, the first day of the month was considered, at approximately 10:30 am and 10:30 pm, and data were manually obtained from the files and entered into an Excel spreadsheet. Eight spreadsheets were created for four months, for both years, and included data for all 216 weather stations at 10:30 am and 10:30 pm, with data in degrees Fahrenheit, which simply needed to be converted to degrees Celsius.

After the Excel files were completed, a point layer needed to be created in ArcGIS. This was done by using the latitude and longitude of each weather station location, which was manually entered into the Excel spreadsheets, and the latitude and longitude were then geocoded in the GIS. Eight point layers were created in the GIS using the eight Excel spreadsheets, as shown in *Figure 45: Locations of 216 NCDC Weather Stations*.

6.4.2 Weather Station Variable Data in ArcGIS

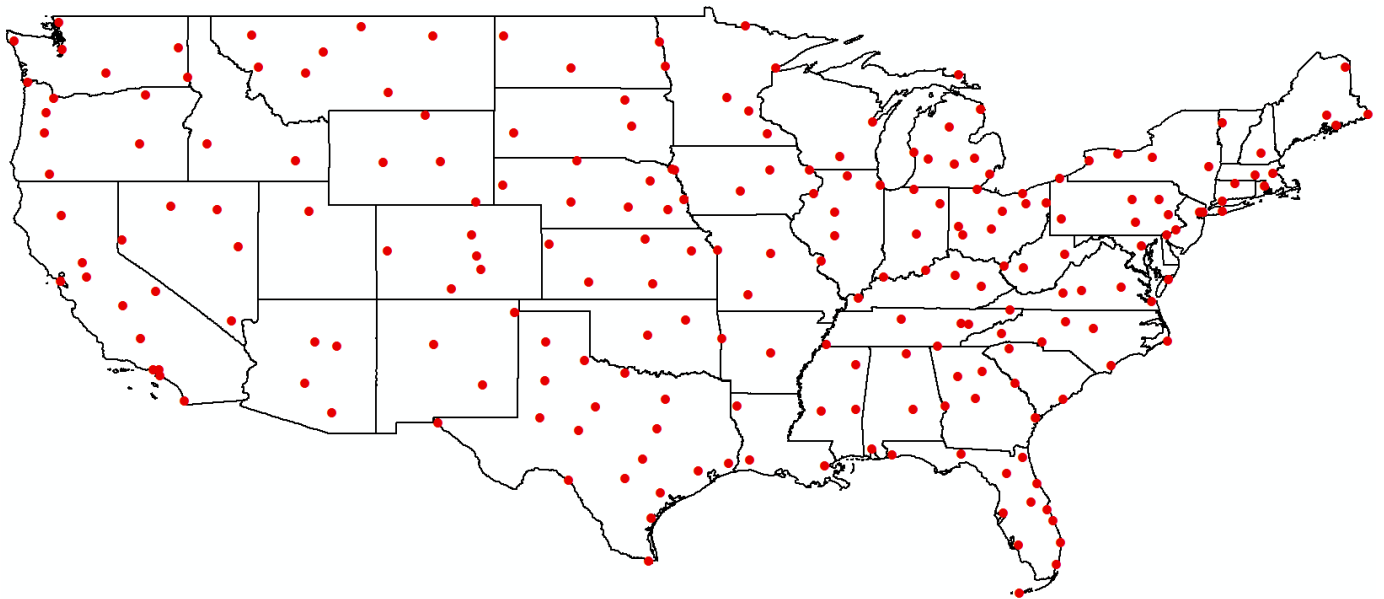


Figure 45: Locations of 216 NCDC Weather Stations

After the point layers were created using the spreadsheets with the data obtained from NCDC, the data associated with each of the 216 points needed to be used to estimate values for the entire U.S. This was done simply by using the Kriging function in ArcToolbox in ArcGIS. Before performing the interpolation, the weather station point layers needed to be reprojected to the Sinusoidal projection so that the layers were in-line with the projection used in the MODIS satellite imagery representing surface temperature values, and the state boundary layer representing the boundaries for all 48 conterminous states (obtained from USGS).

After the point layers were reprojected, the Kriging method of interpolation could then be performed. To do this, the weather station point layer was selected, along with the particular weather station variable from the attribute table (to represent the z value). The cell size was specified to match the resolution of the MODIS satellite imagery (926.6254331), and under the

“environments” tab, the processing extent (which was the state boundary layer) was then selected to limit the processing area. This was done for all five variables (air temperature, wetbulb temperature, dewpoint temperature, relative humidity, and station pressure), for both 2011 and 2013, for four months, both 10:30 am and 10:30 pm. After performing the Kriging method of interpolation, 80 raster layers were created that would then be used to calculate sensible and latent heat; four of which can be found in *Figure 46: Air Temperature Interpolation* though *Figure 50: Relative Humidity Interpolation*.

Summer 2013 10:30 AM Air Temperature

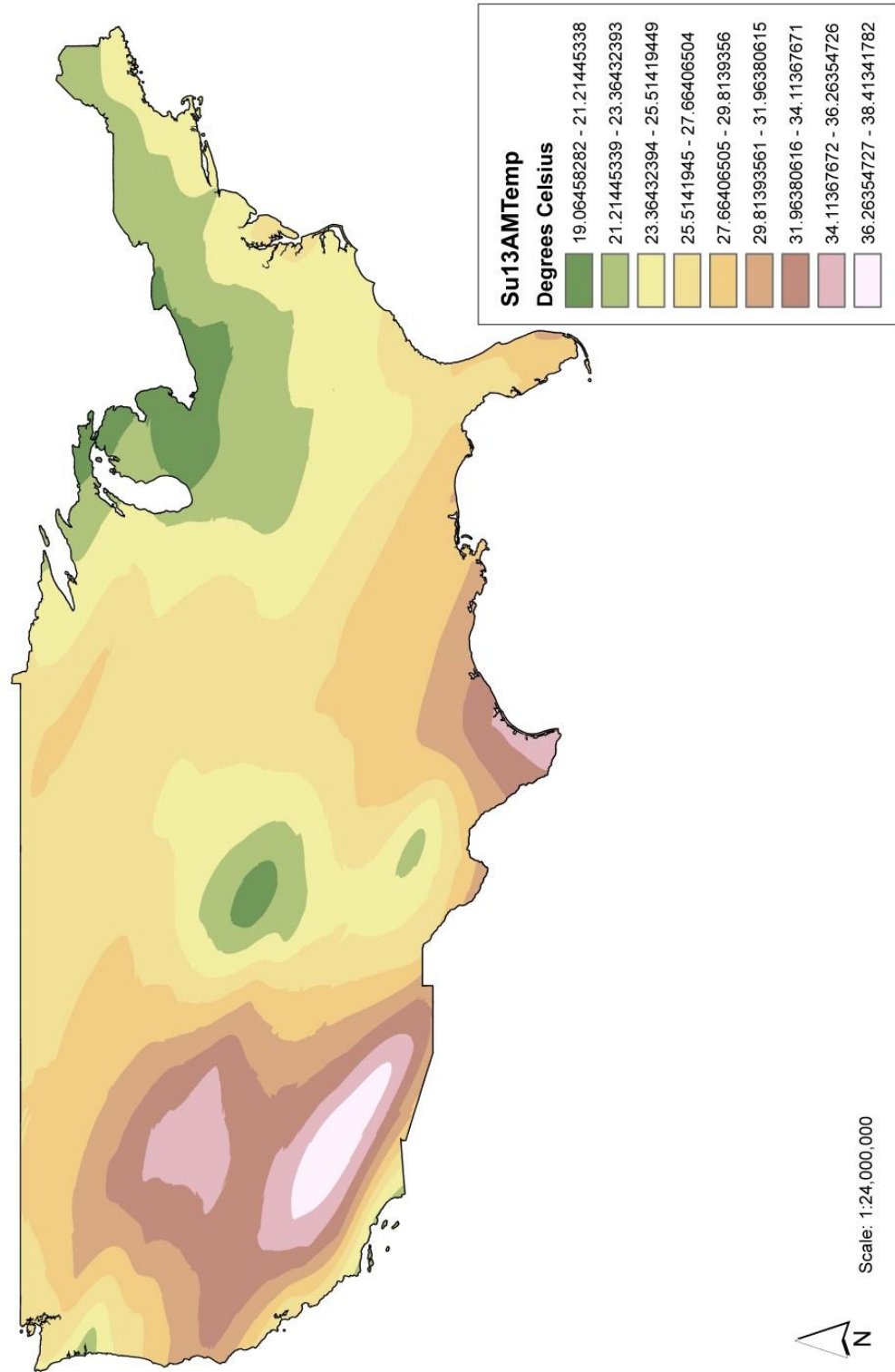


Figure 46: Air Temperature Interpolation

Summer 2013 10:30 AM Dewpoint Temperature

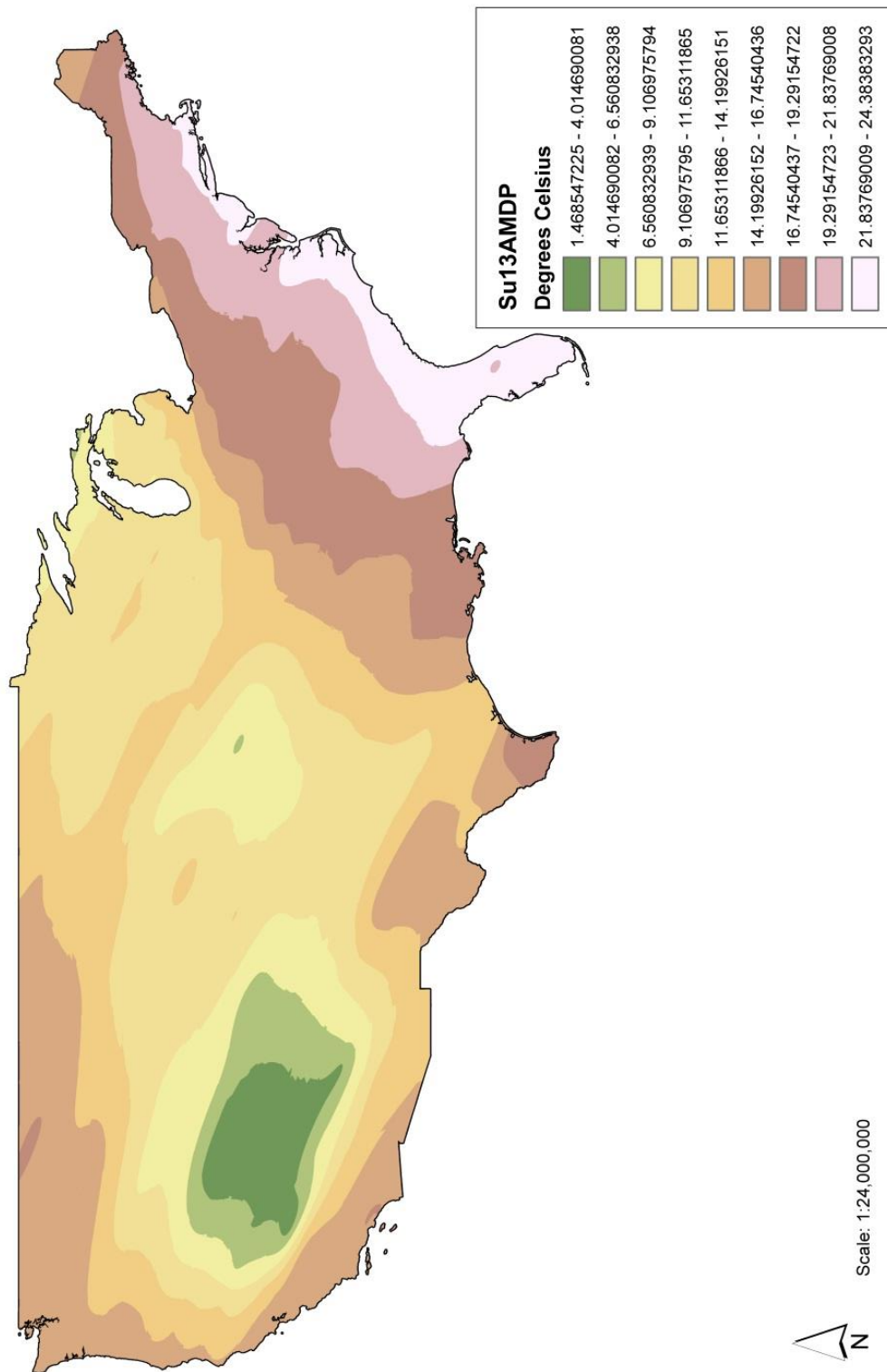


Figure 47: Dewpoint Temperature Interpolation

Summer 2013 10:30 AM Wetbulb Temperature

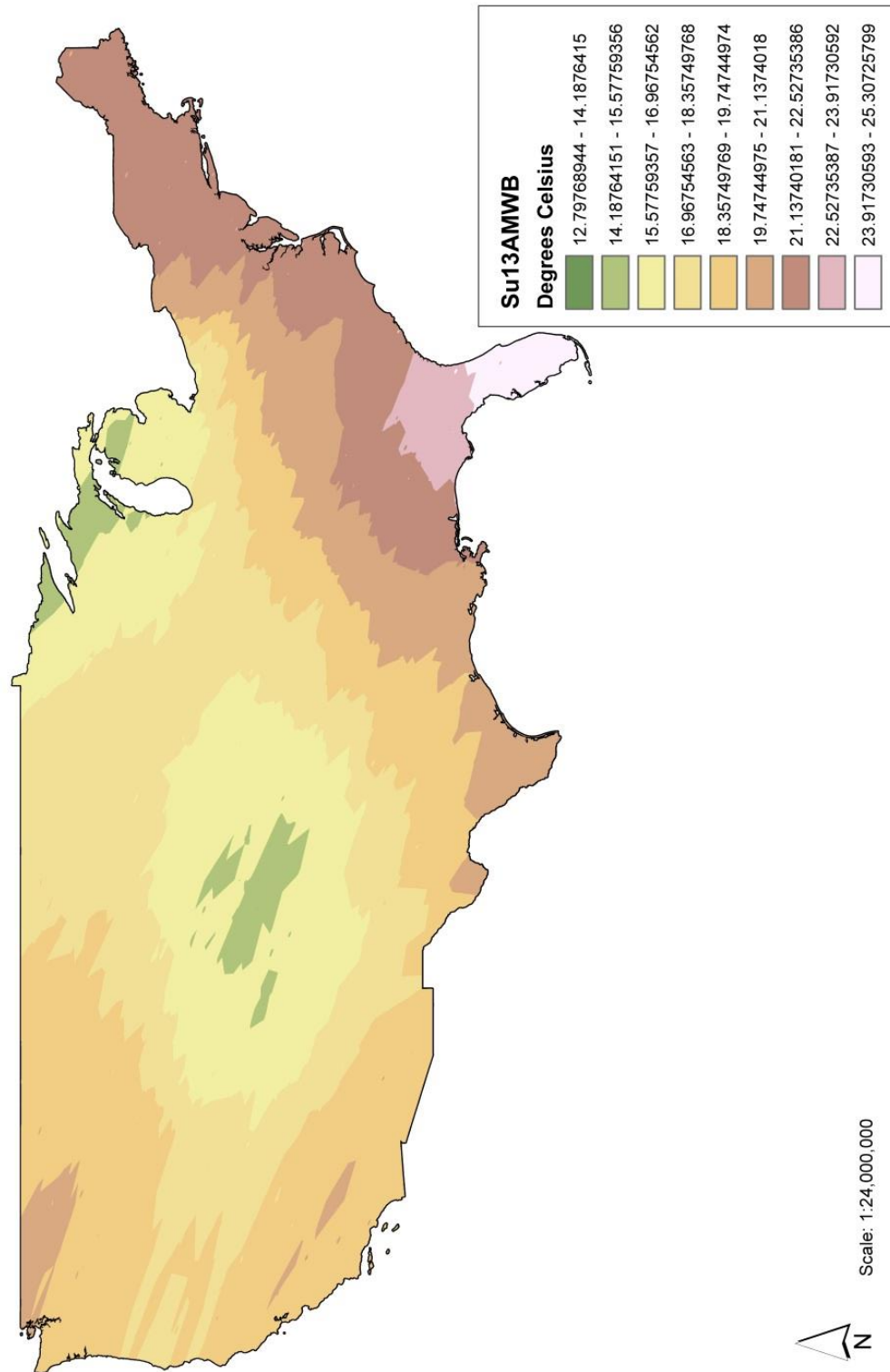


Figure 48: Wetbulb Temperature Interpolation

Summer 2013 10:30 AM Weather Station Pressure

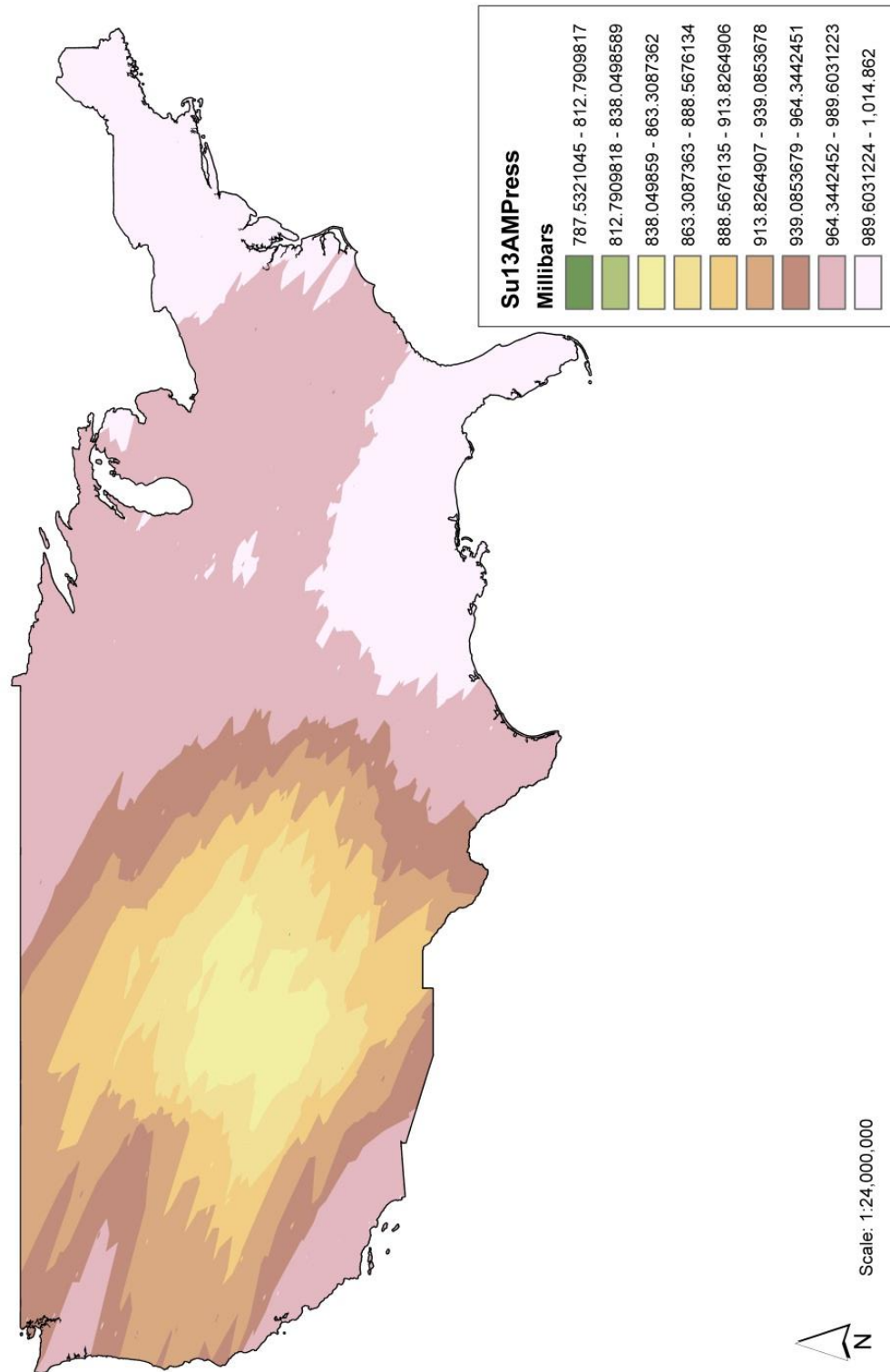


Figure 49: Weather Station Pressure Interpolation

Summer 2013 10:30 AM Relative Humidity

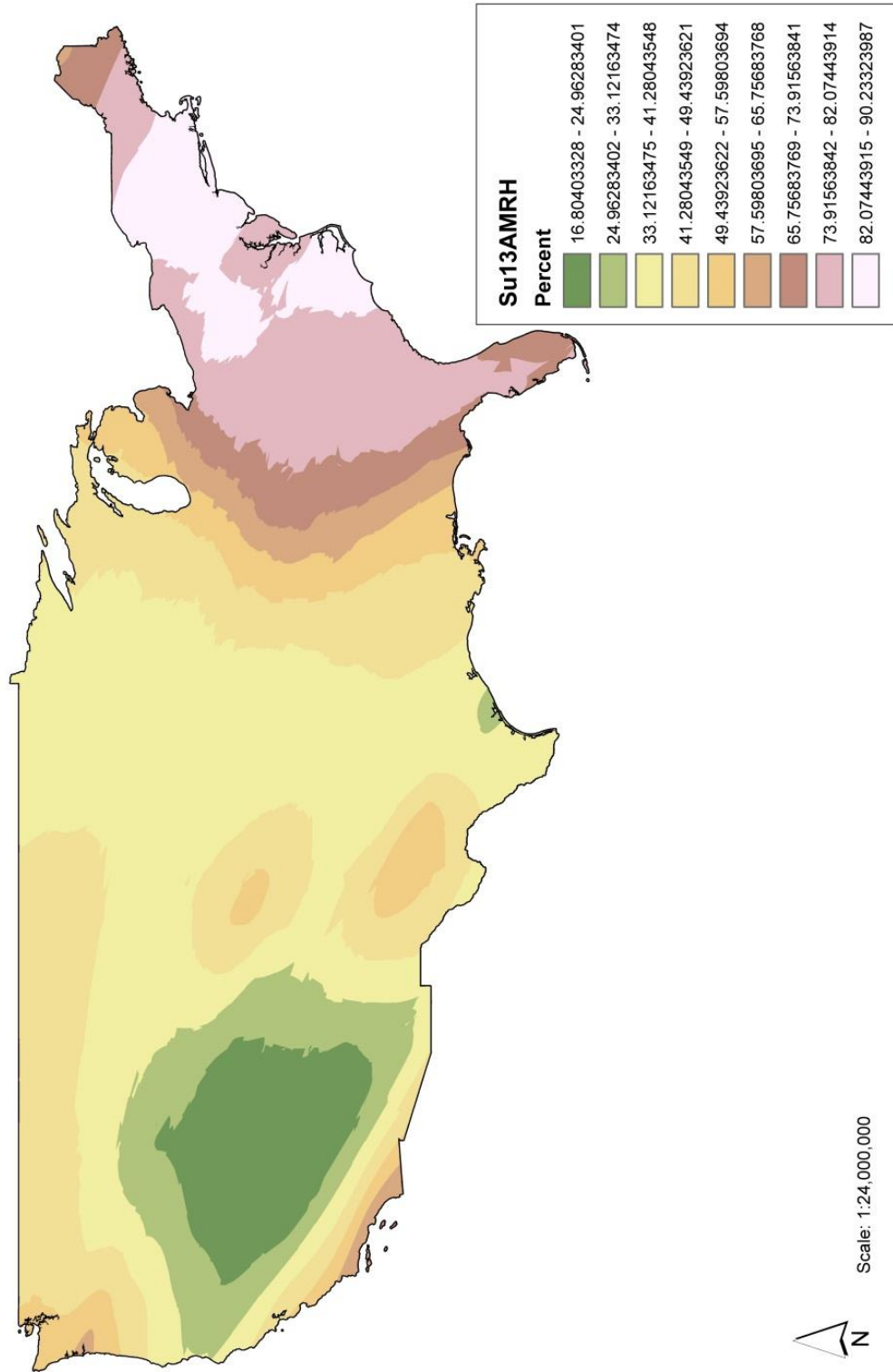


Figure 50: Relative Humidity Interpolation

6.4 Calculation of Sensible and Latent Heat Flux

Due to the fact that concentrated wind systems, like the SoV, rely on the existence of convection, which occurs naturally when solar-heated air at the ground level is warmer than the air directly above it, it was necessary to calculate sensible and latent heat to find potential locations for future systems. The methods used for calculating sensible and latent heat were obtained from two studies by Ma et al (2010 and 2013). Both studies used similar methods for calculating heat flux in the Tibetan Plateau. Both studies also incorporated the use of in-situ data and MODIS satellite imagery in order to calculate sensible and latent heat.

For this study, as was the case in both Ma et al studies, it was necessary to calculate sensible and latent heat values over a heterogeneous landscape. The methods used in Ma et al (2010) were such that calculated sensible and latent heat values when using MODIS data along with surface layer data in areas with vast differences in landscape attributes were compared with sensible and latent heat values calculated from lower resolution MODIS and atmospheric boundary layer data in areas with similar landscape attributes to determine whether these methods resulted in values that were closer to those obtained in in-situ data. The formulas used to calculate sensible and latent heat using surface layer data and MODIS data in this study were obtained from Ma et al (2010).

For this study, as was the case with Ma et al (2013), in-situ values for sensible and latent heat flux in a heterogeneous landscape were compared with MODIS satellite imagery data. The methods used in this study for obtaining and comparing temporal distributions in heat flux for a variety of landscapes were obtained from Ma et al (2013). As in this study, Ma et al (2013) used MODIS data from January, April, July, and October to represent the four seasons. Sensible and latent heat values were then calculated using a specified set of equations. These results were then

compared with results from using in-situ data to derive sensible heat values at morning and evening, which was also performed in this study.

The methods used to calculate sensible heat were based off of methods used in Ma et al (2010), and required the use of the MODIS surface temperature data, and the weather station variable data in order to calculate sensible heat values at one kilometer resolution. It was determined that the calculations could be done solely using ArcGIS using the Raster Calculator tool. In order to perform the necessary calculations, the following variables as show in *Table 5: Variables Needed for Sensible and Latent Heat Calculation*, were needed:

Table 5: Variables Needed for Sensible and Latent Heat Calculation

Variable	Variable Meaning
α	unit-less constant, with value of 1.28
c_p	air specific heat at constant pressure, approximately $1005 \text{ J kg}^{-1} \text{ K}^{-1}$ (Jia et al. 2003)
D	drying power of air
Δ	slope of the saturation vapor pressure deficit at the air temperature
e_0	vapor pressure in the surface layer nearby the surface
e_a	vapor pressure at the reference height
E_a	actual evapotranspiration
E_s	equilibrium evapotranspiration
E_p	potential evapotranspiration
ϕ	relative humidity
G	soil heat flux
γ	Psychrometric constant
H	sensible heat flux
λ	latent heat of vaporization
M_d	molar mass of dry air
M_v	molar mass of vapor
p	actual air pressure
p_d	partial pressure of dry air
p_{sat}	saturation pressure of water vapor at air temperature
p_{sat}^*	saturation pressure of water vapor at wet-bulb temperature
p_v	partial pressure of water vapor
ρ	air density
R	universal gas constant, $8.31447 \text{ J/(mol K)}$
r_{as}	aerodynamic resistance for vapor transfer between the land surface and the reference height
r_{ah}	aerodynamic resistance for heat transfer between the land surface and the reference height
R_n	net radiation flux
T_0	land surface temperature, in $^{\circ}\text{C}$ (from MODIS data)
T_a	air temperature at the reference height (dry bulb temperature), in $^{\circ}\text{C}$ (from weather station data)
T^*	wet-bulb temperature, in $^{\circ}\text{C}$ (from weather station data)
T_d	dewpoint temperature, in $^{\circ}\text{C}$ (from weather station data)

6.4.1 Gamma Calculation

The initial variable needed for the calculation was Gamma, or the Psychrometric constant, which was calculated using the following equation:

$$\gamma = 0.00066(1 + 0.00115T^*)$$

Where T^* represents wetbulb temperature in degrees Celsius, obtained from the weather station data.

6.4.2 Delta Calculation

Delta, or the slope of the saturation vapor pressure deficit at air temperature, was calculated with the following formula:

$$\Delta = \frac{dp_{sat}}{dT_a} = d(6.11 \times 10^{\left(\frac{7.5 \times T_a}{273.3 + T_a}\right)}) / dT_a = 25032.575295 \times 10^{\frac{7.5T_a}{273.3 + T_a}} \times \frac{1}{(273.3 + T_a)^2}$$

Where T_a represents the air temperature at the reference height in degrees Celsius, which was obtained from the weather station data.

6.4.3 p_{sat}^* and VPD Calculation

The following two formulas were obtained from *Principles of Environmental Physics*, (J. L. Monteith & M. H. Unsworth. Edward Arnold, Sevenoaks. 2nd edition, 1990):

p_{sat}^* , or the saturation pressure of water vapor at wet-bulb temperature was calculated using the following formula:

$$p_{sat}^* = 6.11 \times 10^{\left(\frac{7.5 \times T_a}{273.3 + T_a}\right)}$$

Where T_a , is air temperature, which was obtained from weather station data, and measured in degrees Celsius. The result was calculated in millibars and converted to kilopascals.

VPD, or vapor pressure deficit, was calculated using the following formula:

$$VPD = (1 - (\varphi / 100)) * p_{sat}^*$$

Where φ , or relative humidity, is obtained from weather station data, and p_{sat}^* was calculated in the previous equation. The result is measured in millibars and converted to kilopascals.

6.4.4 p_v Calculation

p_v , or the partial pressure of water vapor, was calculated using the following formula:

$$p_v = 6.11 \times 10^{\left(\frac{7.5 \times T_d}{273.3 + T_d}\right)}$$

Where T_d represents the dewpoint temperature in degrees Celsius, which was obtained from weather station data, and the result was measured in millibars.

6.4.5 p_d Calculation

p_d , or the partial pressure of dry air, was calculated using the following formula:

$$p_d = p - p_v$$

Where p is actual pressure recorded at a measuring station, which was obtained from the station pressure interpolation layer, and p_v was calculated previously.

6.4.6 ρ Calculation

ρ , or air density, was calculated using the following formula:

$$\rho = \frac{p_d M_d + p_v M_v}{RT_a}$$

$$M_d = 28.964 \text{ gm/mol}$$

$$M_v = 18.016 \text{ gm/mol}$$

$$R = 8.31447 \text{ J/mol}\cdot\text{k}$$

Where p_d and p_v were calculated previously; T_a is air temperature, in degrees Celsius, obtained from weather station data; the constant, M_d , is the molar mass of dry air, measured in grams per mole; the second constant, M_v , is the molar mass of vapor, measured in grams per mole; and the third constant, R , is the universal gas constant, which is measured in Joules per mole kilogram.

6.4.7 Sensible Heat Calculation

Using the previous formulas, along with two additional variables, sensible heat was calculated using the following formula:

$$H = \rho c_p \frac{T_0 - T_a}{r_{ah}}$$

$$c_p = 1005 \text{ Joules per kilogram Kelvin}$$

$$r_{ah} = 80 \text{ for a.m. / } 200 \text{ for p.m.}$$

Where ρ , or air density, was calculated previously; the constant c_p is the air specific heat at constant pressure; T_0 is surface temperature, in degrees Celsius, obtained from MODIS; T_a is air temperature, obtained from weather station data; and the constant r_{ah} is the aerodynamic resistance for heat transfer between land and surface at the reference height, which varies depending on the time considered for the calculation (morning or night). The result is measured in watts per meter square.

r_{ah} was determined by analysis of Ameriflux sites for differing land cover type classes, and represents how easily heat can leave a surface, with lower resistance resulting in heat leaving a surface faster. It is a function of atmospheric stability, wind speed, and surface roughness. It decreases with an increase in wind speed and an increase in surface roughness, and conversely, it increases with an increase in stability (Powell, 2003).

The completed sensible heat models can be found in *Figure 51: Sensible Heat Flux, January, 2011 (10:30 am)* through *Figure 66: Sensible Heat Flux, October, 2013 (10:30 pm)*.

January 2011 10:30 am

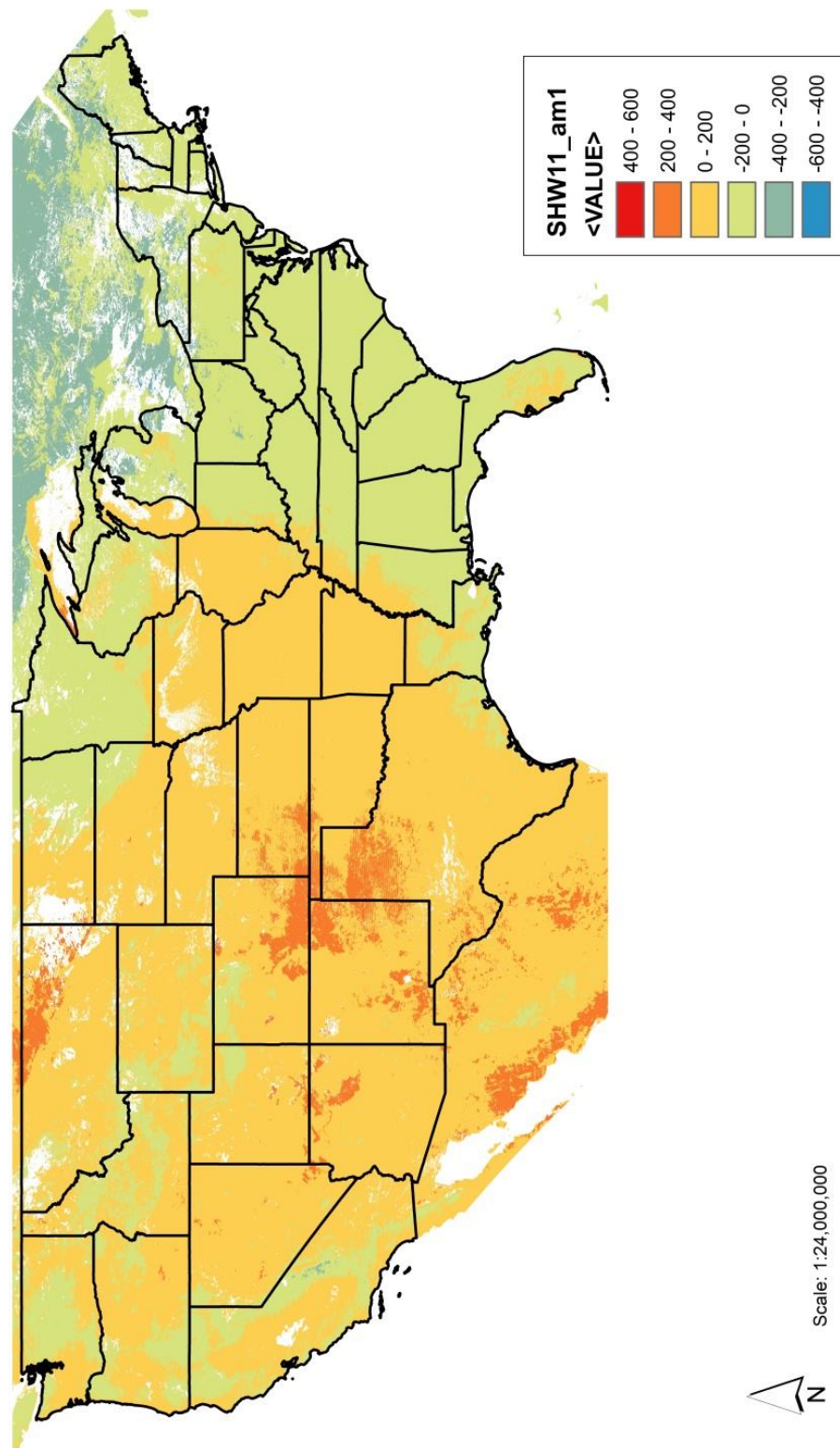


Figure 51: Sensible Heat Flux, January, 2011 (10:30 am)

January 2011 10:30 pm

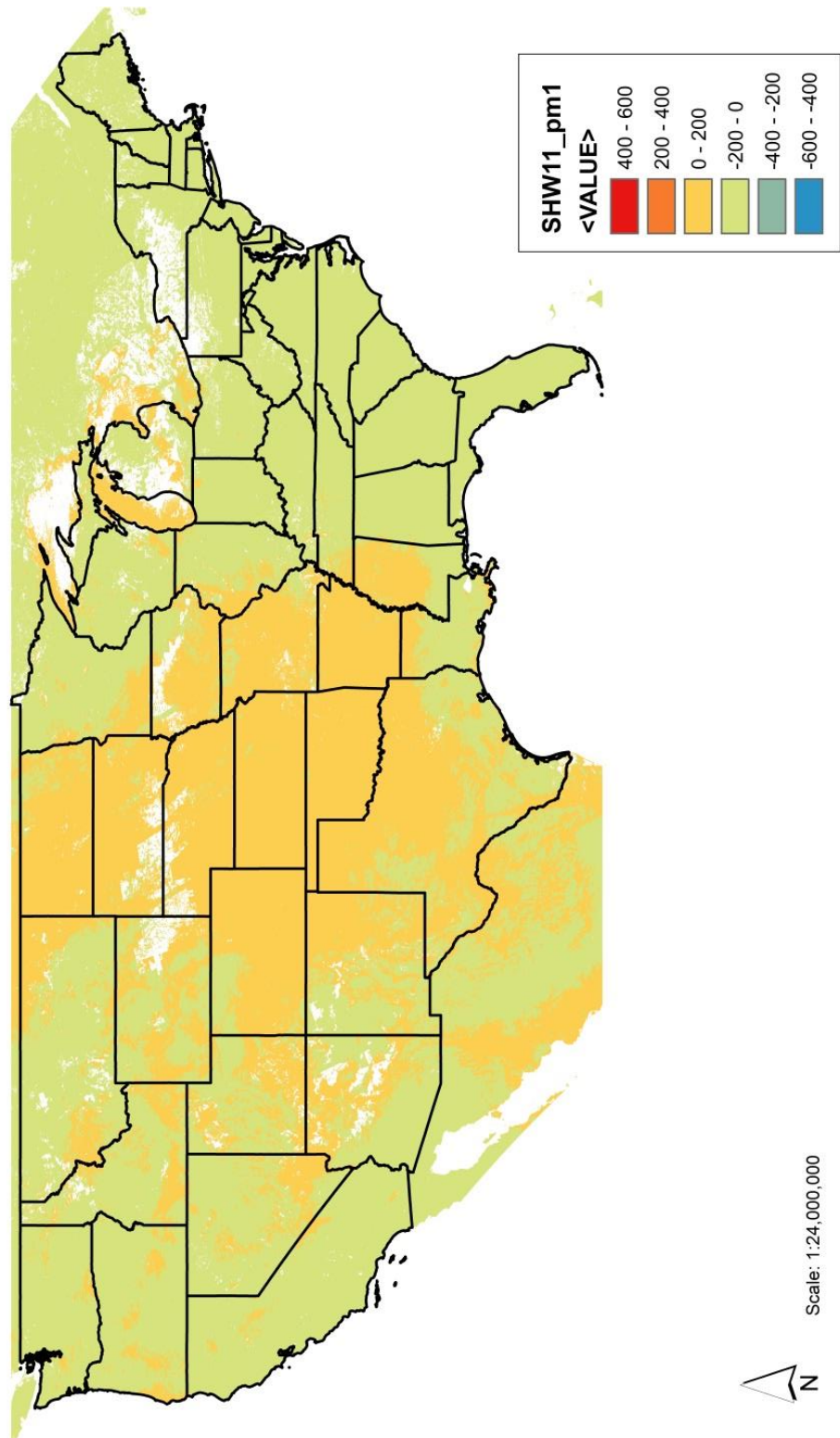


Figure 52: Sensible Heat Flux, January, 2011 (10:30 pm)

January 2013 10:30 am

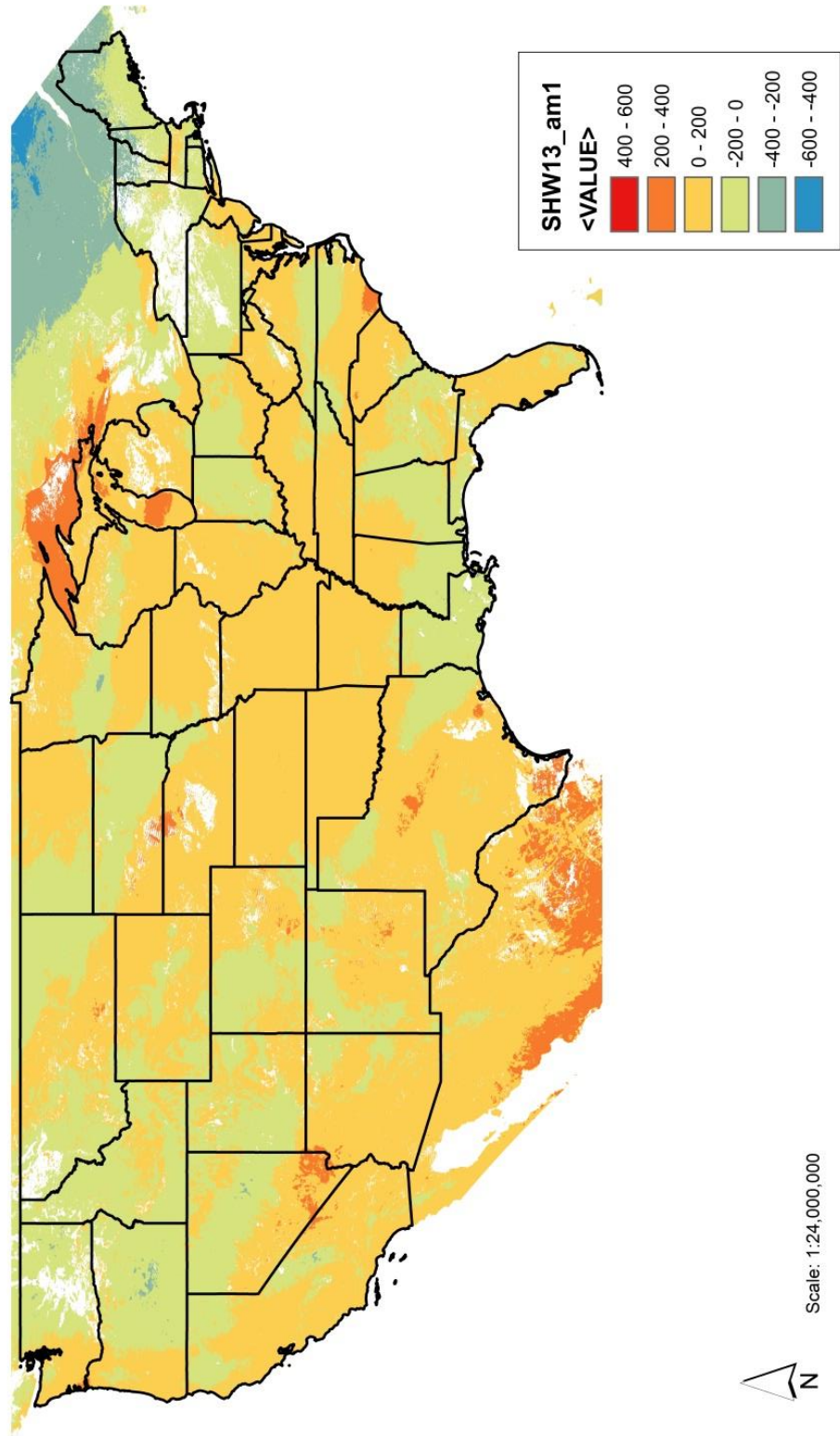


Figure 53: Sensible Heat Flux, January, 2013 (10:30 am)

January 2013 10:30 pm

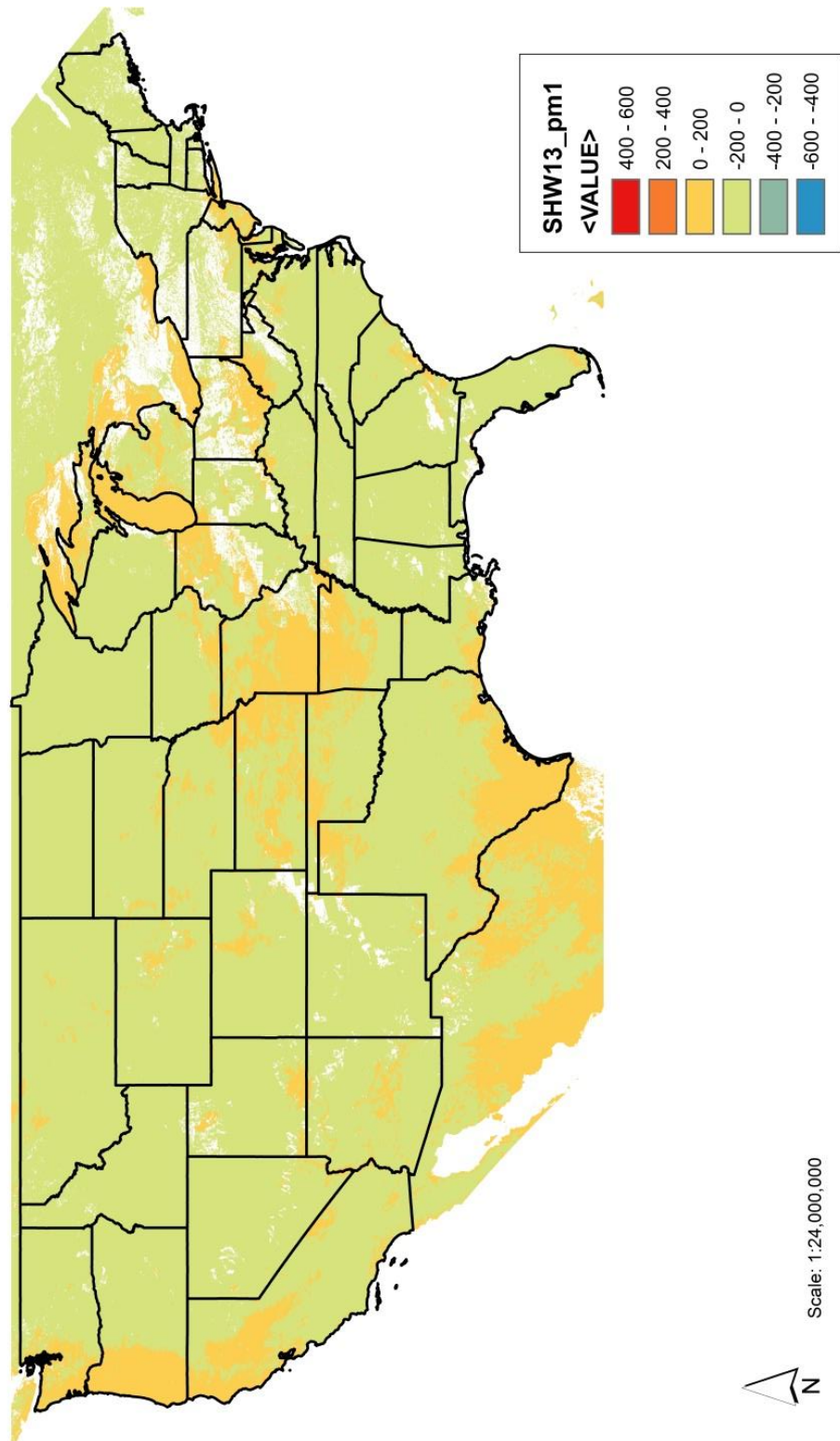


Figure 54: Sensible Heat Flux, January, 2013 (10:30 pm)

April 2011 10:30 am

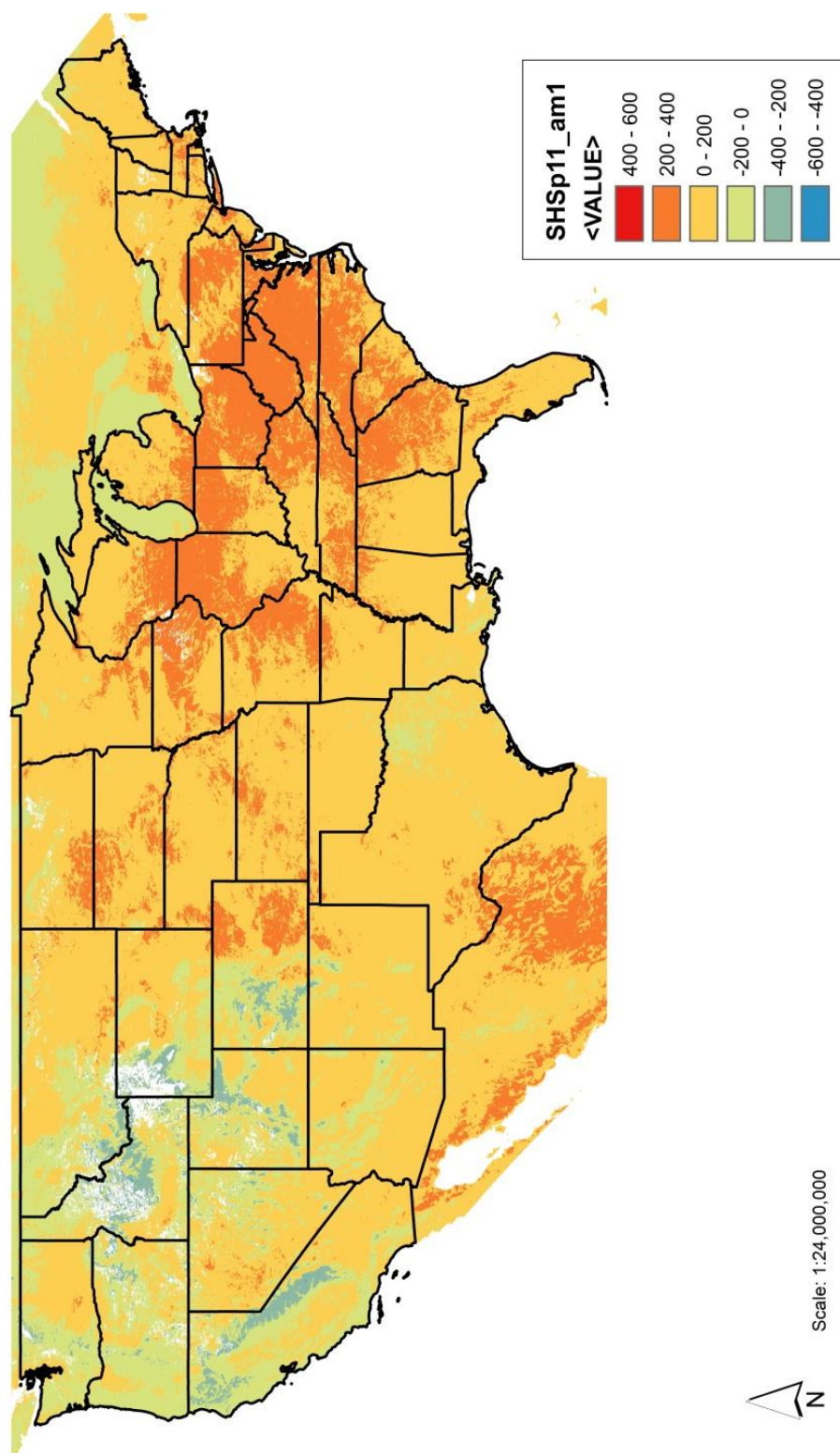


Figure 55: Sensible Heat Flux, April, 2011 (10:30 am)

April 2011 10:30 pm

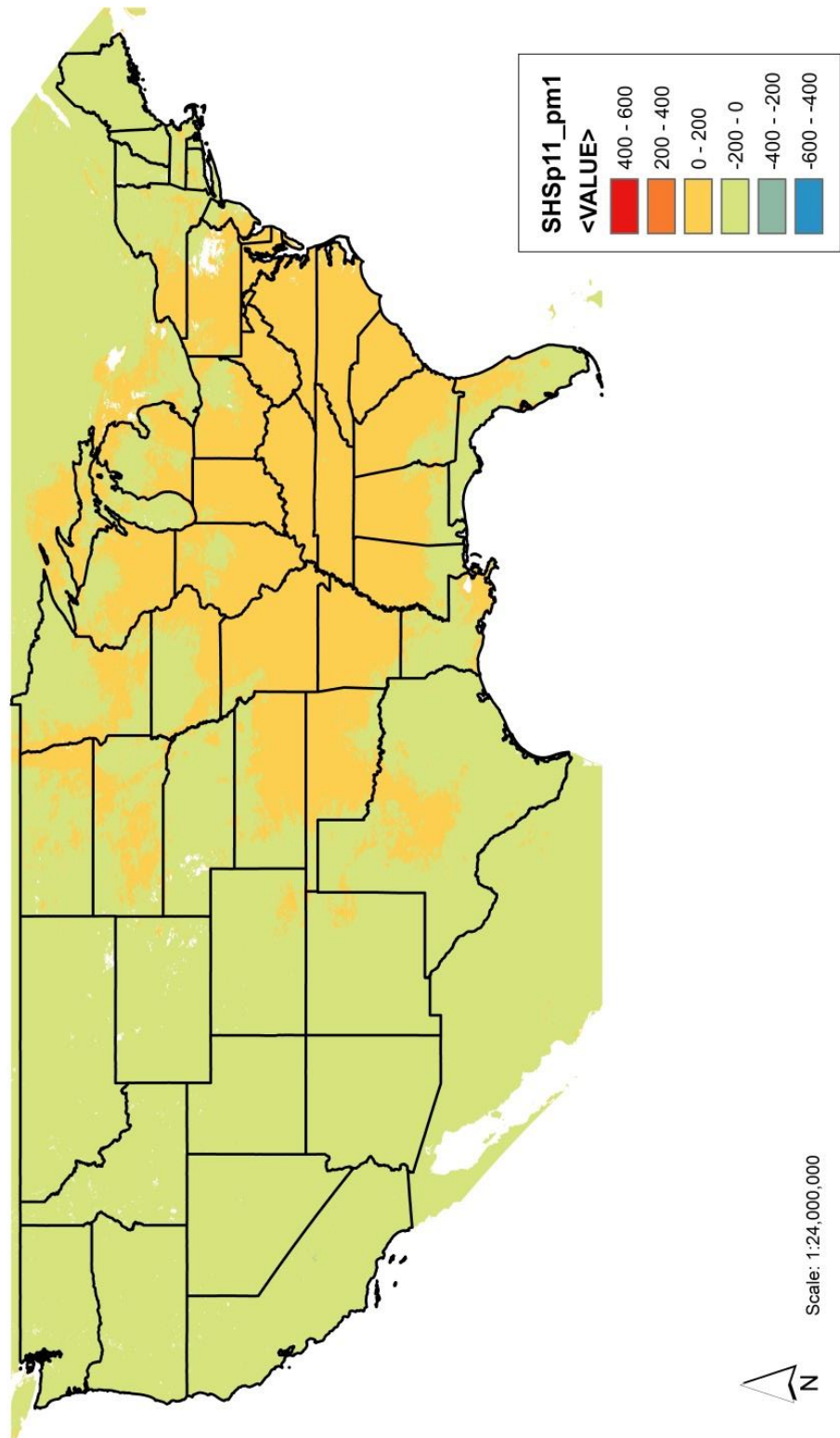


Figure 56: Sensible Heat Flux, April, 2011 (10:30 pm)

April 2013 10:30 am

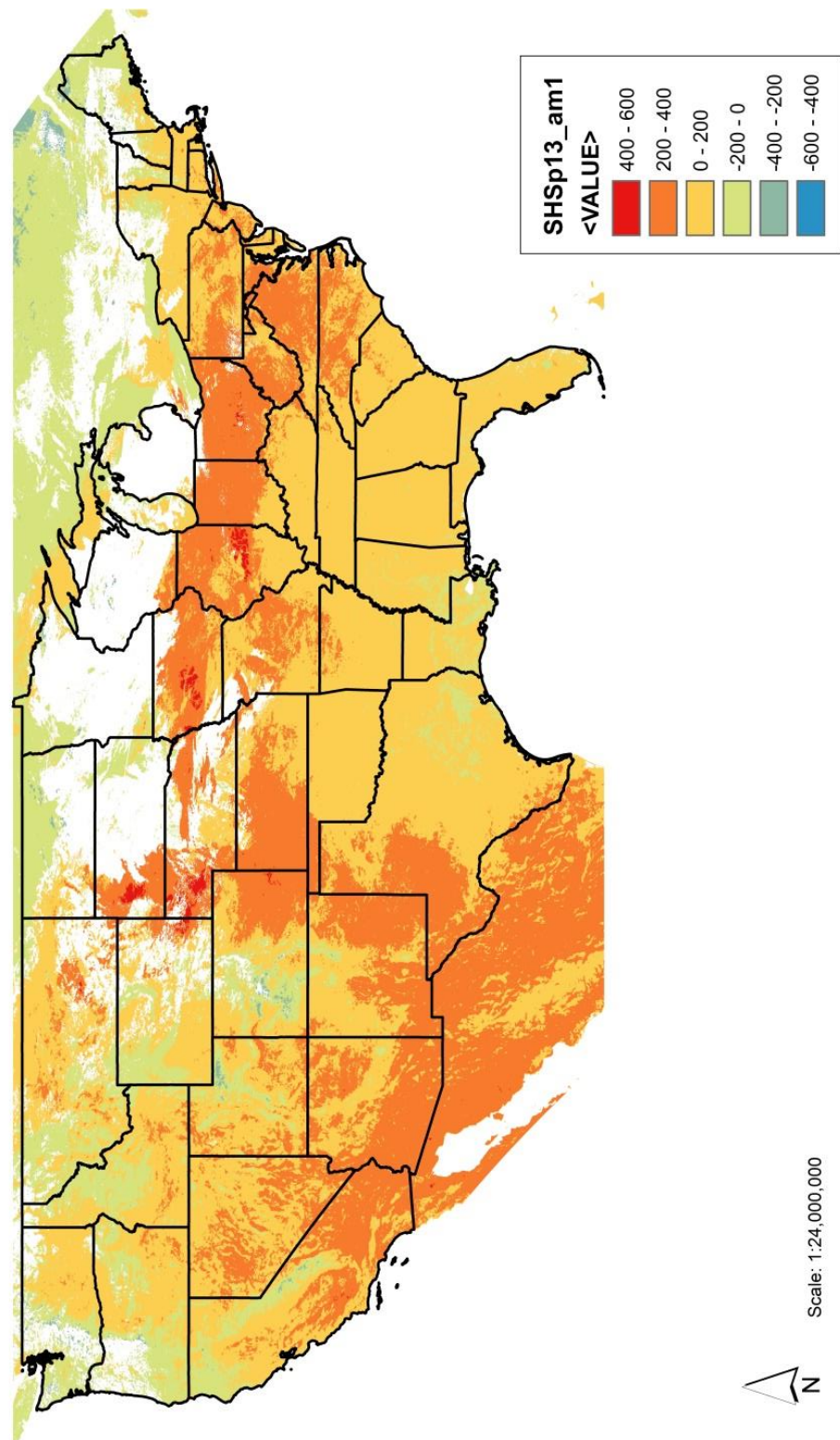


Figure 57: Sensible Heat Flux, April, 2013 (10:30 am)

April 2013 10:30 pm

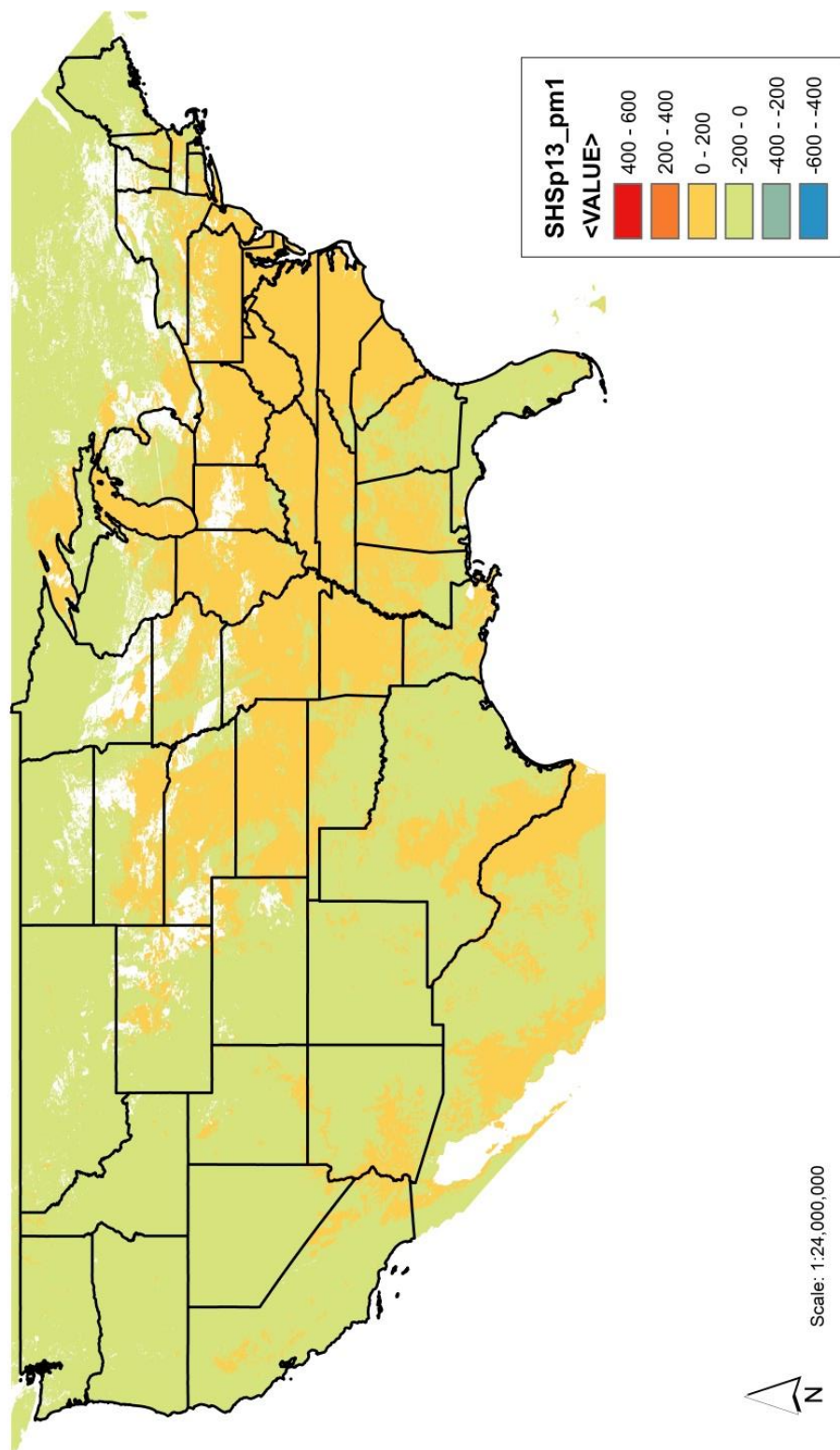


Figure 58: Sensible Heat Flux, April, 2013 (10:30 pm)

July 2011 10:30 am

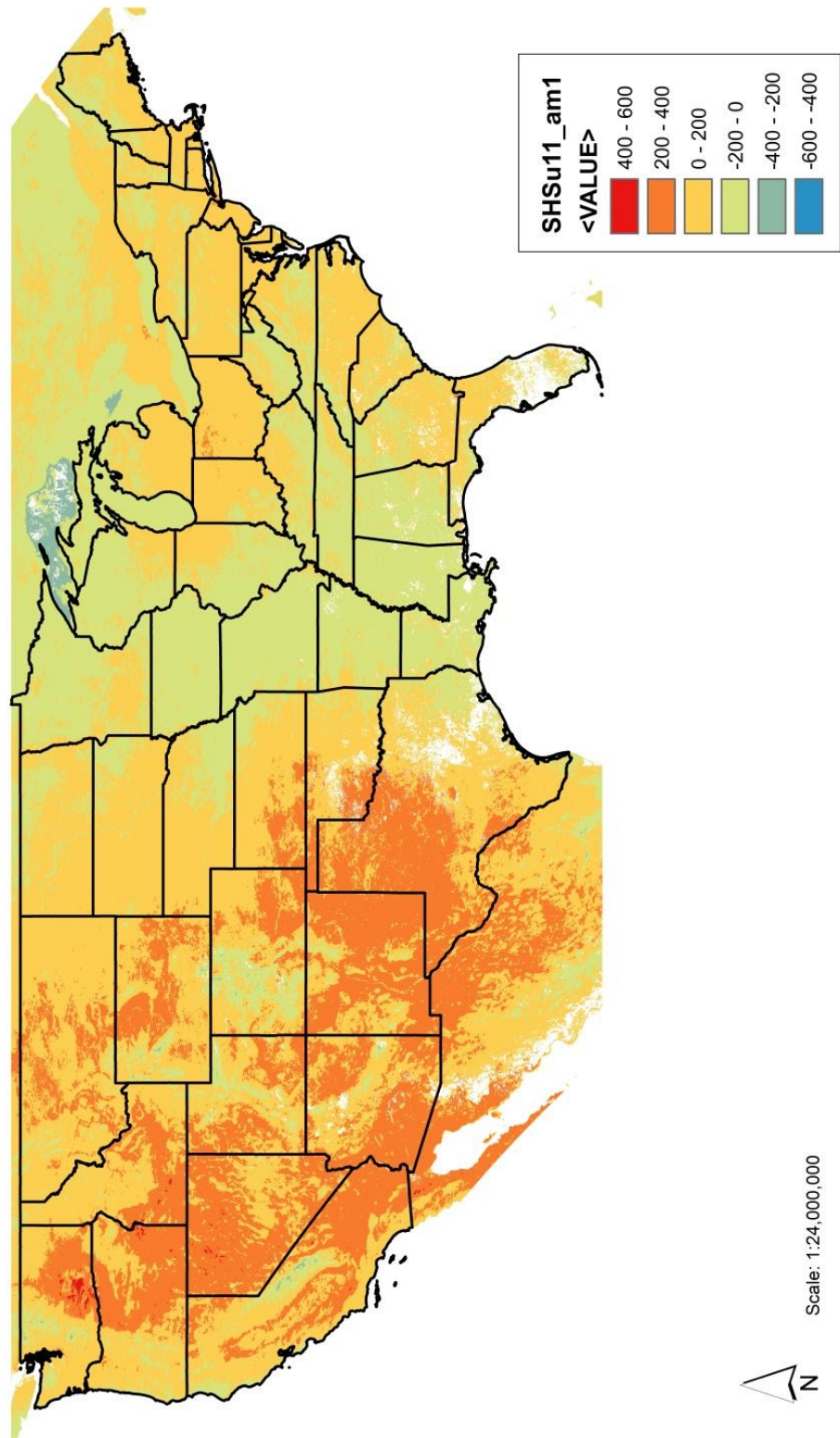


Figure 59: Sensible Heat Flux, July, 2011 (10:30 am)

July 2011 10:30 pm

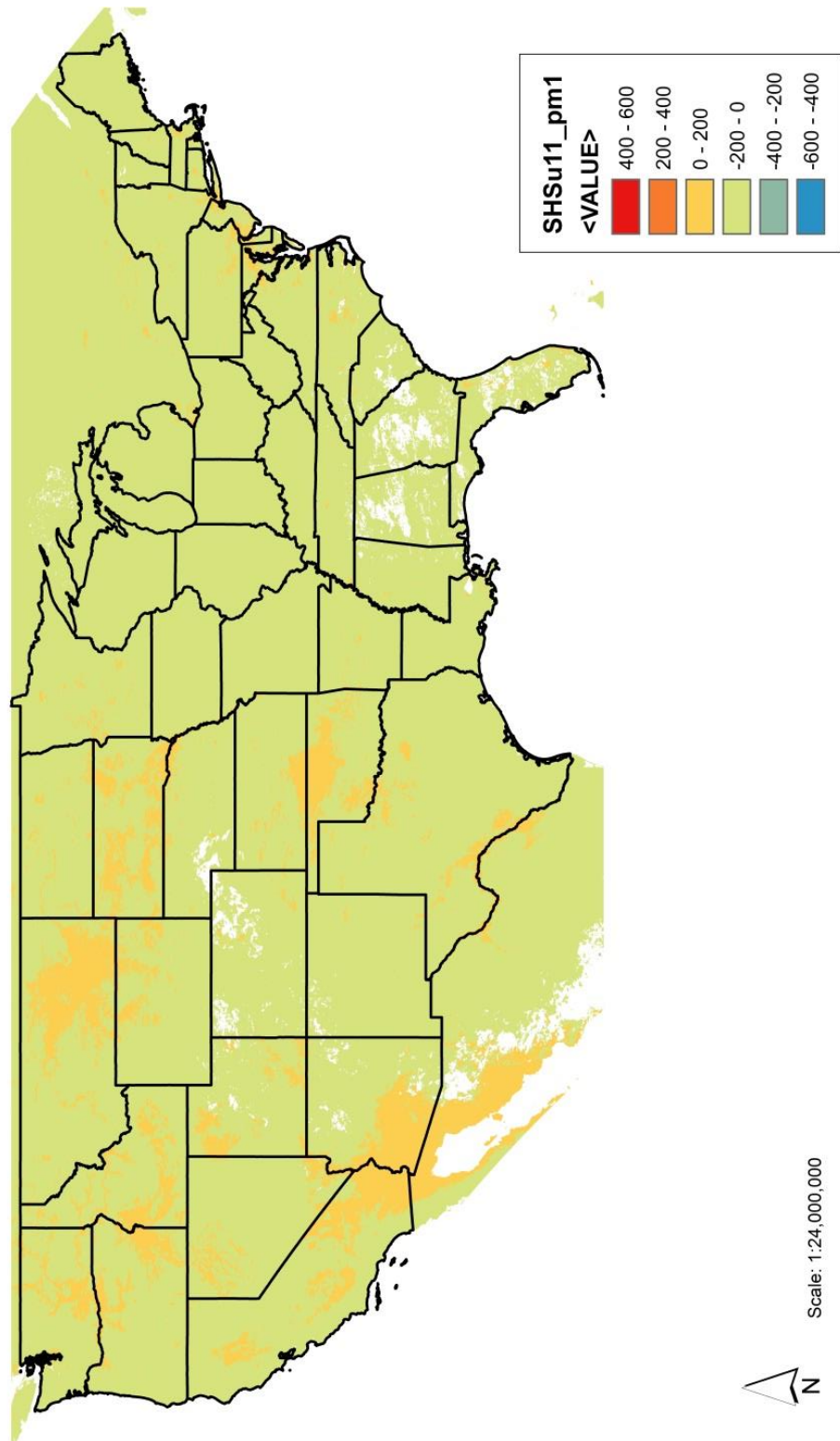


Figure 60: Sensible Heat Flux, July, 2011 (10:30 pm)

July 2013 10:30 am

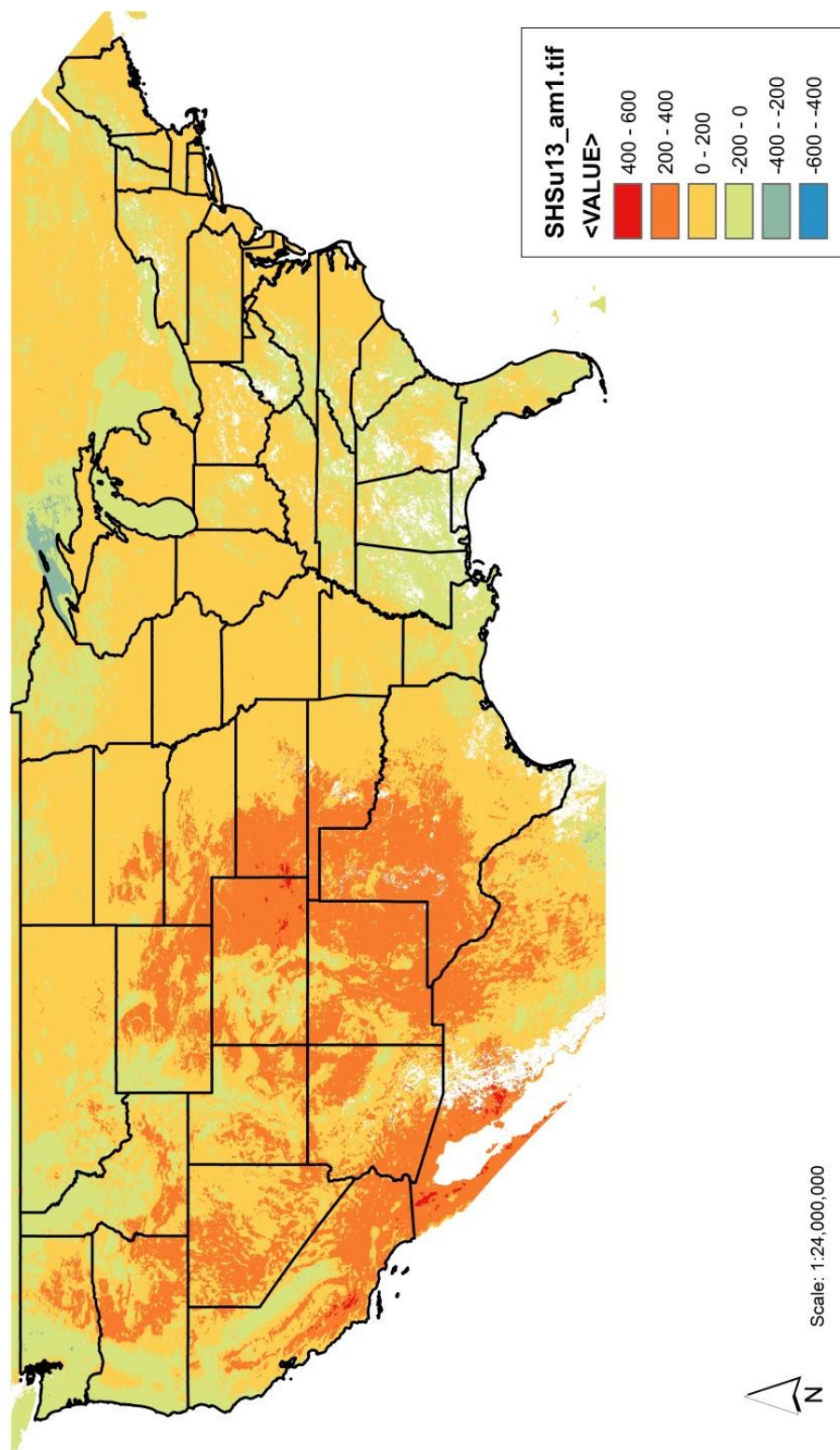


Figure 61: Sensible Heat Flux, July, 2013 (10:30 am)

July 2013 10:30 pm

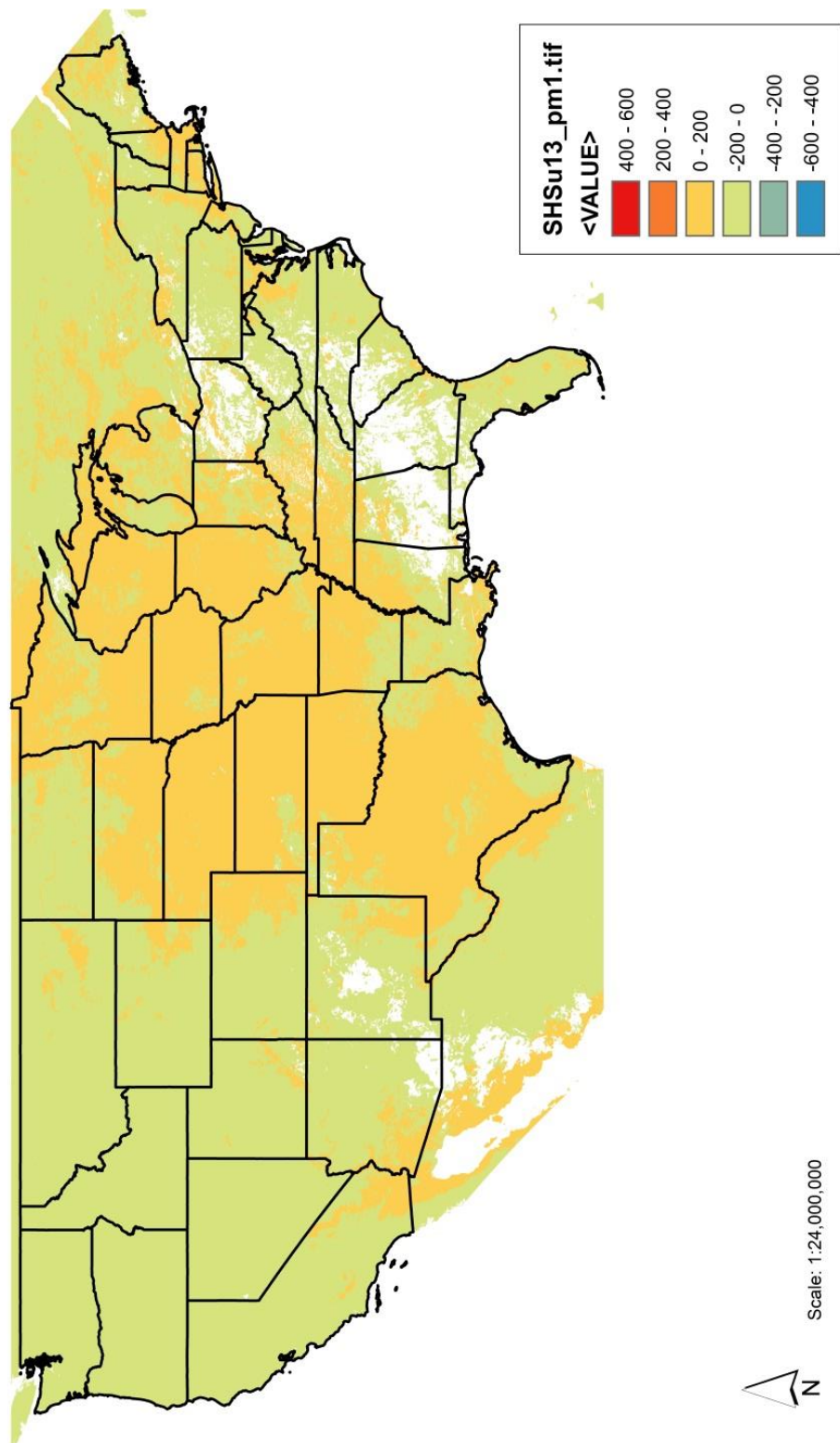


Figure 62: Sensible Heat Flux, July, 2013 (10:30 pm)

October 2011 10:30 am

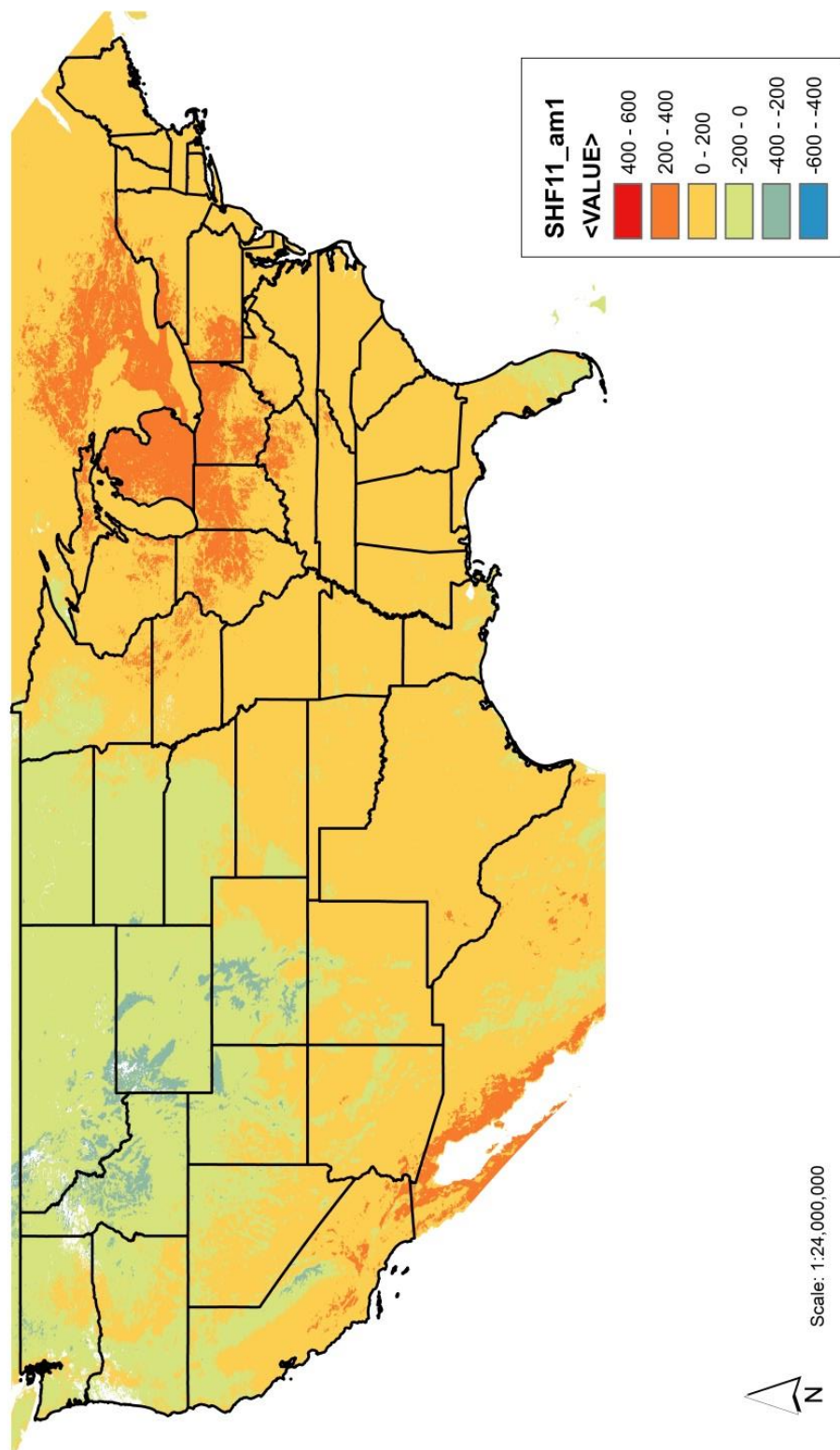


Figure 63: Sensible Heat Flux, October, 2011 (10:30 am)

October 2011 10:30 pm

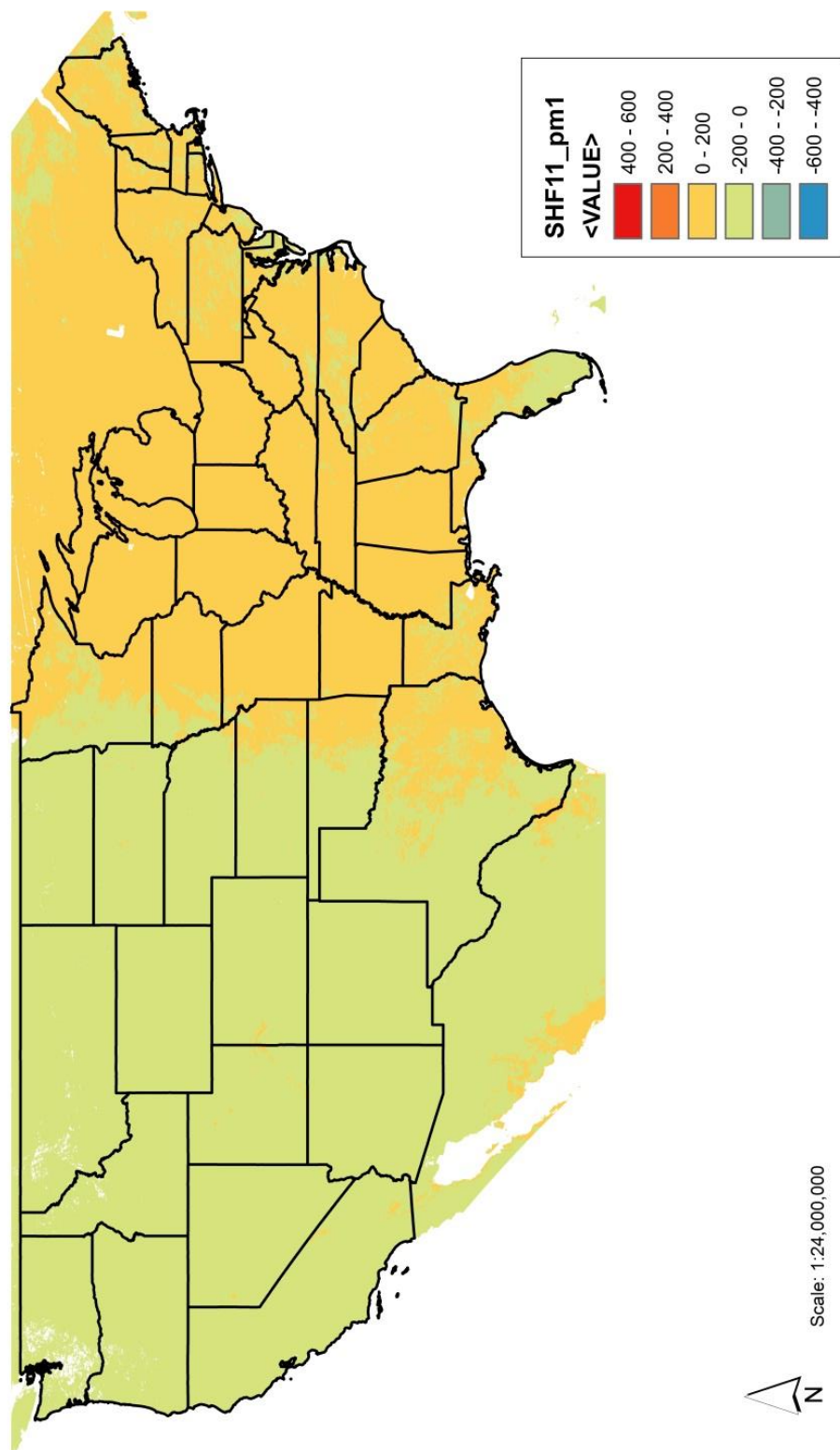


Figure 64: Sensible Heat Flux, October, 2011 (10:30 pm)

October 2013 10:30 am

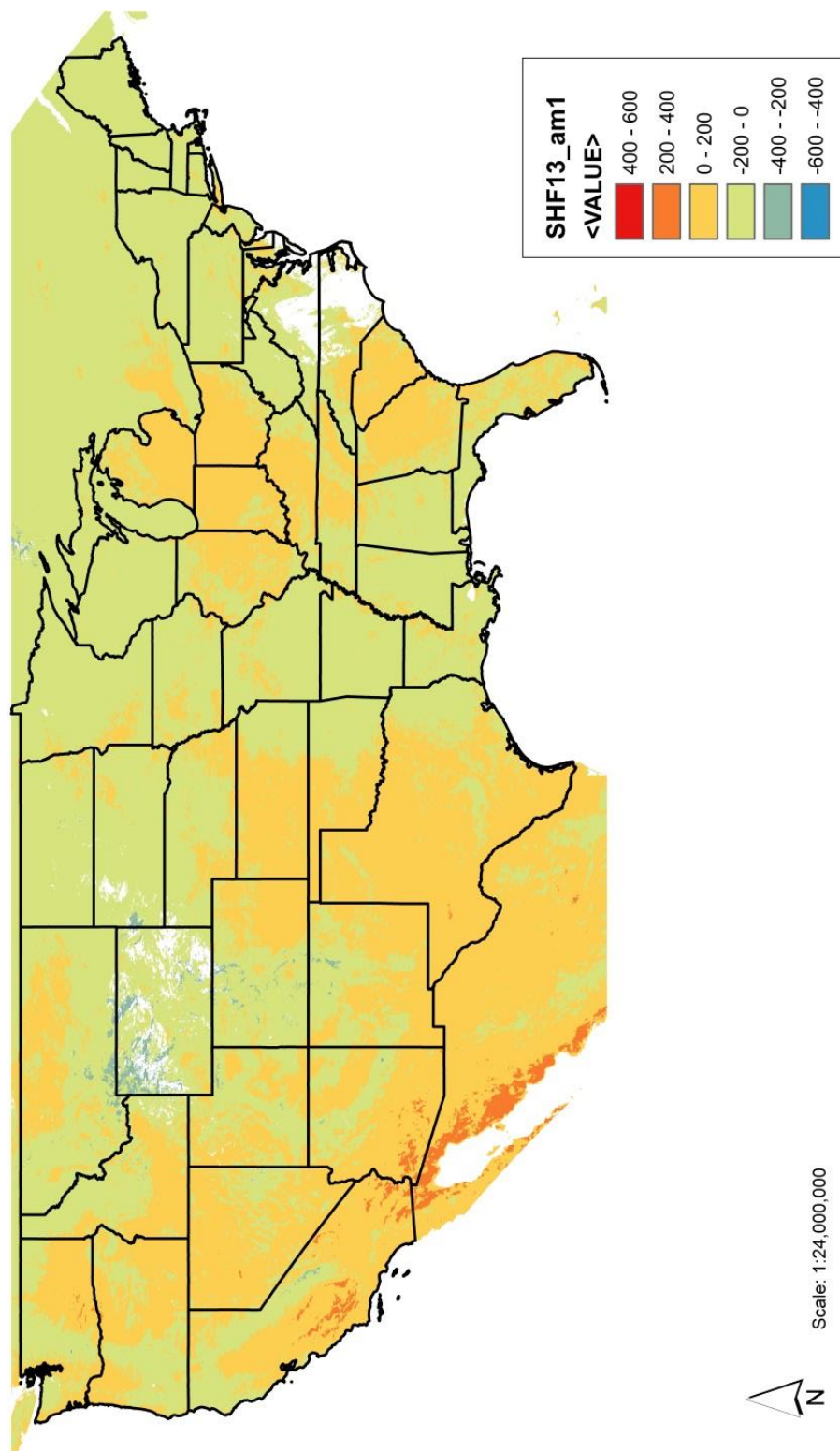


Figure 65: Sensible Heat Flux, October, 2013 (10:30 am)

October 2013 10:30 pm

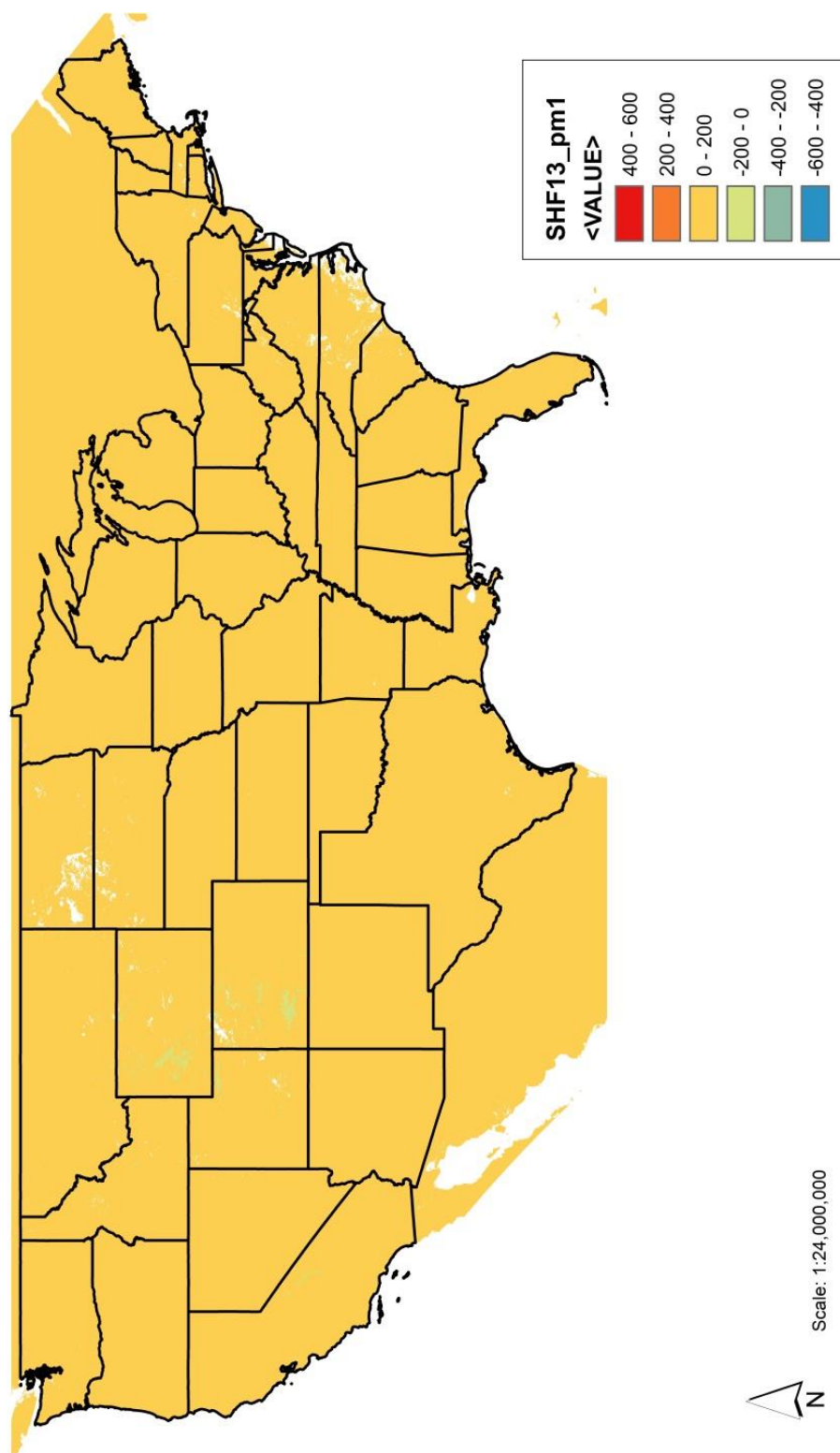


Figure 66: Sensible Heat Flux, October, 2013 (10:30 pm)

6.4.8 Latent Heat Calculation

The methods for calculating latent heat were obtained from Bonan (2002). Using the results obtained from the previous calculations and the interpolation layers, latent heat was calculated using the following formula:

$$\lambda E = \left(\frac{-\rho C_p}{\gamma} \right) \left(\frac{VPD}{r_{ah}} \right)$$

Where ρ , C_p , VPD , r_{ah} , and γ were all calculated previously. The results are measured in watts per meter square.

The raster calculator tool in ArcToolbox was used to perform the latent heat calculations based on the ASCE Standardized Reference Evapotranspiration Equations (Allen, 2005) for saturated vapor pressure, actual vapor pressure, and the vapor pressure deficit, and using the weather station variable interpolation layers:

6.4.9 Saturation Vapor Pressure

$$e_s = 0.6108 \times e^{\left(\frac{17.27 \times T_a}{237.3 + T_a} \right)}$$

T_a represents air temperature, which was obtained from the interpolation layer.

6.4.10 Actual Vapor Pressure

$$e_a = \left(\frac{\varphi}{100} \right) \times e_s$$

Where φ represents relative humidity, which was obtained from the interpolation layer, and e_s represents saturation vapor pressure, which was calculated in the previous equation.

6.4.11 Saturation and Actual Vapor Pressure Deficit

$$PD = e_a - e_s$$

Where the pressure deficit is the difference between the actual vapor pressure and the saturation vapor pressure.

6.5 Raster Calculator

Each variable, excluding constants, was calculated using the Raster Calculator tool in ArcGIS, as shown in *Figure 67: Raster Calculator Tool in ArcGIS*. The formula was entered into Raster Calculator, and a raster layer was created at the resolution of one kilometer. Each time that a new raster layer was created to represent a variable, the raster layer was referenced in Raster Calculator to perform the calculation and create a new raster layer. The variables that were constant were simply entered numerically into Raster Calculator, rather than referencing a raster layer.

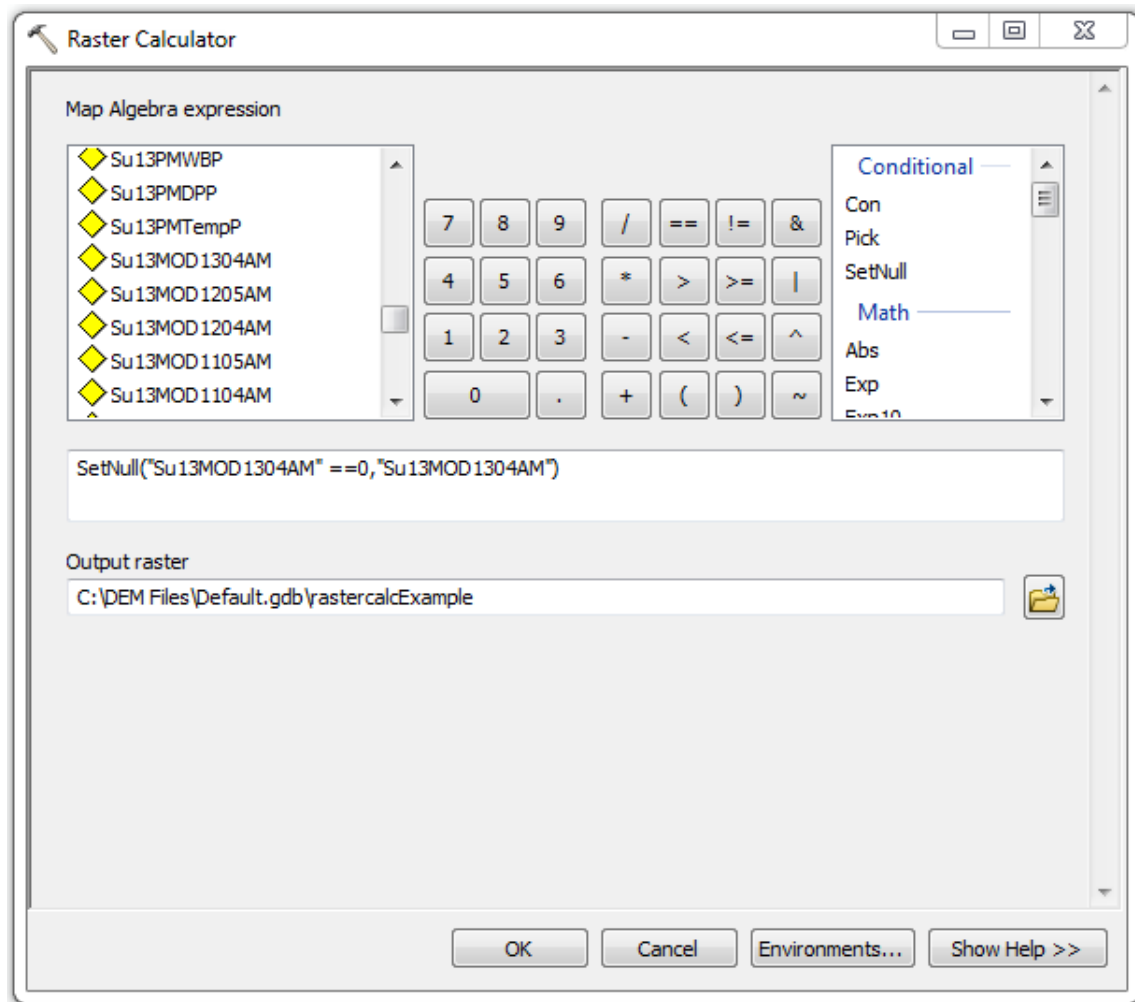


Figure 67: Raster Calculator Tool in ArcGIS

6.6 Contour Elevation Files

A digital representation of variations in elevation was needed for the purpose of examining the landscape in areas that might be suitable for installation of SoV facilities. After contacting USGS and performing a search for a digital elevation model (DEM), it was determined that one needed to be created. After contacting USGS, and learning that contour elevation files were available for the 48 conterminous states, it was determined that the files simply needed to be downloaded and then loaded into ArcGIS.

USGS's National Map Viewer contains data of various themes related to landscape attributes (i.e. contours, boundaries, orthoimagery, and transportation, among others). In the National Map Viewer a state can be selected and the user can simply chose the themes that need to be downloaded. For the purpose of this study, only the contour elevation files were downloaded for each state, and these files were constructed using the 1/3 arc-second National Elevation Dataset (NED) from USGS at 30 meters square resolution.

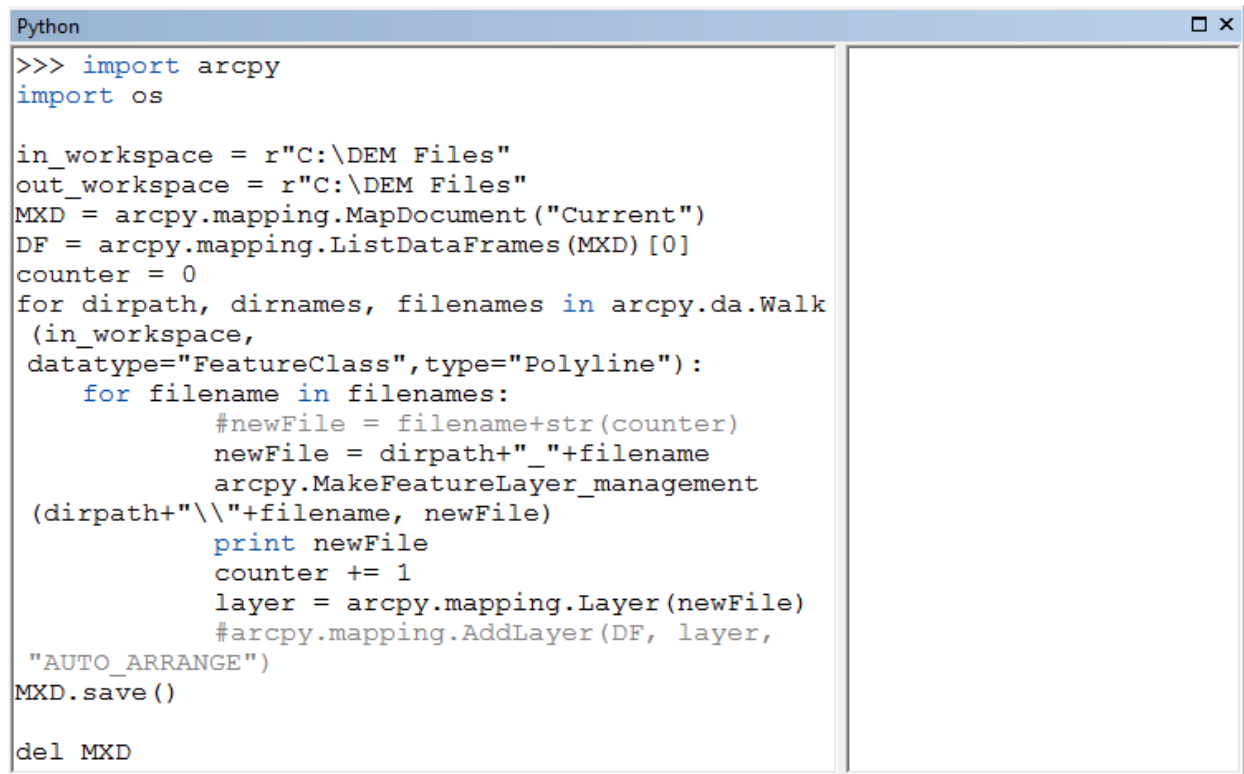
Downloading the files for each state was performed manually. Each state has an average of 20 sets of files to be downloaded (for metropolitan and micropolitan areas). For each state, all files that were in the format suitable for ArcGIS 10.1 were selected to be downloaded. These files were in geodatabase format and there were approximately 2,000 files to be downloaded (at a total of approximately 95 GBs).

6.6.1 Creation of Digital Elevation Model

After all of the contour elevation files were downloaded from USGS's National Map Viewer, the files needed to be loaded into an ArcMap document. This task absolutely could not be attempted to be done manually. A Python script needed to be written to load all of the files into ArcGIS as layers. Because the files were downloaded as geodatabases, the structure of the data, and the means by which the data could be accessed, was tedious. Each state, with its varying number of files, was located in a folder. Inside each folder was a folder for each geodatabase and in many of those folders was another folder which contained all of the necessary files to create the contour elevation feature class. Thus, the way in which the data were arranged, made it complicated to access each file, and the fact that the files were feature classes instead of layers, also made it complicated.

A Python script was then written in order to access the files from within the layers of folders. The script, which was written in ArcPy, which is a variation of Python used specifically in ESRI software, was written in IDLE and run in the Python window in ArcGIS. The script was constructed in a way such that each individual file would be accessed, converted from a feature class to a feature layer, and then loaded into the Table of Contents in the ArcMap document. The script also had to handle the problem that each individual file, for each location, in each state had the same name: “elevation contour,” which posed a problem because the script would initially only run once in order to avoid repeatedly loading files with the same name. A simple means by which to remedy this problem was to add a counter to the file name, which would increment each time a file was added, thus giving each file a unique name, as shown in *Figure 68: ArcPy Window in ArcGIS with DEM Script*.

Due to the fact that the amount of data being loaded into the ArcMap document was so large, the software had difficulty running the script through all 2,000 folders. The script would run for nearly 12 hours, and then crash. To remedy this problem, the script was altered slightly so that only one state could be loaded at a time. This solved the problem of the program crashing, but it also made it more tedious because now the script had to be run 48 separate times instead of only once, and each state had to be loaded into a separate dataframe in the ArcMap document, which then had to be copied and pasted into one dataframe in order for the entire U.S. to render at once after all of the files had been loaded.

A screenshot of the Python window in ArcGIS. The window has a title bar that says "Python" and standard window controls (minimize, maximize, close). The main area contains a Python script for processing DEM files. The script imports arcpy and os, sets workspace paths, gets the current MXD, lists data frames, and then iterates through files in a directory to create new feature layers and add them to the map document. The script is as follows:

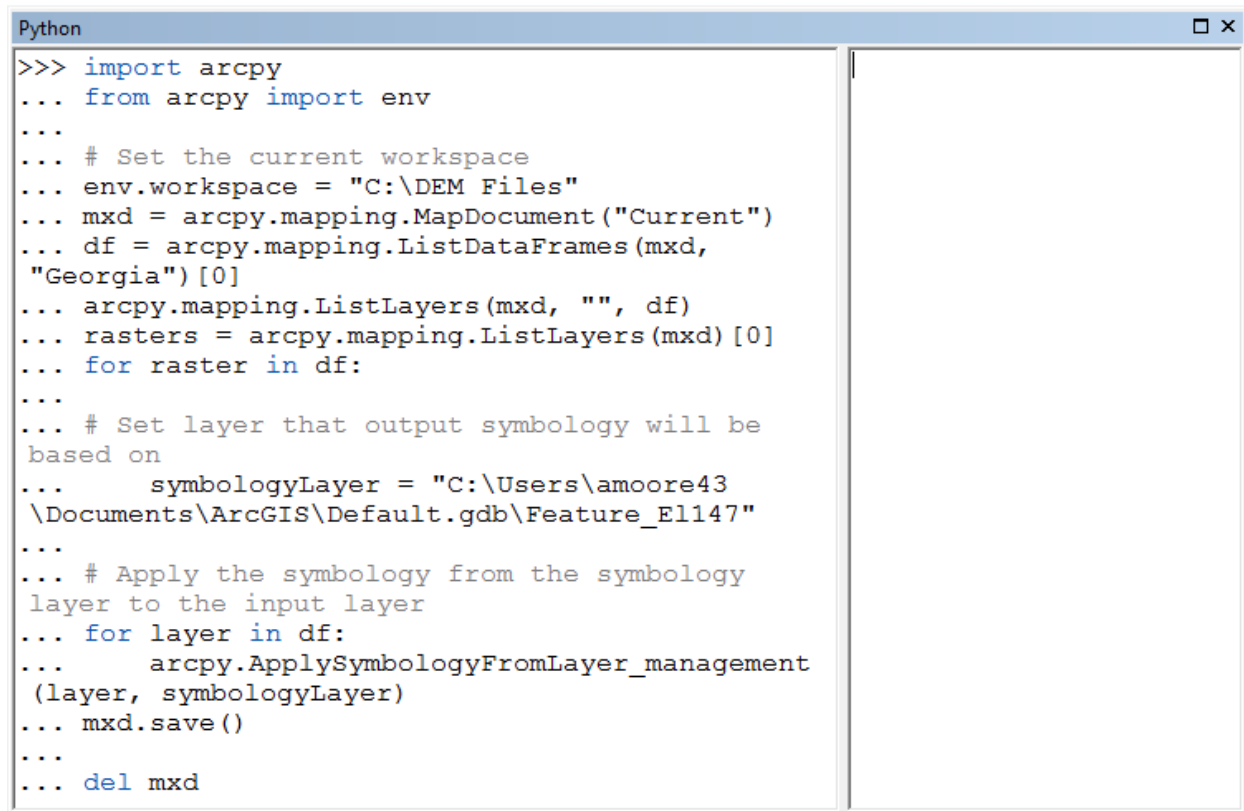
```
>>> import arcpy
import os

in_workspace = r"C:\DEM Files"
out_workspace = r"C:\DEM Files"
MXD = arcpy.mapping.MapDocument("Current")
DF = arcpy.mapping.ListDataFrames(MXD)[0]
counter = 0
for dirpath, dirnames, filenames in arcpy.da.Walk
    (in_workspace,
     datatype="FeatureClass", type="Polyline"):
    for filename in filenames:
        #newFile = filename+str(counter)
        newFile = dirpath+"_"+filename
        arcpy.MakeFeatureLayer_management
        (dirpath+"\\\\"+filename, newFile)
        print newFile
        counter += 1
        layer = arcpy.mapping.Layer(newFile)
        #arcpy.mapping.AddLayer(DF, layer,
        "AUTO_ARRANGE")
MXD.save()

del MXD
```

Figure 68: ArcPy Window in ArcGIS with DEM Script

After all of the 2,000 files were loaded into the Table of Contents in the ArcMap document, it was necessary to apply a uniform symbology to all of the layers so that a range of colors could be used to show variations in elevation that would be the same across the entire U.S. Again, because there were 2,000 files, a script was absolutely necessary. An ArcPy script was written, using the file for the Death Valley area of Nevada as the template, because there is a wide range in elevations. The ArcPy script used the range and intervals of elevation and the color scheme used in the Death Valley, Nevada file and applied it to all of the feature layers in the Table of Contents, which created a unified theme across the entire U.S., as shown in *Figure 69: ArcPy Window in ArcGIS with Symbology Script*.

A screenshot of a Python window in ArcGIS. The window has a title bar that says "Python" and standard window controls (minimize, maximize, close). The main area contains a Python script for applying symbology. The script imports arcpy and env, sets the workspace to "C:\DEM Files", opens the current map document, lists data frames for "Georgia", lists layers, and then iterates through the layers to apply symbology from a specific layer management file. The script ends with saving the map document and deleting the mxs object.

```
>>> import arcpy
... from arcpy import env
...
... # Set the current workspace
... env.workspace = "C:\DEM Files"
... mxd = arcpy.mapping.MapDocument("Current")
... df = arcpy.mapping.ListDataFrames(mxd,
... "Georgia")[0]
... arcpy.mapping.ListLayers(mxd, "", df)
... rasters = arcpy.mapping.ListLayers(mxd)[0]
... for raster in df:
...
... # Set layer that output symbology will be
... based on
...     symbologyLayer = "C:\Users\amoore43
... \Documents\ArcGIS\Default.gdb\Feature_E1147"
...
... # Apply the symbology from the symbology
... layer to the input layer
... for layer in df:
...     arcpy.ApplySymbologyFromLayer_management
... (layer, symbologyLayer)
... mxd.save()
...
... del mxd
```

Figure 69: ArcPy Window in ArcGIS with Symbology Script

Upon completion, it was discovered that several areas, including half of South Dakota, a portion of central North Carolina, an area around Eureka, California, and most of Nye County, Nevada failed to render, as shown in the completed image in *Figure 70: Completed Digital Elevation Model in ArcGIS*. USGS was contacted and the files for South Dakota and North Carolina were re-downloaded and successfully rendered. However, the area around Eureka and most of Nye County never rendered.

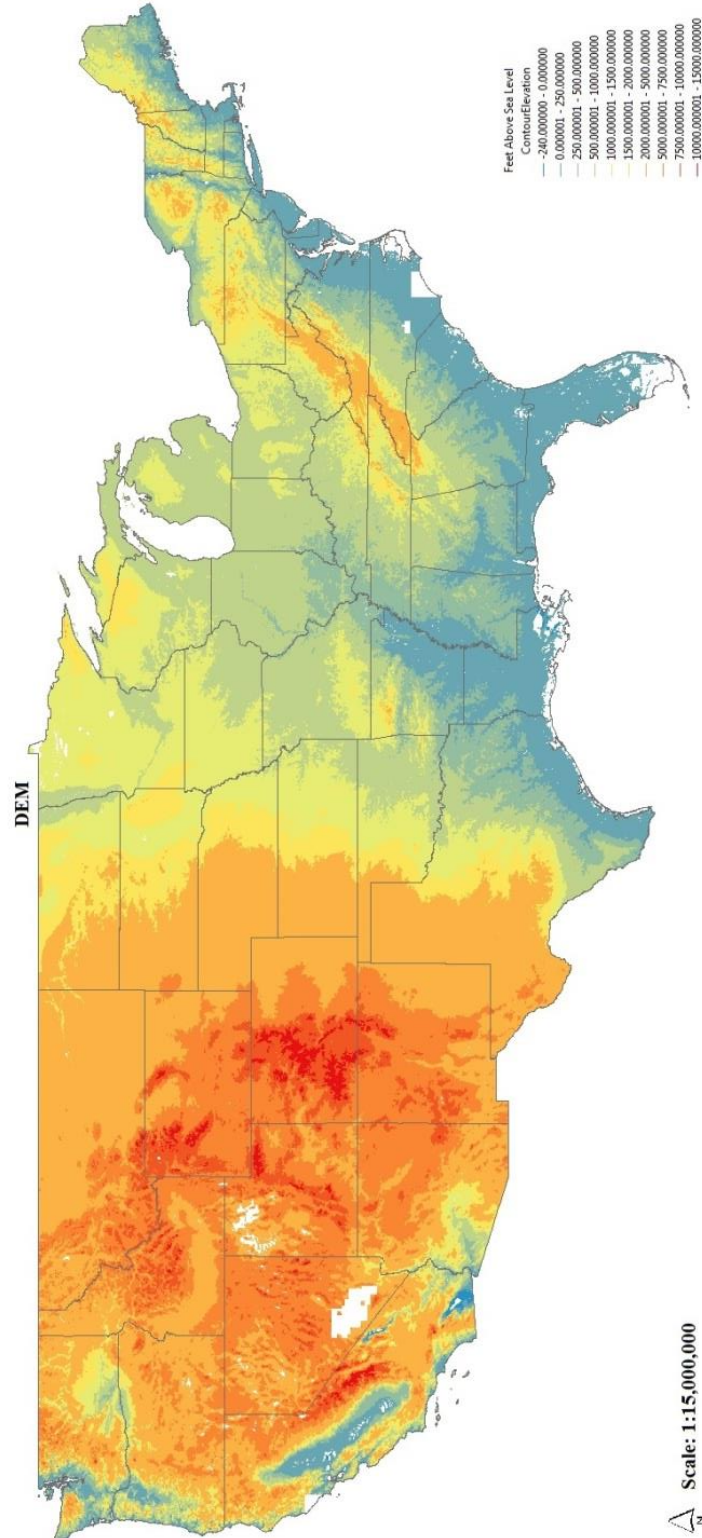


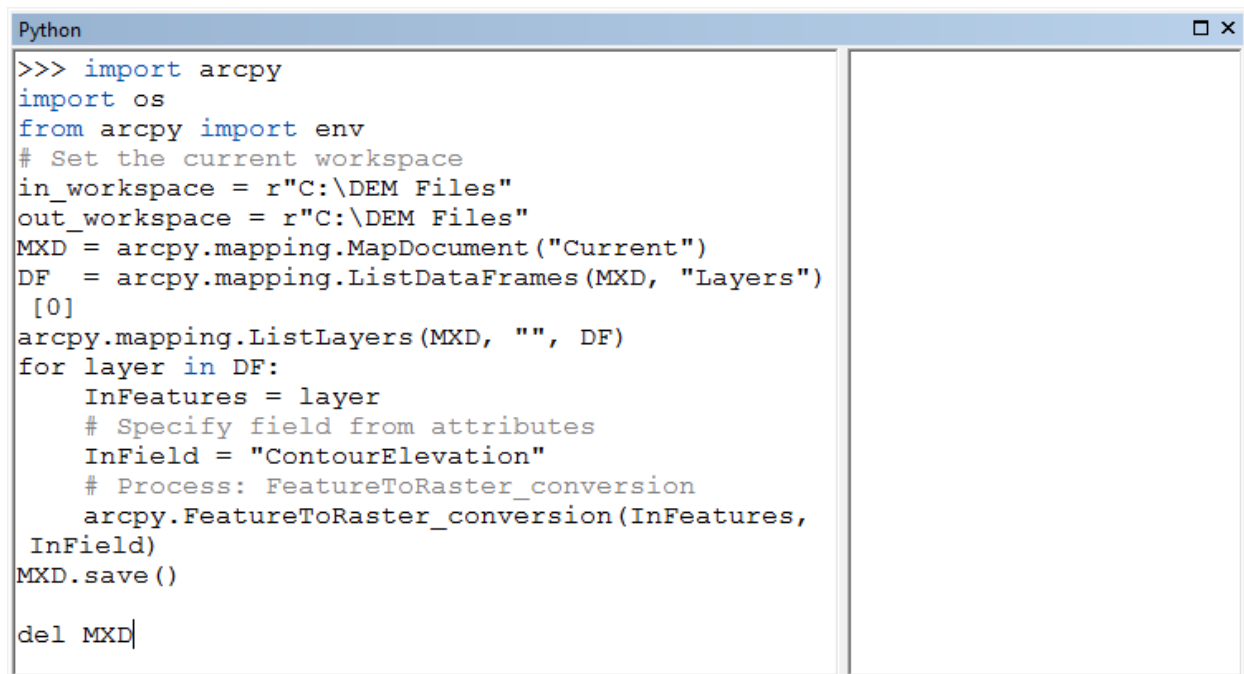
Figure 70: Completed Digital Elevation Model in ArcGIS

6.7 Creation of the Slope Model

A slope map was necessary for evaluating potential areas for installation of SoVs. Because a slope map for the entire U.S. was not readily available, one needed to be created using the contour elevation files used in the creation of the Digital Elevation Model. As with the DEM, creating the slope map would require the loading and manipulation of 2,000 files, therefore, Python scripting was absolutely necessary.

6.7.1 ArcPy Scripts Involved in the Creation of the Slope Model

Initially, a copy of the DEM was needed to form the basis of the slope map. An ArcPy script was then written to convert all of the feature layers from the DEM to raster layers, as shown in *Figure 71: ArcPy Window in ArcGIS with Feature to Raster Conversion Script*. The ArcPy script was to be run on all 2,000 files. The same problem that was encountered during the creation of the DEM, in which ArcGIS had difficulty handling the data load, occurred again but was remedied by running the script on each state, individually, by placing each state in a separate dataframe, and changing the dataframe for each run, depending on which state was being considered. Again, this made the task much more tedious, but it ensured that the ArcPy rasterization script would run successfully each time.

A screenshot of a Python window in ArcGIS. The window has a title bar that says "Python" and standard window controls (minimize, maximize, close). The main area contains a Python script. The script imports arcpy and os, sets the current workspace to "C:\DEM Files", and lists data frames in the current map document. It then iterates through the data frames, selecting the "ContourElevation" field and using the FeatureToRaster_conversion tool to convert each feature layer to a raster. Finally, it saves the map document and deletes the MXD object.

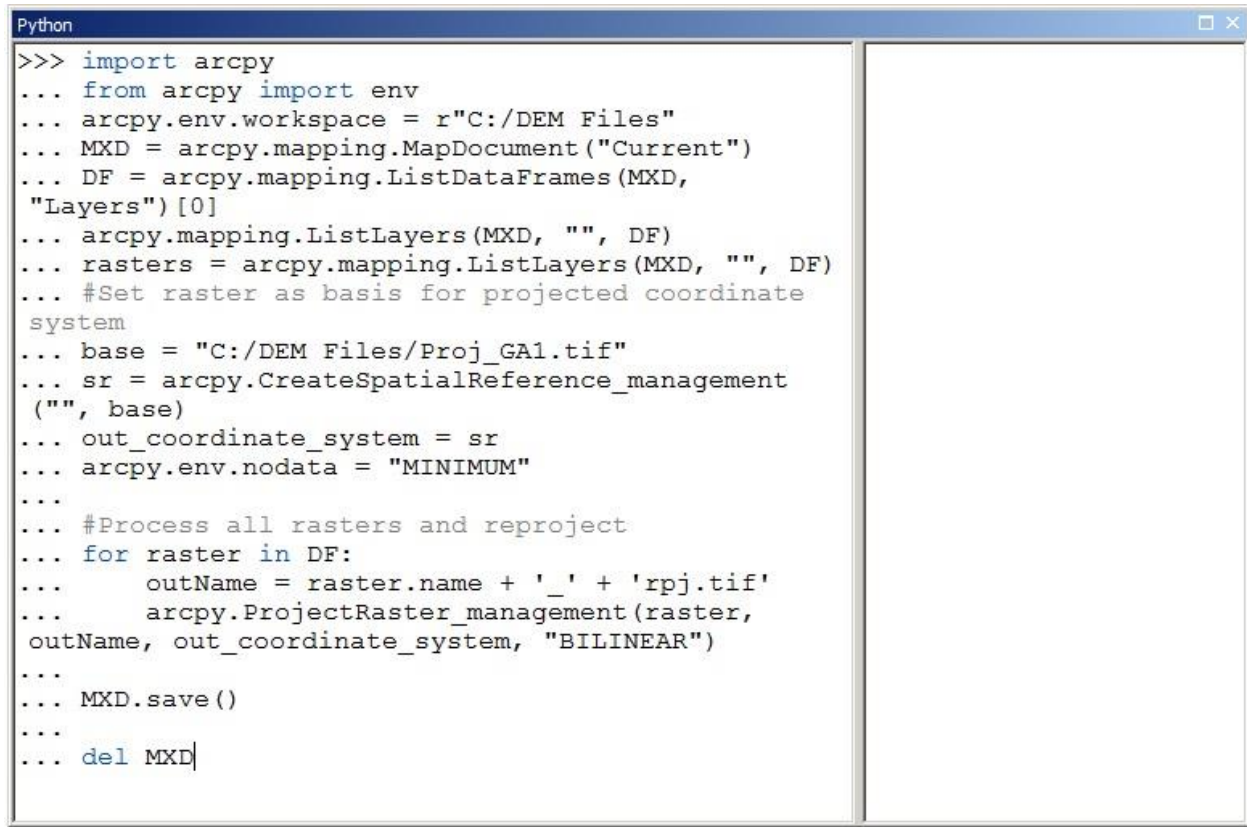
```
>>> import arcpy
import os
from arcpy import env
# Set the current workspace
in_workspace = r"C:\DEM Files"
out_workspace = r"C:\DEM Files"
MXD = arcpy.mapping.MapDocument("Current")
DF = arcpy.mapping.ListDataFrames(MXD, "Layers")
[0]
arcpy.mapping.ListLayers(MXD, "", DF)
for layer in DF:
    InFeatures = layer
    # Specify field from attributes
    InField = "ContourElevation"
    # Process: FeatureToRaster_conversion
    arcpy.FeatureToRaster_conversion(InFeatures,
    InField)
MXD.save()

del MXD
```

Figure 71: ArcPy Window in ArcGIS with Feature to Raster Conversion Script

After the 2,000 contour elevation feature layers were converted to raster layers, the raster layers needed to be reprojected. Initially, the DEM was in an unspecified projection, with measurements in decimal degrees. When slope was initially calculated, the units were in the millions. It was necessary that the raster files be reprojected. A projection using U.S. feet was needed, therefore, the State Plane projection was chosen. For each state, which was in a separate dataframe in the Table of Contents, the appropriate State Plane projection was chosen manually, and applied to one layer using the project raster tool in ArcToolbox. The layer was then exported to a tiff, and loaded into the Table of Contents. An ArcPy script was then written to reproject the remaining raster files within the dataframe to the State Plane projection specified by the example raster layer. It was also necessary to exclude raster cells with null values, so a line was written to account for the cells without data, by setting it to “minimum,” the lowest value within the dataset was applied to the cell. A bilinear interpolation was performed to estimate the values. Bilinear

was chosen instead of the default nearest neighbor or cubic interpolation because bilinear is recommended for contour interval interpolation, as shown in *Figure 72: ArcPy Window in ArcGIS with Raster Reprojection Script*.

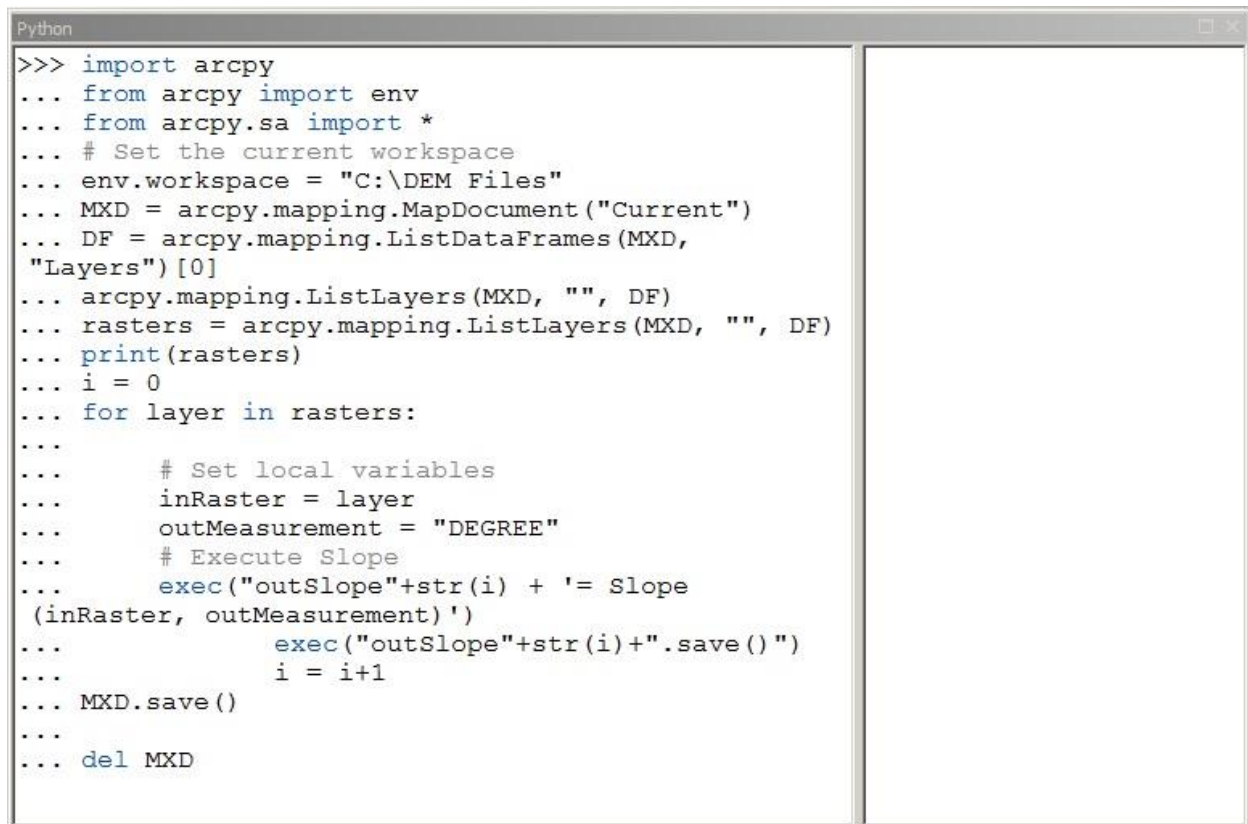
A screenshot of the ArcPy Window in ArcGIS. The window has a title bar that says "Python" and standard window controls (minimize, maximize, close). The main area contains a Python script for raster reprojection. The script imports arcpy and sets the workspace to "C:/DEM Files". It then lists data frames and rasters, sets a base raster and coordinate system, and loops through each raster to reproject it using bilinear interpolation. Finally, it saves the MXD and deletes the MXD object.

```
>>> import arcpy
... from arcpy import env
... arcpy.env.workspace = r"C:/DEM Files"
... MXD = arcpy.mapping.MapDocument("Current")
... DF = arcpy.mapping.ListDataFrames(MXD,
    "Layers")[0]
... arcpy.mapping.ListLayers(MXD, "", DF)
... rasters = arcpy.mapping.ListLayers(MXD, "", DF)
... #Set raster as basis for projected coordinate
system
... base = "C:/DEM Files/Proj_GA1.tif"
... sr = arcpy.CreateSpatialReference_management
    ("", base)
... out_coordinate_system = sr
... arcpy.env.nodata = "MINIMUM"
...
... #Process all rasters and reproject
... for raster in DF:
...     outName = raster.name + '_' + 'rpj.tif'
...     arcpy.ProjectRaster_management(raster,
        outName, out_coordinate_system, "BILINEAR")
...
... MXD.save()
...
... del MXD
```

Figure 72: ArcPy Window in ArcGIS with Raster Reprojection Script

After all of the raster layers had been reprojected to the State Plane projection based on the state for each dataframe, an ArcPy script was written in order to apply the slope function from ArcToolbox to all 2,000 raster layers in the Table of Contents in the ArcMap document, as shown in *Figure 73: ArcPy Window in ArcGIS with Script that Applies the Slope Function*. Again, this script was run on each state, individually, to avoid the occurrence of the script failing

due to the size of the data load. The slope function calculated the degree of slope, rather than the percent rise. Because the units of the State Plane projection were in U.S. feet, which were the same units used in the contour interval files, a z factor was not necessary to convert the units from meters to feet.

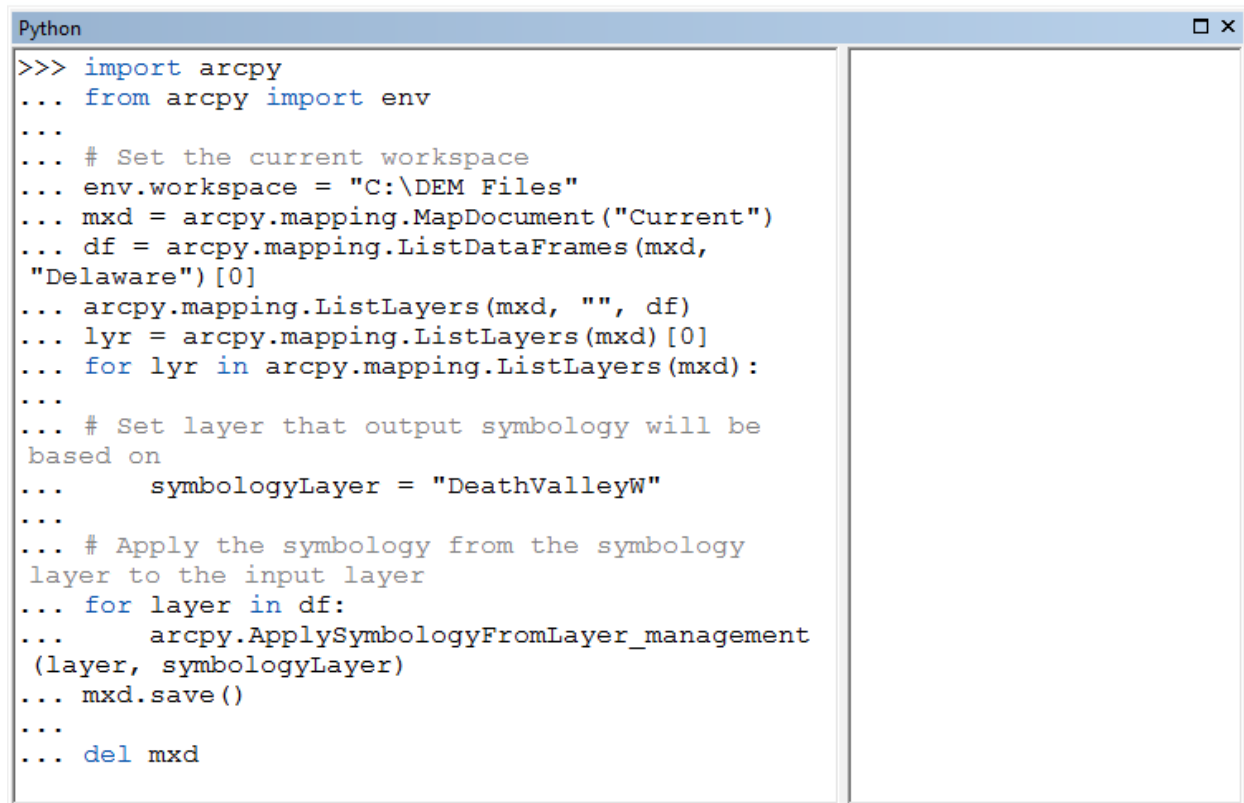


```
>>> import arcpy
... from arcpy import env
... from arcpy.sa import *
... # Set the current workspace
... env.workspace = "C:\DEM Files"
... MXD = arcpy.mapping.MapDocument("Current")
... DF = arcpy.mapping.ListDataFrames(MXD,
... "Layers")[0]
... arcpy.mapping.ListLayers(MXD, "", DF)
... rasters = arcpy.mapping.ListLayers(MXD, "", DF)
... print(rasters)
... i = 0
... for layer in rasters:
...     # Set local variables
...     inRaster = layer
...     outMeasurement = "DEGREE"
...     # Execute Slope
...     exec("outSlope"+str(i) + '= Slope
... (inRaster, outMeasurement)')
...     exec("outSlope"+str(i)+".save()")
...     i = i+1
... MXD.save()
... del MXD
```

Figure 73: ArcPy Window in ArcGIS with Script that Applies the Slope Function

After the ArcPy slope script was run on all 2,000 files, with each state in a separate dataframe, a third ArcPy script was needed in order to apply a unified symbology to all of the raster slope layers. Using the original ArcPy symbology script written for the DEM, changes were made to apply the symbology of the Death Valley, Nevada file (as with the DEM ArcPy symbology script) and apply it to all raster layers in the Table of Contents in order to create a

unified color scheme to show variations in slope across the entire U.S., as shown in *Figure 74*: *ArcPy Window in ArcGIS with Script that Applies a Unified Symbolology* and *Figure 75*: *Completed Slope Model in ArcGIS*.

The image shows a screenshot of the 'Python' window in ArcGIS. The window has a title bar with 'Python' and standard window controls. The main area contains a Python script that uses the arcpy module to apply symbology from one layer to others in a map document. The script sets the workspace to 'C:\DEM Files', opens the current map document, lists data frames, and then iterates through layers to apply the symbology of the 'DeathValleyW' layer to each. The script ends with deleting the map document object.

```
>>> import arcpy
... from arcpy import env
...
... # Set the current workspace
... env.workspace = "C:\DEM Files"
... mxd = arcpy.mapping.MapDocument("Current")
... df = arcpy.mapping.ListDataFrames(mxd,
... "Delaware")[0]
... arcpy.mapping.ListLayers(mxd, "", df)
... lyr = arcpy.mapping.ListLayers(mxd)[0]
... for lyr in arcpy.mapping.ListLayers(mxd):
...
... # Set layer that output symbology will be
... based on
...     symbologyLayer = "DeathValleyW"
...
... # Apply the symbology from the symbology
... layer to the input layer
... for layer in df:
...     arcpy.ApplySymbologyFromLayer_management
... (layer, symbologyLayer)
... mxd.save()
...
... del mxd
```

Figure 74: ArcPy Window in ArcGIS with Script that Applies a Unified Symbolology

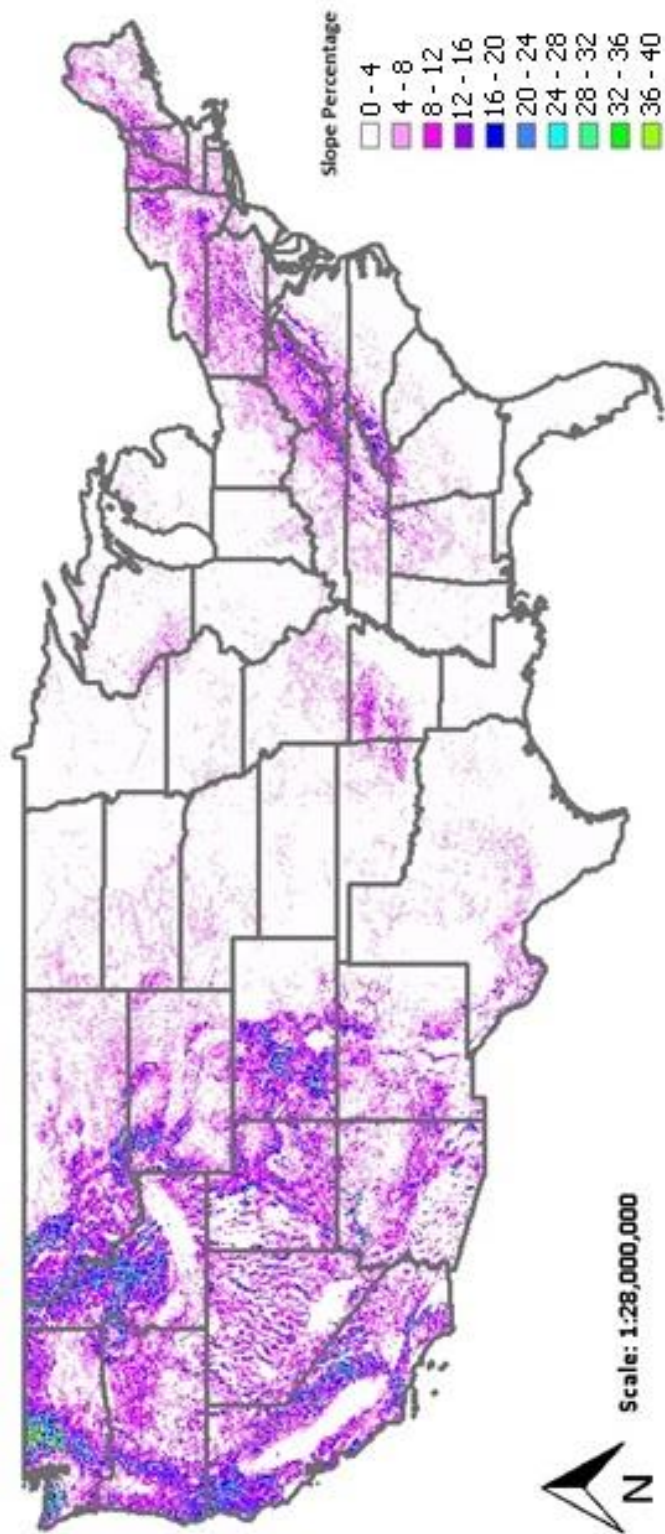


Figure 75: Completed Slope Model in ArcGIS

6.8 Threshold Model

Estimated potential power output for the conterminous U.S. was performed using the sensible heat flux raster layers created in ArcGIS, in-conjunction with in-situ data of temporal distributions at varying physiographic regions across the U.S. The statistical computing and graphics software, R, was used to calculate power output based on the matrices in each sensible heat flux raster layer created in the GIS. Raster layers were created in R, and imported back into the GIS. As with the resolution of the sensible heat flux raster layers, the results from the model are in one kilometer resolution. Currently, the initial model used to estimate power output potential is lacking latent heat flux, and relies on sensible heat and temporal distributions of sensible heat across varying landscapes across the U.S. Later models will incorporate latent heat flux.

6.8.1 Representative Distributions

In-situ data were necessary to compare with heat flux values calculated in the GIS. Obviously, in-situ heat flux values at the resolution used in the GIS (one kilometer), were not available for the conterminous U.S., so locations were chosen to represent varying physiographic region types, and temporal distributions were obtained from these locations, as shown in *Figure 76: Physiographic Region Types Across U.S. with Ameriflux Sites*.

The conterminous U.S. is divided into approximately 500 physiographic areas, which are divided into eight regions. 14 Ameriflux sites were chosen to represent these varying types of physiographic regions, as shown in *Figure 77: Representative Distributions from Ameriflux Sites*. Ameriflux, which is managed by the DOE and Lawrence Berkeley National Lab, maintains monitoring sites across North and South America. Weather data, CO₂, and heat flux, among other data, are measured at these different locations. Data is available on their Website, in the

form of text and Excel files. Olga Kemenova, at the Georgia Tech Research Institute, was responsible for obtaining and analyzing the Ameriflux data used in this study.

Ameriflux Sites Across Physiographic Region Types

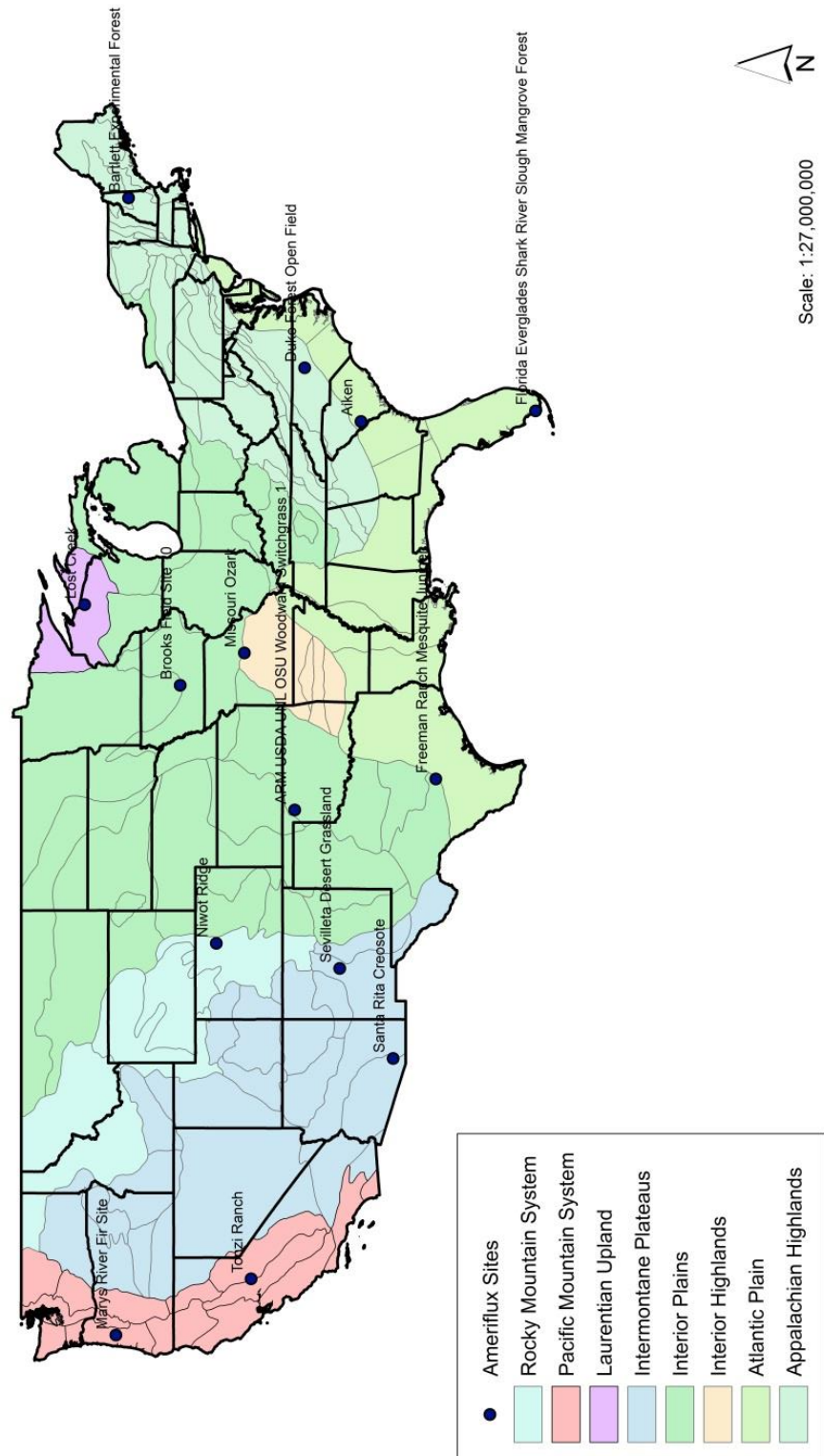


Figure 76: Physiographic Region Types Across U.S. with Ameriflux Sites

Site Name	Land Cover	State	Division	Province	Section
Santa Rita Creosote	Open shrublands	AZ	Intermontane Plateaus	Basin And Range	Sonoran Desert
Aiken	Mixed forest	SC	Atlantic Plain	Coastal Plain	Sea Island
USDA Woodward Switchgrass	Grassland	OK	Interior Plains	Central Lowland	Osage Plains
Tonzi Ranch	Woody savanna	CA	Pacific Mountain System	Cascade-Sierra Mountains	Sierra Nevada
Brooks Field Site 10	Cropland	IA	Interior Plains	Central Lowland	Western Lake
Missouri Ozark	Deciduous broadleaf forest	MO	Interior Highlands	Ozark Plateaus	Springfield-Salem Plateaus
Duke Forest Open Field	Grassland	NC	Appalachian Highlands	Piedmont	Piedmont Upland
Lost creek	Closed shrublands	WI	Laurentian Upland	Superior Upland	
Niwot Ridge	Evergreen needleleaf forest	CO	Rocky Mountain System	Southern Rocky Mountains	
Florida Everglades Shark River Slough Mangrove Forest	Evergreen broadleaf forest	FL	Atlantic Plain	Coastal Plain	Floridian
Sevilleta Desert Grassland	Grassland	NM	Intermontane Plateaus	Basin And Range	Mexican Highland
Bartlett Experimental Forest / US-Bar	Deciduous broadleaf forest	NH	Appalachian Highlands	New England	White Mountain
Marys River Fir Site / US-MRf	Evergreen needleleaf forest	OR	Pacific Mountain System	Pacific Border	Oregon Coast Range
Freeman Ranch Mesquite Juniper / US-FR2	Woody savanna	TX	Interior Plains	Great Plains	Edwards Plateau

Figure 77: Representative Distributions from Ameriflux Sites

6.8.2 Analysis of In-Situ Data

Olga Kemenova was responsible for performing various statistical analyses on the Ameriflux data. She used the statistical software JMP. After obtaining the text and Excel files from Ameriflux, she cleaned the data by recoding some of the variables. The data obtained from Ameriflux consisted of heat flux, both sensible and latent, for the 14 sites, measured hourly, every day, for several years (typically from 2006 to 2012). Missing data was an issue; ANOVA tests were performed across the datasets for each site to determine statistical significance. For each site, the dataset with the least amount of data was chosen to represent the site. After the ANOVA was performed, data from previous years were used as substitutes for the missing data.

After handling the problem of missing data, Olga created probability distributions of the heat flux data for each site, as shown in *Figure 78: Bimodal Distribution of Heat Flux at Santa Rita Creosote Site*, and applied an outlier box plot to each distribution. She obtained mean values for 10:30 am and 10:30 pm. She then fit the distributions with a mixture of three normal distributions because many of the distributions had three peaks in the data. She then obtained a mean μ , standard deviation σ , and percentage of the overall distribution which fell into each of the three distributions π , for each of the three normal distributions for each site (some sites, such as the Santa Rita Creosote site, were bimodal, and only two normal distributions were needed). After these parameters were obtained, she performed regression analyses to determine how well the parameters for each of the distributions could be used to predict the overall means for the distributions at 10:30 am and 10:30 pm, as shown in *Figure 79: Measured vs. Predicted (Santa Rita Creosote site)*

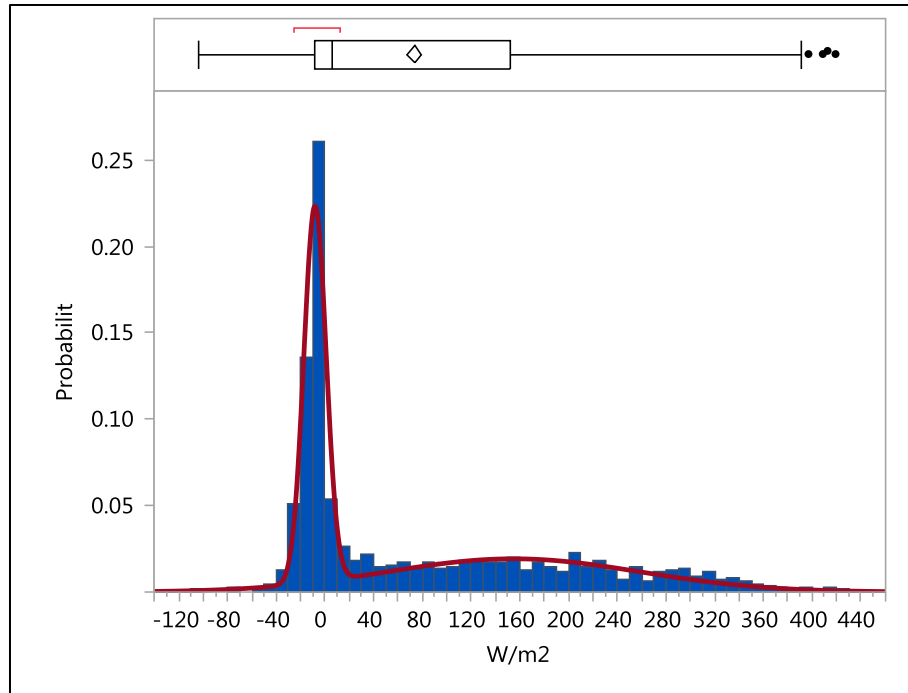


Figure 78: Bimodal Distribution of Heat Flux at Santa Rita Creosote Site

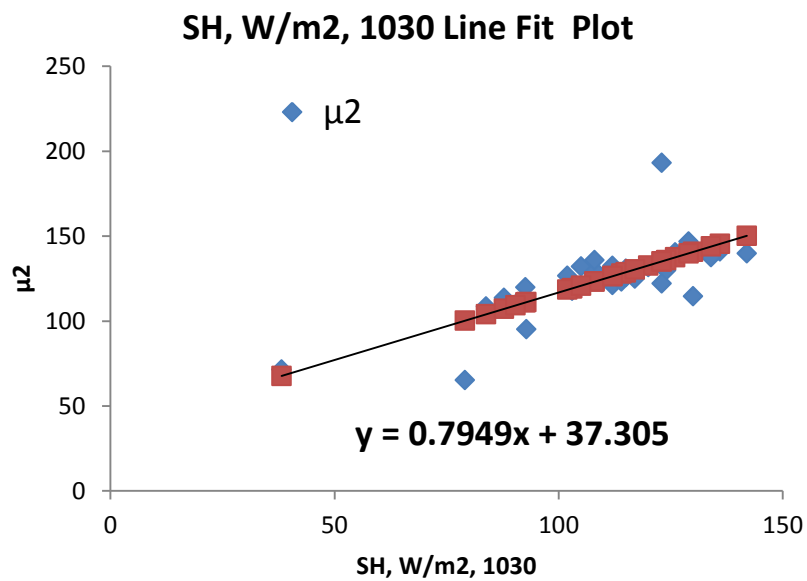


Figure 79: Measured vs. Predicted (Santa Rita Creosote site)

```

R Untitled - R Editor
setwd("C:/Power Output")
pars<-read.csv(file="ameriflux_normaldist_052615_yx_SH.csv",header=TRUE)

library(raster)
library(rgdal)

am_RMS_july<-raster("RMS_ClipAM1.tif",native=T)
pm_RMS_july<-raster("RMS_ClipPM1.tif",native=T)
pars_current<-pars[which(pars$site=="NRE"&pars$month==7),]
attach(pars_current)
mu1<-a1+b_am1*am_RMS_july+b_pm1*pm_RMS_july
mu2<-a2+b_am2*am_RMS_july+b_pm2*pm_RMS_july
mu3<-a3+b_am3*am_RMS_july+b_pm3*pm_RMS_july
nr=dim(am_RMS_july)[1]
nc=dim(am_RMS_july)[2]
alpha=50
PowerGen<-matrix(rep(0,nr*nc),nrow=nr,ncol=nc)
for (i in 1:nr){
  for (j in 1:nc){
    if((is.na(mu1[i,j])==FALSE)&(is.na(mu2[i,j])==FALSE)&(is.na(mu3[i,j])==FALSE)){
      dist<-function(z){(pi1*dnorm(z,mu1[i,j],sd1)+pi2*dnorm(z,mu2[i,j],sd2)+pi3*dnorm(z,mu3[i,j],sd3))*z}

      PowerGen[i,j]<-integrate(dist,lower=alpha,upper=maxValue(am_RMS_july))$value
    }
    else{
      PowerGen[i,j]<-NA
    }
  }
}
detach(pars_current)
plot(am_RMS_july)
PGLayer<-raster(PowerGen,template=am_RMS_july)
plot(PGLayer)
writeRaster(PGLayer,"PowerGen_RMS_July2013AM.tif",format="GTiff")

```

Figure 80: R Code Used in Estimation of Power Output

6.8.3 Threshold Model Steps

Using the sensible heat layers created previously in ArcGIS, raster layers were created to represent the 14 physiographic regions. Using the physiographic layers as boundaries, the sensible heat layers for AM and PM were “clipped” using the raster clip function in ArcToolbox. After layers were created for all 14 physiographic regions, for AM and PM, for all four seasons, for both 2011 and 2013, these 224 files were exported to tiff files, which would be necessary to run the R script.

Using an Excel spreadsheet (Appendix) created by Olga Kemenova, which contained the regression coefficients for all 14 Ameriflux sites’ sensible heat distributions, and the 224 sensible

heat physiographic regions' geotiff files, power output was estimated using R. The variables names were assigned based on the physiographic region and the season. The script used the cell matrix in the AM sensible heat layer to perform the necessary calculations using the normal distributions created by the values found in the Excel spreadsheet. An arbitrary alpha value of 50 was used based on the assumption that the SoV would not be able to “startup” until sensible heat measurements were at least 50 w/m². Using the integrate function in R, the power output estimation was generated by simply integrating below the curve of the normally-distributed sensible values provided by the Ameriflux sites in the Excel spreadsheet. A beta value was applied using the completed power output raster layers in Raster Calculator. The beta value of 24.73 was obtained from results of the prototype. This beta value represents the amount of sensible heat that the SoV unit will convert to vortex energy. The assumption is that, at 50 watts per meter square sensible heat, the relationship between sensible heat and vortex energy is linear. Refer to *Figure 81: Threshold Model Assumptions*.

$$\text{Power Output } (W/m^2) = \int_{\alpha}^{Inf} F(x)P(x)dx$$

where

x is the sensible heat flux in W/m^2

$P(x)$ is the probability density function

$F(x)$ is the relationship between power output and sensible heat flux; in this case

$$F(x) = \begin{cases} 0, & \text{if } x < \alpha \\ \beta x, & \text{if } x \geq \alpha \end{cases}$$

Where $\alpha = 50$ and $\beta = 24.73$

Figure 81: Threshold Model Assumptions

The R script, shown in *Figure 80: R Code Used in Estimation of Power Output*, then generated a geotiff raster file, shown in *Figure 82: Power Output Estimation for California and Baja California*, using the dimensions previously specified in the script based on the dimensions of the AM sensible heat raster layer. The images generated using the R script representing each month for 2011 and 2013 can be found in the Appendix. The completed model representing annual power output for 2011 and 2013 are shown in *Figure 83: 2011 Annual Power Output (from Threshold Model)* and *Figure 84: 2013 Annual Power Output (from Threshold Model)*.

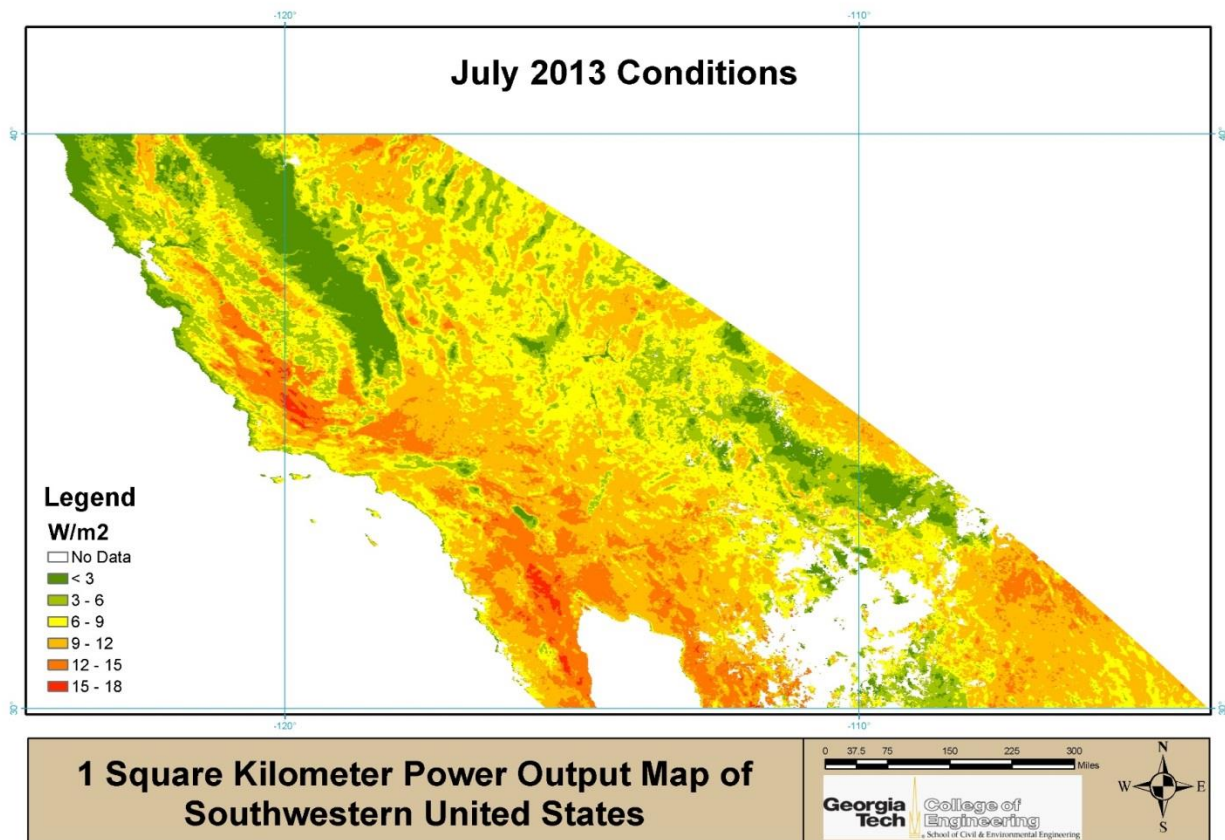


Figure 82: Power Output Estimation for California and Baja California

Threshold Model: 2011 Annual Power Output

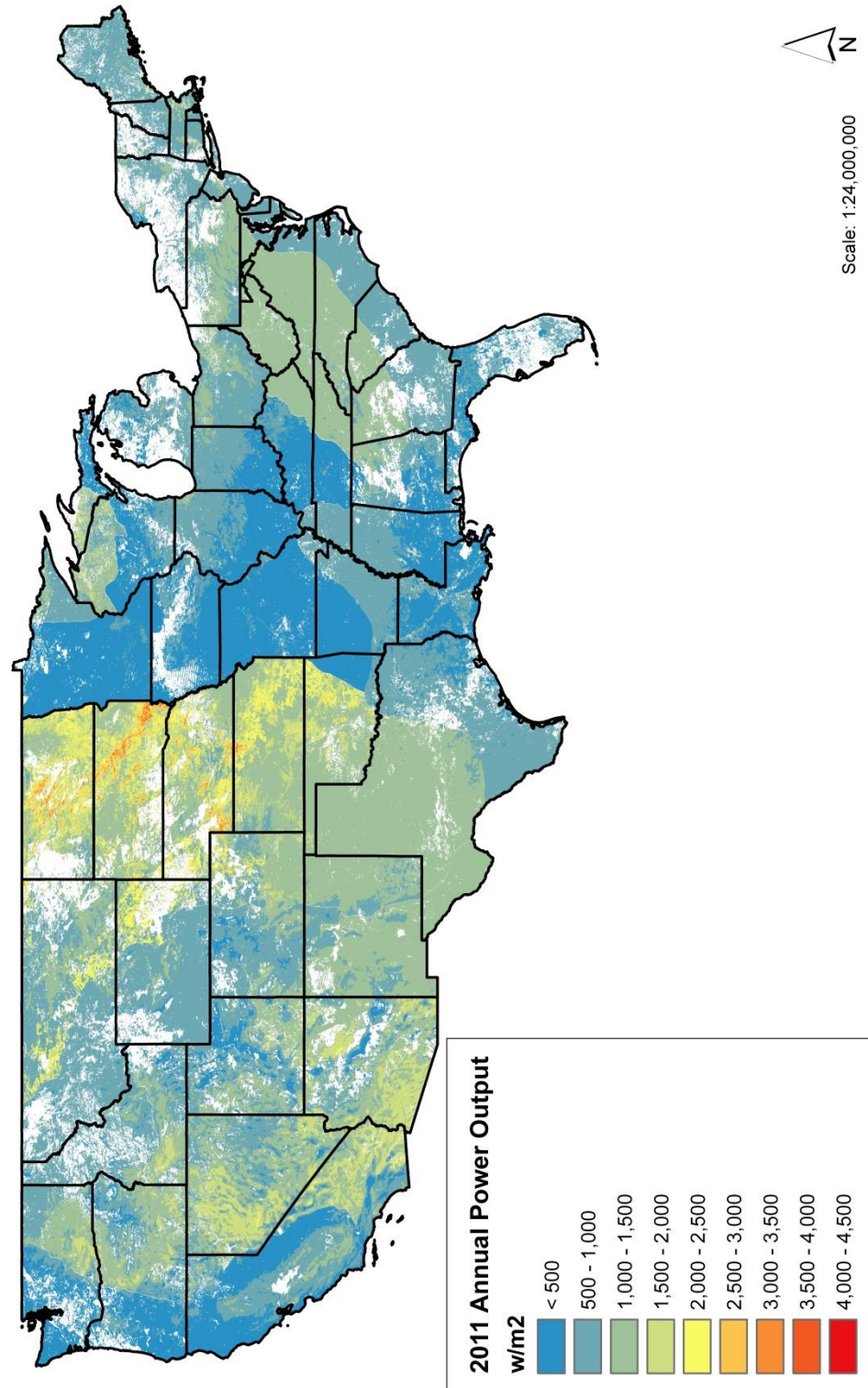


Figure 83: 2011 Annual Power Output (from Threshold Model)

Threshold Model: 2013 Annual Power Output

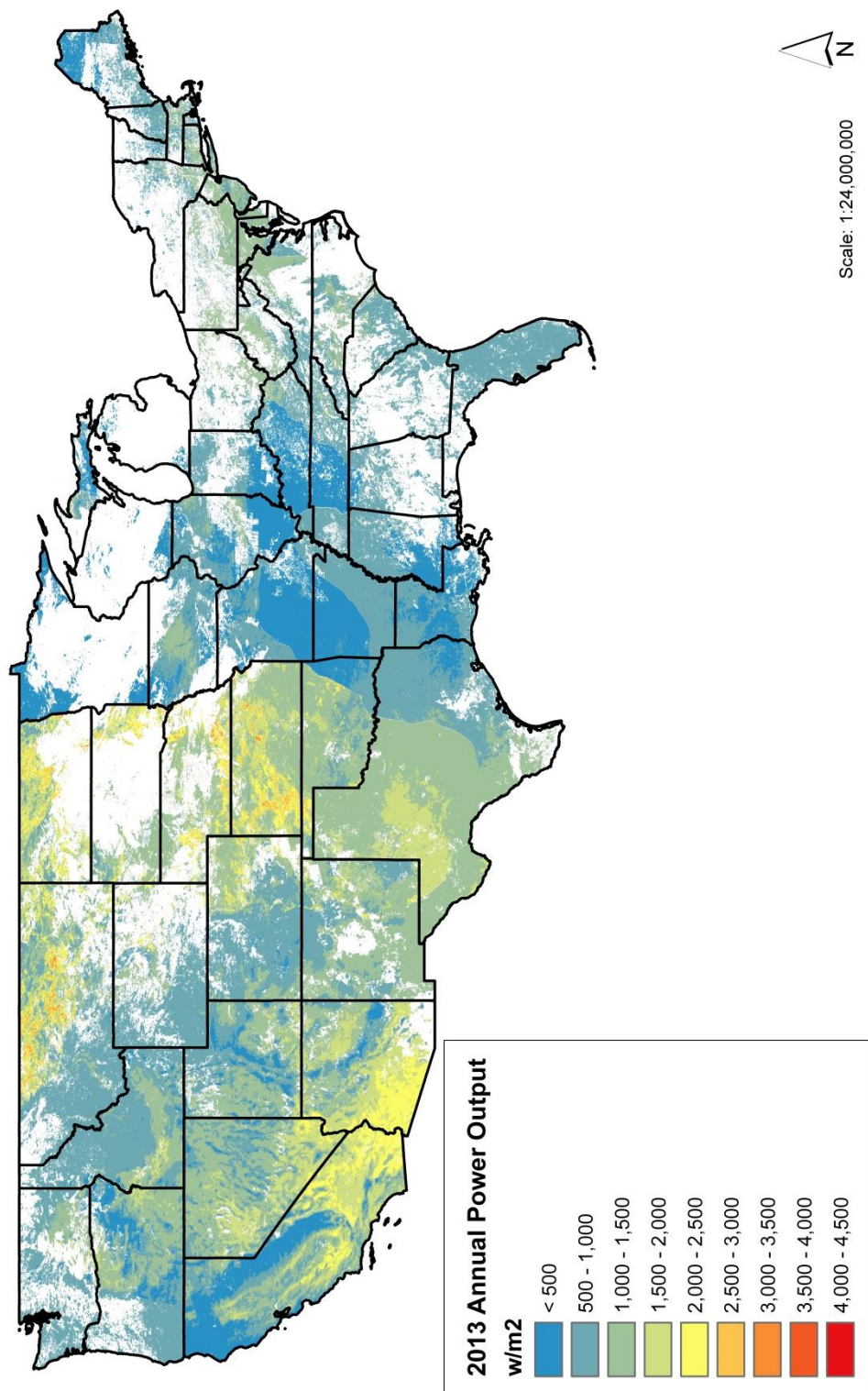


Figure 84: 2013 Annual Power Output (from Threshold Model)

6.9 Linear Model

The final model incorporates the sensible and latent heat calculations, and the slope model to calculate potential energy generated by the SoV. For the purposes of this research, the completed model will be used to calculate vortex energy for both the Mesa, Arizona (location of SoV prototype) and Zion National Park, Utah (location of case study) areas.

6.9.1 Final Model Assumptions

6.9.1.1. Vortex Power Assumption

Based on the results from the six-meter diameter SoV prototype located in Mesa, Arizona, it is assumed that:

$$\text{Vortex Energy (VE)} = (H) \times (C_a) \times (C_E)$$

Where SoV power is a function of sensible heat H , the footprint of the SoV where sensible heat is obtained and utilized by the unit (the collection area, C_a , and measure of conversion efficiency C_E , by which the SoV converts sensible heat to power.

Using the six-meter diameter prototype located in Mesa, Arizona, it was found that:

$$\begin{aligned} (VE)_6 &= (1,500 \text{ kw}) = (237.4 \text{ w/m}^2) \times (C_a) \times (C_E) = \\ (C_a) \times (C_E) &= \left(\frac{1500}{237.4} \right) = 6.32 \end{aligned}$$

The collection area (C_a) represents the area around the SoV unit in which energy will be drawn into the unit. Both collection area (C_a) and the conversion efficiency factor (C_E) are unknown, but the assumption from this model is that the product of the two is equal to 6.32.

Thus, for the final prototype model, which had a diameter of 10 meters, it is assumed that r^4 , such that:

$$(VE)_{10} = 6.32 \times \left(\frac{10}{6}\right)^4 \times H = 6.32 \times 7.71 \times H \\ = 48.75 \times H$$

Only sensible heat is considered in this model, due to the prototype being located in a desert, which lacks latent heat. Slope was also not considered for this model due to the flat location.

6.9.1.2 Daytime Electrical Power Produced by SoV

Using the value obtained from the Vortex Power equation at a 10-meter diameter, it is then assumed that the daytime production power for the SoV (at approximately 10:30 AM) can be found using:

$$\text{Daytime Electrical Power } VE_D = (VE)_{10} \times (G_E)$$

Where the generation efficiency factor, G_E , is either .3, .4, or .5, representing a 30 to 50 percent efficiency in the unit converting sensible heat to electrical power.

6.9.1.3 Average Daytime Electrical Power Produced by SoV

The average daytime electrical power produced (VE_{AD}) by the unit can then be determined by multiplying the daytime electrical power produced by a conversion factor obtained from the Ameriflux data. The conversion factor is based on the ratio of the measured sensible heat flux at the Ameriflux site located in the same physiographic region as the location used in the model, and the sensible heat flux obtained from the GIS results. For Mesa, Arizona, the Santa Rita Creosote site was used, resulting in:

$$(VE_{AD}) = (R_F) \times (VE)_{10} \times (G_E)$$

For the Santa Rita Creosote site:

$$(R_F) = \left(\frac{154}{148}\right)$$

6.9.1.4 Average Monthly Daytime Electrical Power Produced by SoV

Lastly, to find average monthly daytime electrical power production, VE_{AM} , the average daytime electrical power is used to calculate the following:

$$VE_{AM} = \left(\frac{VE_{AD}) \times 12 \times 30}{1000}\right)$$

The result is measured in kilowatt-hours.

6.9.1.5 Average Daytime Electrical Power Produced by SoV for All Locations

For all other locations where latent heat and slope are factors, the final model is:

$$(VE) = (R_F) \times 48.75 \times (H + .1\lambda E) \times (1 + (2 \times ((\frac{\delta}{100})))) \times (G_E)$$

Where sensible heat H and latent heat λE and slope δ were calculated in the GIS, and the result is measured in kilowatt-hours.

6.9.1.6 Relationship between Sensible and Latent Heat and Slope

It was assumed that both latent heat and slope extend operational time of the SoV. Latent heat, which is assumed to be approximately 10 percent as effective as sensible heat, was considered in the model, as the sum of sensible heat and 10 percent of the latent heat:

$$(H + .1\lambda E)$$

It was also assumed that two percent of each percent of slope will extend the operational time of the SoV. As mentioned previously, it was assumed that, although an SoV facility will need to be installed on level ground, upward or downward swept winds from sloping ground adjacent to the facility may influence the start-up time.

$$(1 + (2 \times ((\frac{\delta}{100}))))$$

6.9.1.7 Potential Withdrawal of Power

Final vortex energy is assumed to fall within a range of 30 to 50 percent of the energy calculated by the model. This estimate is based on the UTRC estimate of potential withdrawal of power. It is assumed that 30 to 50 percent of the energy will be converted to electricity by the SoV unit, with 30 being the lower estimate, 40 being an intermediate estimate, and 50 being the upper estimate. The final values were obtained using the raster calculator tool.

6.9.1.8 Mesa, Arizona Calculation Methods

As with previous calculations, the raster calculator tool in ArcGIS was used to perform the calculations for the final model. The sensible and latent heat layers (AM values only), the power output estimation layer and table containing the average, monthly sensible heat values from Ameriflux, and the slope model were needed to perform the calculations. A Mesa, Arizona boundary polygon layer was obtained from the City of Mesa's Website, and was used to perform the "extract by mask" function in ArcToolbox to clip the area within the Mesa boundary from the aforementioned raster layers. The completed July 2013 monthly average daytime vortex energy estimations can be found in *Figure 85: Mesa, Arizona Summer 2013 Vortex Energy (Low Estimate)* though *Figure 87: Mesa, Arizona Summer 2013 Vortex Energy (High Estimate)*.

Mesa, Arizona: July 2013 Monthly Average Daytime Vortex Energy

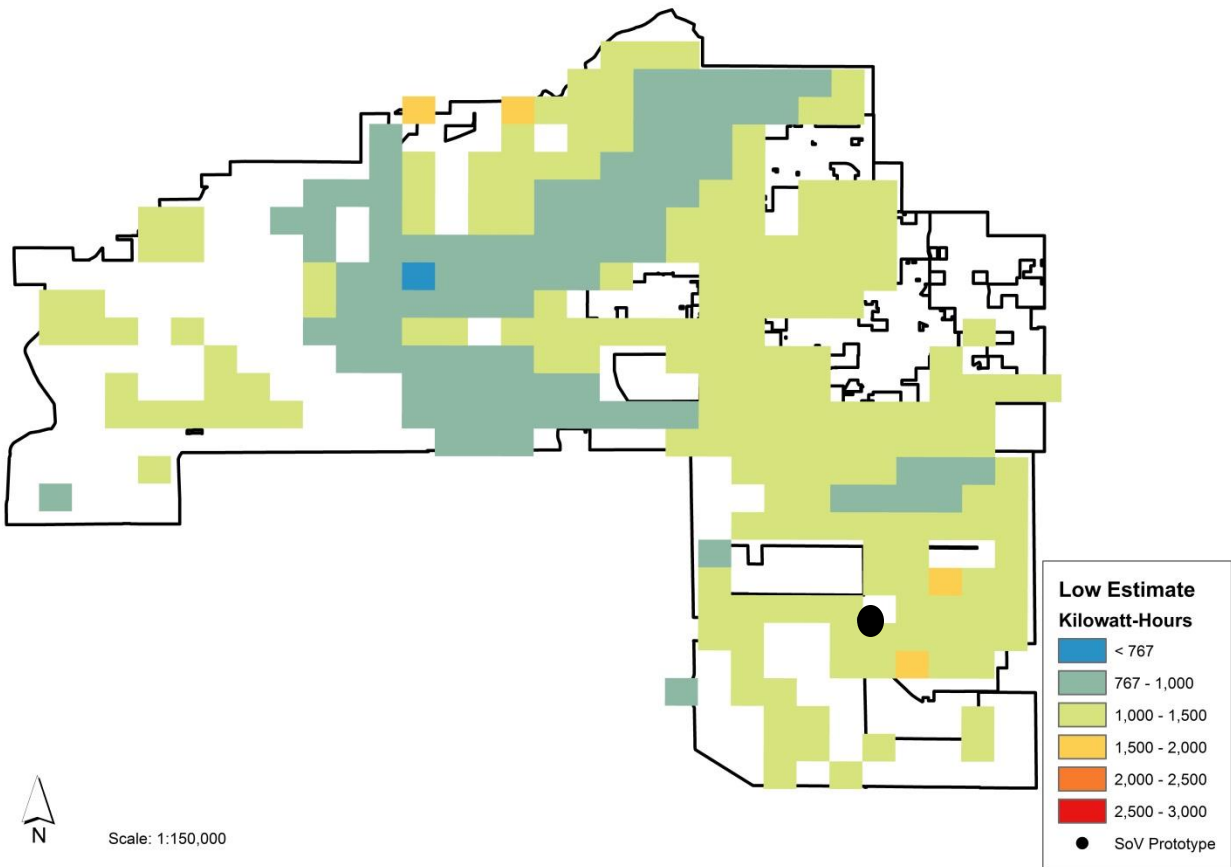


Figure 85: Mesa, Arizona Summer 2013 Vortex Energy (Low Estimate)

Mesa, Arizona: July 2013 Monthly Average Daytime Vortex Energy

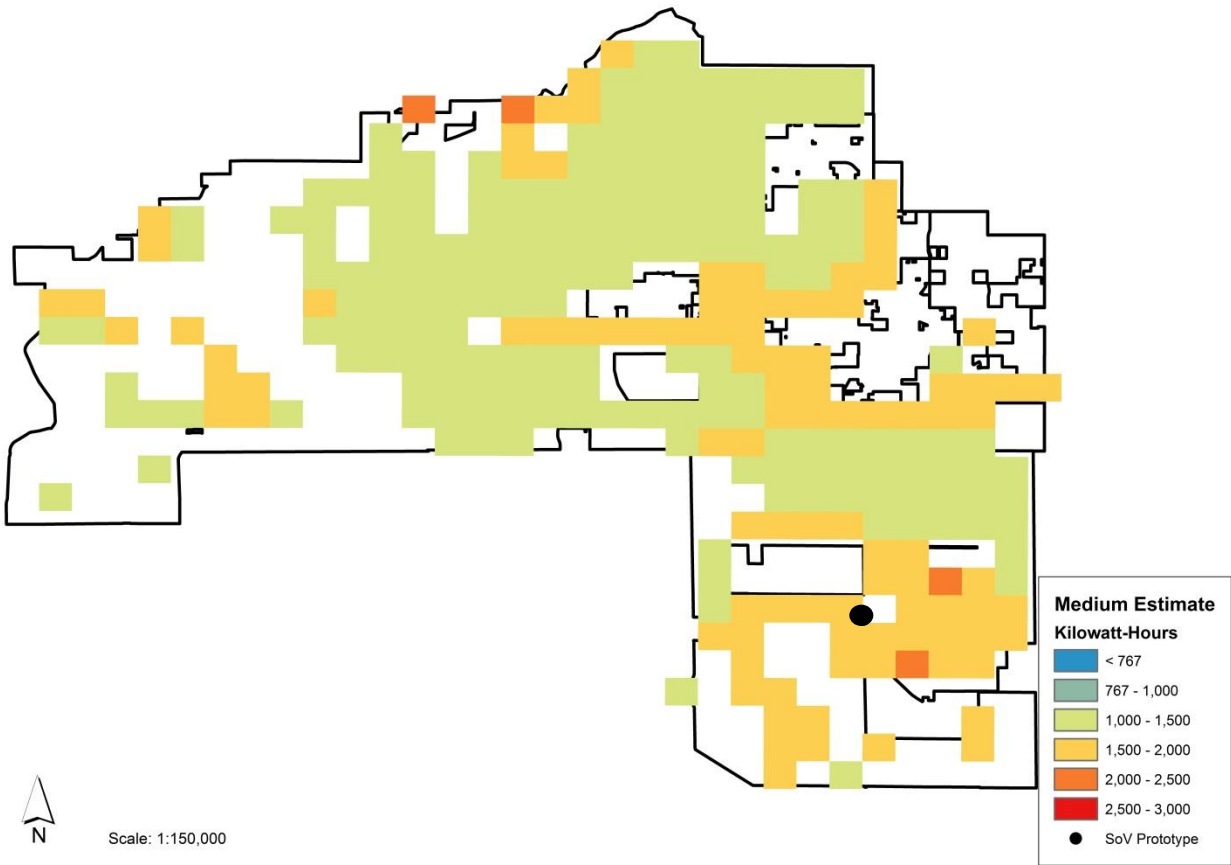


Figure 86: Mesa, Arizona Summer 2013 Vortex Energy (Medium Estimate)

Mesa, Arizona: July 2013 Monthly Average Daytime Vortex Energy

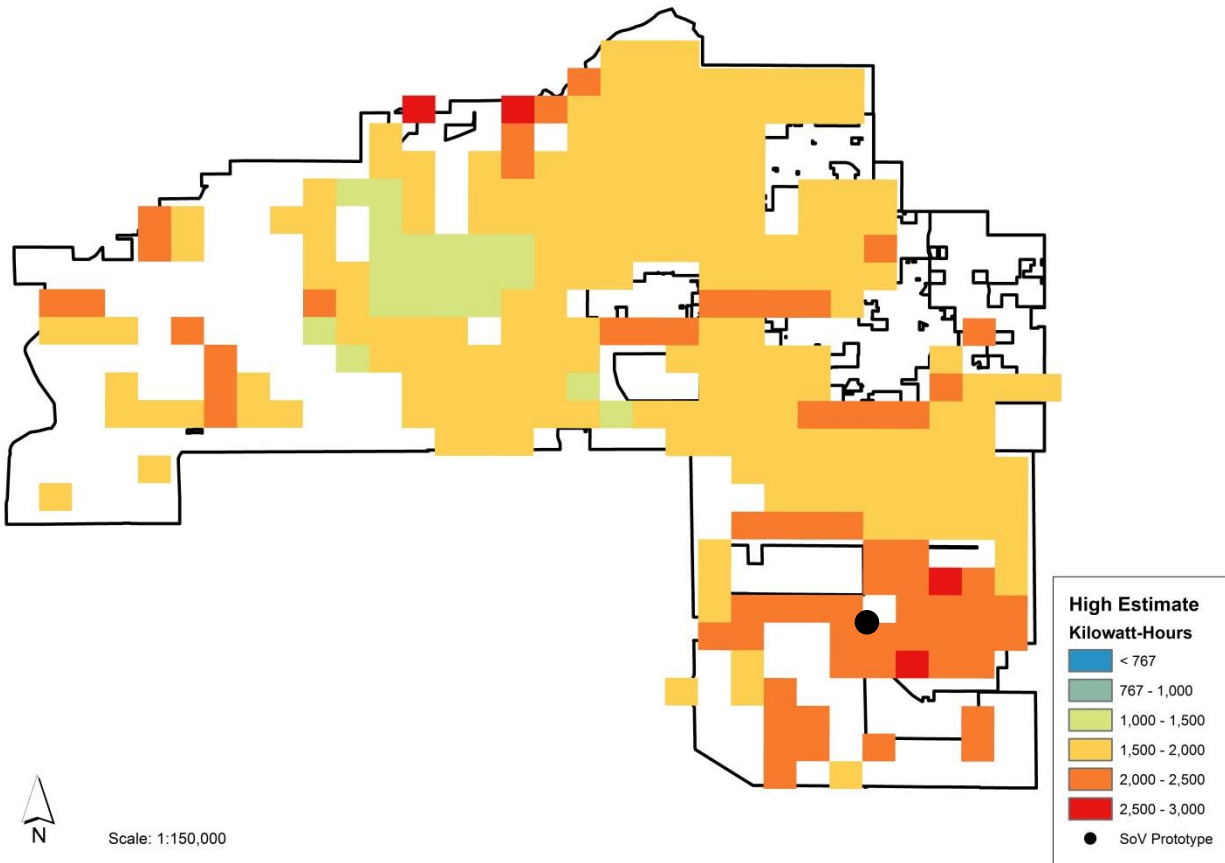


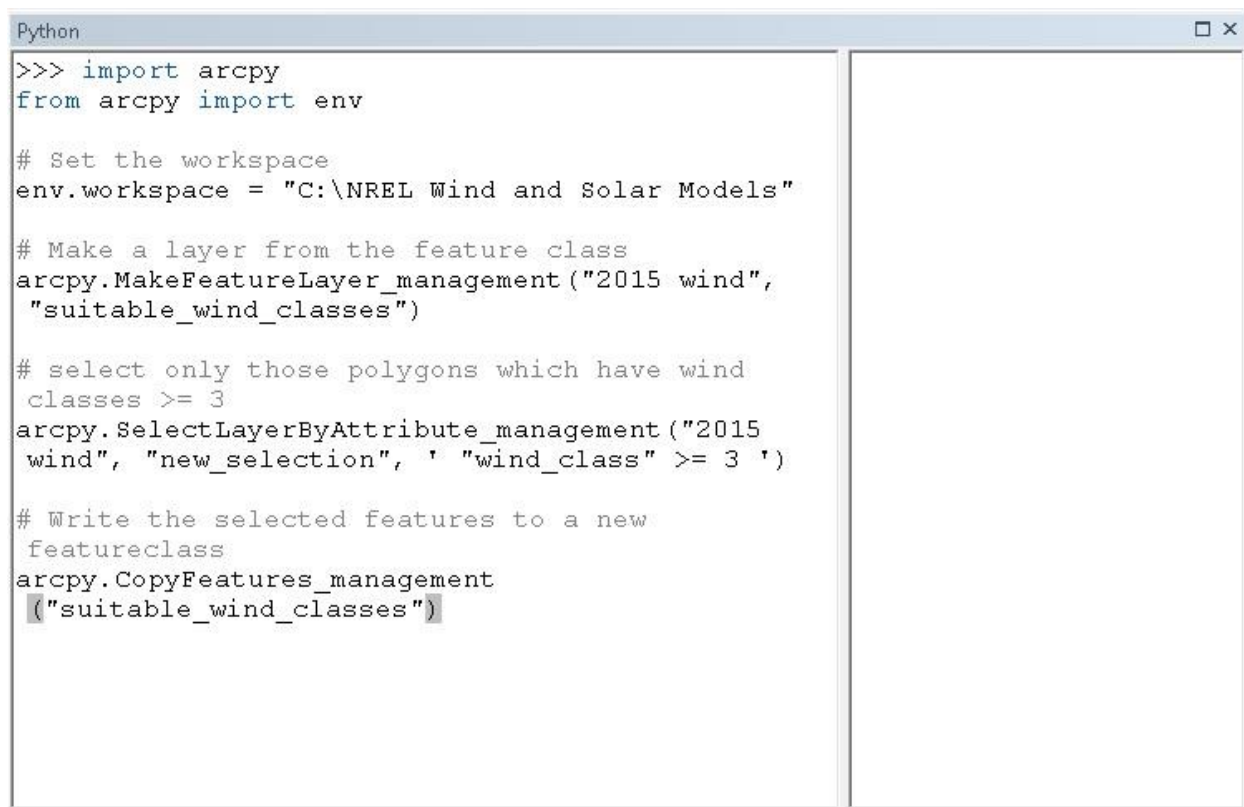
Figure 87: Mesa, Arizona Summer 2013 Vortex Energy (High Estimate)

CHAPTER 7: THE NATIONAL PARKS

7.1 Locating National Parks Using NREL's Wind and Solar Models

7.1.1 Parks Suitable for Wind Facilities

NREL's wind resource data, which consists of vectors, or polygons, displays varying wind classes for the lower 48 States, was loaded into ArcGIS. An ArcPy script was written, as shown in *Figure 88: ArcPy Script for Selecting Areas with Assigned Wind Classes Greater than, or Equal to Three*, to perform the task of selecting areas from the model that have an assigned wind class of three or higher. The value of three was chosen based on NREL's specifications for locations suitable for large-scale wind facilities. Although the documentation states that areas with assigned wind classes of two can accommodate small-scale wind turbines (NREL, 2015), these locations were excluded due to the assumption that the National parks' transportation energy needs, and overall energy needs, would require larger facilities than a small-scale turbine.

A screenshot of a Python script editor window titled "Python". The script is written in Python and uses the ArcPy library. It sets a workspace, creates a feature layer, selects features based on a wind class attribute, and copies the selected features to a new feature class.

```
>>> import arcpy
from arcpy import env

# Set the workspace
env.workspace = "C:\NREL Wind and Solar Models"

# Make a layer from the feature class
arcpy.MakeFeatureLayer_management("2015 wind",
    "suitable_wind_classes")

# select only those polygons which have wind
# classes >= 3
arcpy.SelectLayerByAttribute_management("2015
wind", "new_selection", ' "wind_class" >= 3 ')

# Write the selected features to a new
# featureclass
arcpy.CopyFeatures_management
(["suitable_wind_classes"])
```

Figure 88: ArcPy Script for Selecting Areas with Assigned Wind Classes Greater than, or Equal to Three

After the areas with assigned wind classes of three or higher were selected using the ArcPy script, it was necessary to write an additional ArcPy script that would then select the National parks that are located within these areas, as shown in *Figure 89: ArcPy Script for Selecting National Parks within Areas with Wind Classes Greater than, or Equal to Three*.

```

Python
>>> import arcpy
... from arcpy import env
...
... # Set the workspace
... env.workspace = "C:\NREL Wind and Solar
Models"
...
... # Make a layer from the feature class
... arcpy.MakeFeatureLayer_management
("National_Parks", "suitable_National_Parks")
...
... # Select all National Parks which overlap
suitable wind class polygons
... arcpy.SelectLayerByLocation_management
("suitable_National_Parks", "intersect",
"suitable_wind_classes", 0, "new_selection")
...
... # Write the selected features to a new
featureclass
... arcpy.CopyFeatures_management
("suitable_National_Parks", "wind_parks")

```

Figure 89: ArcPy Script for Selecting National Parks within Areas with Wind Classes Greater than, or Equal to Three

The results from the model included the following 12 National parks:

Table 6: Suitable National Parks for Wind Facilities

Park	State
Acadia	Maine
Badlands	South Dakota
Capital Reef	Utah
Carlsbad Caverns	New Mexico
Channel Islands	California
Crater Lake	Oregon
Death Valley	California/Nevada
Guadalupe Mountains	Texas
Lassen Volcanic	California
Mount Rainier	Washington
Olympic	Washington
Rocky Mountain	Colorado
Theodore Roosevelt	North Dakota
Wind Cave	South Dakota

As shown in *Table 6: Suitable National Parks for Wind Facilities* and *Figure 90: National Parks in Areas with Assigned Wind Class of 3 to 7 (NREL, 2015)*, 12 parks were chosen using the model. The only National park selected in the model that currently has existing wind facilities is Channel Islands National Park in California. Mount Rainier National Park in Washington does not have wind facilities that provide power to the park, although wind farms are currently in-operation adjacent to park property, and are managed privately. Further examination will be required to determine the suitability of the remaining 10 National parks selected in the model.

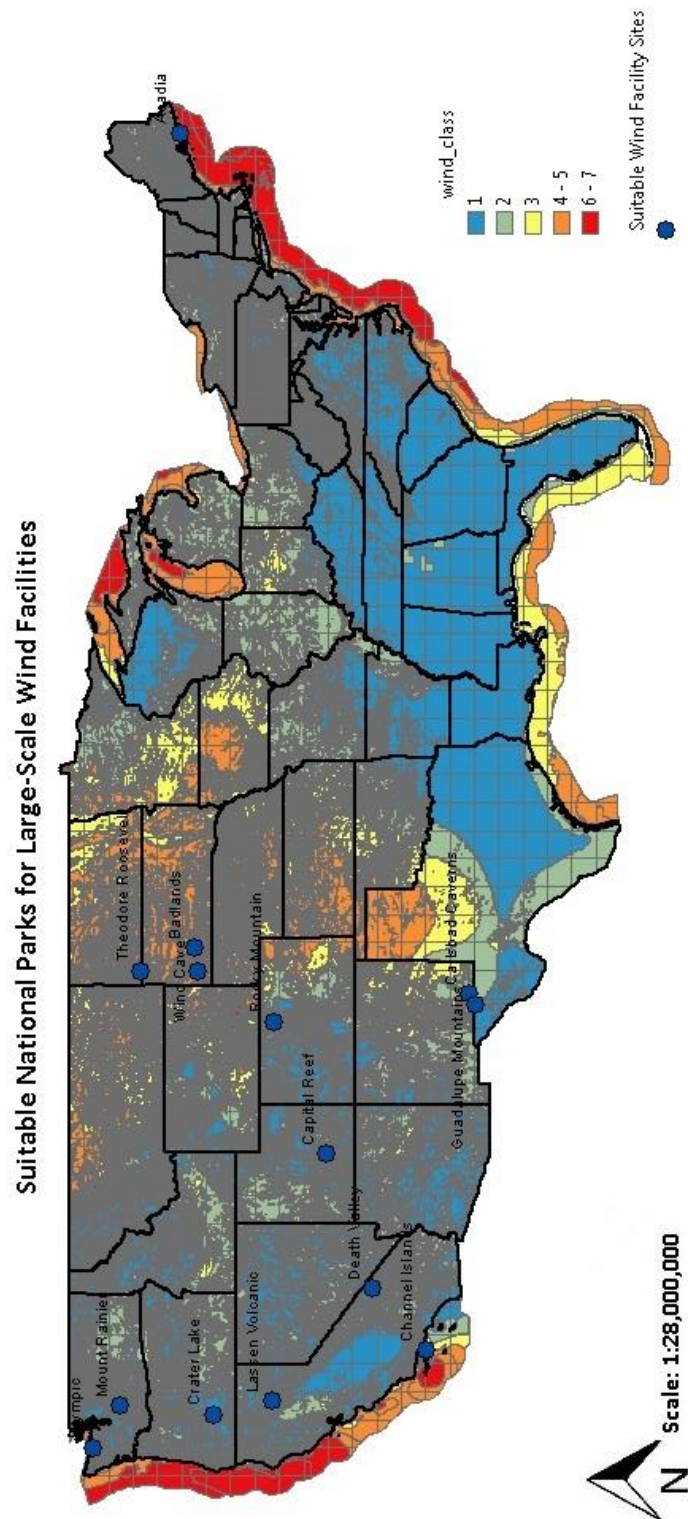
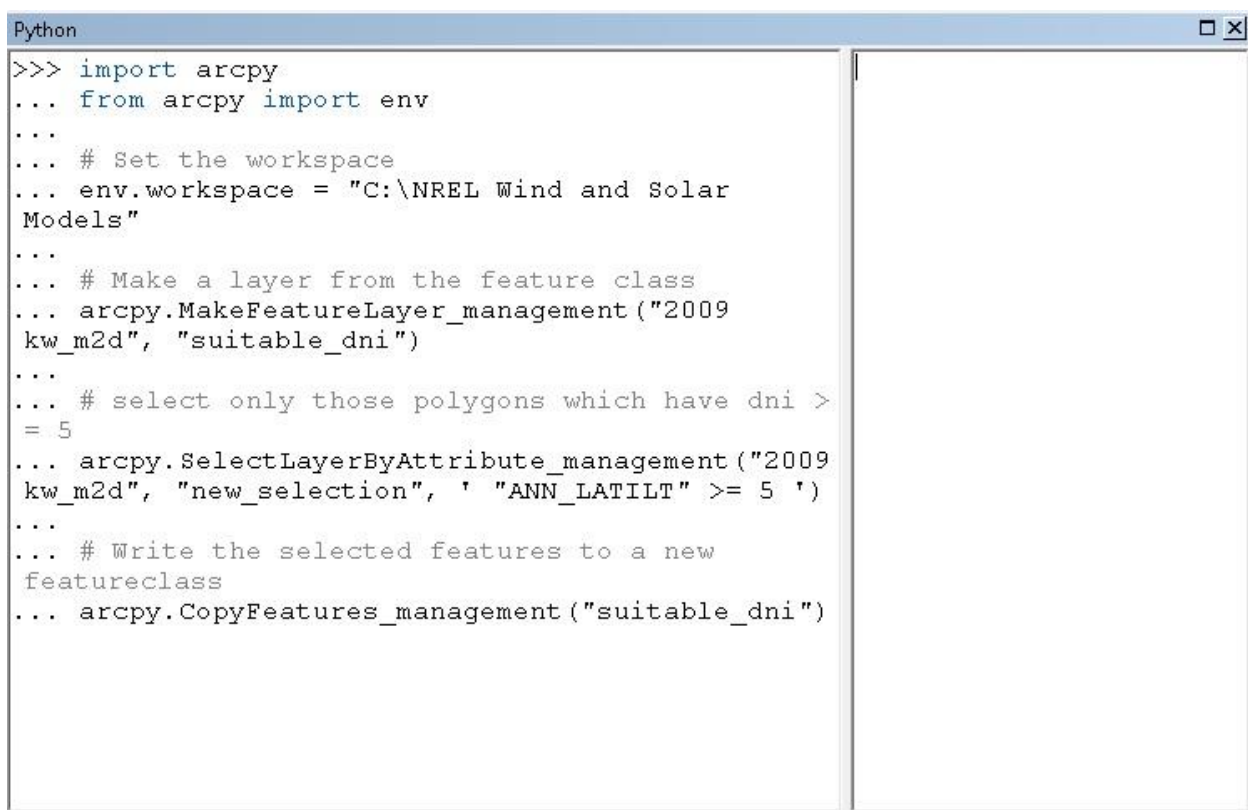


Figure 90: National Parks in Areas with Assigned Wind Class of 3 to 7 (NREL, 2015)

7.1.2 Parks Suitable for Solar PV Facilities

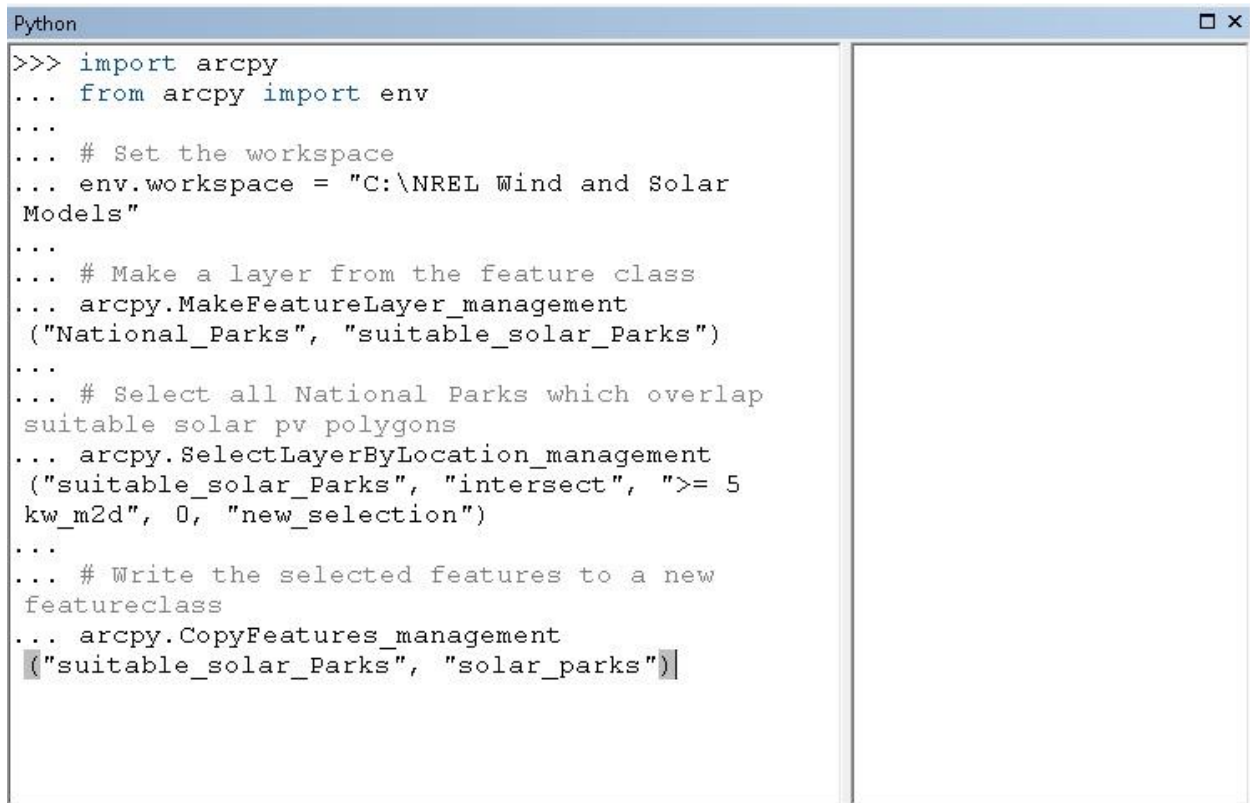
Similar methods were used to locate National parks that are located in areas suitable for solar pv facilities. NREL's solar resource model was loaded into ArcGIS. The solar resource data, which also consists of vectors, or polygons, displays the average, annual, and monthly, energy potential for solar pv facilities in kilowatts per square meter day for the lower 48 States. An ArcPy script was written to perform the task of selecting areas from the model that have solar pv energy potential of five kw/m2d or higher, as shown in *Figure 91: ArcPy Script for Selecting Areas with Kilowatts per Square Meter per Day (kw/m2d) Greater than, or Equal to Five*. The value of five was chosen arbitrarily.



```
Python
>>> import arcpy
... from arcpy import env
...
... # Set the workspace
... env.workspace = "C:\NREL Wind and Solar
Models"
...
... # Make a layer from the feature class
... arcpy.MakeFeatureLayer_management("2009
kw_m2d", "suitable_dni")
...
... # select only those polygons which have dni >
= 5
... arcpy.SelectLayerByAttribute_management("2009
kw_m2d", "new_selection", ' "ANN_LATILT" >= 5 ')
...
... # Write the selected features to a new
featureclass
... arcpy.CopyFeatures_management("suitable_dni")
```

Figure 91: ArcPy Script for Selecting Areas with Kilowatts per Square Meter per Day (kw/m2d) Greater than, or Equal to Five

After the areas with solar pv energy potential of five or greater were selected using the ArcPy script, it was necessary to write an additional ArcPy script that would then select the National parks that are located within these areas, as shown in *Figure 92: ArcPy Script for Selecting National Parks within Areas with Kilowatts per Square Meter per Day (kw/m2d) Greater than, or Equal to Five.*

A screenshot of a Python script editor window titled "Python". The window contains a script that uses the ArcPy library to select national parks based on solar energy potential. The script is as follows:

```
>>> import arcpy
... from arcpy import env
...
... # Set the workspace
... env.workspace = "C:\NREL Wind and Solar
Models"
...
... # Make a layer from the feature class
... arcpy.MakeFeatureLayer_management
("National_Parks", "suitable_solar_Parks")
...
... # Select all National Parks which overlap
suitable solar pv polygons
... arcpy.SelectLayerByLocation_management
("suitable_solar_Parks", "intersect", ">= 5
kw_m2d", 0, "new_selection")
...
... # Write the selected features to a new
featureclass
... arcpy.CopyFeatures_management
(["suitable_solar_Parks", "solar_parks"])
```

Figure 92: ArcPy Script for Selecting National Parks within Areas with Kilowatts per Square Meter per Day (kw/m2d) Greater than, or Equal to Five

The results from the model included the following 30 National parks:

Table 7: Suitable National Parks for Solar PV Facilities

Park	State
Arches	Utah
Badlands	South Dakota
Big Bend	Texas
Biscayne	Florida
Black Canyon of the Gunnison	Colorado
Bryce Canyon	Utah
Canyonlands	Utah
Capital Reef	Utah
Carlsbad Caverns	New Mexico
Channel Islands	California
Conagree	South Carolina
Crater Lake	Oregon
Death Valley	California/Nevada
Everglades	Florida
Grand Canyon	Arizona
Great Basin	Nevada
Great Sand Dunes	Colorado
Guadalupe Mountains	Texas
Joshua Tree	California
Kings Canyon	California
Lassen Volcanic	California
Mesa Verde	Colorado
Petrified Forest	Arizona
Pinnacles	California
Rocky Mountain	Colorado
Saguaro	Arizona
Sequoia	California
Theodore Roosevelt	North Dakota
Wind Cave	South Dakota
Yellowstone	Wyoming/Montana/Idaho
Yosemite	California
Zion	Utah

As shown in *Table 7: Suitable National Parks for Solar PV Facilities* and *Figure 93: National Parks in Areas with $kw/m^2d \geq 5$* , 32 parks were chosen using the model. Several of the National Parks selected in the model currently have solar pv facilities on park property, including: Canyonlands, Death Valley, Yosemite, and Zion. Although several of the National parks were excluded from this list, this is simply because the value of five was chosen arbitrarily. It is possible that several of the other National parks not selected in the model may be suitable

for small-scale solar pv facilities. An example of this is the Great Smoky Mountains National Park, which has small-scale solar pv facilities, but was excluded from the model results.

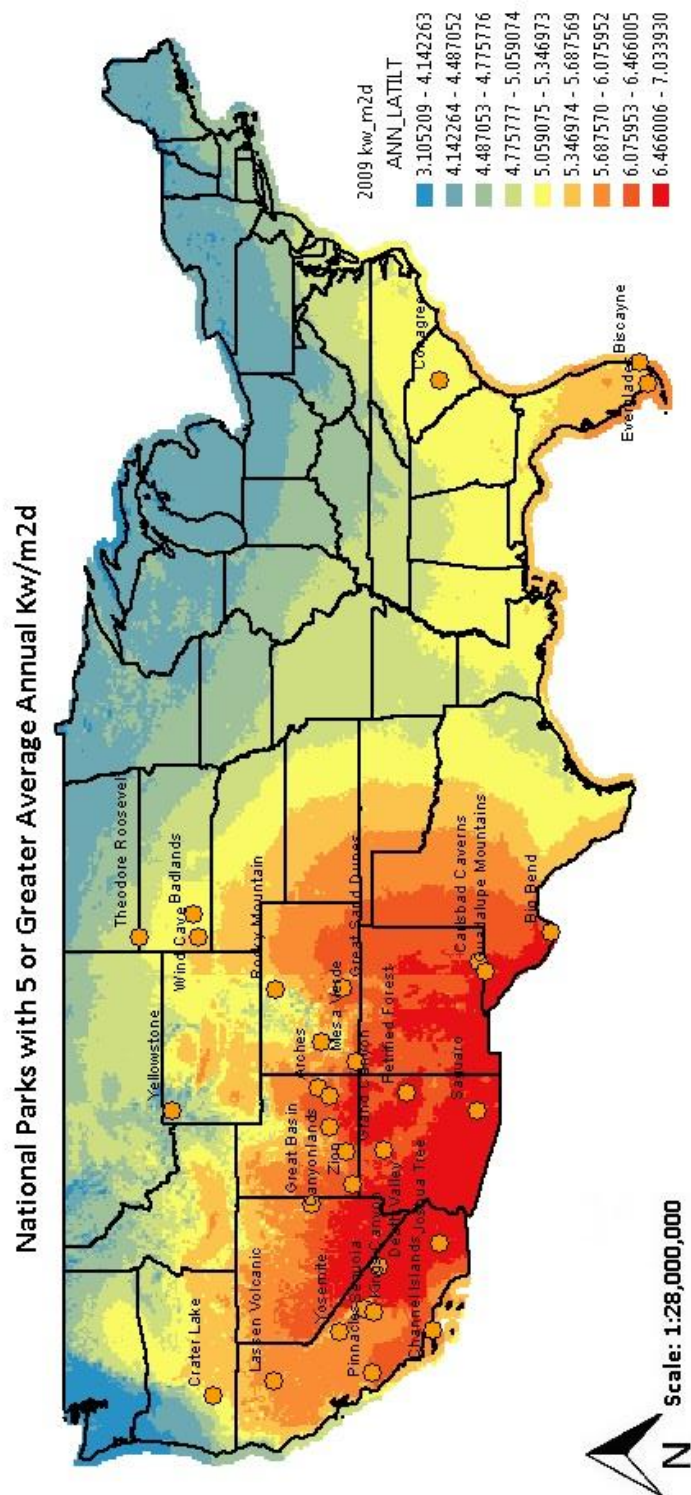


Figure 93: National Parks in Areas with kw/m²d \geq 5

CHAPTER 8: ANALYSIS, RESULTS, AND DISCUSSION OF CASE STUDY IN ZION NATIONAL PARK

Zion National Park near Springdale, Utah, as shown in *Figure 94: Zion National Park Boundary (Google Earth)*, was chosen for the case study in this research due to its remote location and its assumed suitability for installation of SoV facilities. The following section contains a brief overview of Zion National Park, and its current park transportation. The results from both the linear model and the threshold model will then be provided. Lastly, suggestions will be provided regarding suitable locations for SoV units and ways to incorporate SoV usage into the Park's transportation system. This case study is to be used as an example of how both the linear and threshold models can be applied to varying locations to determine site suitability for SoV installation. Installation of SoV units in the specified location in the case study, or another location in Zion also depends on other considerations other than power output potential. The following table shown in *Table 8: Additional SoV Site Selection Criteria* contains additional considerations for park managers. SoV power output potential should not be the only consideration, and park management may find that small scale wind or additional solar pv systems may be a more suitable solution for providing renewable power to Zion.

SoV Site Selection Criteria for Park Managers
Criteria
Land Availability
Aesthetics
Wildlife Impacts
Habitat Encroachment
Water Resource Impacts
Stormwater Management

Table 8: Additional SoV Site Selection Criteria

8.1 Overview of Zion National Park

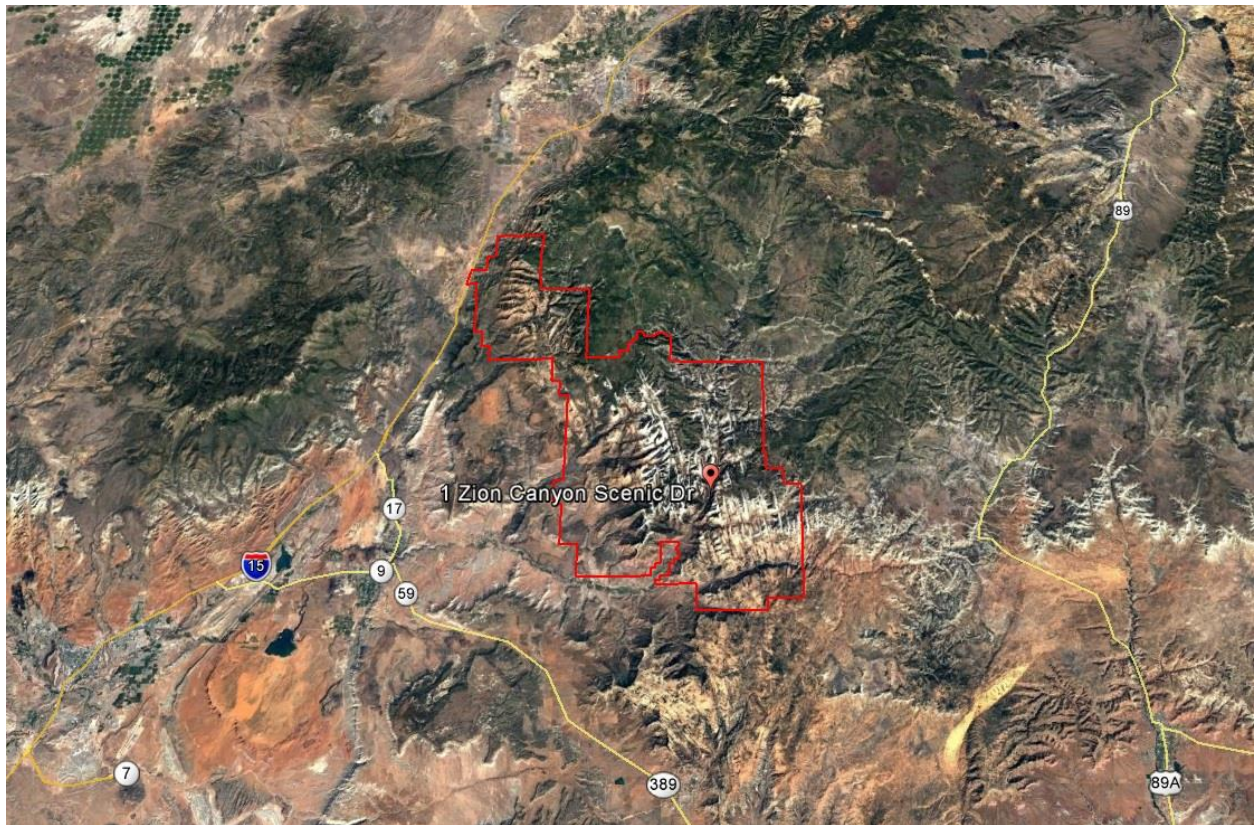


Figure 94: Zion National Park Boundary (Google Earth)

Frank Austin, the general manager at Parks Transportation Incorporated, provided information regarding the park shuttle fleet size for Zion. According to Mr. Austin, the current fleet size consists of 39 Eldorado National propane-powered buses. Each bus is 30 feet long, and seats 31 passengers. The park also has a fleet of 23 Eldorado National passenger trailers that are 30 feet long and seat 37 passengers. These trailers are run in-tandem with the buses, similar to an articulated bus. Also according to Mr. Austin, although the tandem bus and trailers seat 68 passengers total, typically there are 100 passengers on the combined units due to standing passengers, and there are often 45 to 50 passengers on the buses alone, also due to standing passengers.

The shuttles and trailers are typically housed in a parking lot, which also contains a garage, located adjacent to the Zion National Park Visitor Center, as shown in *Figure 95: Zion Shuttle Parking and Garage (Google Earth)*. This parking lot, and the area located to the north of the shuttle garage and parking lot would likely be a suitable location for SoV units. The area north of the parking lot is approximately 22,000 square meters (approximately 5.4 acres), and would accommodate an array of approximately six SoVs, as shown in *Figure 96: Area North of Shuttle Parking Considered for SoV Installation*. This number is based on the assumption that, based on the size of the unit (with a ten-meter diameter vortex), and the size of the collection area, 320 units can fit within a square kilometer. These units could then provide power to charging stations located near the shuttle parking lot. Although initial capital costs would be high, it is suggested that part of Zion's current fleet could then be converted to electric. Power from the SoVs could also be used to provide power to the garage facilities.

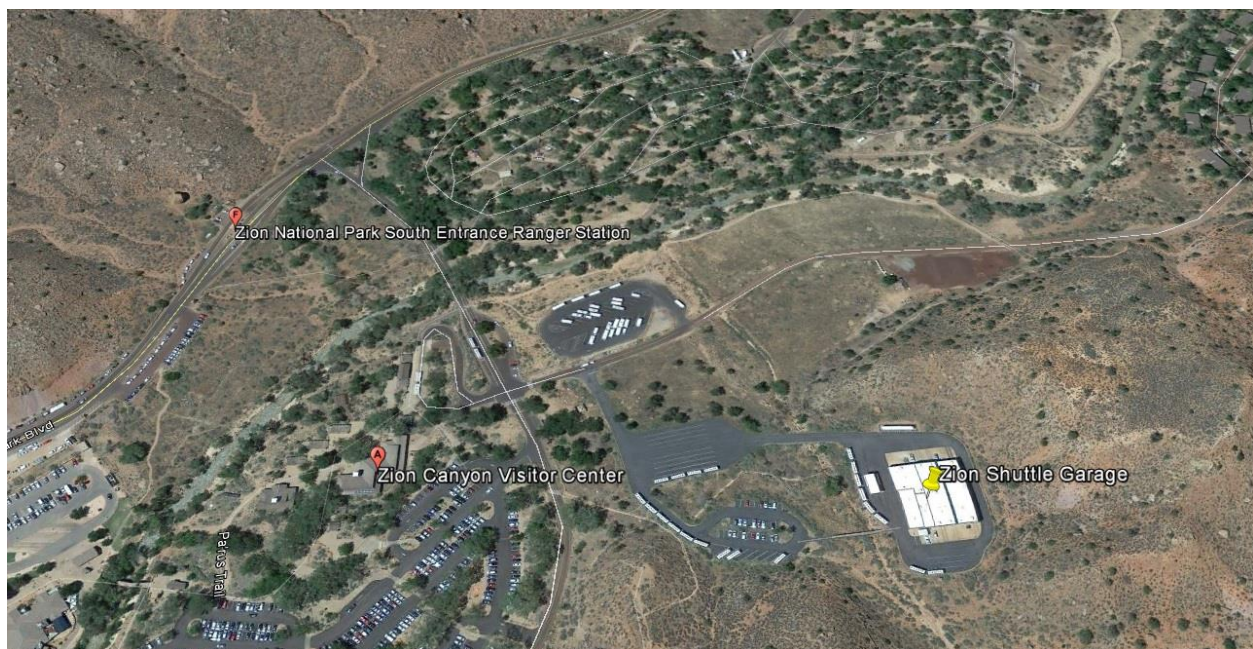


Figure 95: Zion Shuttle Parking and Garage (Google Earth)

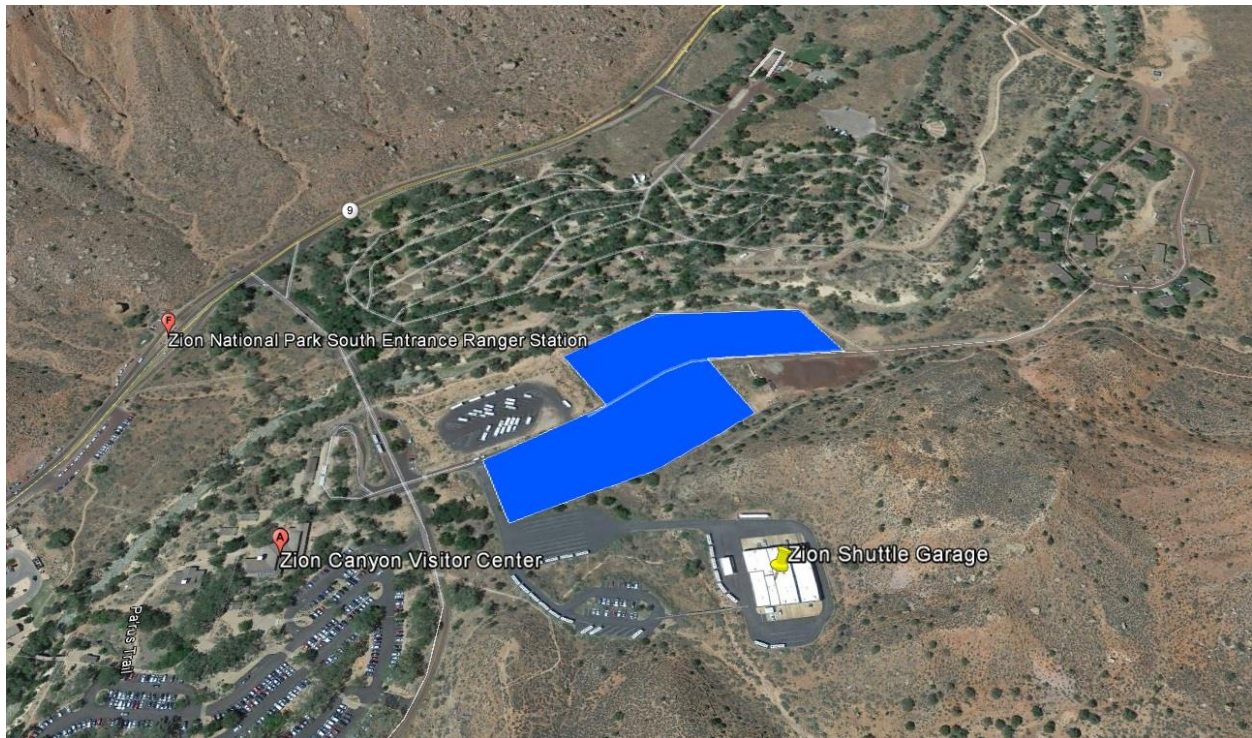


Figure 96: Area North of Shuttle Parking Considered for SoV Installation

A polygon of the area north of the shuttle parking lot was created in Google Earth. After the polygon was created, the measuring tool in Google Earth was used to measure the lengths, and the area was then calculated. The polygon was saved as a kml file and converted to a layer in ArcGIS using the conversion tool in ArcToolbox.

8.2 Calculation of Vortex Energy Potential Using Models

The calculation of vortex energy using both the threshold model and the full linear model needed to be performed in order to determine if the area adjacent to the shuttle parking lot and garage would be suitable for installation of SoV units. The Zion park boundary was used to “clip” the necessary model layers to be used in the calculation, including the slope model, as shown in *Figure 97: Zion National Park Slope Model*. The output from the two models, including close-up images, can be found in *Figure 98: Zion Monthly Average Daytime Vortex*

Energy (Low Estimate – Linear Model) through Figure 109: Zion Shuttle Parking, Visitor Center, and Potential SoV Facility Locaiton (High Estimate – Threshold Model).

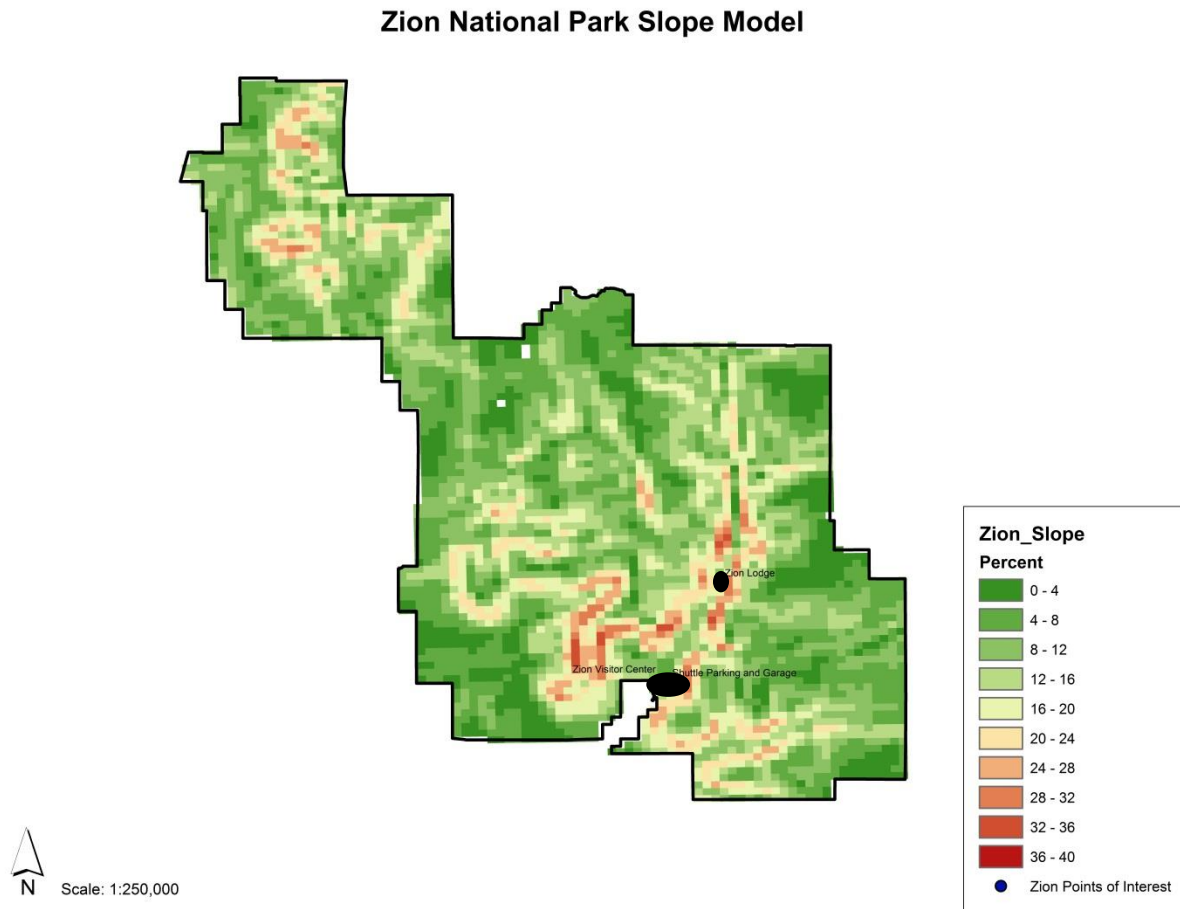


Figure 97: Zion National Park Slope Model

8.3 Results from the Linear Model

Zion National Park: July 2013 Monthly Average Daytime Vortex Energy

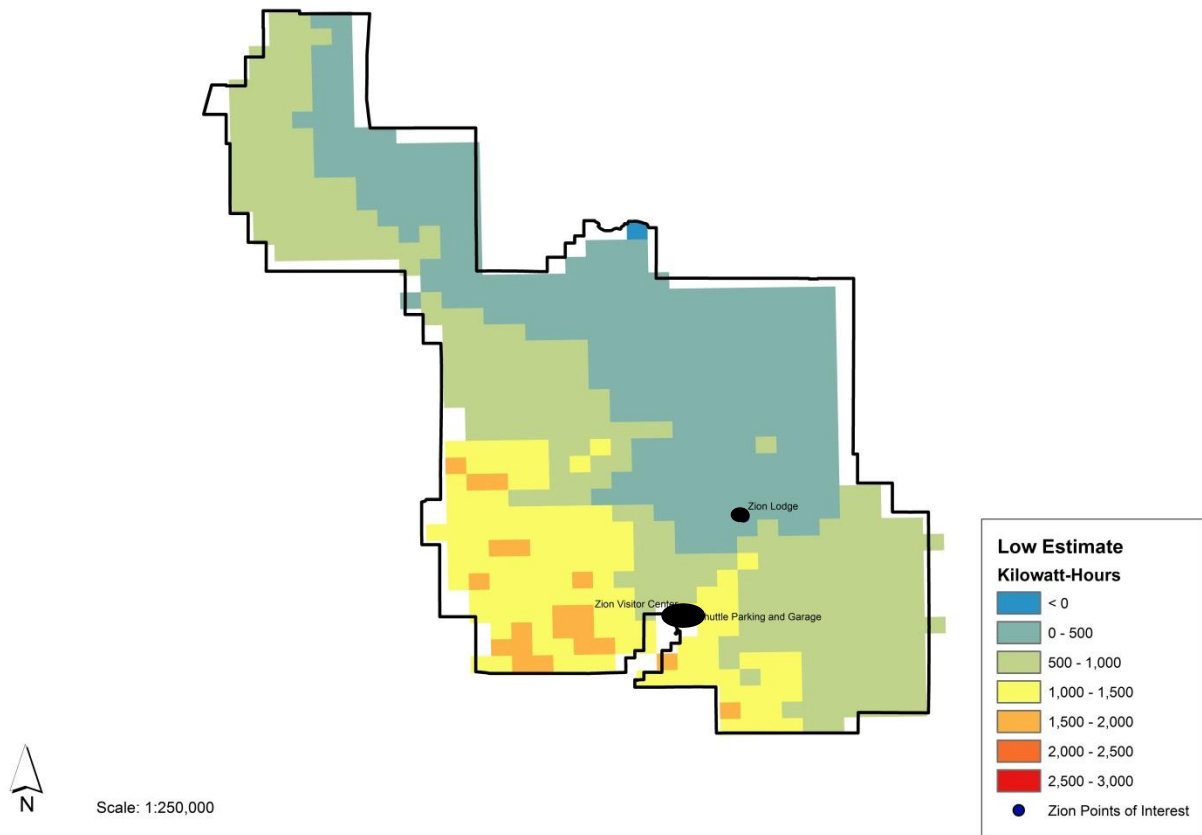


Figure 98: Zion Monthly Average Daytime Vortex Energy (Low Estimate – Linear Model)

Zion National Park: July 2013 Monthly Average Daytime Vortex Energy

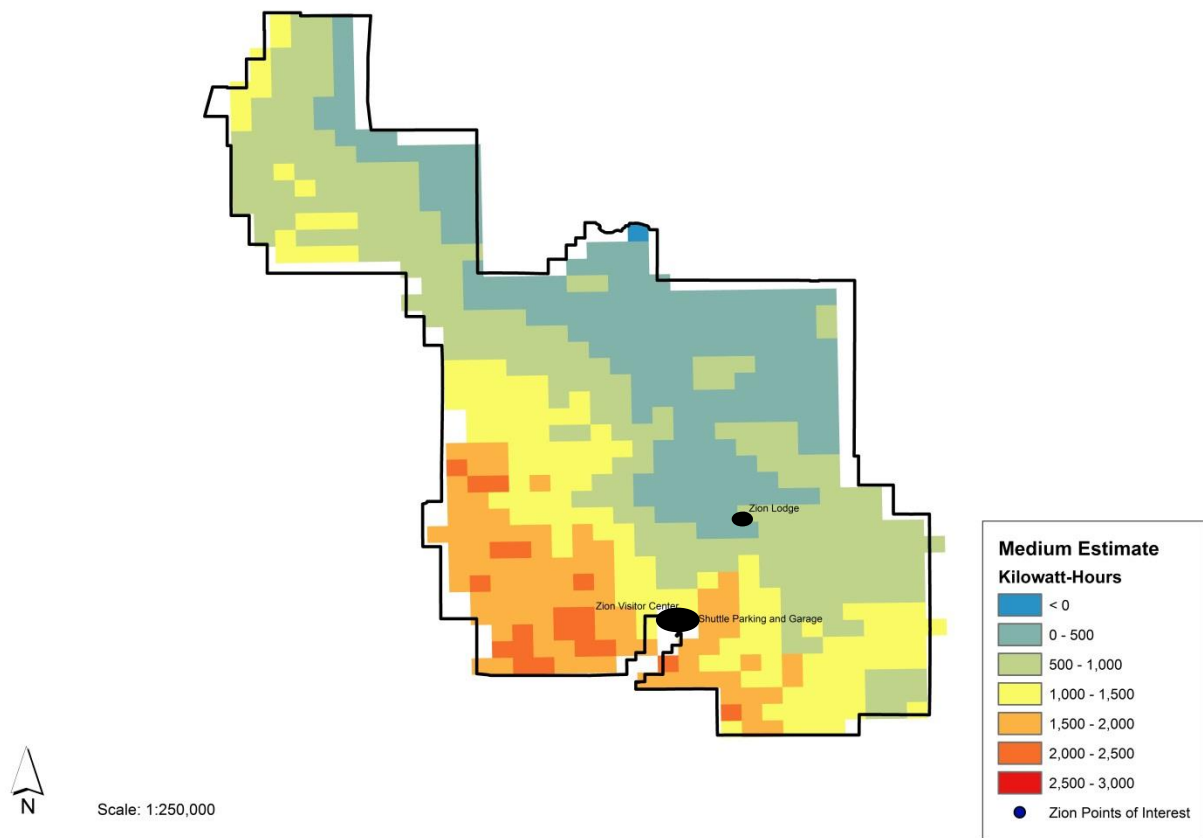


Figure 99: Zion Monthly Average Daytime Vortex Energy (Medium Estimate– Linear Model)

Zion National Park: July 2013 Monthly Average Daytime Vortex Energy

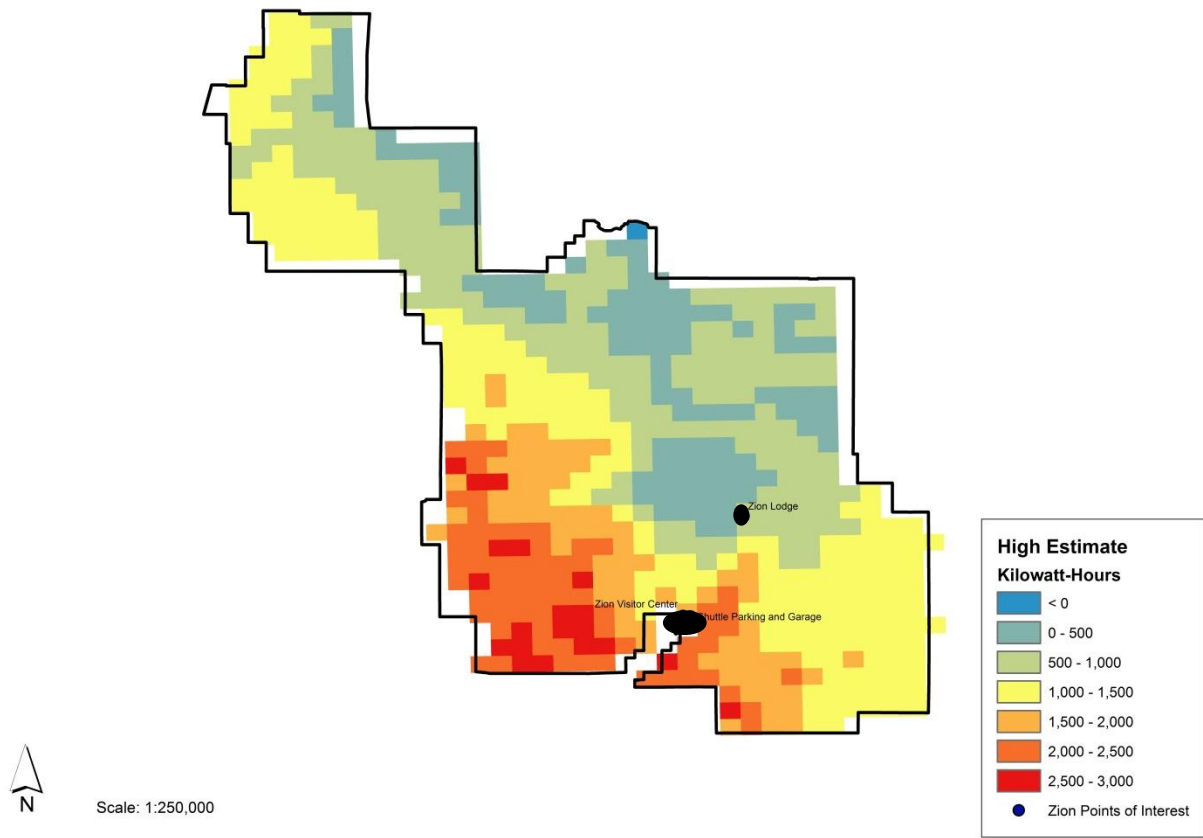


Figure 100: Zion Monthly Average Daytime Vortex Energy (High Estimate- Linear Model)

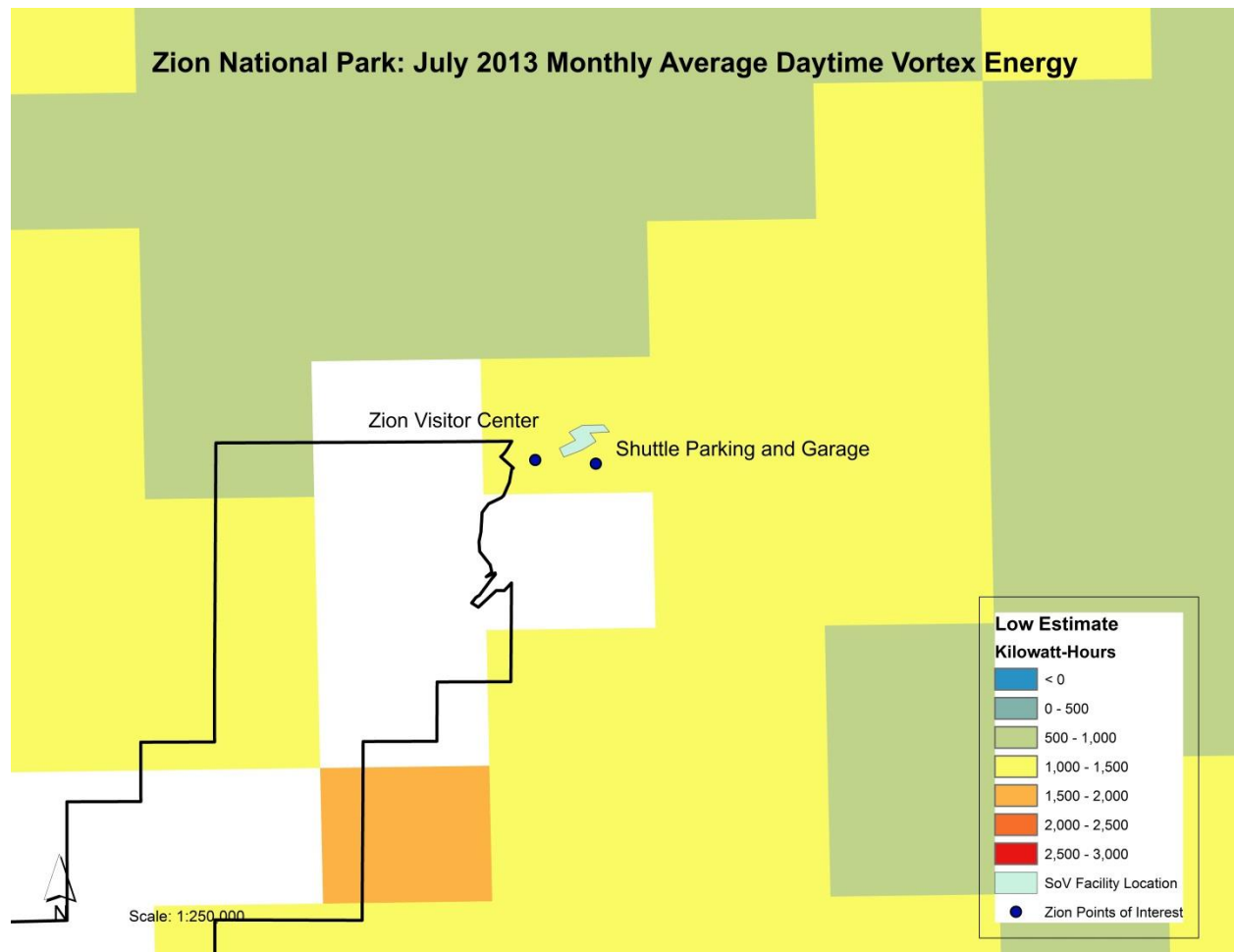


Figure 101: Zion Shuttle Parking, Visitor Center, and Potential SoV Facility Location (Low Estimate – Linear Model)

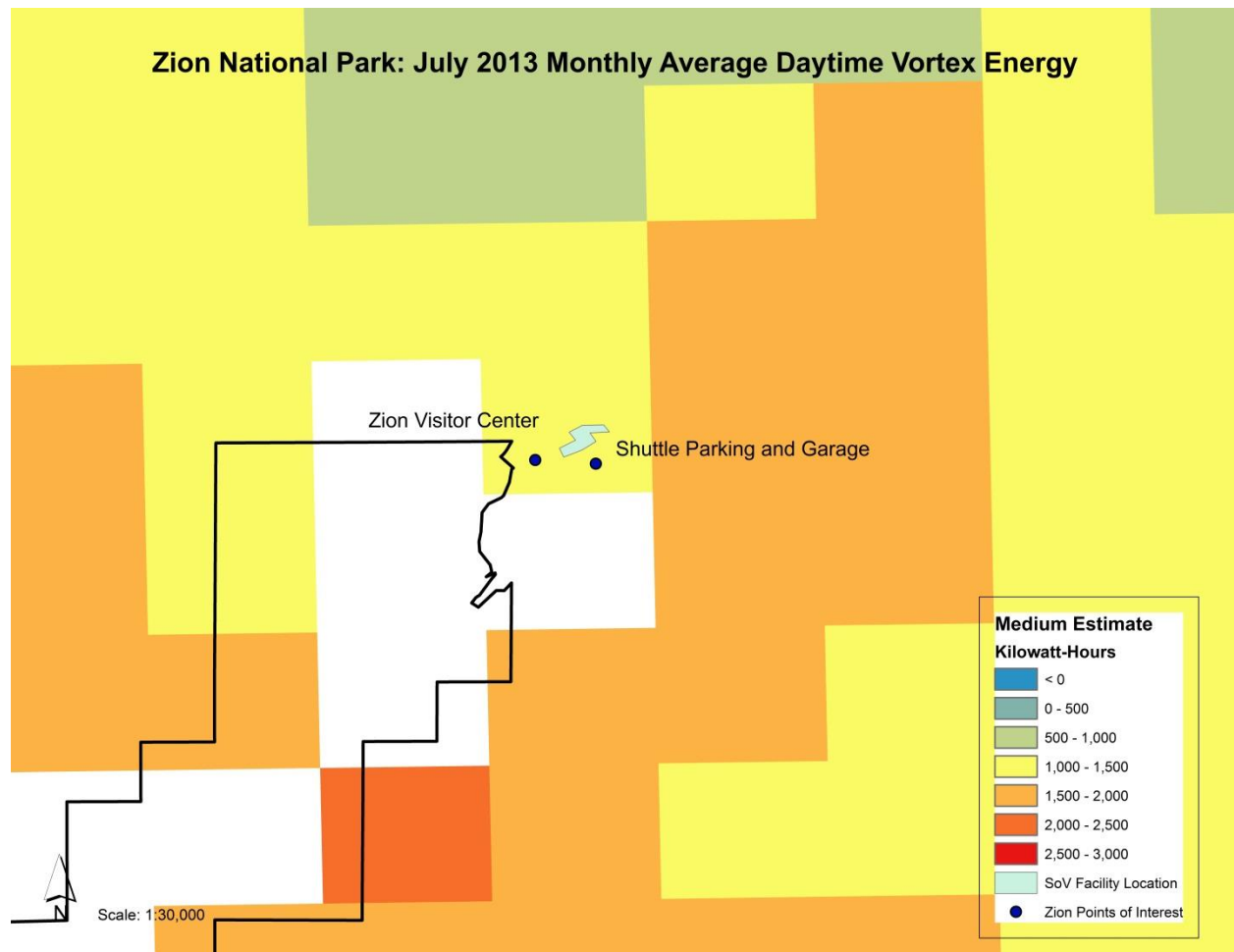


Figure 102: Zion Shuttle Parking, Visitor Center, and Potential SoV Facility Location (Medium Estimate – Linear Model)

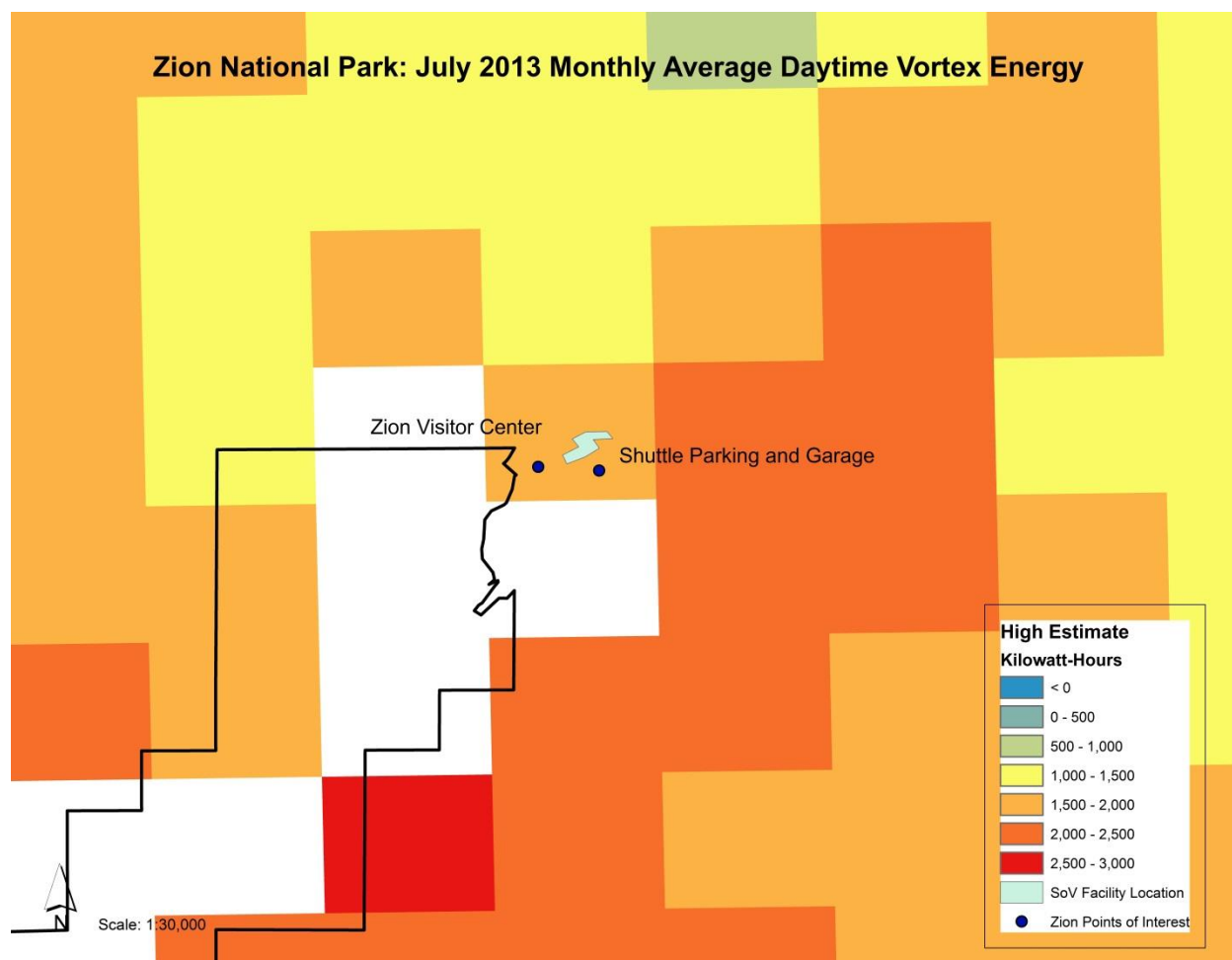


Figure 103: Zion Shuttle Parking, Visitor Center, and Potential SoV Facility Location (High Estimate – Linear Model)

Further analysis will be needed to determine the number and exact locations for SoV installation based on collection area. However, based on the results from the linear model, it appears that the area located to the north of the shuttle parking lot would be suitable for the installation of six SoV units. According to the model, the monthly average daytime power production range is between 1,000 and 2,000 kilowatt-hours, per 10-meter diameter unit. Thus, the monthly average daytime power production ranges from 6,000 to 12,000 kilowatt-hours for six units.

8.4 Results from the Threshold Model

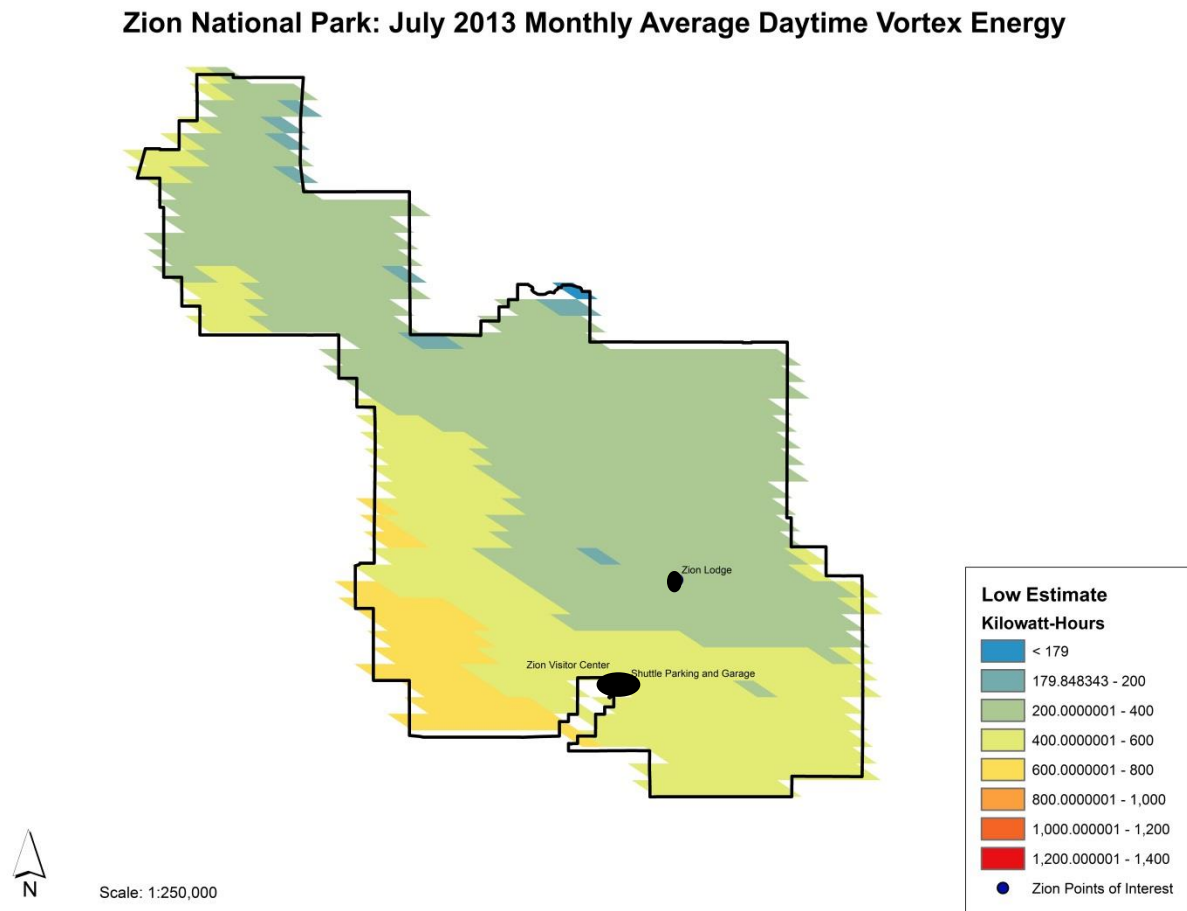


Figure 104: Zion Monthly Average Daytime Vortex Energy (Low Estimate – Threshold Model)

Zion National Park: July 2013 Monthly Average Daytime Vortex Energy

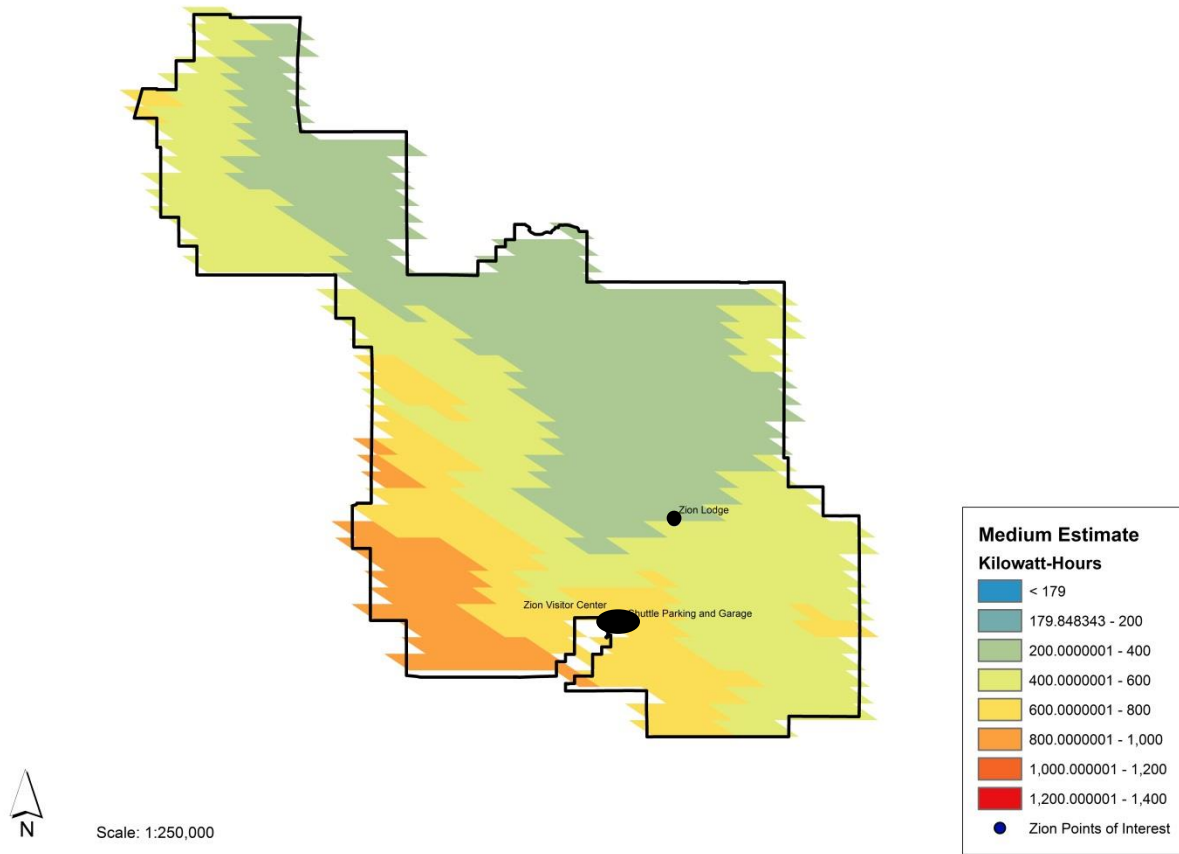


Figure 105: Zion Monthly Average Daytime Vortex Energy (Medium Estimate – Threshold Model)

Zion National Park: July 2013 Monthly Average Daytime Vortex Energy

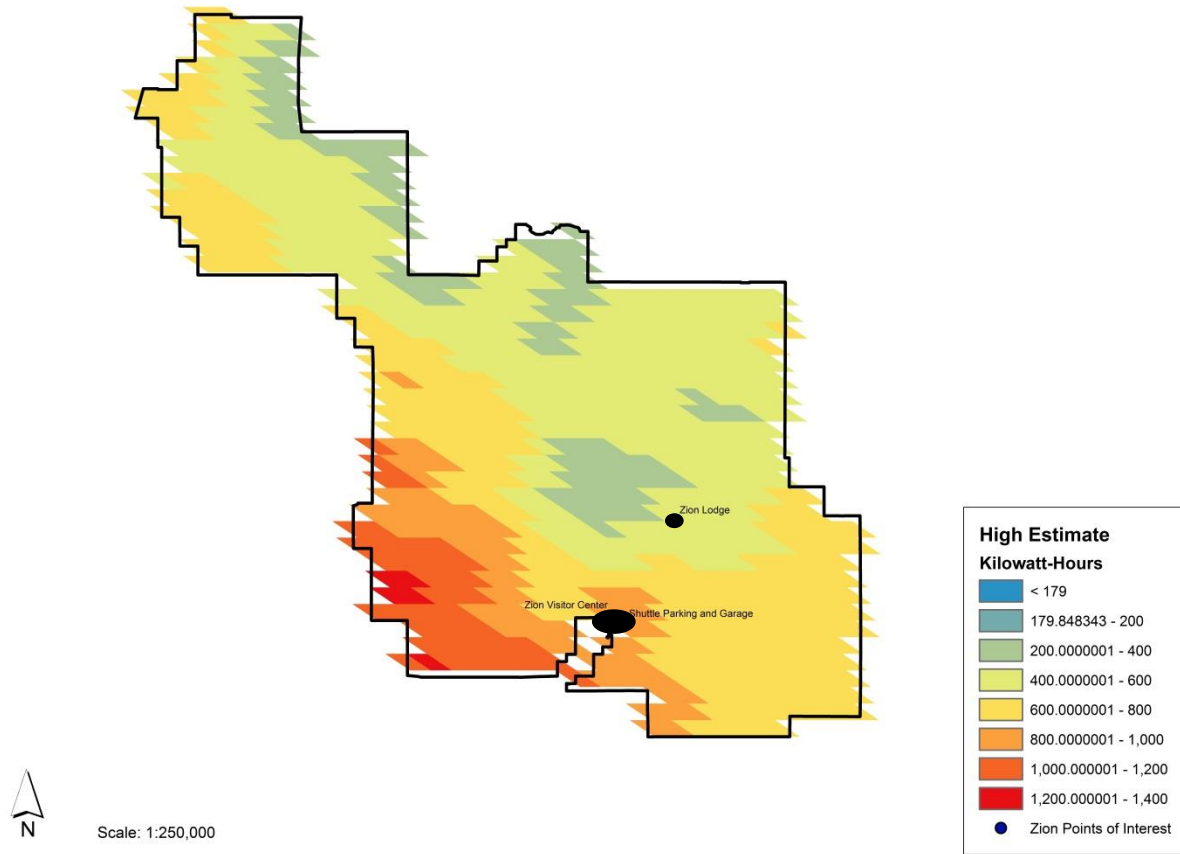


Figure 106: Zion Monthly Average Daytime Vortex Energy (High Estimate – Threshold Model)

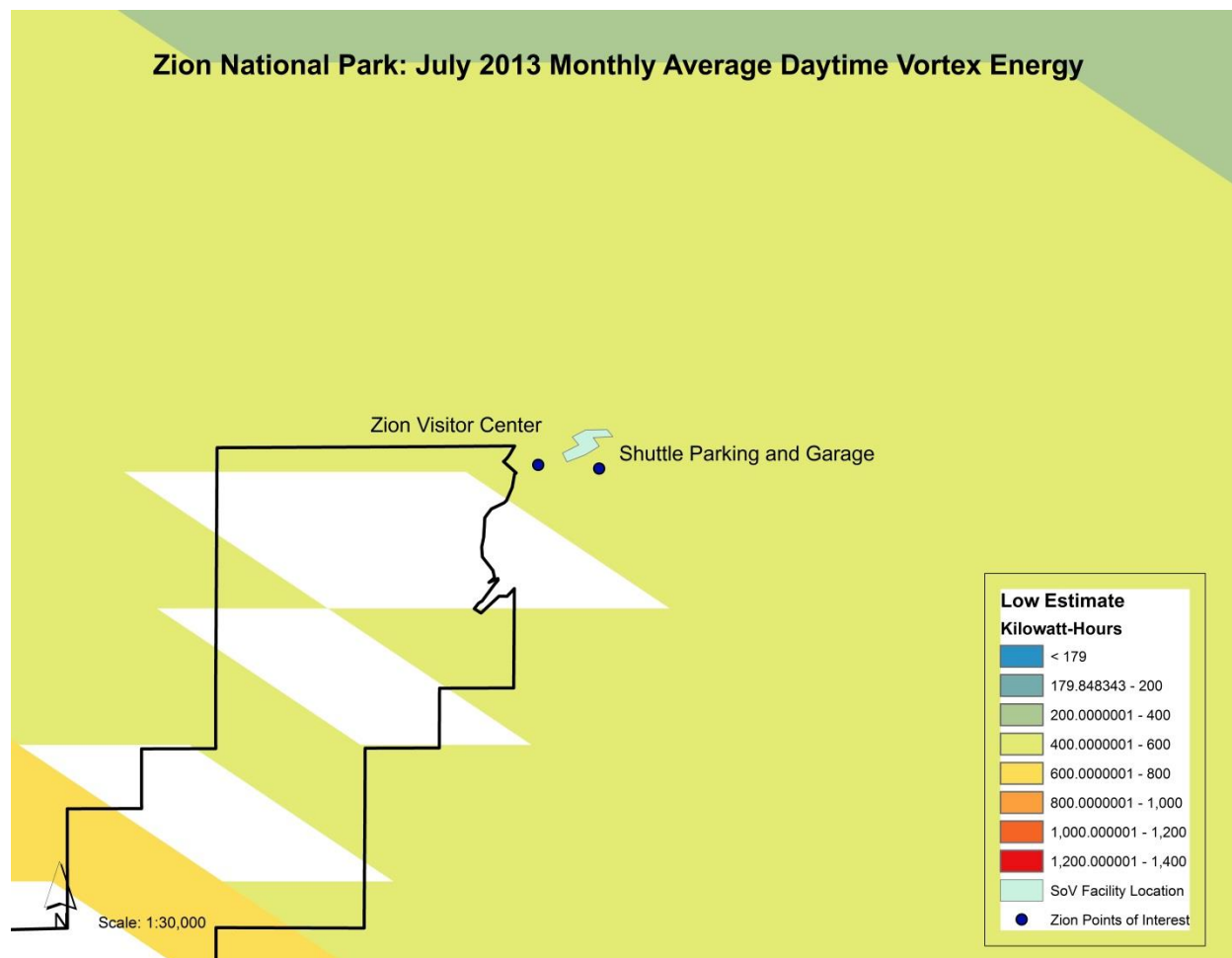


Figure 107: Zion Shuttle Parking, Visitor Center, and Potential SoV Facility Location (Low Estimate – Threshold Model)

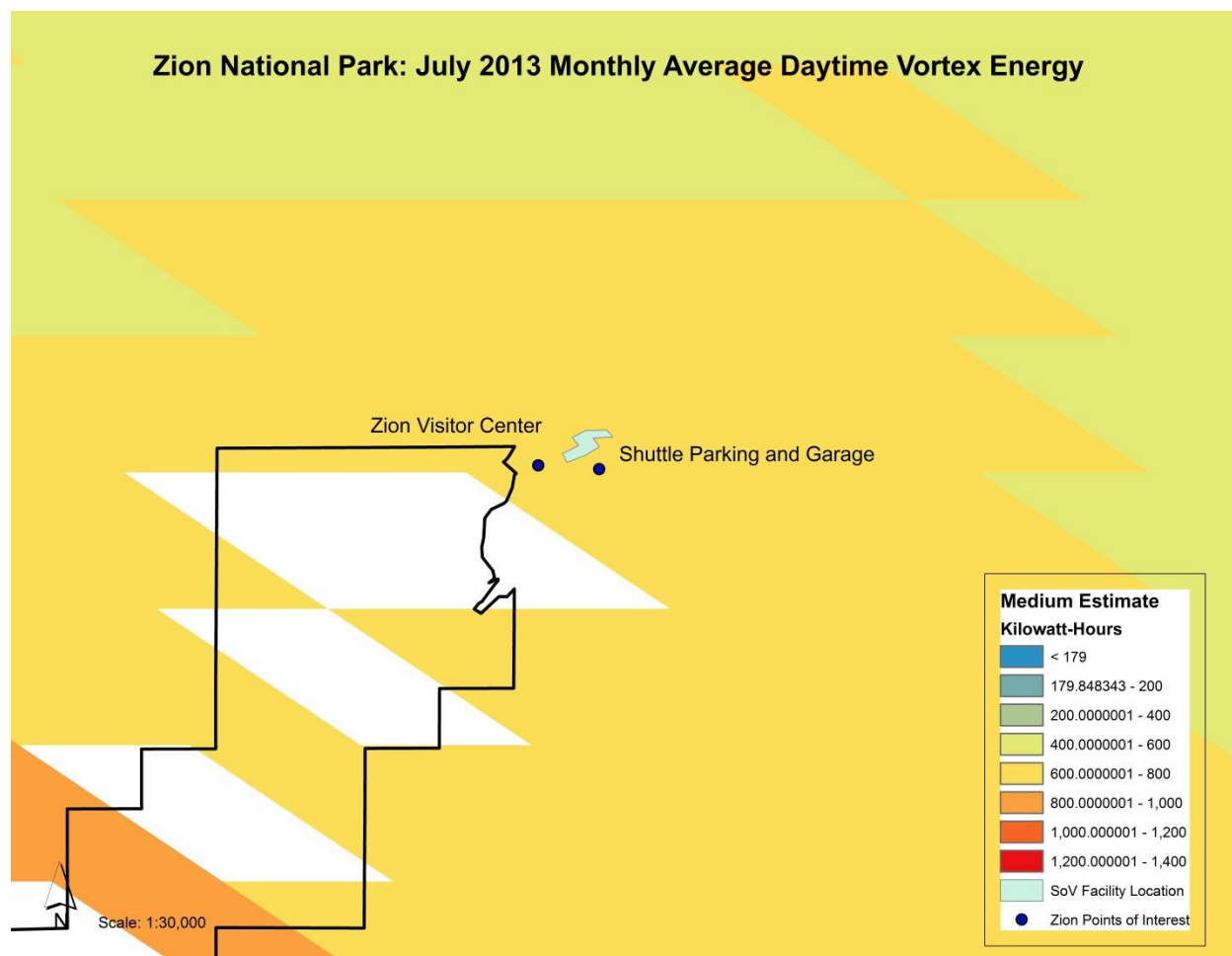


Figure 108: Zion Shuttle Parking, Visitor Center, and Potential SoV Facility Location (Medium Estimate – Threshold Model)

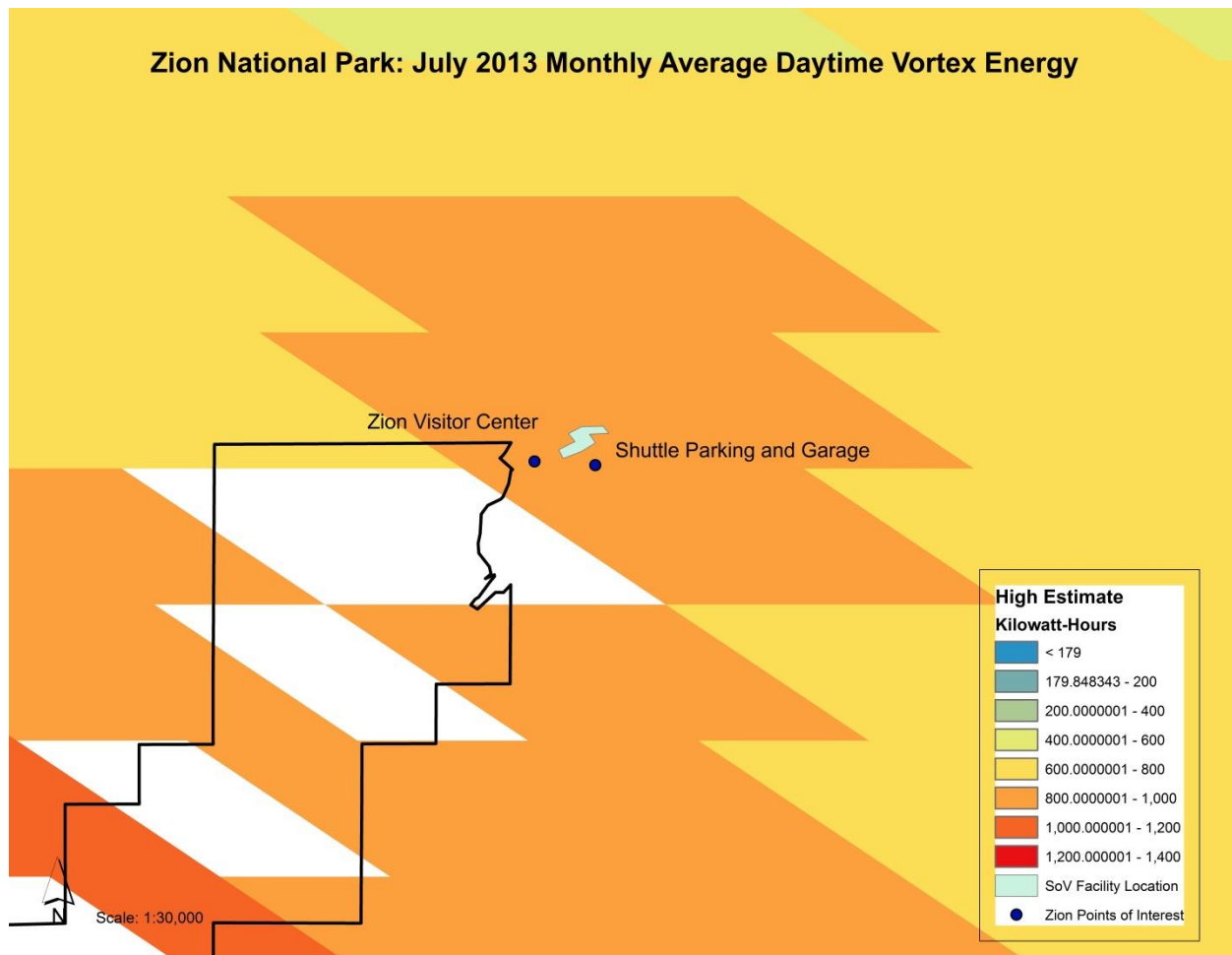


Figure 109: Zion Shuttle Parking, Visitor Center, and Potential SoV Facility Location (High Estimate – Threshold Model)

Although the results from the threshold model were lower than the estimated values from the linear model, the range of values for monthly average daytime power production for the area near the shuttle parking lot and area north of the parking lot are still between 600 to 1,000 kilowatt-hours, per 10-meter diameter SoV unit. Thus, for six SoV units, the monthly average power production ranges from 3,600 to 6,000 kilowatt-hours.

8.5 Discussion

The estimated SoV average monthly power production for summer (July) for the approximately 22,000 square meters (approximately 5.4 acres) area near the Zion shuttle parking lot and garage ranges from 6,000 to 12,000 kilowatt-hours for the full linear model, and 3,600 to 6,000 kilowatt-hours for the threshold model. The summer season (July) was considered for the case study because that is Zion's peak season, and the shuttles are not run throughout the year when park visitation is not as high.

The estimated power needed to provide a full charge to a fully-electric shuttle comparable in size to the Eldorado National shuttles used by Zion is approximately 324 kilowatt-hours (Hill, 2015). This full charge would allow a fully-electric bus, comparable in size to Zion's, to cover the approximate 162 miles needed each day to cover the shuttle loop around the park. With a fleet of 39 shuttles, 12,636 kilowatt-hours of power would be needed each day to fully charge the batteries for all 39 shuttles. Based on the estimates from the full linear model and threshold model, the highest estimate for the monthly average would not be enough to cover fully charging the entire fleet. Based on the higher end of the estimates, there would be enough power to fully charge one fully-electric shuttle for the month (9,720 kilowatt-hours per 30 days), which likely would not be suitable. However, using the six SoV units to provide power to charging stations for electric golf carts and ranger vehicles, which require much less power to fully charge: approximately five kilowatt-hours (ziparoundcarts, 2015), may be an alternative.

CHAPTER 9: CONTRIBUTIONS, LIMITATIONS, AND FUTURE WORK

9.1 Contributions

A major goal of this study was to develop a concentrated wind resource model. This GIS model was used for resource evaluation, to determine off-grid locations where a concentrated wind system, like the SoV, could be used in an effort to reduce GHG emissions, specifically in the National Parks, although the application can also be used in other locations. The methods and results of this study will be useful in a variety of other applications related to GIS and spatial modeling, alternative energy distribution, natural resource evaluation, site selection based on weather or landscape dependency, increasing electric vehicle usage, and furthering green efforts, including, but not limited to, the National Parks.

The GIS models created to represent heat flux, slope, and power output estimation using both the linear and threshold models, as well as the proposed methods used and scripts generated, can be used in other applications in engineering and planning, such as in land development and large-scale agricultural applications. The results from the GIS model, and the recommendations comparisons made for Zion National Park in the case study can be useful for planning purposes, and in future installation of green technologies in other National Parks and in other locations, such as in the conversion to all-electric fleets of vehicles at businesses in regions that are suitable for SoV facilities, or other concentrated wind energy production facility installation.

9.2 Limitations

A major limitation of this study is obviously the lack of data from the SoV prototype. Further testing will be needed to improve the power output estimation models based on results

from future prototypes and simulation. Additional estimation models will likely be developed to further improve estimation of power production from the SoV.

Another limitation of the study is the lack of a more detailed evaluation of Zion National Park's transportation. Although suggestions were provided and an approximation of the area suitable for SoV installation was also provided, a further, in-depth evaluation is needed. In the case of Zion National Park, a detailed cost comparison of the current transportation system and the conversion to electric shuttles is needed to provide Park officials with the information needed to make future decisions regarding the Park's transportation needs. Capital costs involved in purchasing vehicles, converting current vehicles, installing charging stations, and installing SoV facilities, and cost comparisons of maintaining and operating electric vehicles versus the current propane-powered fleet, should all be considered in future research. Lastly, and most importantly to this research, environmental costs should be determined.

9.3 Future Work

A goal of this research is to use the models developed to estimate SoV power production for the entire U.S. Although in this research, the models were only applied to small areas (Mesa, Arizona and Zion National Park, Utah), the models were developed to be applied to the 48 conterminous U.S. Upon further testing of the SoV prototype, and further improvement of the linear and threshold models developed in this research, SoV power production can then be estimated for the entire U.S.

APPENDIX A

RESULTS FROM THRESHOLD MODEL

The following eight images shown in *Figure 110: January 2011: Average Monthly Daytime Power Output (using Threshold Model)* through *Figure 117: October 2013: Average Monthly Daytime Power Output (using Threshold Model)*, were produced using the threshold model. These images represent SoV power output for the 48 conterminous U.S. These values represent daytime averages, and are based off of the daytime (approximately 10:30 AM) sensible heat flux values generated in the GIS.

January 2011 Power Output (based on Sensible Heat)

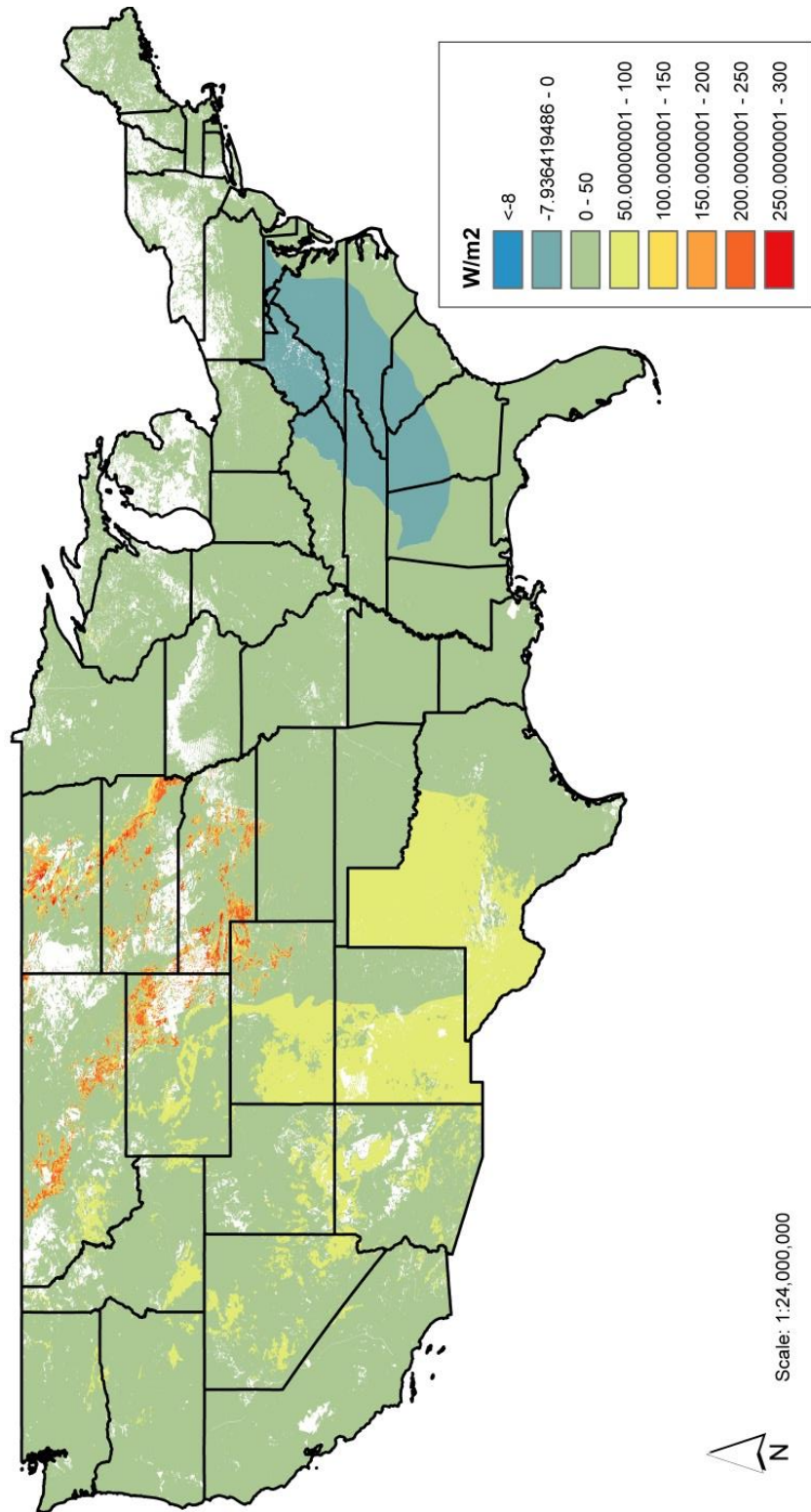


Figure 110: January 2011: Average Monthly Daytime Power Output (using Threshold Model)

January 2013 Power Output (based on Sensible Heat)

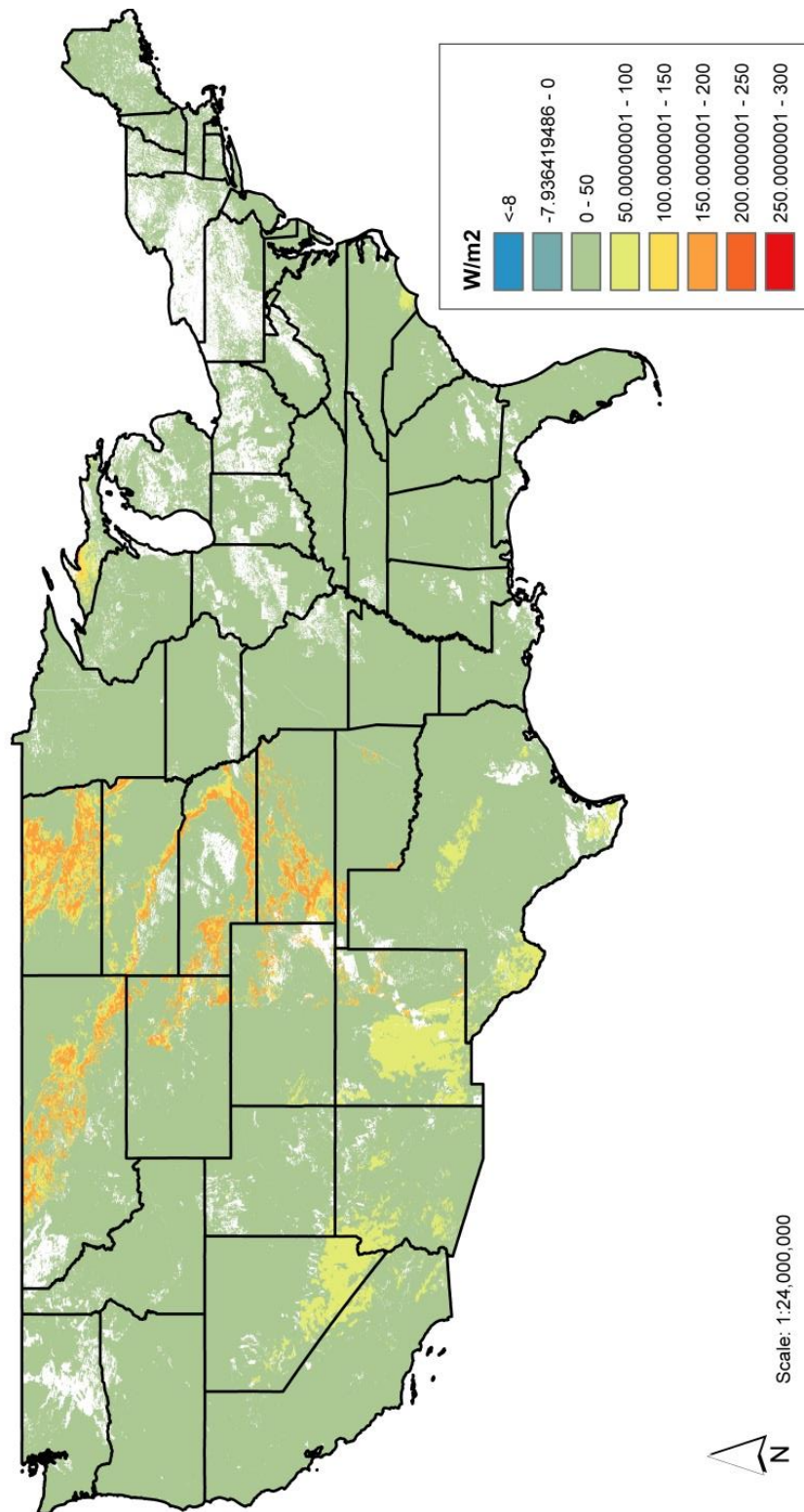


Figure 111: January 2013: Average Monthly Daytime Power Output (using Threshold Model)

April 2011 Power Output (based on Sensible Heat)

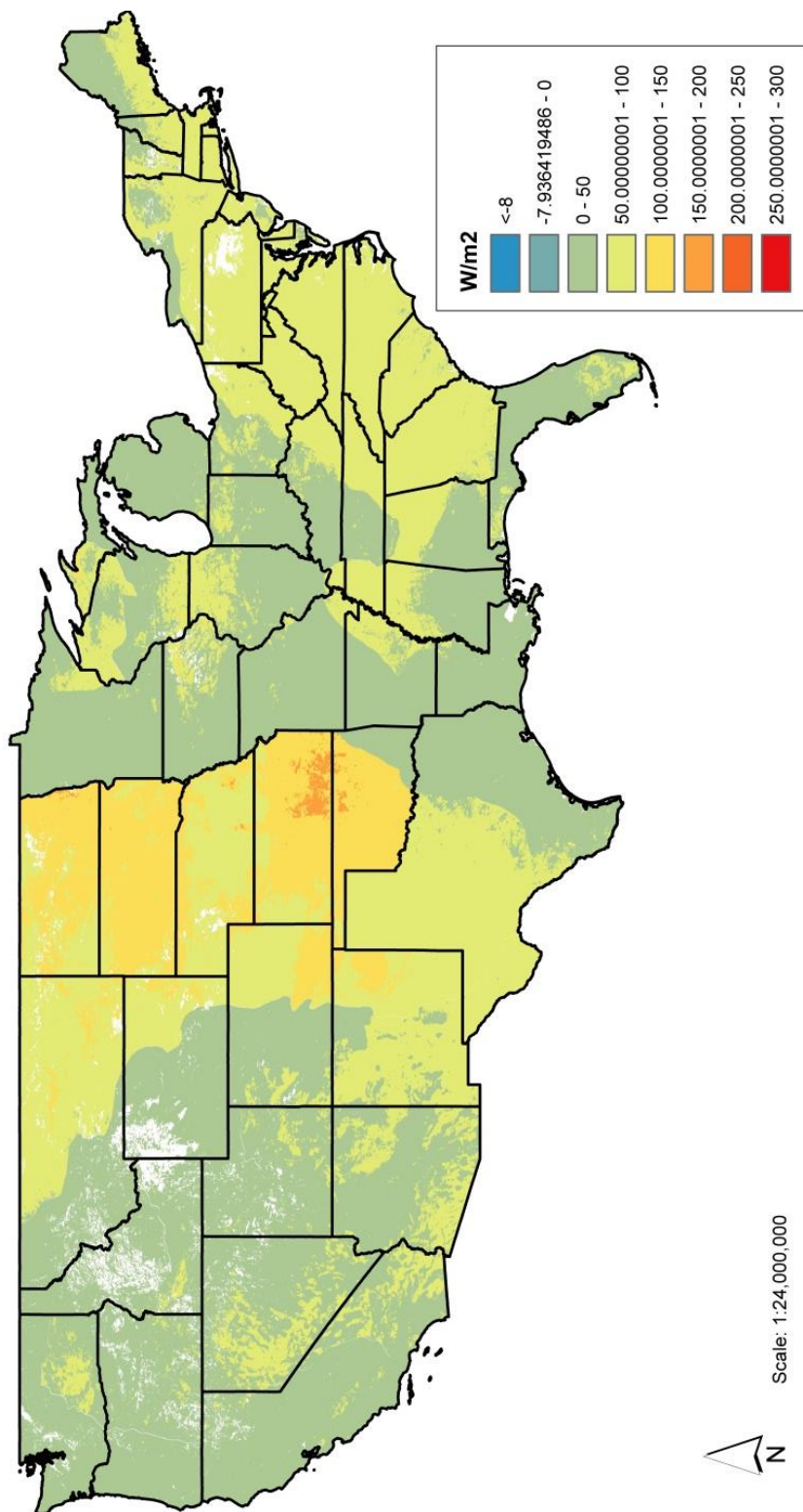


Figure 112: April 2011: Average Monthly Daytime Power Output (using Threshold Model)

April 2013 Power Output (based on Sensible Heat)

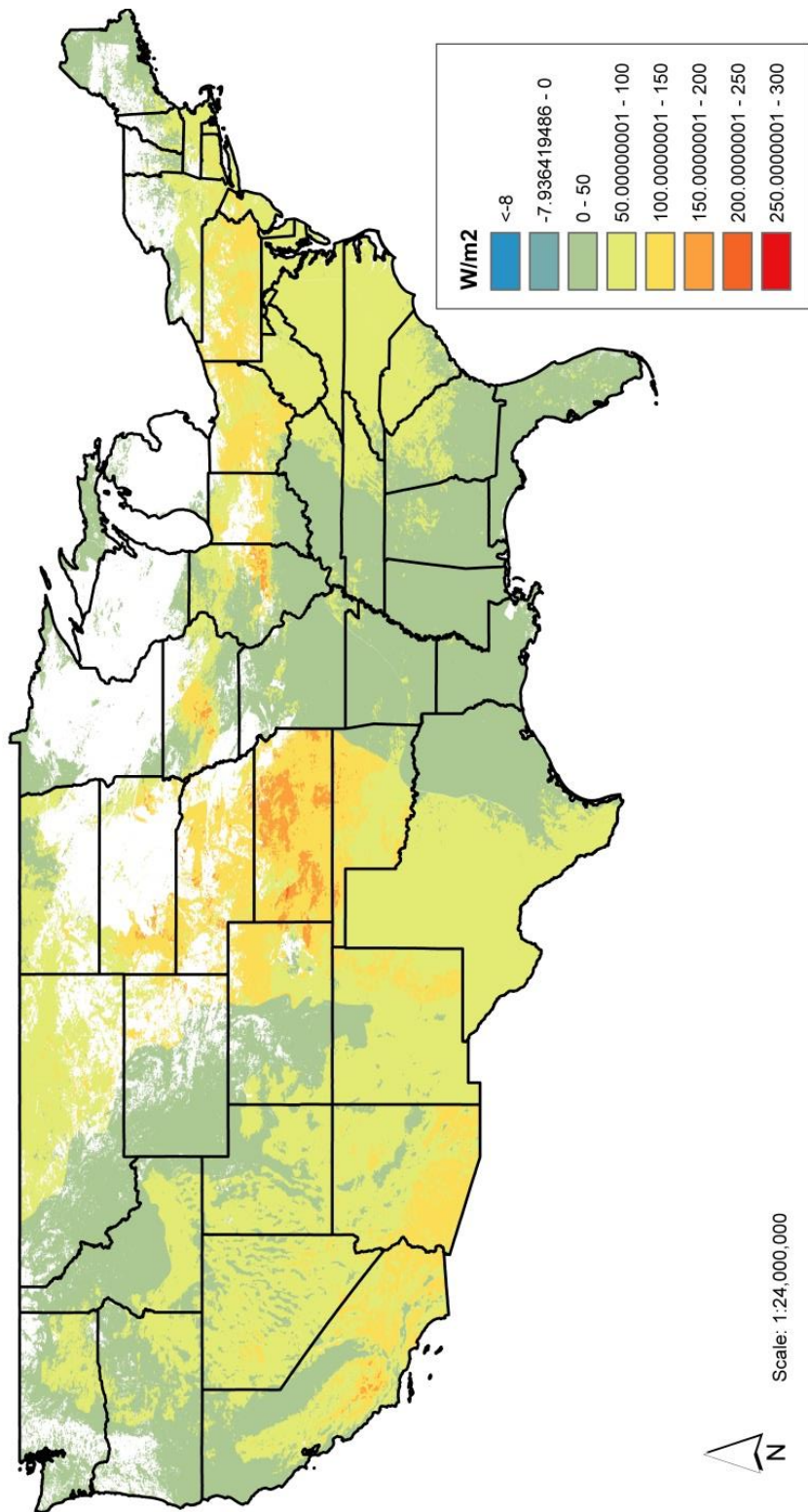


Figure 113: April 2013: Average Monthly Daytime Power Output (using Threshold Model)

July 2011 Power Output (based on Sensible Heat)

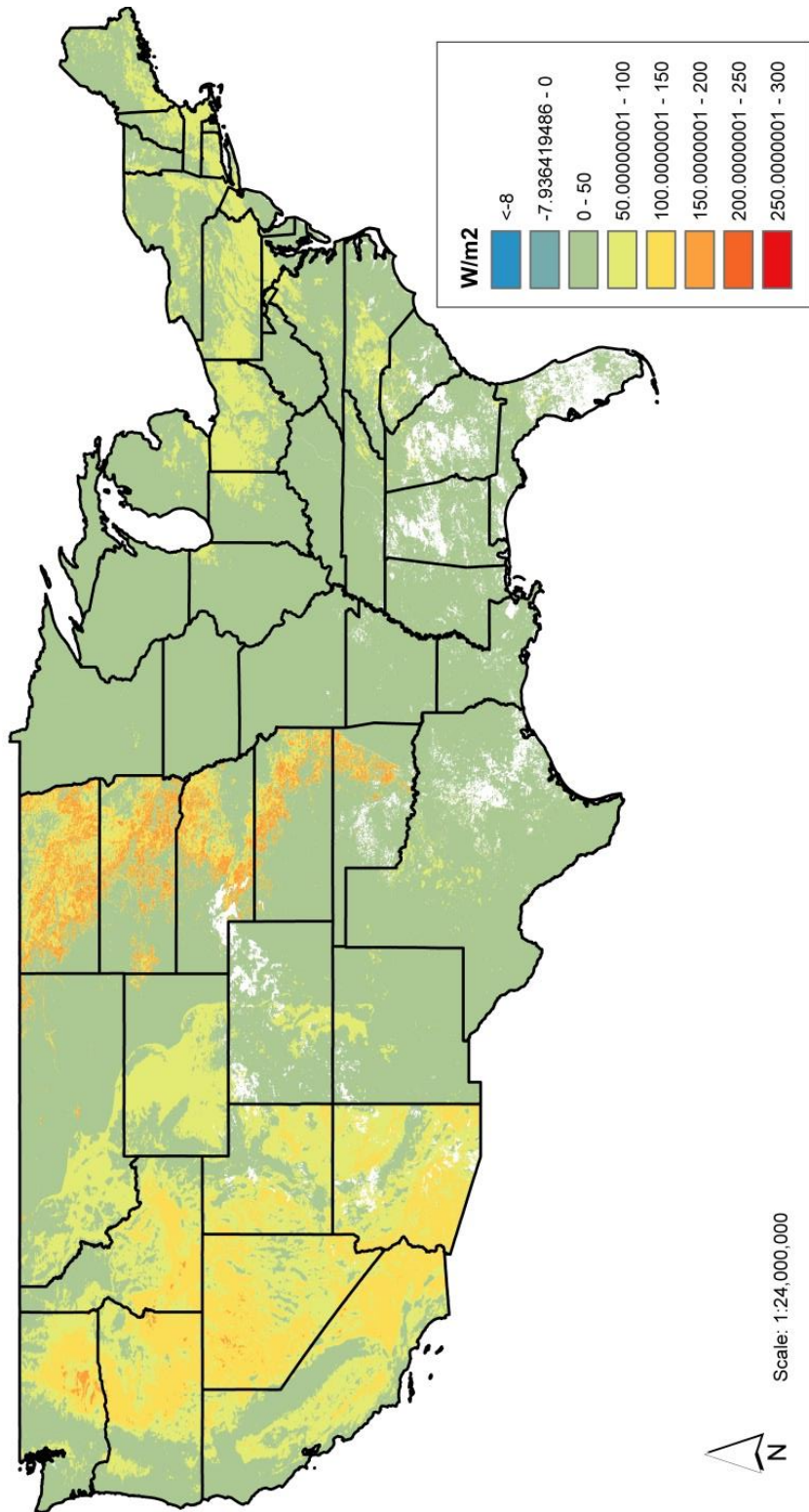


Figure 114: July 2011: Average Monthly Daytime Power Output (using Threshold Model)

July 2013 Power Output (based on Sensible Heat)

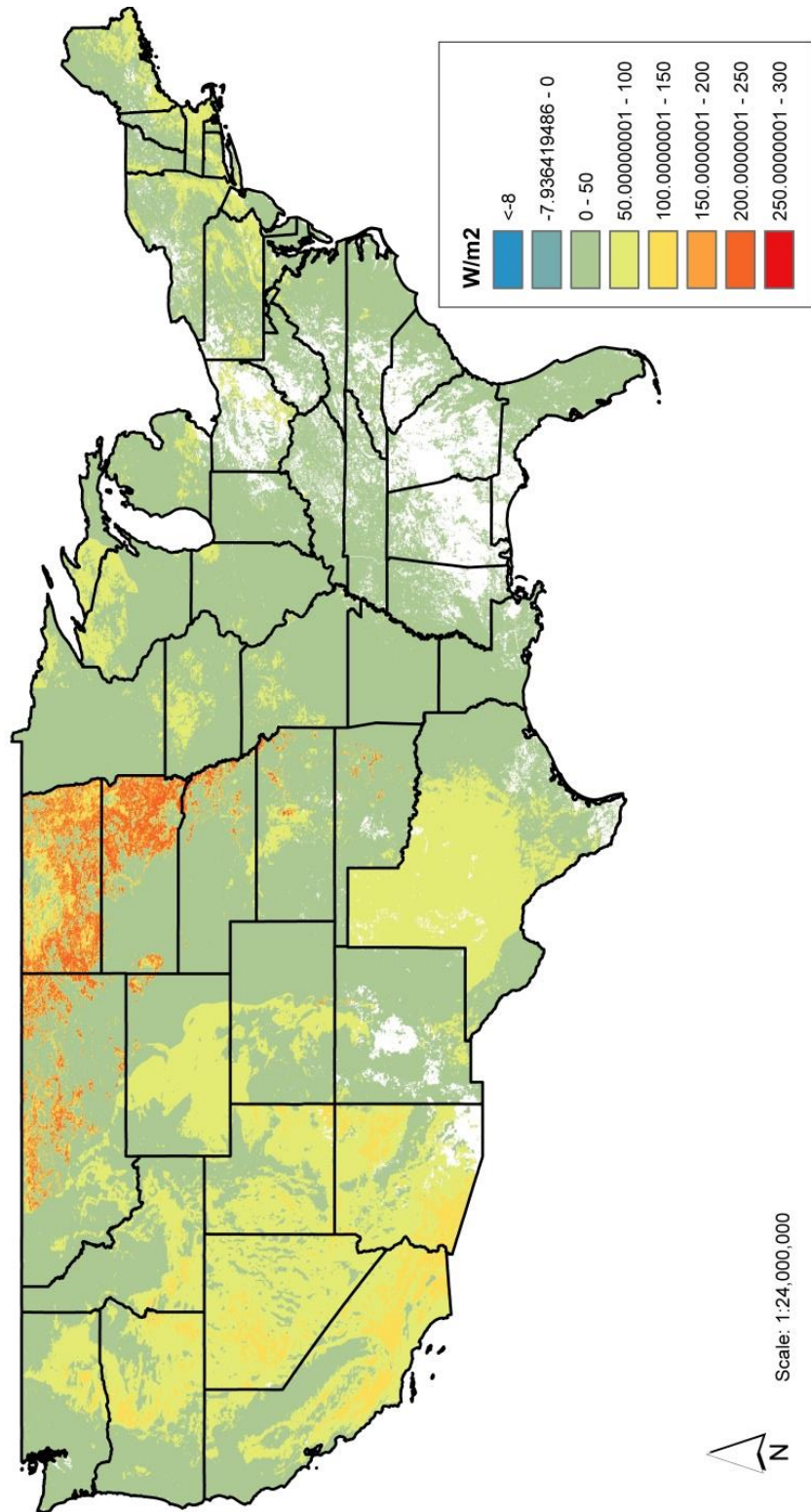


Figure 115: July 2013: Average Monthly Daytime Power Output (using Threshold Model)

October 2011 Power Output (based on Sensible Heat)

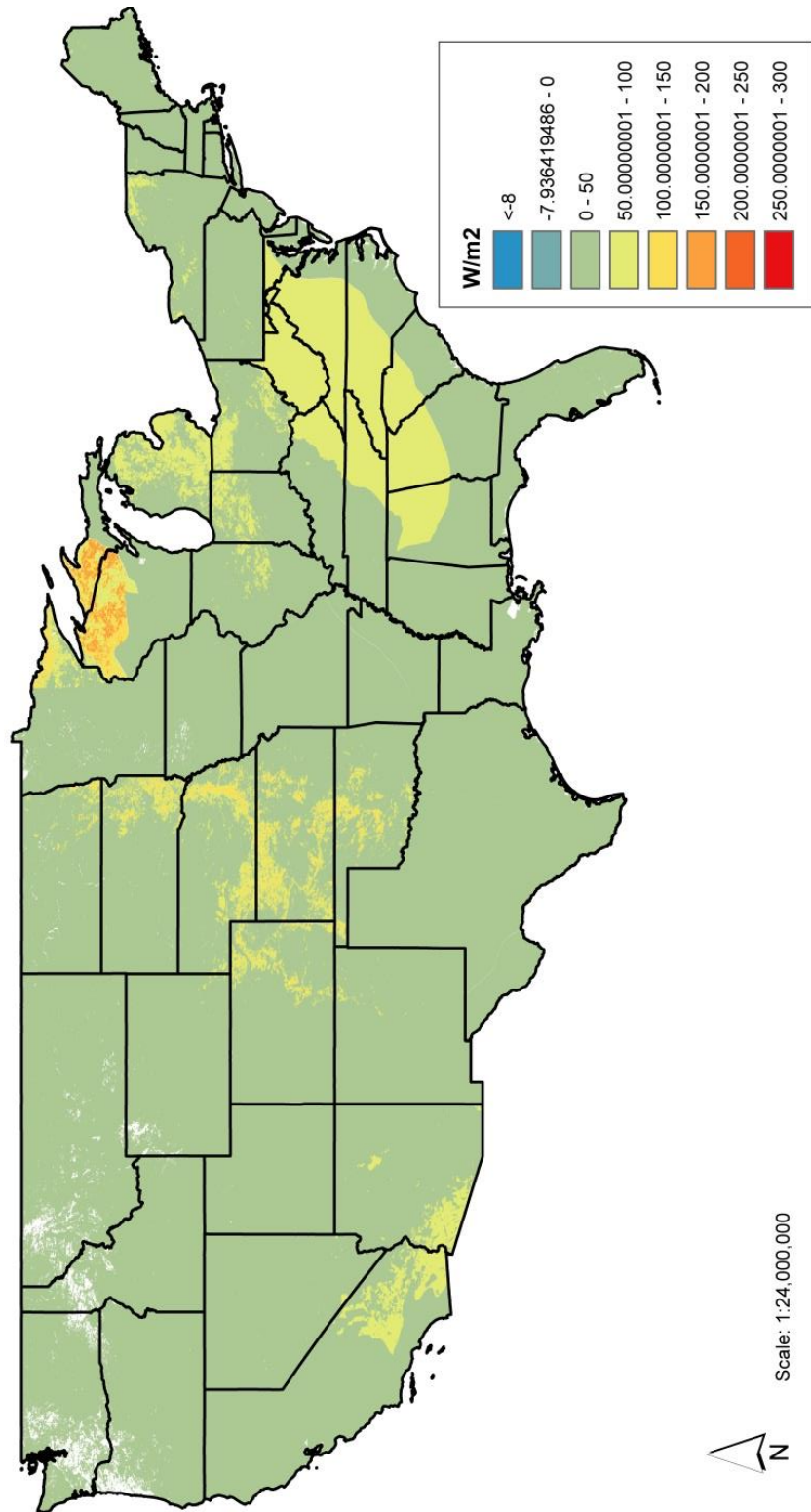


Figure 116: October 2011: Average Monthly Daytime Power Output (using Threshold Model)

October 2013 Power Output (based on Sensible Heat)

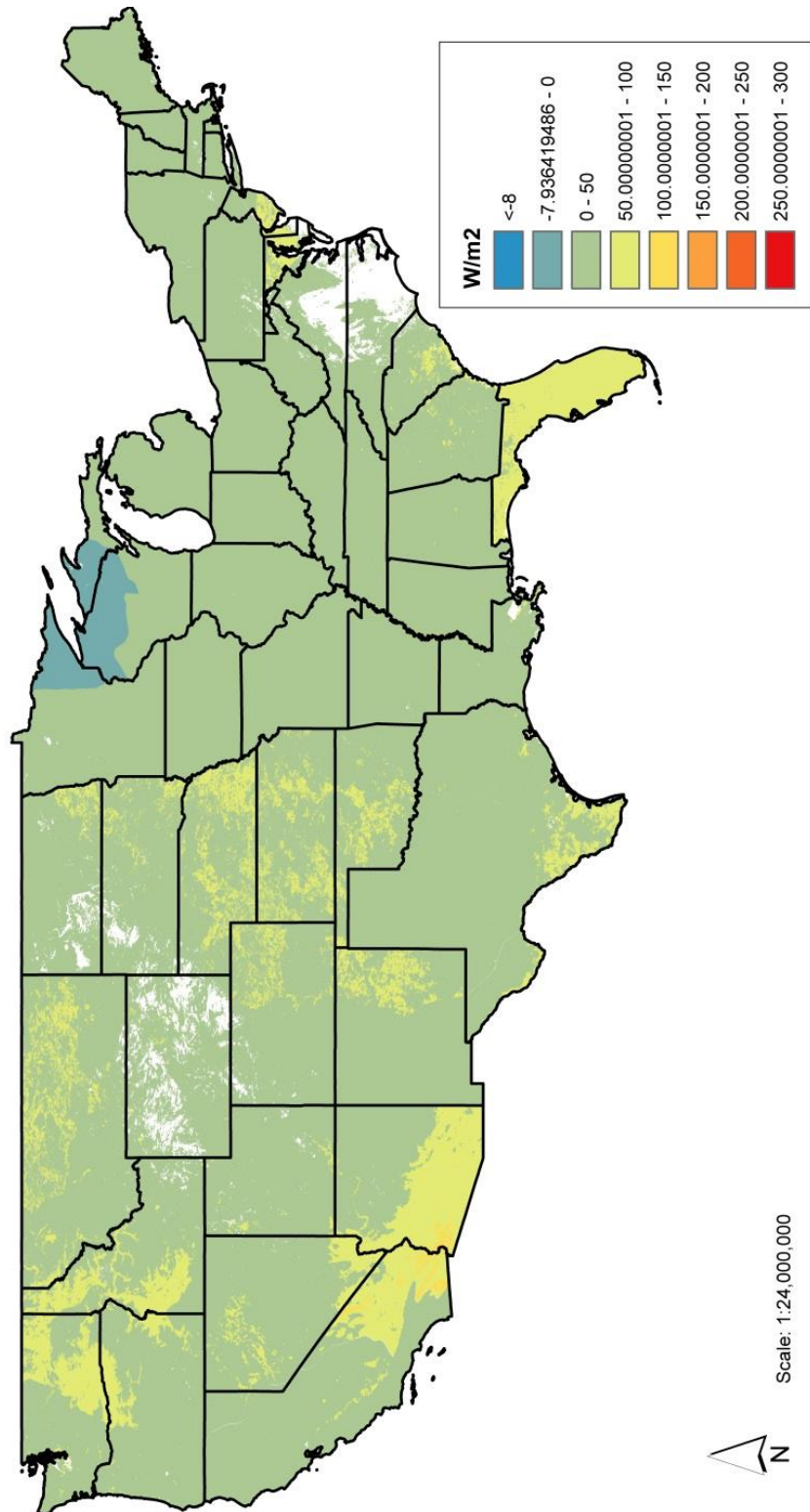


Figure 117: October 2013: Average Monthly Daytime Power Output (using Threshold Model)

APPENDIX B

RESULTS FROM LATENT HEAT MODEL

The following 16 images, shown in *Figure 118: January 2011 Latent Heat (10:30 AM)* through *Figure 133: October 2013 Latent Heat (10:30 PM)*, were generated using the Bonan (2002) method of calculating latent heat for the 48 conterminous U.S. using the interpolation layers generated in the GIS. The following images represent daytime (approximately 10:30 AM) and nighttime (approximately 10:30 PM) values, for four seasons, for both 2011 and 2013. The color scale used (low to high) is relative to the range of latent heat values in the images.

January 2011: Latent Heat (10:30 AM)

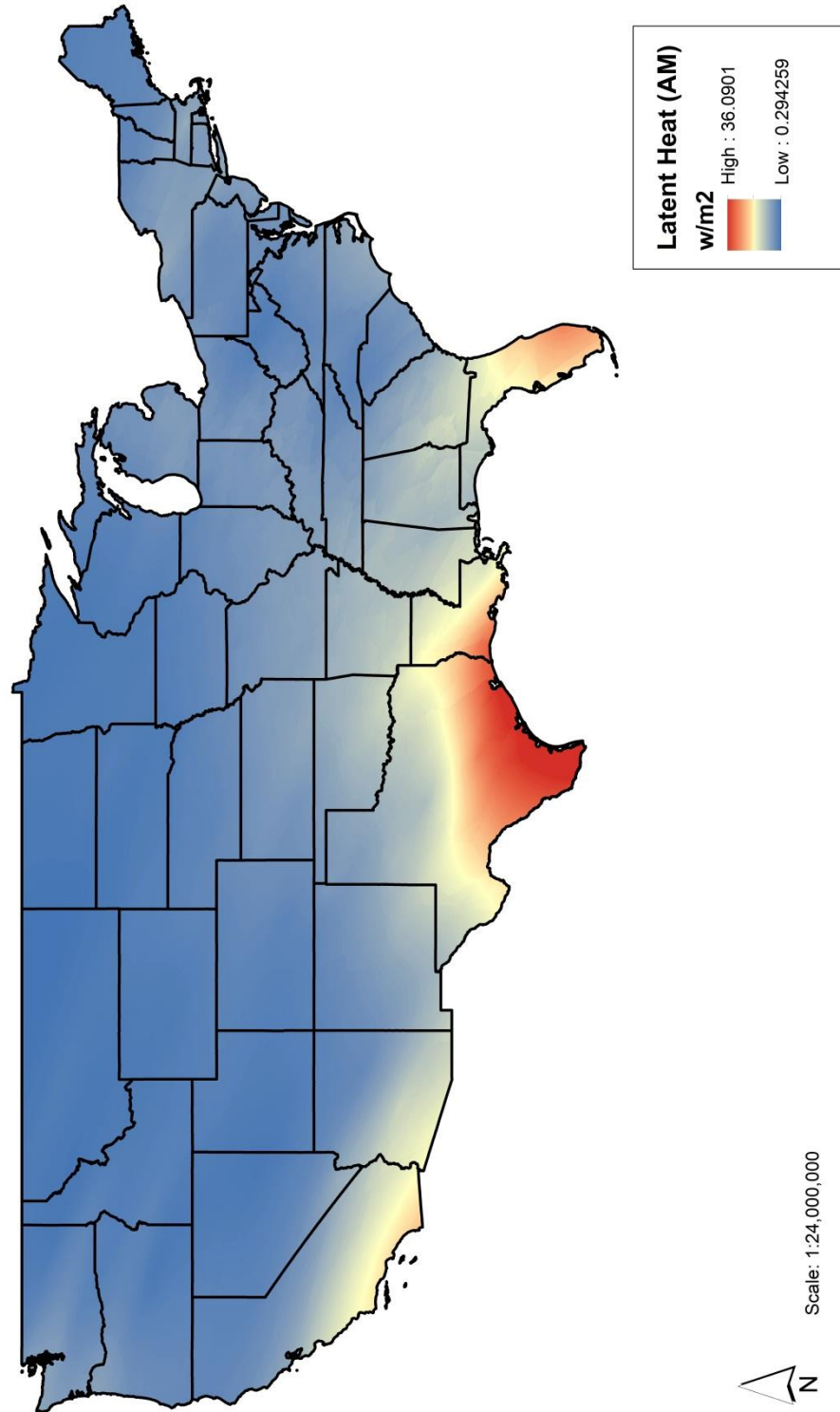


Figure 118: January 2011 Latent Heat (10:30 AM)

January 2011: Latent Heat (10:30 PM)

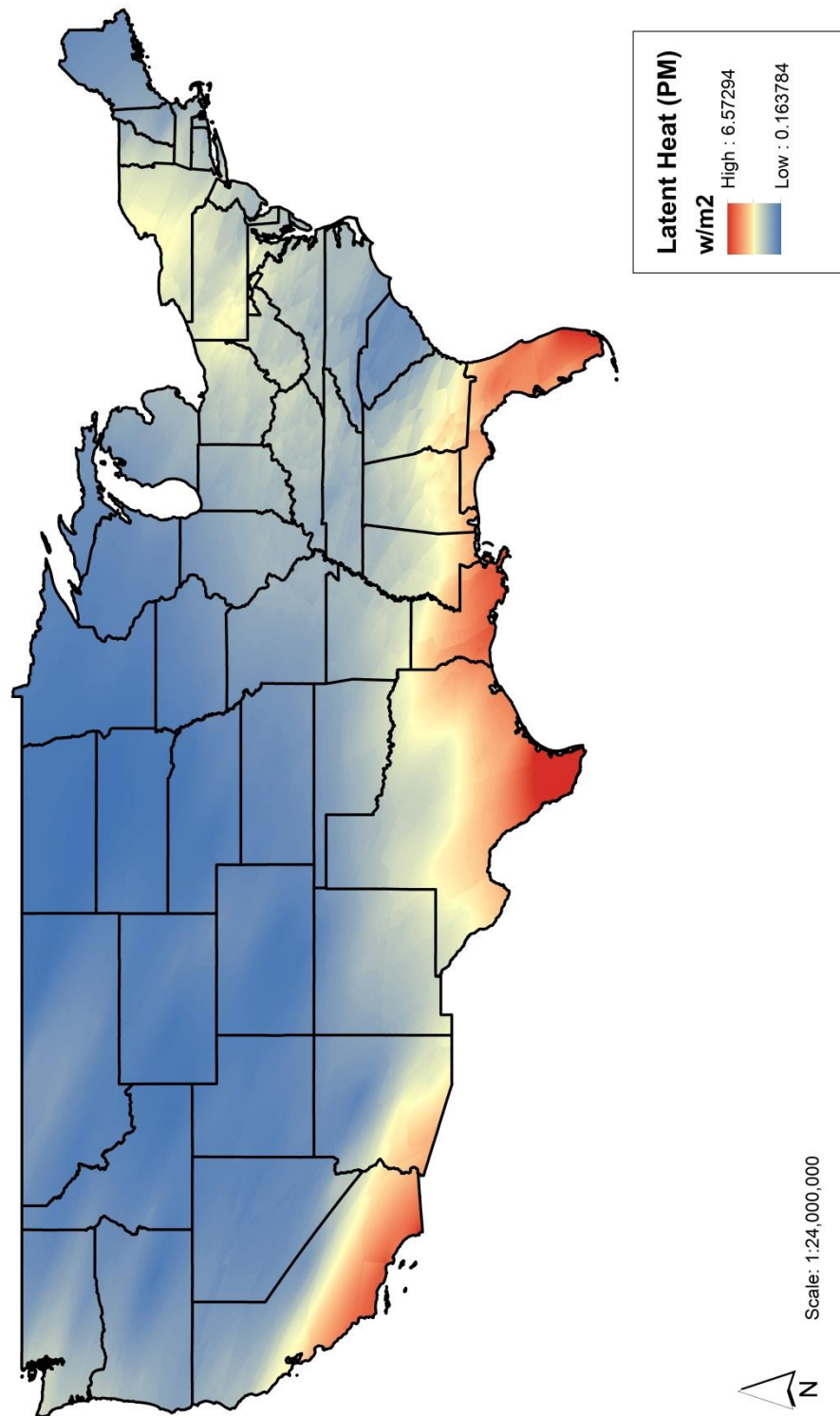


Figure 119: January 2011 Latent Heat (10:30 PM)

January 2013: Latent Heat (10:30 AM)

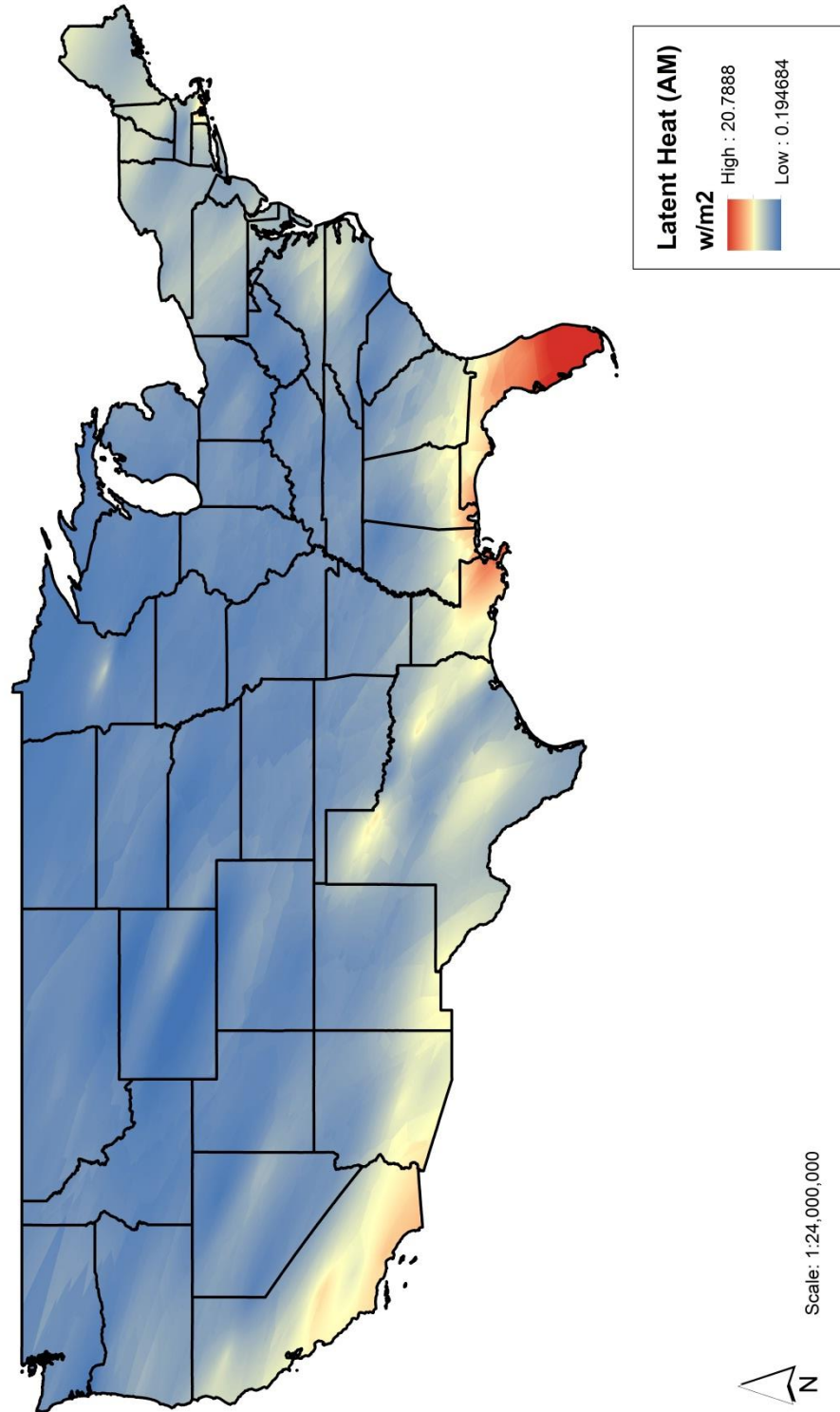


Figure 120: January 2013 Latent Heat (10:30 AM)

January 2013: Latent Heat (10:30 PM)

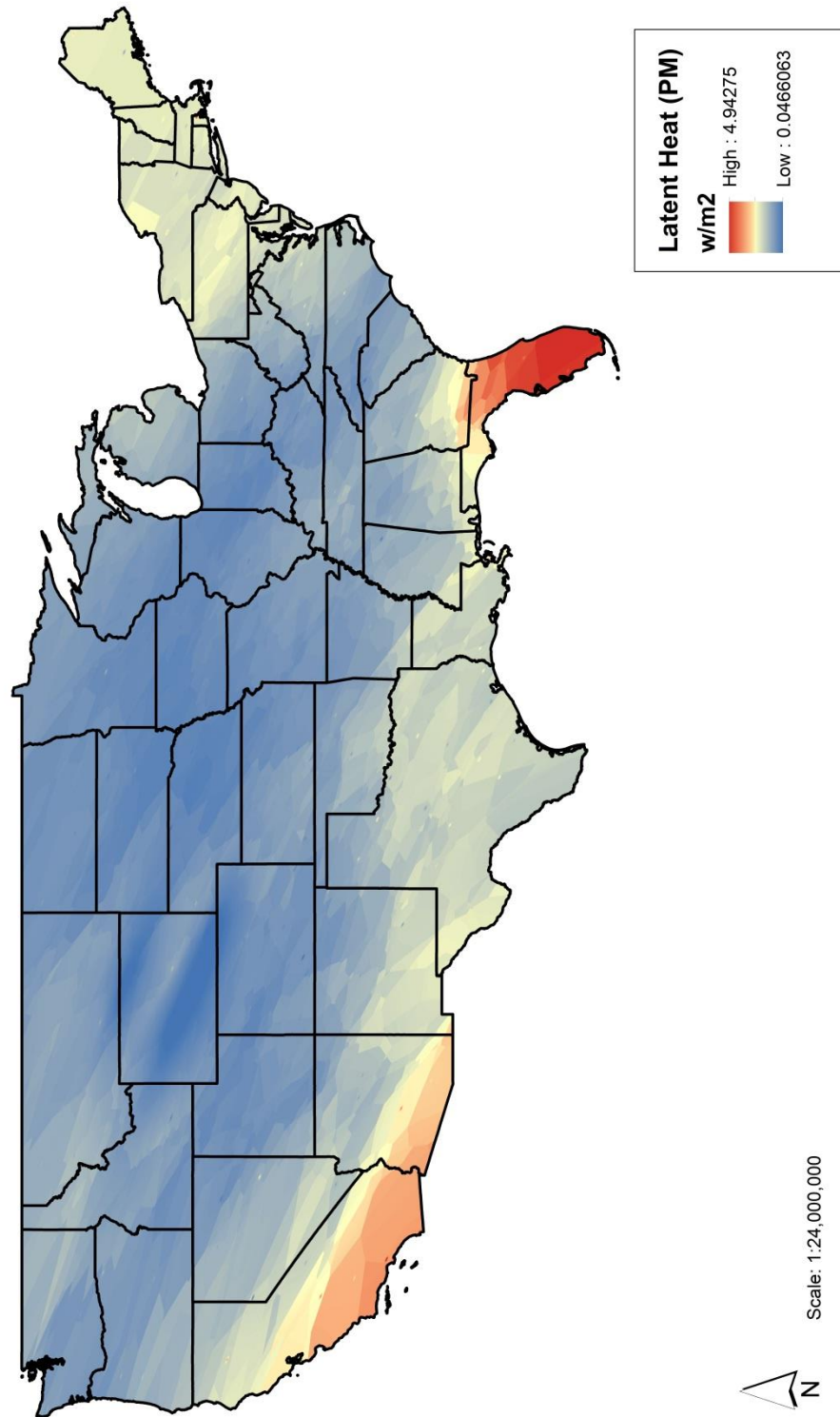


Figure 121: January 2013 Latent Heat (10:30 PM)

April 2011: Latent Heat (10:30 AM)

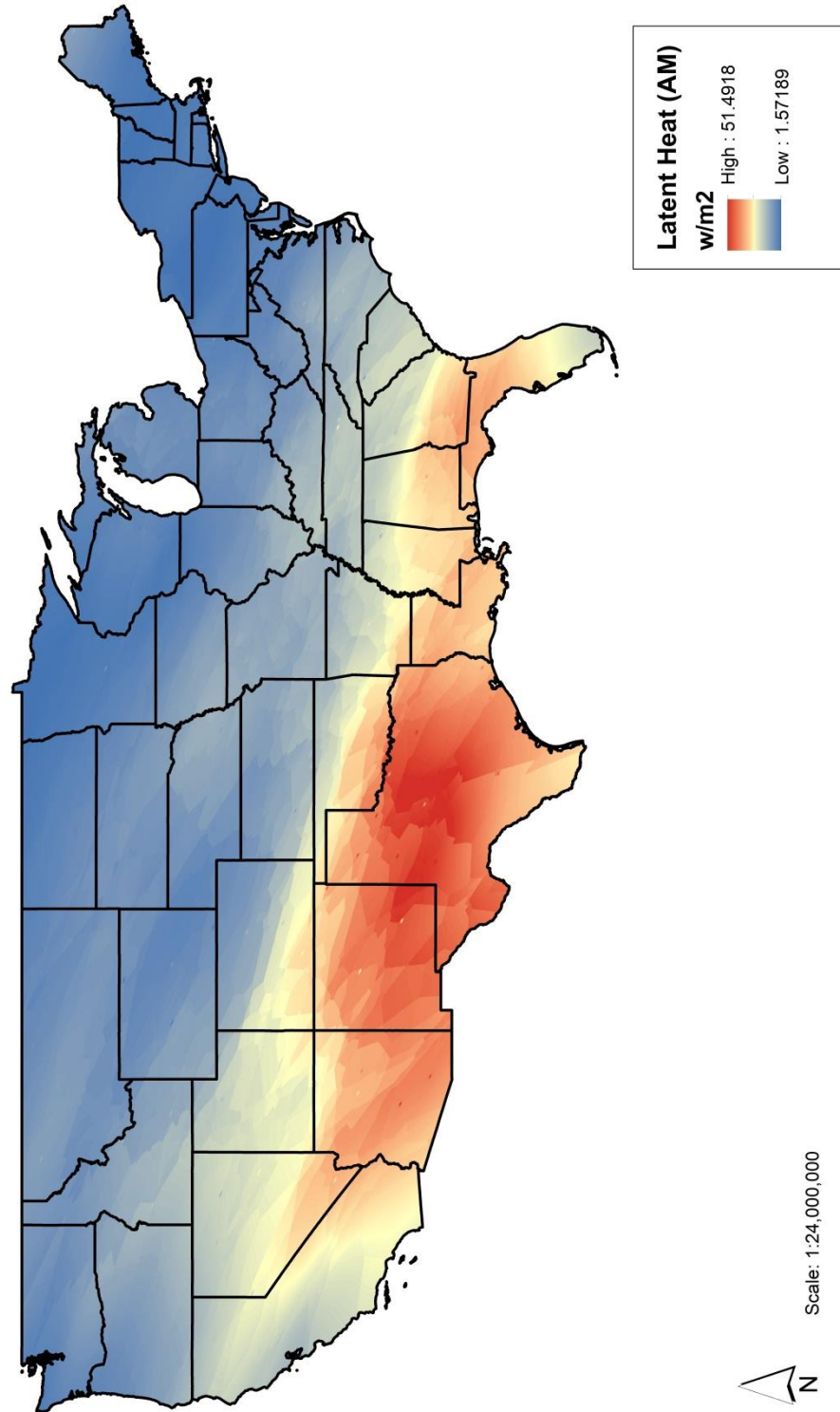


Figure 122: April 2011 Latent Heat (10:30 AM)

April 2011: Latent Heat (10:30 PM)

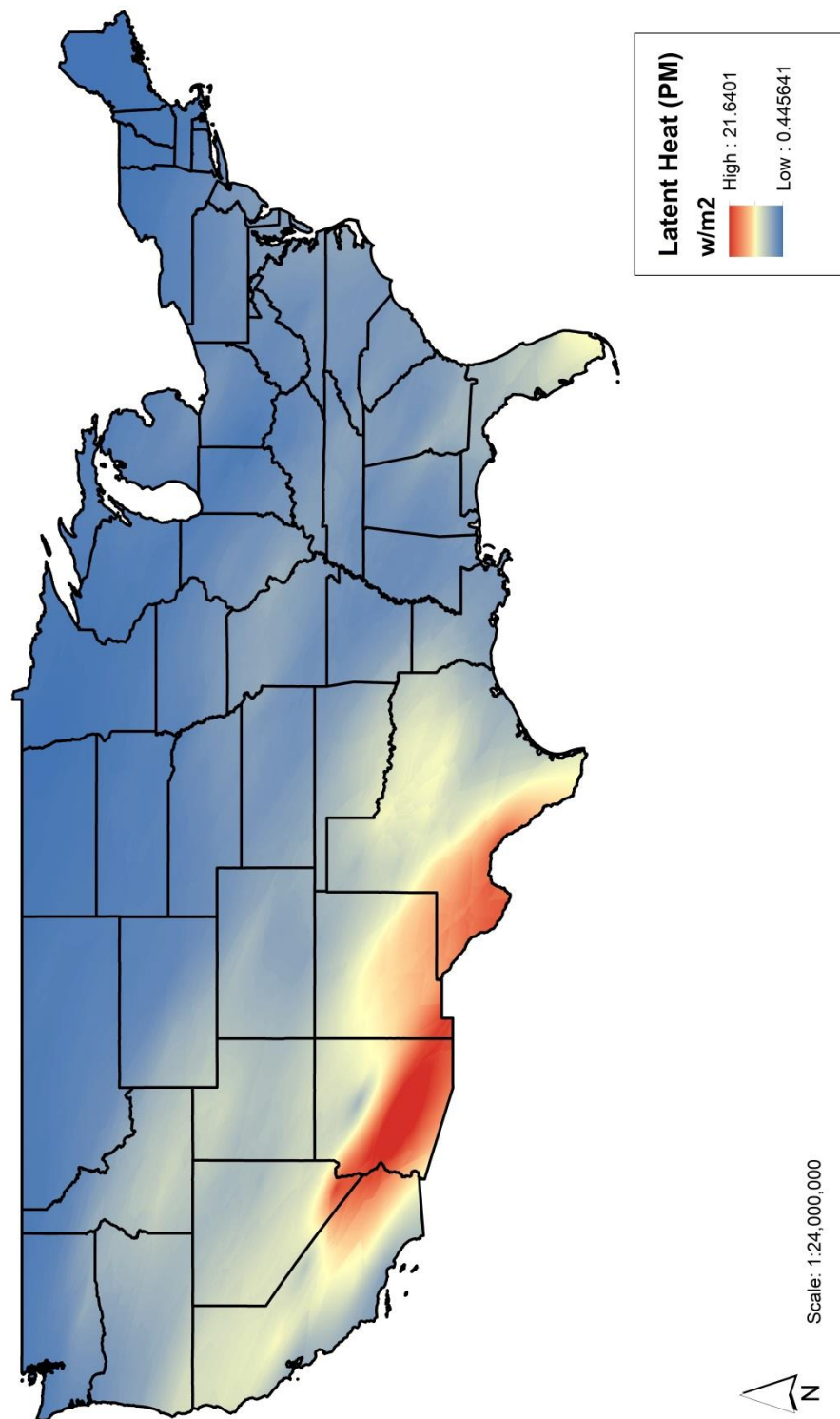


Figure 123: April 2011 Latent Heat (10:30 PM)

April 2013: Latent Heat (10:30 AM)

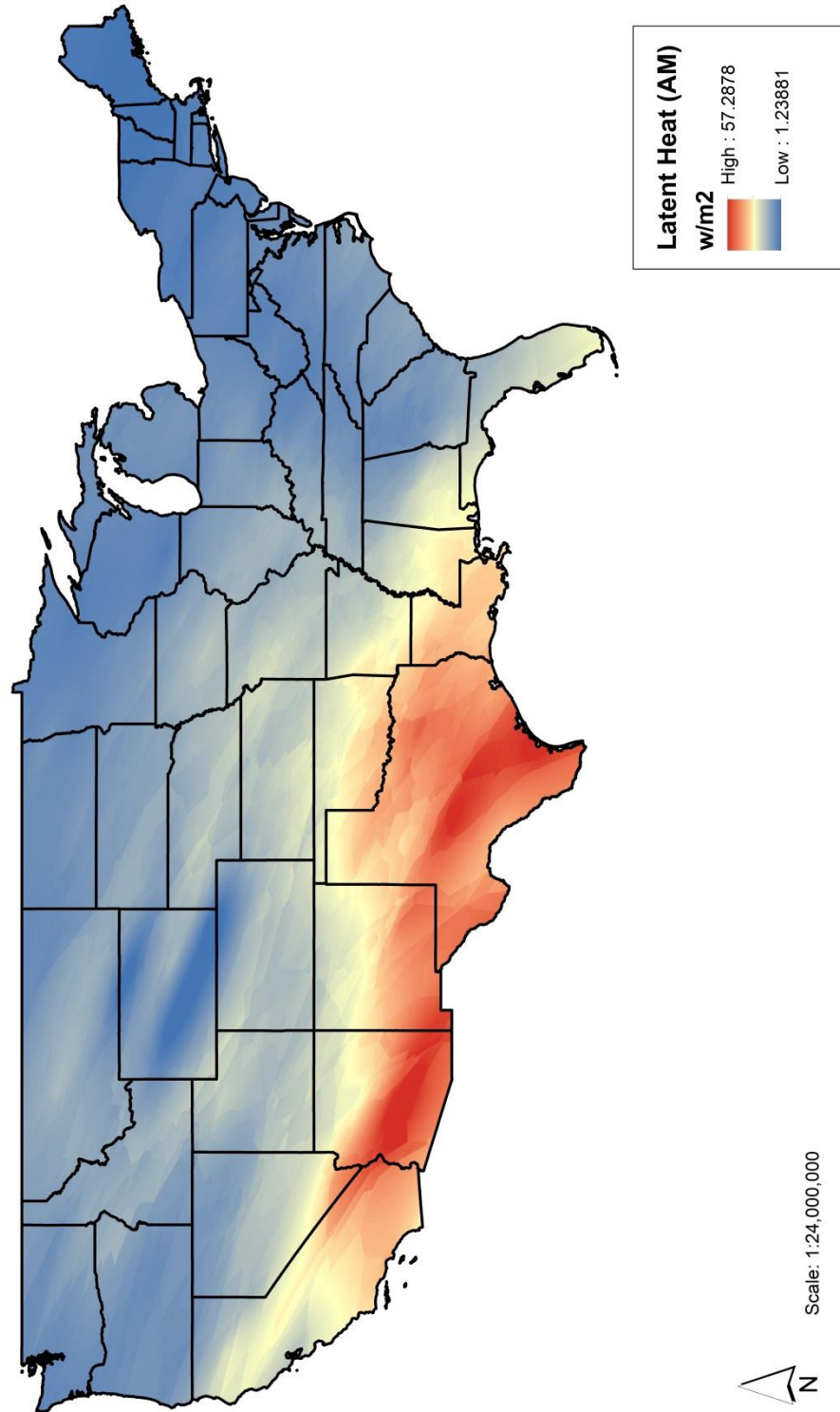


Figure 124: April 2013 Latent Heat (10:30 AM)

April 2013: Latent Heat (10:30 PM)

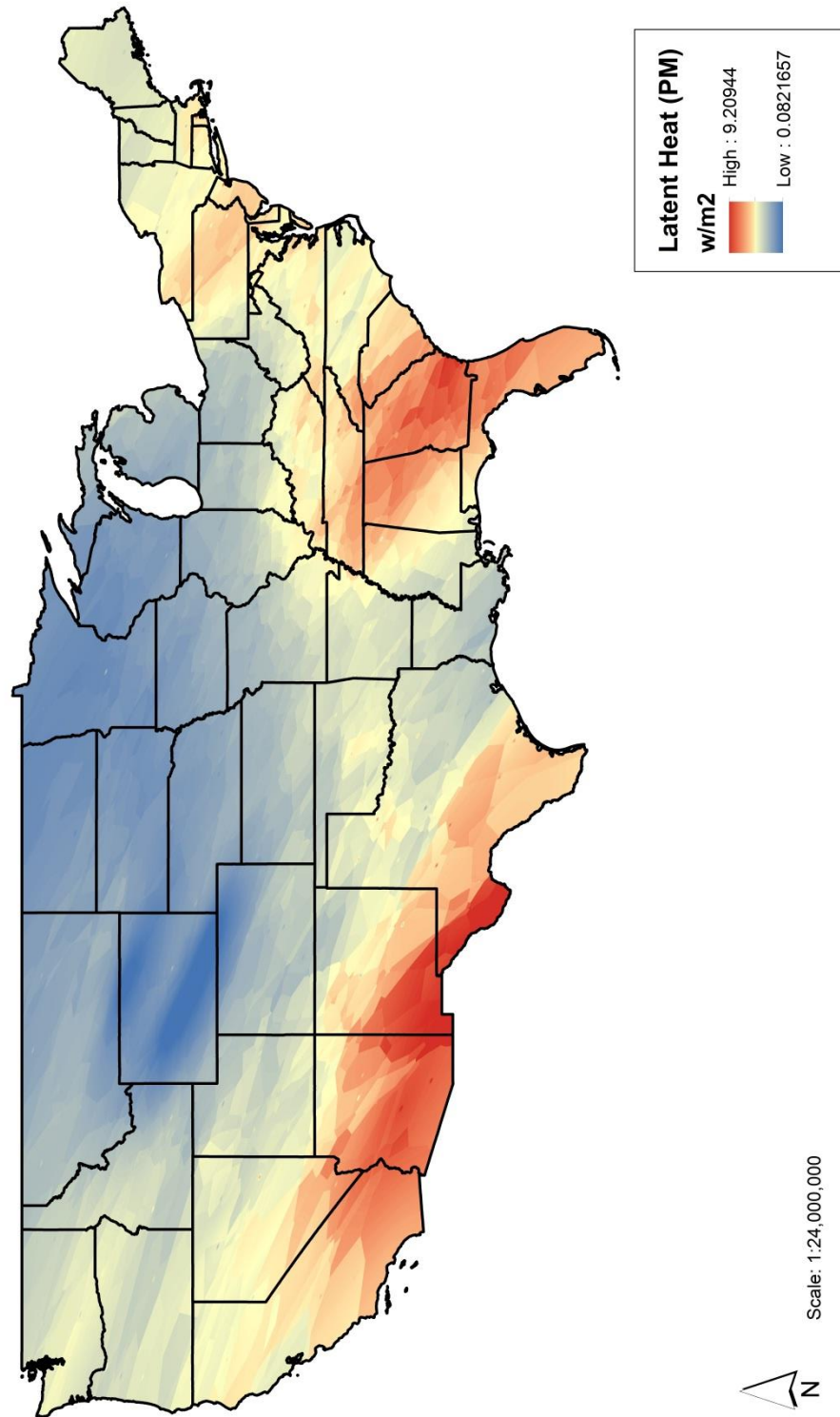


Figure 125: April 2013 Latent Heat (10:30 PM)

July 2011: Latent Heat (10:30 AM)

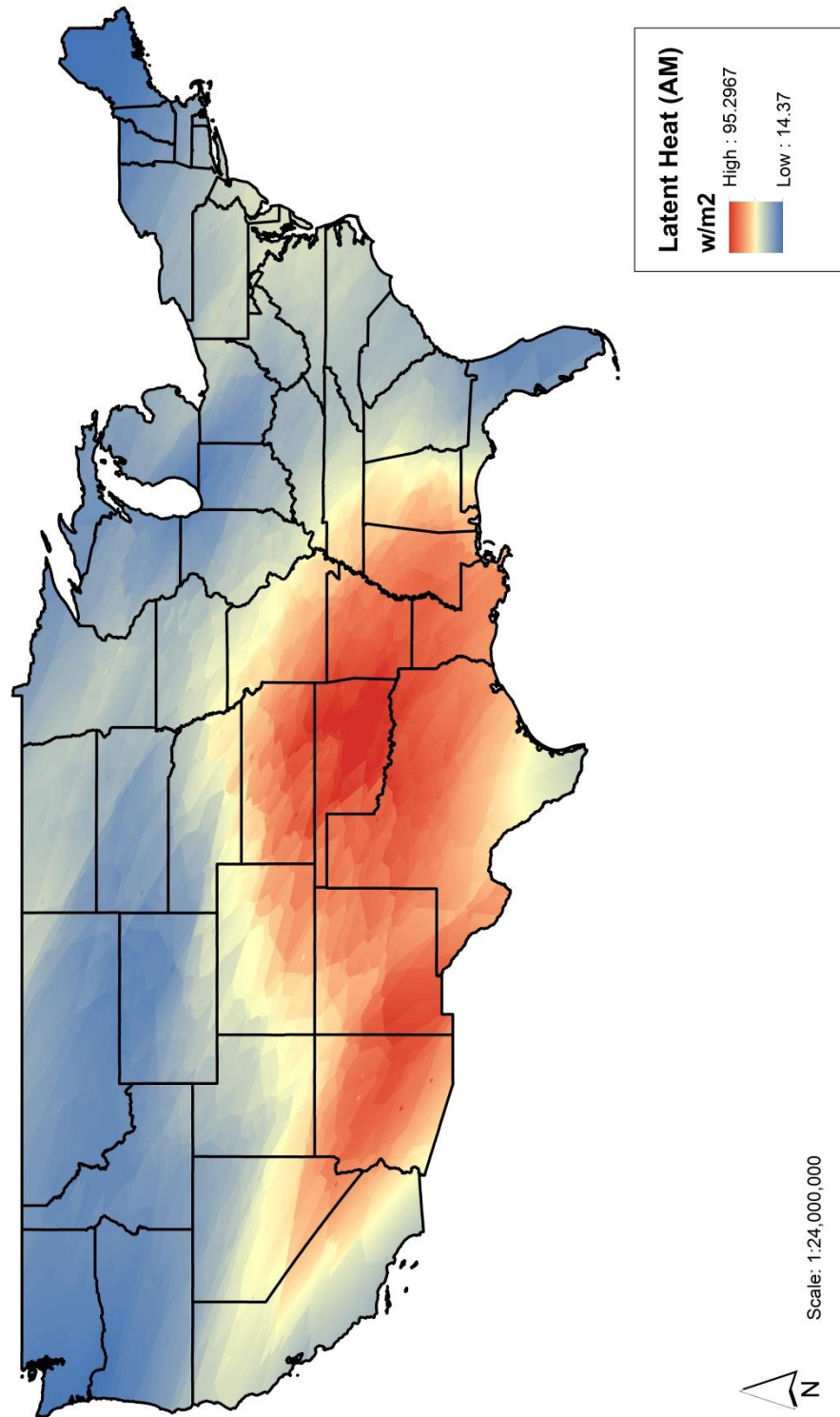


Figure 126: July 2011 Latent Heat (10:30 AM)

July 2011: Latent Heat (10:30 PM)

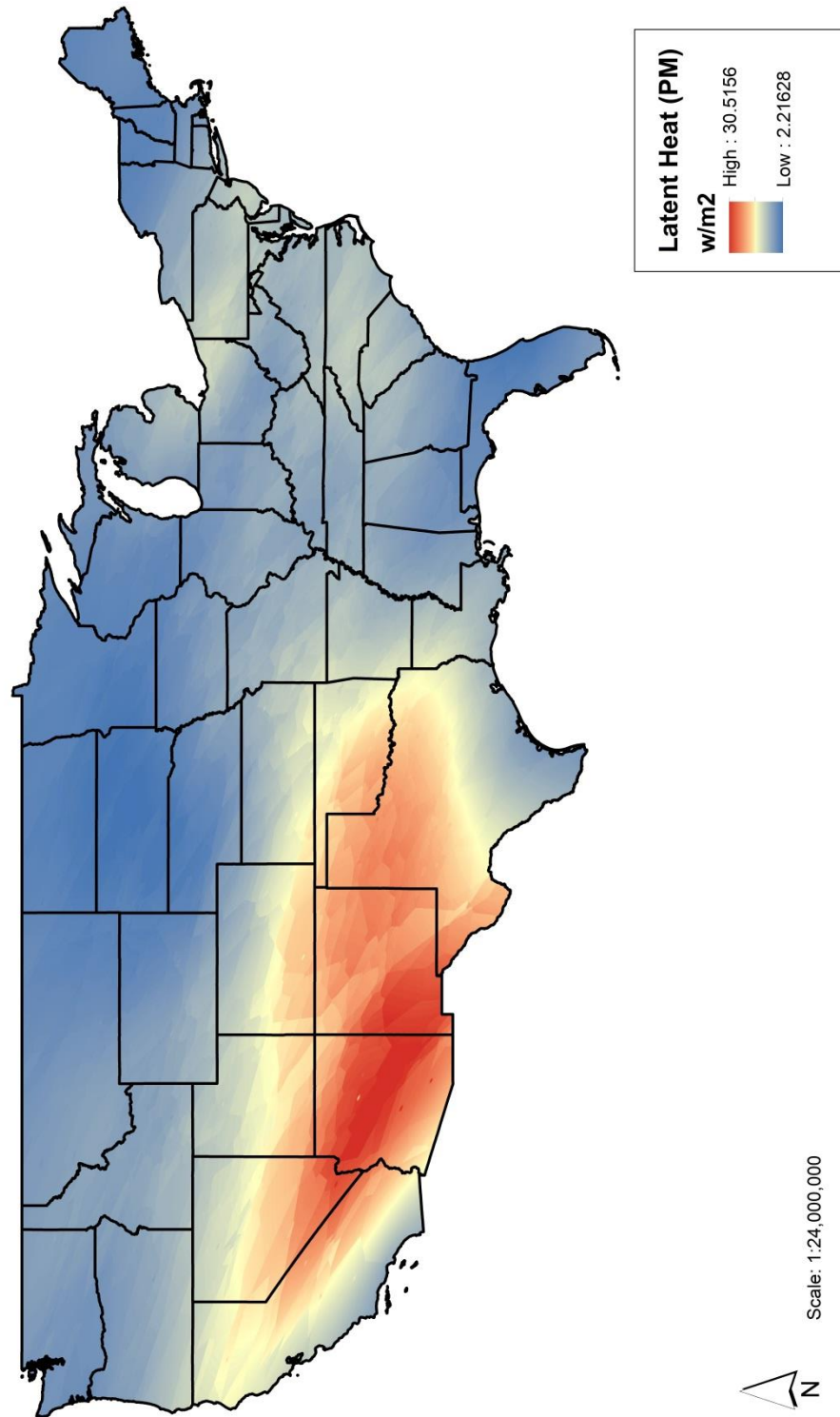


Figure 127: July 2011 Latent Heat (10:30 PM)

July 2013: Latent Heat (10:30 AM)

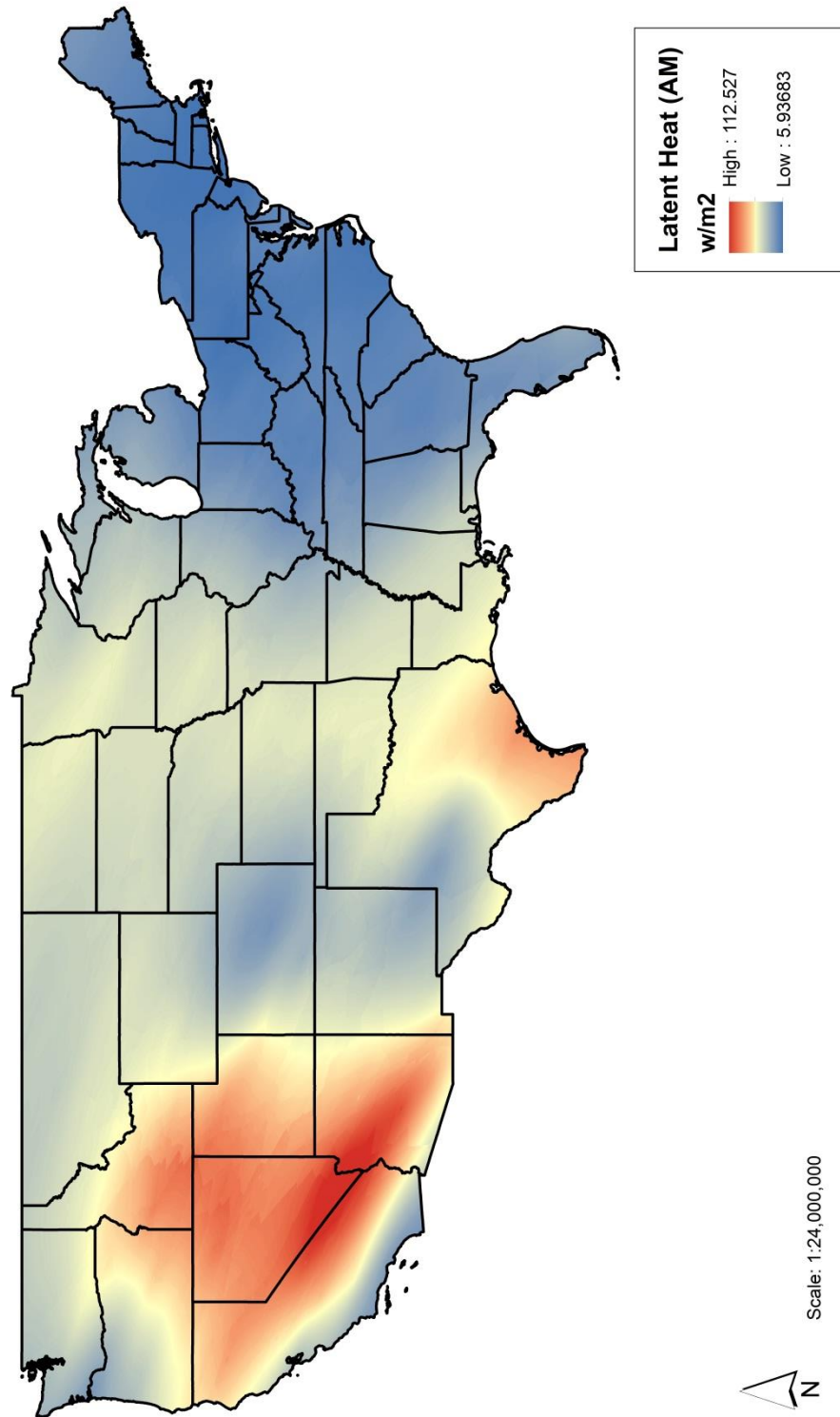


Figure 128: July 2013 Latent Heat (10:30 AM)

July 2013: Latent Heat (10:30 PM)

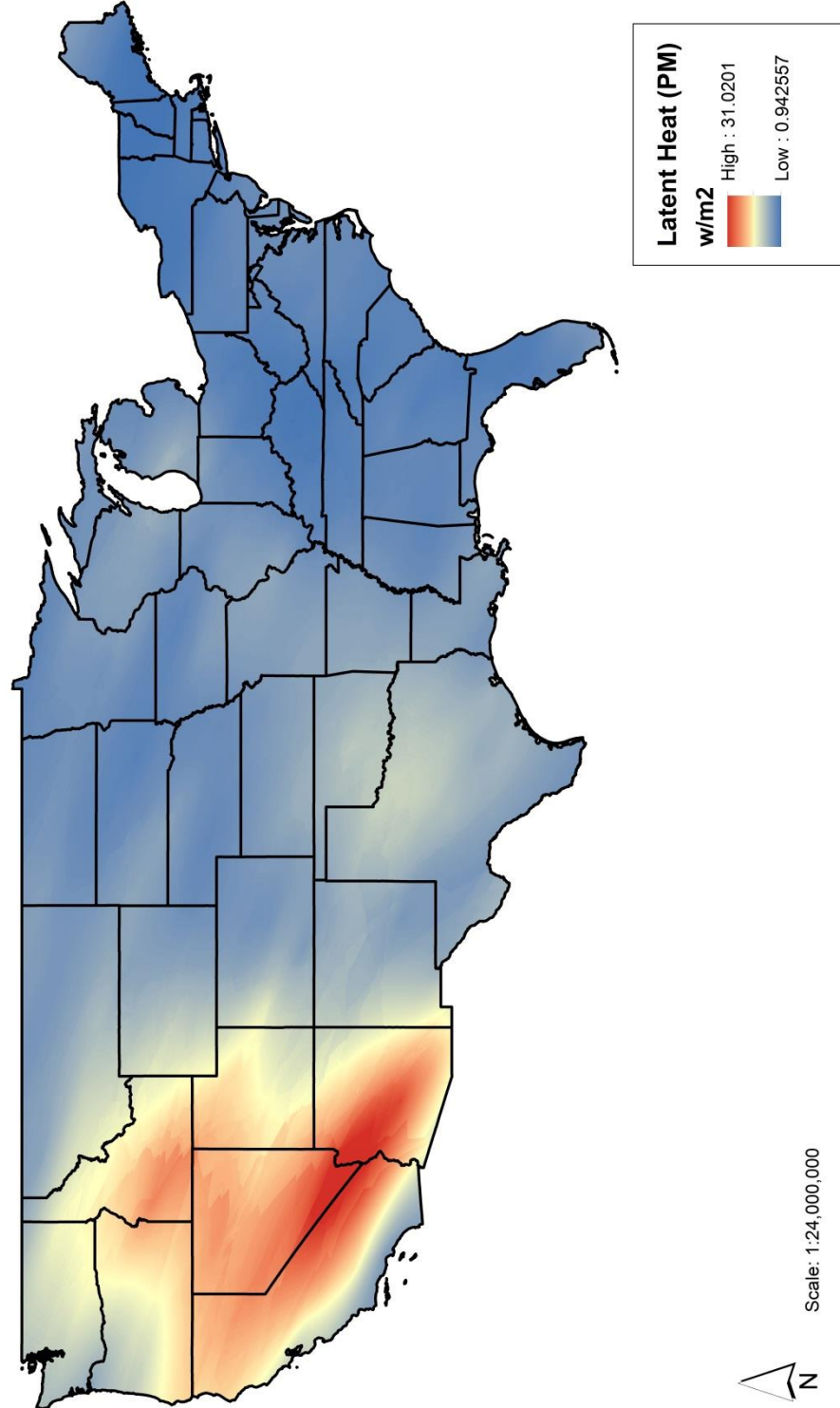


Figure 129: July 2013 Latent Heat (10:30 PM)

October 2011: Latent Heat (10:30 AM)

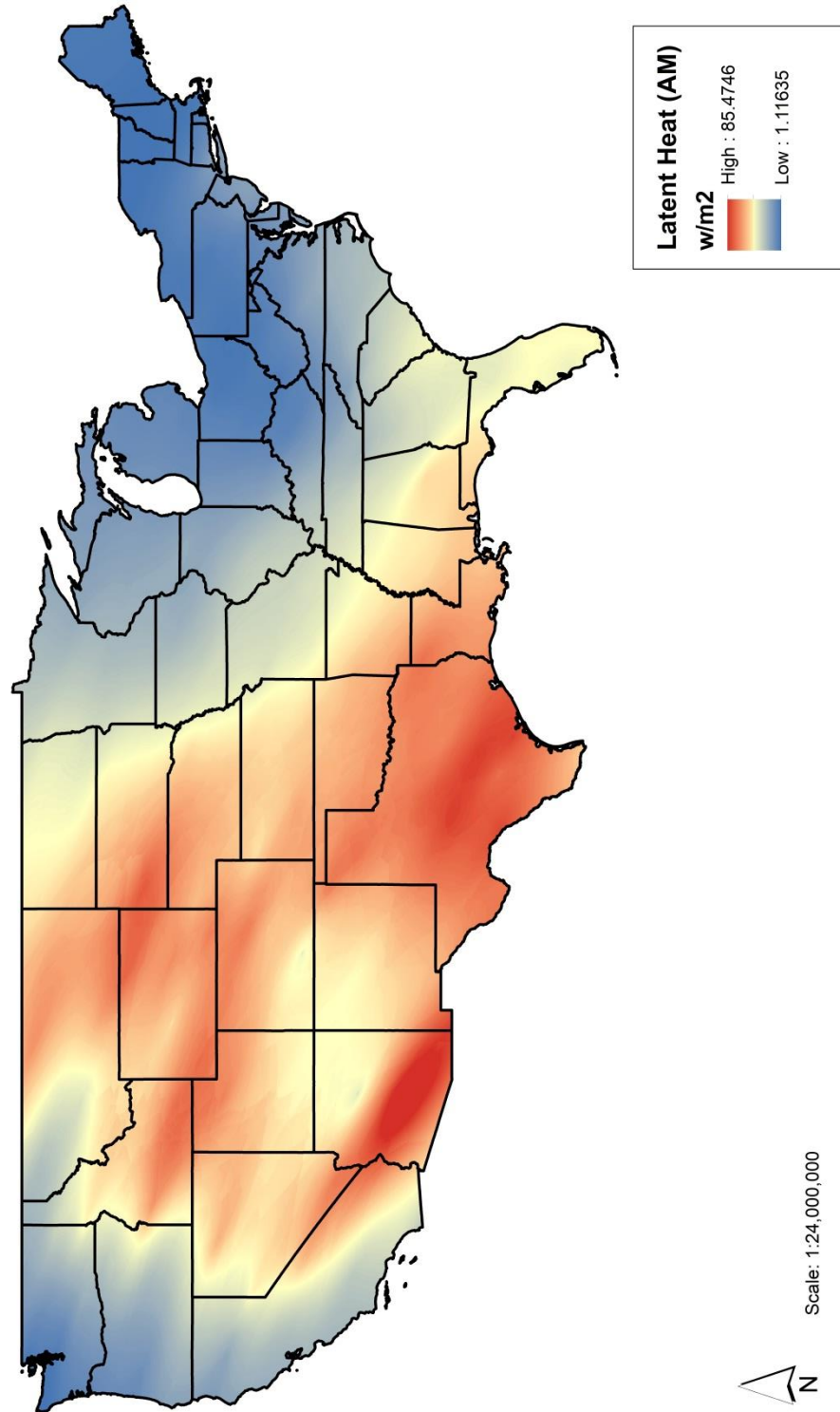


Figure 130: October 2011 Latent Heat (10:30 AM)

October 2011: Latent Heat (10:30 PM)

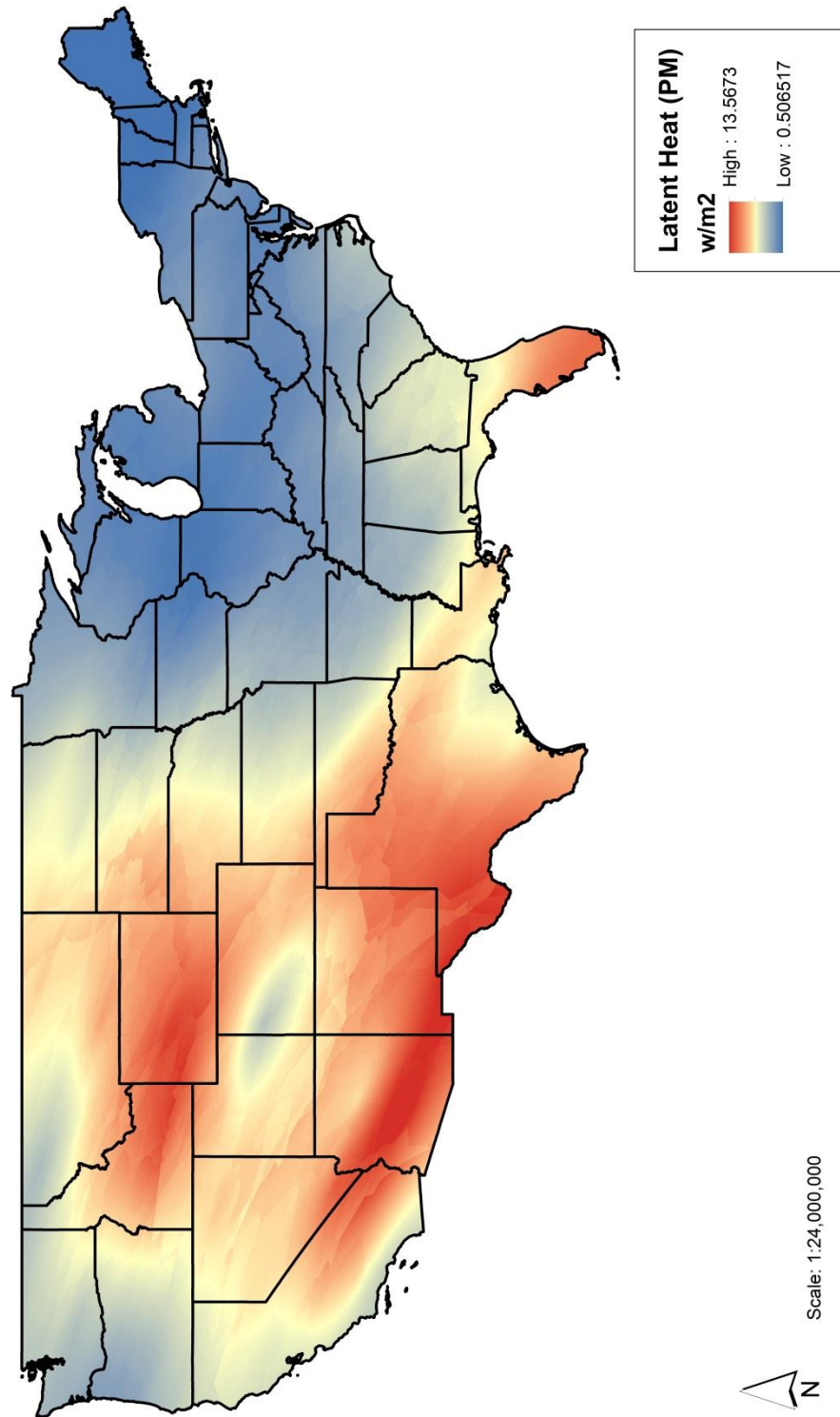


Figure 131: October 2011 Latent Heat (10:30 PM)

October 2013: Latent Heat (10:30 AM)

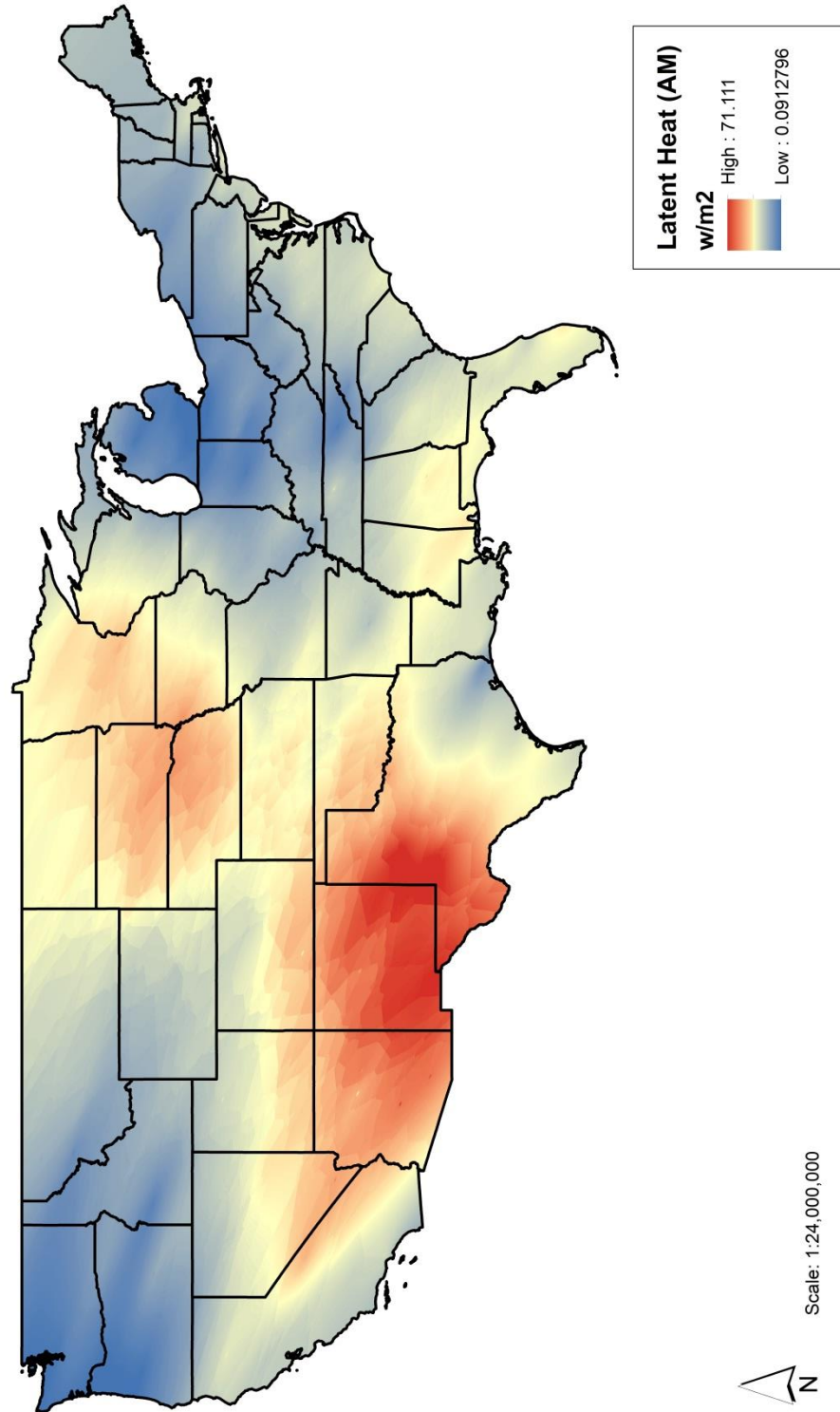


Figure 132: October 2013 Latent Heat (10:30 AM)

October 2013: Latent Heat (10:30 PM)

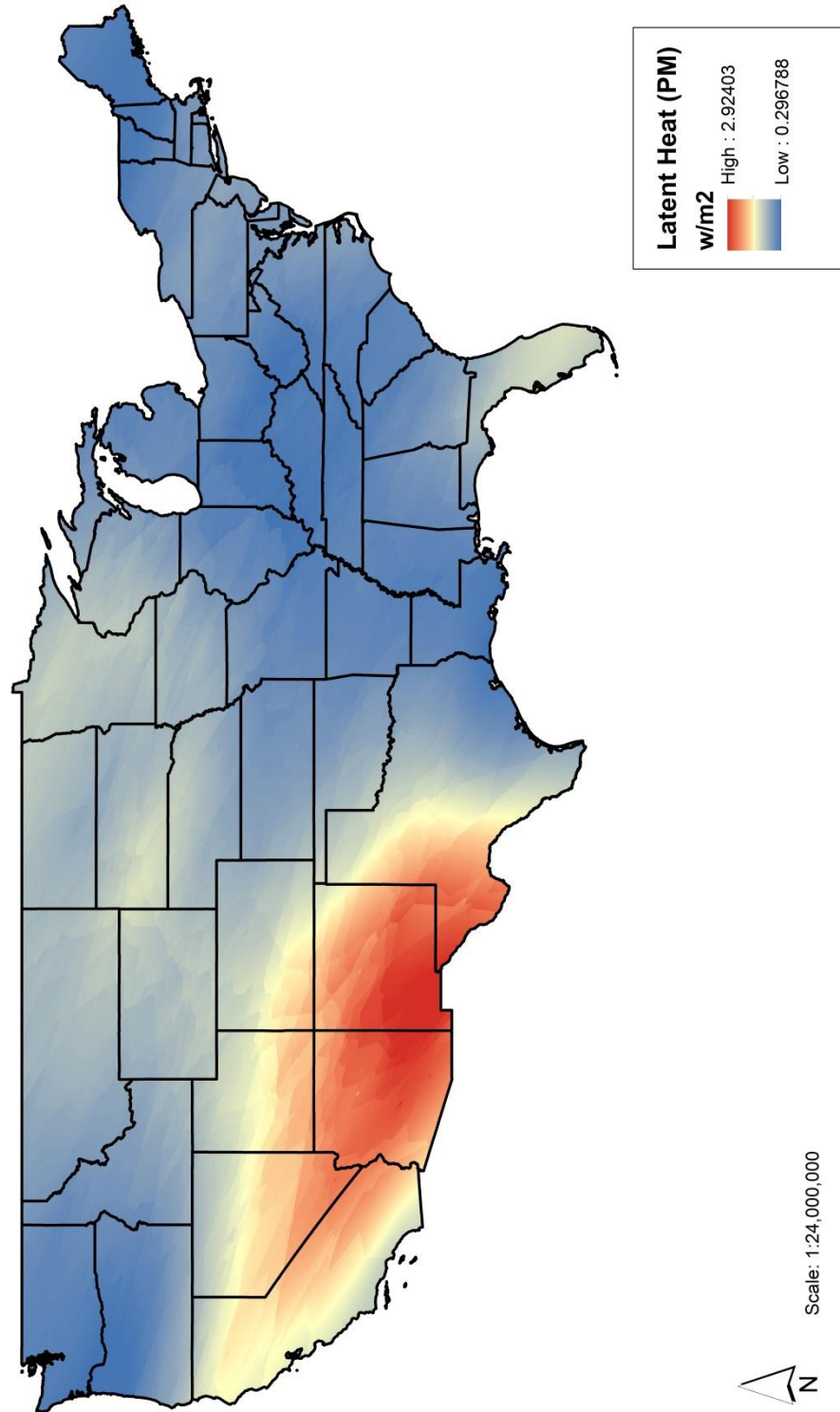


Figure 133: October 2013 Latent Heat (10:30 PM)

APPENDIX C

RESULTS FROM LINEAR MODEL APPLIED TO ENTIRE U.S.

The following four images, shown in *Figure 134: January 2013 Power Output (10:30 AM - Using Linear Model)* through *Figure 137: October 2013 Power Output (10:30 AM - Using Linear Model)*, represent the SoV power output in kilowatts based on the 10:30 AM sensible and latent heat flux values using the linear model. The regional factor and slope were excluded from this model. The images shown represent the four seasons for 2013.

January 2013: 10:30 AM Power Production

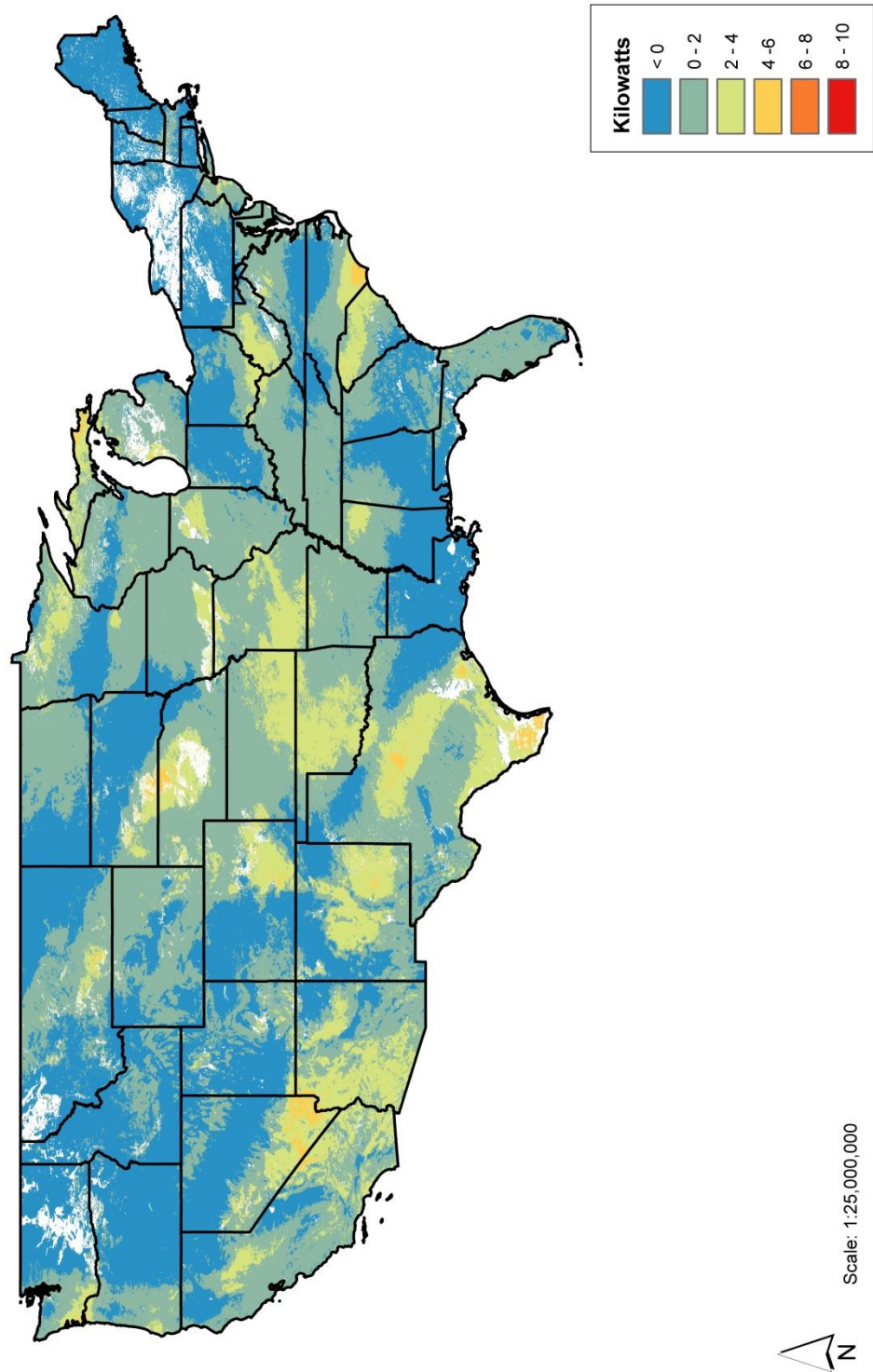


Figure 134: January 2013 Power Output (10:30 AM - Using Linear Model)

April 2013: 10:30 AM Power Production

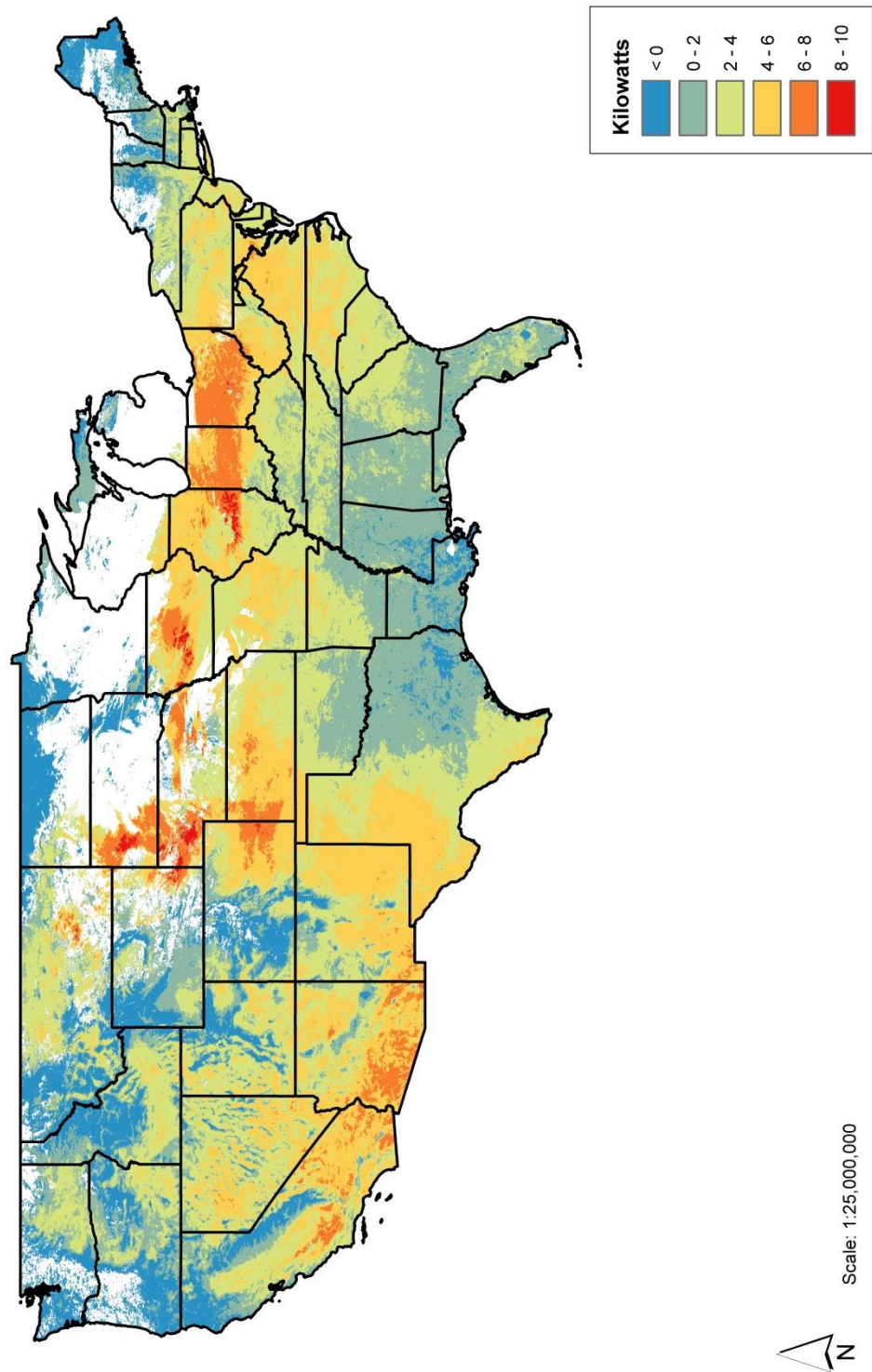


Figure 135: April 2013 Power Output (10:30 AM - Using Linear Model)

July 2013: 10:30 AM Power Production

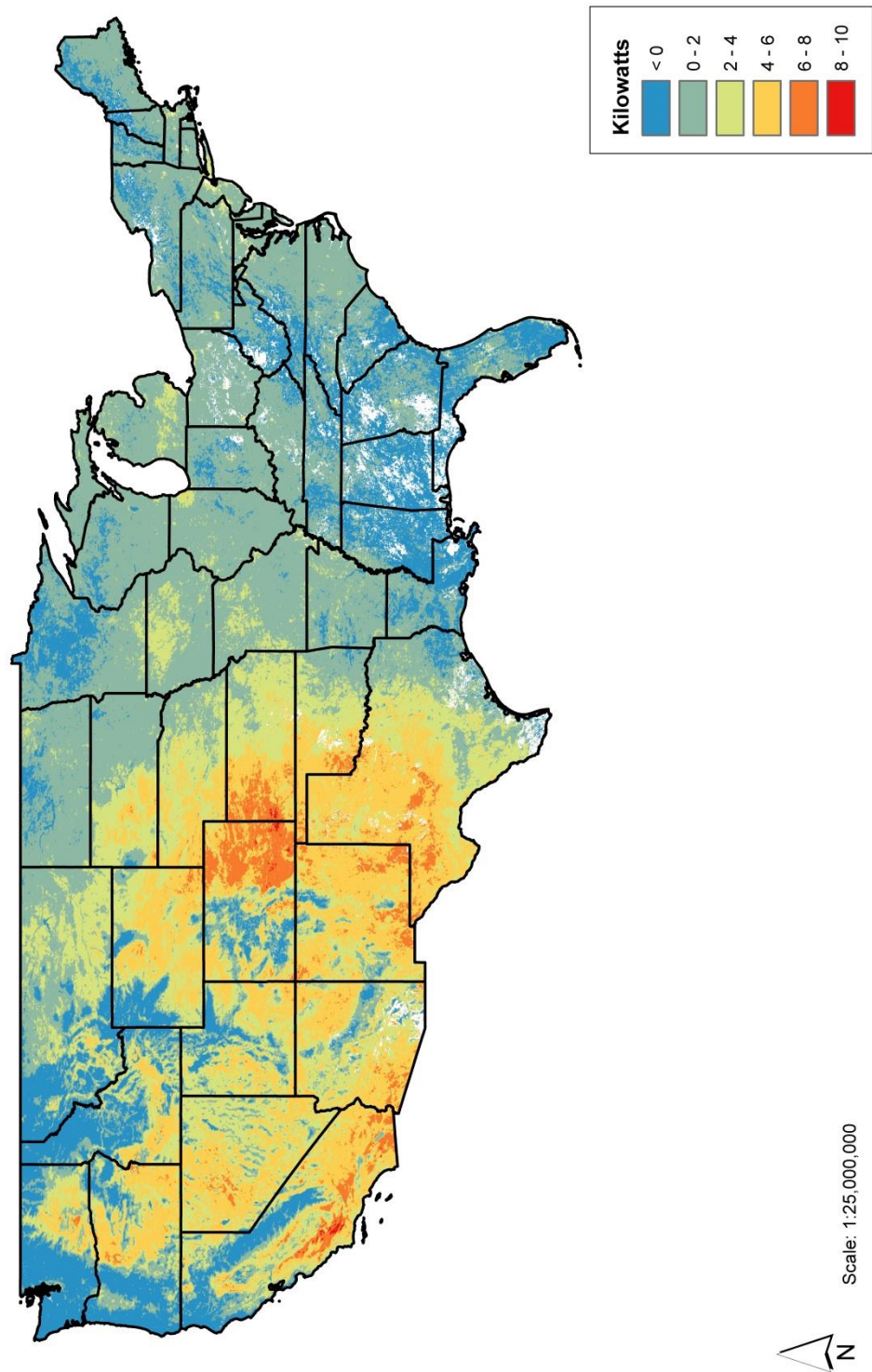


Figure 136: July 2013 Power Output (10:30 AM - Using Linear Model)

October 2013: 10:30 AM Power Production

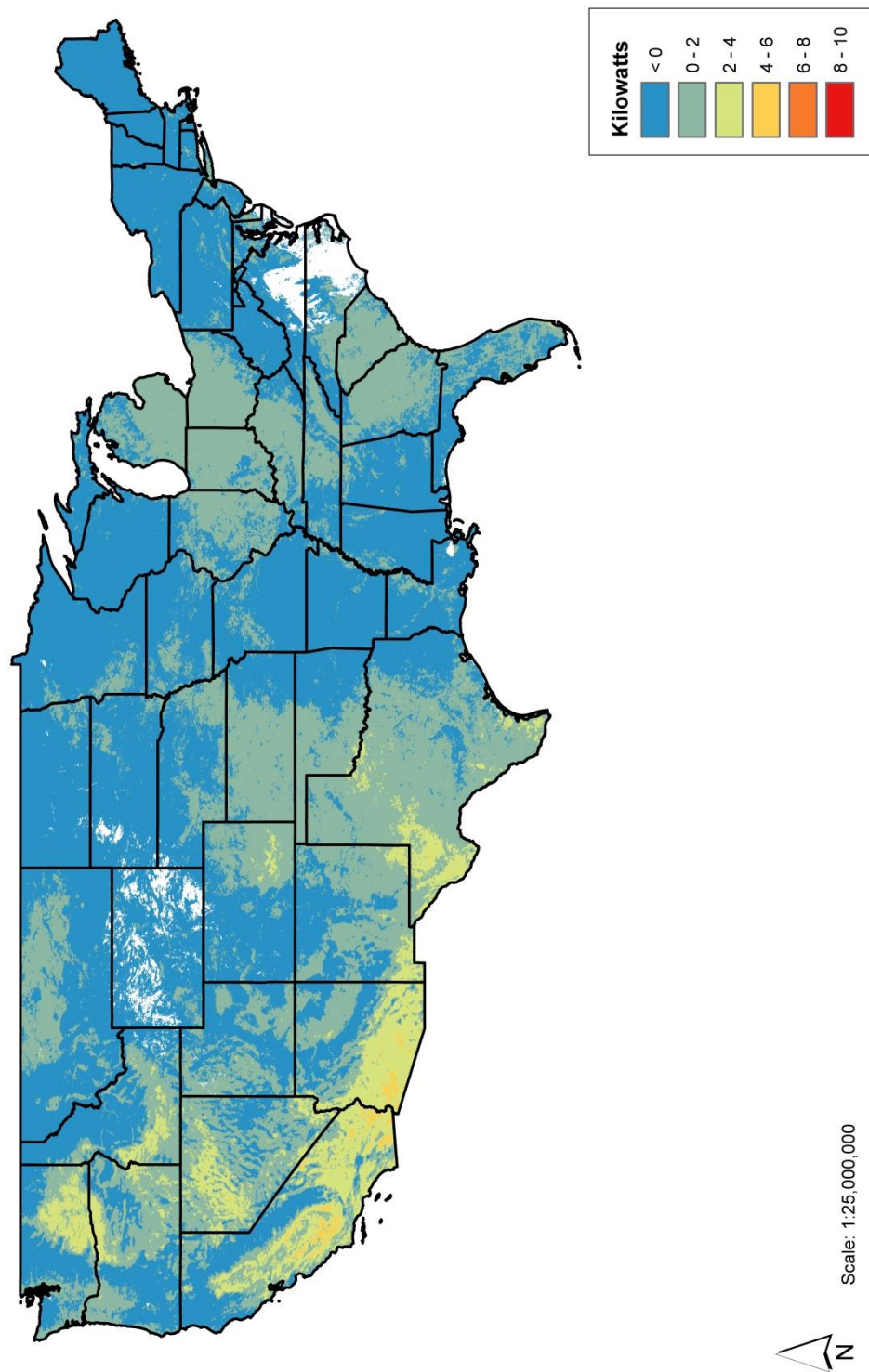


Figure 137: October 2013 Power Output (10:30 AM - Using Linear Model)

APPENDIX D

RESULTS FROM LINEAR MODEL APPLIED TO CITY OF ATLANTA

The following four images, shown in *Figure 138: January 2013: City of Atlanta 10:30 AM Power Production (Full Linear Model)* through *Figure 141: October 2013: City of Atlanta 10:30 AM Power Production (Full Linear Model)*, represent the SoV power production at 10:30 AM for the City of Atlanta, Georgia. The full linear model was used, which incorporated the regional factor and slope model. The images represent the four seasons for 2013.

January 2013: City of Atlanta 10:30 AM Power Production

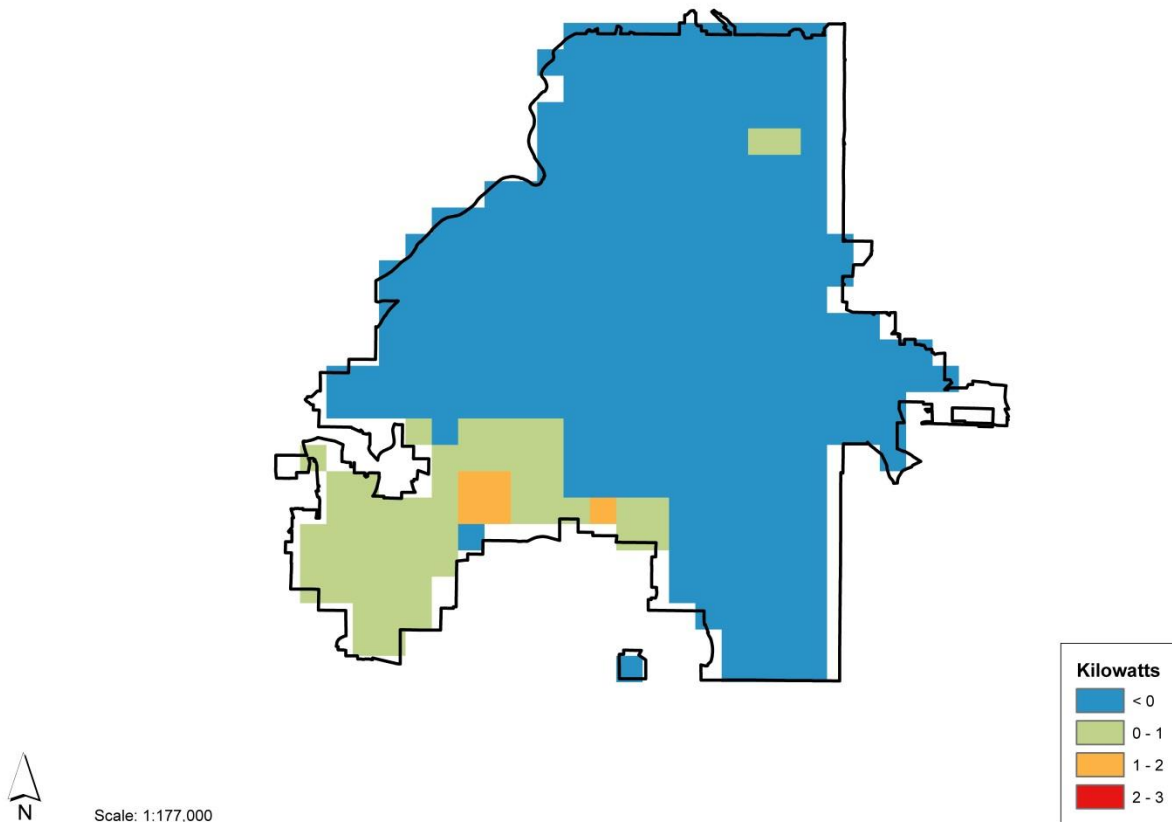


Figure 138: January 2013: City of Atlanta 10:30 AM Power Production (Full Linear Model)

April 2013: City of Atlanta 10:30 AM Power Production

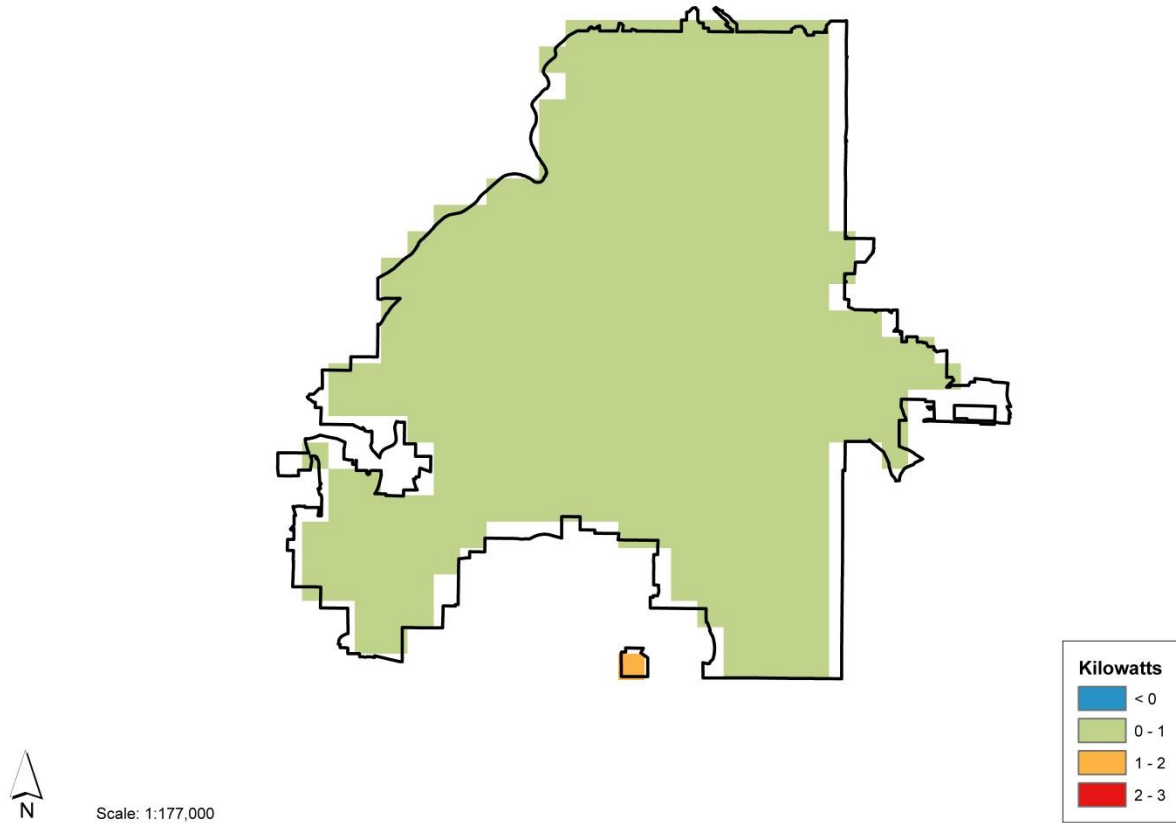


Figure 139: April 2013: City of Atlanta 10:30 AM Power Production (Full Linear Model)

July 2013: City of Atlanta 10:30 AM Power Production

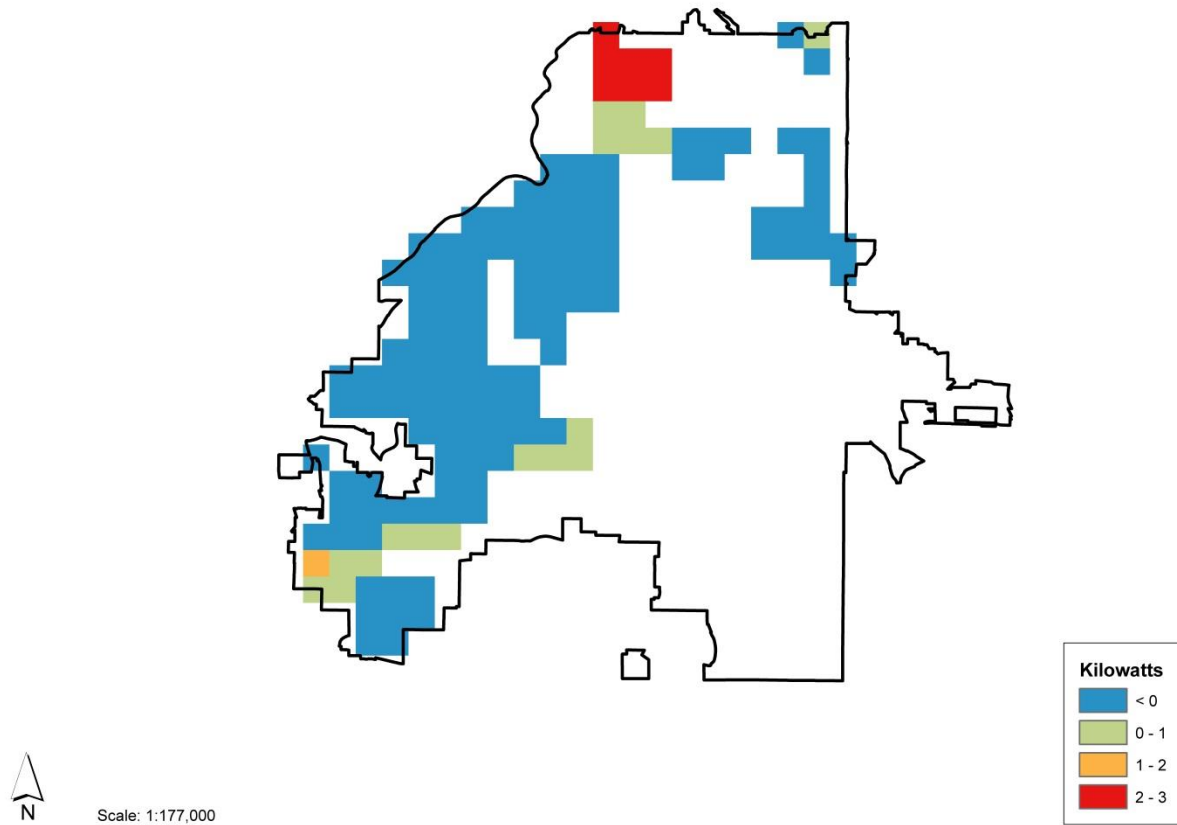


Figure 140: July 2013: City of Atlanta 10:30 AM Power Production (Full Linear Model)

October 2013: City of Atlanta 10:30 AM Power Production

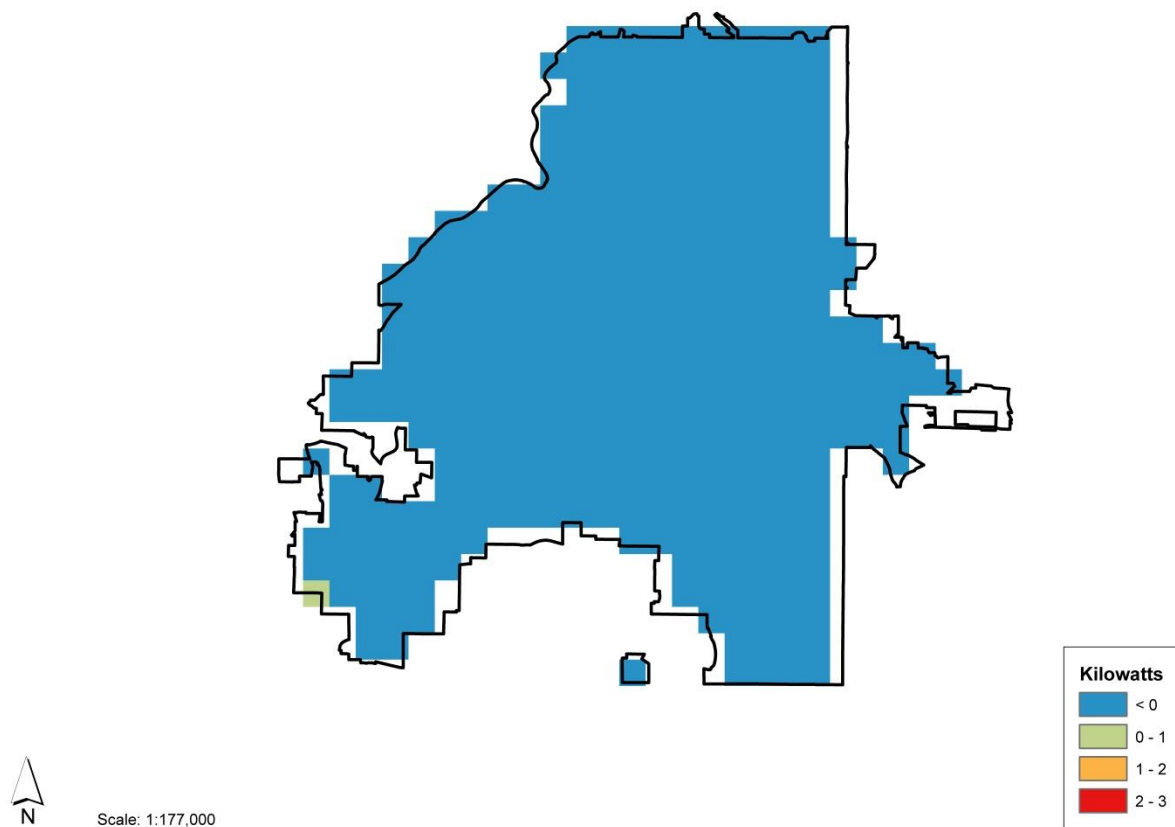


Figure 141: October 2013: City of Atlanta 10:30 AM Power Production (Full Linear Model)

REFERENCES

- Alexander-Kearns, M. and Thakar, N. (2015). “The Greening of Our National Parks.” <https://www.americanprogress.org/issues/green/report/2015/10/14/123076/the-greening-of-our-national-parks/.pdf> (July 2015).
- Allen, R. G. (2005). *The ASCE Standardized Reference Evapotranspiration Equation*. Reston, VA.
- American Physical Society. (2007). “National Policy: Climate Change.” http://www.aps.org/policy/statements/07_1.cfm (July 2015).
- Anderson, L., Manning, R., Valliere, W., Reigner, N., Pettengill, P., & Pierce, V. (2015). “Assessing the Full Circle Trolley: Implications for Alternative Transportation Systems in the National Parks.” *Journal of Park and Recreation Administration*, 33(1), 112-131.
- Bonan, G. (2002). *Ecological Climatology: Concepts and Applications*. New York: Cambridge University Press.
- Bureau of Land Management. (2014). “Wind Energy Development Programmatic EIS.” <http://www.windeis.anl.gov> (July 2015).
- Build Your Dreams. (2015). “Electric Bus.” <http://www.byd.com/na/auto/ElectricBus.html> (July 2015).
- California Energy Commission. (2015a). “Biodiesel as a Transportation Fuel.” <http://www.consumerenergycenter.org/transportation/afvs/biodiesel.html> (July 2015).
- California Energy Commission. (2015b). “Compressed Natural Gas (CNG) as a Transportation Fuel.” <http://www.consumerenergycenter.org> (July 2015).
- California Energy Commission. (2015c). “Frequently Asked Questions about LNG.” <http://www.energy.ca.gov/lng/faq.html#200> (July 2015).
- California Energy Commission. (2015). “LPG – Propane as a Transportation Fuel.” http://www.Consumerenergycenter.org/transportation/afvs/lpg_propane.html (July 2015).
- Center for Climate and Energy Solutions. (2014). “Cogeneration: Combined Heat and Power.” <http://www.c2es.org/technology/factsheet/CogenerationCHP> (June 2015).
- Department of Energy. (2014). “Alternative Fuel Excise Tax Credit.” <http://www.afdc.energy.gov/laws/319> (June 2015).

- Department of Energy. (2015). "Alternative Fuels Data Center: Biodiesel Fuel Basics." http://www.adfc.energy.gov/fuels/biodiesel_basics.html (June 2015).
- Department of Energy. (2014). "Alternative Fuels Data Center." http://www.afdc.energy.gov/vehicles/flexible_fuel_emissions.html (June 2015).
- Department of Energy. (2015) "Alternative Fuels Data Center." http://www.afdc.energy.gov/fuels/propane_benefits.html (June 2015).
- Department of Energy. (2015). "Clean Cities National Parks Initiative." http://www1.eere.energy.gov/cleancities/national_parks.html#blue (June 2015).
- Department of Energy. (2015). "Energy Efficiency and Renewable Energy: Clean Cities." <https://cleancities.energy.gov/technical-assistance/green-rides/> (June 2015).
- Department of Energy. (2014). "National Parks Roll on with Alternative Fuels." <http://energy.gov/eere/articles/national-parks-roll-alternative-fuels> (July 2015).
- Department of Energy. (2015). "San Clemente Islands." <http://energy.gov/eere/femp/san-clemente-island-channel-islands-national-park-california> (June 2015).
- Dirjish, Matt. (2012). "What's the Difference Between Thin-Film and Crystalline-Silicon Solar Panels?" *Electronic Design*. <http://www.electronicdesign.com/power-sources> (July 2015).
- Dunning, A. (2005). "Impacts of Transit in National Parks and Gateway Communities." *Transportation Research Record: Journal of the Transportation Research Board*, (1931), 129-136.
- Environmental Protection Agency. (2015). "Overview of Greenhouse Gas Emissions." <http://www3.epa.gov/climatechange/ghgemissions/gases.html> (June 2015).
- Environmental Protection Agency. (2015). "Sources of Greenhouse Gas Emissions." <http://www3.epa.gov/climatechange/ghgemissions/sources/transportation.html> (June 2015).
- Federal Transit Authority. (2014). "Low or No Emission Vehicle Deployment Program (LoNo Program)." http://www.fta.dot.gov/grants/13077_15782.html (November 2015).

- Georgia Institute of Technology. (2013). "Fluid Mechanics Research Laboratory." <<http://www.fmrl.gatech.edu/drupal/projects/solarvortex>> (July 2014).
- Green Sun Rising. (2015). "Solar PV." <<http://www.greensunrising.com/solar-pv.htm>> (June 2015).
- Hallo, J. and Manning, R. (2009). "Transportation and recreation: a case study of visitors driving for pleasure at Acadia National Park." *Journal of Transport Geography*, 17, 491–499.
- Hill, D. (2015). "Battery Bus Range: It's All in the Math." <<http://www.masstransitmag.com/article/12131451/battery-bus-range-its-all-in-the-math>> (November 2016).
- Ma, Y., Menenti, M., & Feddes, R. (2010). "Parameterization of Heat Fluxes at Heterogeneous Surfaces by Integrating Satellite Measurements with Surface Layer and Atmospheric Boundary Layer Observations." *Advances in Atmospheric Sciences*, 27(2), 328-336.
- Ma, Y., Han, C., Zhong, L., Wang, B., Zhu, Z., Wang, Y., and Amatya, P. (2013). "Using MODIS and AVHRR Data to Determine Regional Surface Heating Field and Heat Flux Distributions Over the Heterogeneous Landscape in the Tibetan Plateau." *Theory of Applied Climatology*, 117(3-4), 643-652.
- Mace, B., Marquit, J., & Bates, S. (2014). "Visitor Assessment of the Mandatory Alternative Transportation System at Zion National Park." *Environmental Management*, 52, 1271-1285.
- MacKechnie, C. (2015). "Electric Buses: An Introduction." >http://publictransport.about.com/od/Transit_Vehicles/a/Electric-Buses-An-Introduction.htm> (June 2015).
- Manning, R., Lawson, S., Newman, P., Hallo, J., & Monz, C. (2014). "Principles of Sustainable Transportation in National Parks." *TRB 93rd Annual Meeting Compendium of Papers*. Washington, D.C.
- Manning, R., Lawson, S., Newman, P., Hallo, J., & Monz, C. (2013). "Sustainable Transportation and the National Parks: From Acadia to Zion." University Press of New England, Hanover and London.
- National Aeronautics and Space Administration. (2016). "Scientific Consensus: Earth's Climate is Warming." <<http://climate.nasa.gov/scientific-consensus/>> (June 2015).
- National Parks Conservation Association. (2012). "Solar Energy, National Parks, and

- Landscape Protection in the Desert Southwest: Executive Summary.”
<<https://npca.s3.amazonaws.com/.../aa610927-8501-468b-90f3-7d7834fbb56a.pdf>> (June 2015).
- National Parks Service. (2003). “Accomplishments in Alternative Transportation.”
<http://www.fta.gov/documents/Natl_Park_Svc_Trans_Report.pdf>
(June 2015).
- National Parks Service. (2003). “Alternative Fuels in National Park Units.”
<http://www.nps.gov/transportation/pdfs/ATP_altfuels.pdf>
(June 2015).
- National Parks Service. (2012). “Green Parks Plan.”
<http://www.nps.gov/greenparksplan/downloads/NPS_2012_Green_Parks_Plan.pdf> (August 2015).
- National Parks Service. (2011). Yosemite National Park Unveils Largest Solar Energy System in National Park System.
<<http://www.nps.gov/yose/learn/news/epsolar11.htm>> (June 2015).
- National Parks Service. (2011). “National Parks Index.”
<http://www.nps.gov/hfc/products/pubs/NPS_index2009_11.pdf> (August 2015).
- National Parks Service. (2010). “Recovery Act Provides Gas Powered Shuttle Buses for Grand Canyon National Park.”
<http://www.nps.gov/grca/learn/news/2aug10_news.htm> (August 2015).
- National Parks Service. (2016). Yellowstone.
<<http://www.nps.gov/yell/learn/management/sustainability-energy.htm>>
(July 2015).
- National Renewable Energy Lab. (2015). “Dynamic Maps, GIS Data, and Analysis Tool.”
<http://www.nrel.gov/gis/data_solar.html> (September 2015).
- National Renewable Energy Lab. (2015). “Dynamic Maps, GIS Data, and Analysis Tool.”
<http://www.nrel.gov/gis/data_wind.html> (September 2015).
- National Renewable Energy Lab. (1998). “Using CNG Trucks in National Parks.”
<<http://www.afdc.energy.gov/pdfs/CNGTrk.pdf>> (March 2015).
- National Renewable Energy Lab. (2012). Metadata on NREL Solar DNI Data.”
<http://www.nrel.gov/gis/data_solar.html> (September 2015).
- National Wind Watch. (2014). “Presenting the Facts About Industrial Wind Power.”
<<https://www.wind-watch.org/faq-size.php>> (June 2015).

- Nature's Furnace. (2014). "Energy from Biowaste." <<http://www.naturesfurnace.com>> (July 2015).
- Navigant Research. (2014). "U.S. National Parks and Electric Vehicles." <<https://www.navigantresearch.com/blog/u-s-national-parks-and-electric-vehicles-a-match-made-in-heaven>> (June 2015).
- Oregonian. (2012). "The National Parks Service Expresses Concerns Over Proposed LNG Terminal at Warrenton." <http://www.oregonlive.com/environment/index.ssf/2012/11/national_park_service_expresse.html> (July 2015).
- Pettebone, D., Newman, P., Lawson, S., Hunt, L., Monz, C., Zwiefka, J. (2011). Estimating visitors' travel mode choices along the Bear Lake Road in Rocky Mountain National Park. *Journal of Transport Geography*, 19, 1210–1221.
- Powell, M., Vickery, P., and Reinhold, T. (2003). Reduced Drag Coefficient for High Wind Speeds in Tropical Cyclones. *Nature* 422, 279-283.
- Proterra. (2015). "Advantages." <<http://www.proterra.com/advantages/overview/>> (July 2015).
- Shiftan, Y., Vary, D., and Geyer, D. (2006). "Demand for Park Shuttle Services – A Stated-Preference Approach." *Journal of Transport Geography*, 14, 52-59.
- Simpson, M., Pearlstein, A., and Glezer, A. (2013). "Electric Power Generation Using Buoyancy-Induced Vortices." *Renewable Energy and Power Quality Journal*, (11).
- Sims, C., Hodges, D., Fly, M., & Stephens, B. (2005). "Modeling Visitor Acceptance of a Shuttle System in the Great Smoky Mountains National Park." *Journal of Park and Recreation Administration*, 23(3), 25-44.
- Solar Energy Industries Association. (2015). Concentrating Solar Power. <http://www.seia.org/policy/solar-technology/concentration_solar_power.pdf> (September 2015).
- Solar Tower UK. (2016). "Meteorological Reactors." <<http://www.solar-tower.org.uk/quick-start.php>> (September 2015).
- Taff, D., Newman, P., Pettebone, D., White, D., Lawson, S., Monz, C., Vagias, W. (2013). "Dimensions of alternative transportation experience in Yosemite and Rocky Mountain National Parks." *Journal of Transport Geography*, 30, 37-46.
- Toyota Pressroom. (2015). "Toyota Flips the Switch to Sustainable Power at Yellowstone National Park."

- <<http://corporatenews.pressroom.toyota.com/releases/toyota+sustainable+power+yellowstone+may12.htm>> (July 2015).
- U.S. Energy Information Agency. (2015). "Electric Power Monthly."
<<http://www.eia.gov/electricity/monthly/>> (June 2015).
- U.S. Department of Transportation. (2014). "Paul S. Sarbanes Transit in Parks Program."
<http://www.fta.dot.gov/grants/13094_6106.html> (August 2015).
- Westport. (2013). "CNG and LNG: What's Best for Your Fleet?"
<http://www.westport.com/file_library/files/webinar/2013-06-19_CNGandLNG.pdf> (June 2015).
- Winter, A. (2014). "National Park Adds Propane Buses and Trucks."
<<http://www.businessfleet.com/article/story/2014/09/going-green-with-propane.aspx>> (July 2015).
- Yellowstone-Teton Clean Cities. (2014). "National Parks Initiative."
<<https://ytcleancities.org/what-we-are-doing-why/initiatives/>> (June 2015).
- Zion National Park. (2016). "Electric Vehicle Station."
<http://www.zionlodge.com/sustainability/electric-vehicle-charging-station>
(July 2015).
- Zip Around Carts. (2015). "Energy Savings." <<http://http://www.ziparoundcarts.com/Energy-Savings.html>> (November 2016).